

**ABSOLUTE OPTICAL OSCILLATOR STRENGTHS FOR
ELECTRONIC EXCITATIONS OF NOBLE GAS
ATOMS AND DIATOMIC MOLECULES**

By

Wing-Fat Chan

B. Sc. (Chemistry) The Chinese University of Hong Kong, 1984

M. Phil. (Chemistry) The Chinese University of Hong Kong, 1986

A THESIS SUBMITTED IN PARTIAL FULFILLMENT OF
THE REQUIREMENTS FOR THE DEGREE OF
DOCTOR OF PHILOSOPHY

in

THE FACULTY OF GRADUATE STUDIES
DEPARTMENT OF CHEMISTRY

We accept this thesis as conforming
to the required standard

THE UNIVERSITY OF BRITISH COLUMBIA

September 1992

© Wing-Fat Chan, 1992

In presenting this thesis in partial fulfilment of the requirements for an advanced degree at the University of British Columbia, I agree that the Library shall make it freely available for reference and study. I further agree that permission for extensive copying of this thesis for scholarly purposes may be granted by the head of my department or by his or her representatives. It is understood that copying or publication of this thesis for financial gain shall not be allowed without my written permission.

(Signature)

Chemistry

Sept 23,

Abstract

A new high resolution dipole (e,e) method is described for the measurement of absolute optical oscillator strengths (cross sections) for electronic excitation of free atoms and molecules throughout the discrete region of the valence shell spectrum. The technique, utilizing the virtual photon field of a fast electron inelastically scattered at negligible momentum transfer, avoids many of the difficulties and errors associated with the various direct optical techniques which have traditionally been used for absolute optical oscillator strength measurements. In particular, the method is free of the bandwidth (line saturation) effects which can seriously limit the accuracy of photoabsorption cross section measurements for discrete transitions of narrow linewidth obtained using the Beer-Lambert law ($I_0/I = \exp(nl\sigma_p)$). Since these perturbing "line saturation" effects are not widely appreciated and are only usually considered in the context of peak heights a detailed new analysis of this problem is presented considering the integrated cross section (oscillator strength) over the profile of each discrete peak.

Using a low resolution dipole (e,e) spectrometer (~1 eV FWHM), absolute optical oscillator strengths for the photoabsorption of the five noble gases He, Ne, Ar, Kr and Xe have been measured up to 180, 250, 500, 380 and 398 eV respectively. The absolute scales for the measurements of helium and neon were obtained by TRK sum rule normalization and it was not necessary to make the difficult determinations of photon flux or target density required in conventional absolute cross section determinations. Single point continuum normalization to absolute optical data was employed for the

measurements of argon, krypton and xenon due to the closely space in the subshells of these targets which cause problems in the extrapolation procedures required for TRK sum-rule normalization. The newly developed high resolution dipole (e,e) method (0.048 eV FWHM) has then been used to obtain the absolute optical oscillator strengths for the valence discrete excitations of the above five noble gases with the absolute scale normalized to the low resolution dipole (e,e) measurements in the smooth ionization continuum region. The measured dipole oscillator strengths for helium excitation ($1^1S \rightarrow n^1P$, $n=2-7$) are in excellent quantitative agreement with the calculations reported by Schiff and Pekeris (Phys. Rev. **134**, A368 (1964)) and by Fernley *et al.* (J. Phys. B **20**, 6457 (1987)). High resolution absolute optical oscillator strengths are also reported for the autoionizing resonances, corresponding to the double excitation of two valence electrons and/or single excitation of a inner valence electron, of the above five noble gases.

High resolution absolute optical oscillator strengths (0.048 eV FWHM) for discrete and continuum transitions for the photoabsorption of five diatomic gases (H_2 , N_2 , O_2 , CO and NO) throughout the valence shell region are reported. The absolute scales were obtained by normalization in the smooth continuum to TRK sum rule normalized data determined using the low resolution dipole (e,e) spectrometer. Absolute optical oscillator strengths for the vibronic transitions of the Lyman and Werner bands of hydrogen, the $b^1\Pi_u$ and $b^1\Sigma_u^+$ valence excited states, the $c^1\Pi_u$, $c^1\Sigma_u^+$ and $o^1\Pi_u$ Rydberg states and the $e^1\Pi_u$ and $e^1\Sigma_u^+$ states of nitrogen, the $A^1\Pi$, $C^1\Sigma^+$, $B^1\Sigma^+$ and $E^1\Pi$ states of carbon monoxide, and the γ ($A^2\Sigma^+-X^2\Pi$), β ($B^2\Pi-X^2\Pi$), δ ($C^2\Pi-X^2\Pi$) and ϵ ($D^2\Sigma^+-X^2\Pi$) systems of nitric oxide,

were determined. Absolute intensities for the Schumann–Runge continuum region and for the discrete bands below the first ionization potential of oxygen are also reported. The variation of the electronic transition moment with internuclear distance was studied for the Lyman and Werner bands of hydrogen and for the vibronic bands of the $X^1\Sigma^+ \rightarrow A^1\Pi$ transition of carbon monoxide. The dipole strengths of the Lyman and Werner bands of hydrogen at the equilibrium internuclear distance (0.741 Å) are also reported. The present results are compared with previously published experimental data and theoretical calculations. The results for molecular hydrogen are in excellent agreement with high level theory (Allison and Dalgarno, *At. Data* **1**, 289 (1970)).

Table of Contents

Abstract		ii
Table of Contents		v
List of Tables		ix
List of Figures		xiv
Acknowledgements		xx
1	General Introduction	1
2	Measurement of Absolute Optical Oscillator Strengths by Photoabsorption and Electron Impact Methods	6
	2.1 Photoabsorption Cross Section Measurements <i>via</i> the Beer-Lambert Law	6
	2.2 Optical Methods for Determining Absolute Optical Oscillator Strengths for Discrete Transitions	9
	2.3 "Line Saturation" Effects in Beer-Lambert Law Photoabsorption for Discrete Transitions	15
	2.4 Electron Impact Methods	29
	2.4.1 Theoretical Background for Fast Electron Impact Techniques	30
	2.4.2 Experimental Approach	33
3	Experimental Methods	38
	3.1 The Low Resolution Dipole (e,e) Spectrometer	38
	3.2 The High Resolution Dipole (e,e) Spectrometer	42
	3.3 Experimental Considerations and Procedures	47
	3.4 Energy Calibration	52
	3.5 Sample Handling and Background Subtraction	53
4	Absolute Optical Oscillator Strengths for the Electronic Excitation of Helium	55
	4.1 Introduction	55
	4.2 Results and Discussion	56

4.2.1	Low Resolution Optical Oscillator Strengths Measurements for Helium	56
4.2.2	High Resolution Optical Oscillator Strengths Measurements for Helium	63
4.2.2.1	The Discrete Transition of $1^1S \rightarrow n^1P$ ($n=2-7$)..	63
4.2.2.2	The Autoionizing Excited State Resonances	72
4.3	Conclusions	74
5	Absolute Optical Oscillator Strengths for the Electronic Excitation of Neon	76
5.1	Introduction.....	76
5.2	Results and Discussion.....	84
5.2.1	Low Resolution Measurements of the Photoabsorption Oscillator Strengths for Neon up to 250 eV.....	84
5.2.2	High Resolution Measurements of the Photoabsorption Oscillator Strengths for the Discrete Transitions of Neon Below the 2p Ionization Threshold.....	92
5.2.3	High Resolution Photoabsorption Oscillator Strengths for Neon in the 40–55 eV Region of the Autoionizing Excited State Resonances.....	104
5.4	Conclusion.....	107
6	Absolute Optical Oscillator Strengths for the Electronic Excitation of Argon, Krypton and Xenon.....	109
6.1	Introduction.....	109
6.2	Results and Discussion.....	118
6.2.1	Low Resolution Measurements of the Photoabsorption Oscillator Strengths for Argon, Krypton and Xenon	118
6.2.1.1	Low Resolution Measurements for Argon.....	118
6.2.1.2	Low Resolution Measurements for Krypton	133
6.2.1.3	Low Resolution Measurements for Xenon	141

6.2.2	High Resolution Measurements of the Photoabsorption Oscillator Strengths for the Discrete Transitions Below the mp Ionization Thresholds for Argon (m=3), Krypton (m=4) and Xenon (m=5).....	152
6.2.3	High Resolution Measurements of the Photoabsorption Oscillator Strengths in the Autoionizing Resonance Regions due to Excitation of the Inner Valence s Electrons	176
6.4	Conclusions	182
7	Absolute Optical Oscillator Strengths (11–20 eV) and Transition Moments for the Lyman and Werner Bands of Molecular Hydrogen.....	184
7.1	Introduction.....	184
7.2	Results and Discussion.....	192
7.2.1	Absolute Oscillator Strengths	192
7.2.2	The Variation of Transition Moment with the Internuclear Distance for the Lyman and Werner Bands.....	205
7.3	Conclusions	212
8	Absolute Optical Oscillator Strengths for the Discrete and Continuum Photoabsorption of Molecular Nitrogen (11–200 eV)	213
8.1	Introduction.....	213
8.2	Results and Discussion.....	221
8.2.1	Low Resolution Absolute Photoabsorption Oscillator Strength Measurements for Molecular Nitrogen (11–200 eV).....	221
8.2.2	High Resolution Absolute Photoabsorption Oscillator Strength Measurements for Molecular Nitrogen (12–22 eV).....	227
8.3	Conclusions	245

9	Absolute Optical Oscillator Strengths for the Photoabsorption of Molecular Oxygen (5–30 eV)	248
	9.1 Introduction.....	248
	9.2 Results and Discussion.....	252
	9.3 Conclusions	267
10	Absolute Optical Oscillator Strengths for the Discrete and Continuum Photoabsorption of Carbon Monoxide (7–200 eV) and Transition Moments for the $X^1\Sigma^+ \rightarrow A^1\Pi$ System	269
	10.1 Introduction.....	269
	10.2 Results and Discussion.....	275
	10.2.1 Low Resolution Absolute Photoabsorption Oscillator Strength Measurements for Carbon Monoxide (7–200 eV)	276
	10.2.2 High Resolution Absolute Photoabsorption Oscillator Strength measurements for carbon monoxide (12–22 eV)	281
	10.2.3 The Variation of Transition moment with Internuclear Distance for the Vibronic Bands of the $X^1\Sigma^+ \rightarrow A^1\Pi$ Transition	297
	10.3 Conclusions	300
11	Absolute Optical Oscillator Strengths for the Photoabsorption of Nitric Oxide (5–30 eV)	302
	11.1 Introduction.....	302
	11.2 Results and Discussion.....	307
	11.3 Conclusions	323
12	Concluding Remarks	325
	References.....	327

List of Tables

Table	Page
2.1	Methods of obtaining optical oscillator strengths for discrete electronic transitions at high resolution..... 11
3.1	Sources and stated minimum purity of samples..... 54
4.1	Absolute differential optical oscillator strengths for helium obtained using the low resolution (1 eV FWHM) dipole (e,e) spectrometer (24.6–180 eV)..... 58
4.2	Theoretical and experimental determinations of the absolute optical oscillator strengths for the ($1^1S \rightarrow n^1P$, $n=2$ to 7) transitions in helium..... 68
5.1	Absolute differential optical oscillator strengths for neon obtained using the low resolution (1 eV FWHM) dipole (e,e) spectrometer (21.6–250 eV)..... 87
5.2	Theoretical and experimental determinations of the absolute optical oscillator strengths for the $2s^2 2p^6 \rightarrow 2s^2 2p^5 (2P_{3/2,1/2}) 3s$ discrete transitions of neon..... 95
5.3	Theoretical and experimental determinations of the absolute optical oscillator strengths for discrete transitions of neon (19.5–20.9 eV) 97
5.4	Theoretical and experimental determinations of the absolute optical oscillator strengths for discrete transitions of neon (20.9–21.2 eV) 99

6.1	Absolute differential optical oscillator strengths for the photoabsorption of argon above the first ionization potential obtained using the low resolution (1 eV FWHM) dipole (e,e) spectrometer (16–500 eV).....	122
6.2	Absolute differential optical oscillator strengths for the photoabsorption of krypton above the first ionization potential obtained using the low resolution (1 eV FWHM) dipole (e,e) spectrometer (14.7–380 eV).....	136
6.3	Absolute differential optical oscillator strengths for the photoabsorption of xenon above the first ionization potential obtained using the low resolution (1 eV FWHM) dipole (e,e) spectrometer (13.5–398 eV).....	145
6.4	Theoretical and experimental determinations of the absolute optical oscillator strengths for the $3s^23p^6 \rightarrow 3s^23p^5(2P_{3/2,1/2})4s$ discrete transitions of argon.....	159
6.5	Theoretical and experimental determinations of the absolute optical oscillator strengths for discrete transitions of argon. (a) in the energy region 13.80–14.85 eV (b) in the energy region 14.85–15.30 eV.....	161
6.6	Theoretical and experimental determinations of the absolute optical oscillator strengths for the $4s^24p^6 \rightarrow 4s^24p^5(2P_{3/2,1/2})5s$ discrete transitions of krypton....	163
6.7	Theoretical and experimental determinations of the absolute optical oscillator strengths for discrete transitions of krypton. (a) in the energy region 11.90–13.05 eV, (b) in the energy region 13.05–13.50 eV.....	165

6.8	Theoretical and experimental determinations of the absolute optical oscillator strengths for the $5s^2 5p^6 \rightarrow 5s^2 5p^5 ({}^2P_{3/2,1/2}) 6s$ discrete transitions of xenon.....	167
6.9	Theoretical and experimental determinations of the absolute optical oscillator strengths for discrete transitions of xenon. (a) in the energy region 9.80–11.45 eV (b) in the energy region 11.45–11.80 eV.....	169
7.1	Absolute oscillator strengths for the vibronic transitions of the Lyman band of molecular hydrogen	196
7.2	Absolute oscillator strengths for the vibronic transitions of the Werner band of molecular hydrogen.....	197
7.3	Total integrated absolute oscillator strengths for the Lyman and Werner bands of molecular hydrogen.....	203
7.4	Dipole strengths $D_e(r_0)$ for the Lyman and Werner bands of molecular hydrogen	211
8.1	Absolute differential optical oscillator strengths for the photoabsorption of molecular nitrogen obtained using the low resolution (1 eV FWHM) dipole (e,e) spectrometer (11–200 eV).....	224
8.2	Absolute optical oscillator strengths for discrete transitions from the ground state of molecular nitrogen in the energy region 12.50–14.68 eV.....	233
8.3	Absolute optical oscillator strengths for transitions to the vibronic bands of the valence $b^1\Pi_u$ state from the ground state of molecular nitrogen.....	237

8.4	Absolute optical oscillator strengths for transitions to the vibronic bands of the valence $b^1\Sigma_u^+$ state from the ground state of molecular nitrogen	238
8.5	Absolute optical oscillator strengths for transitions to the vibronic bands of the lowest member of the Rydberg $c^1\Sigma_u^+$ state from the ground state of molecular nitrogen	239
8.6	Absolute optical oscillator strengths for transitions to the vibronic bands of the lowest member of the Rydberg $c^1\Pi_u$ state from the ground state of molecular nitrogen	240
8.7	Absolute optical oscillator strengths for transitions to the vibronic bands of the lowest member of the Rydberg $o^1\Pi_u$ state from the ground state of molecular nitrogen	241
8.8	Total absolute optical oscillator strengths for transitions to the $b^1\Pi_u$ and $b^1\Sigma_u^+$ valence states, and the lowest members of the $c^1\Pi_u$, $c^1\Sigma_u^+$ and $o^1\Pi_u$ Rydberg states from the ground state of molecular nitrogen	244
8.9	Integrated absolute optical oscillator strengths in selected regions over the energy range 14.92–16.91 eV for excitation of molecular nitrogen.....	245
9.1	Absolute optical oscillator strengths for the photoabsorption of molecular oxygen in the energy region 9.75–11.89 eV	260
9.2	Integrated absolute optical oscillator strengths for the photoabsorption of molecular oxygen over intervals in the energy region 12.07–18.29 eV.....	264

10.1	Absolute differential optical oscillator strengths for the photoabsorption of carbon monoxide obtained using the low resolution (1 eV FWHM) dipole (e,e) spectrometer (7–200 eV).....	278
10.2	Absolute optical oscillator strengths for the vibronic bands of the $X^1\Sigma^+ \rightarrow A^1\Pi$ transition of carbon monoxide.....	285
10.3	Absolute total optical oscillator strengths for the $X^1\Sigma^+ \rightarrow A^1\Pi$ transition of carbon monoxide.....	288
10.4	Absolute optical oscillator strengths for the vibronic bands from the $X^1\Sigma^+$ ground state to the $B^1\Sigma^+$, $C^1\Sigma^+$ and $E^1\Pi$ excited electronic states of carbon monoxide.....	290
10.5	Integrated absolute optical oscillator strengths for the photoabsorption of carbon monoxide over energy intervals in the region 12.13–16.98 eV.....	295
11.1	Absolute optical oscillator strengths for discrete transitions of nitric oxide in the energy region 5.48–7.44 eV.....	313
11.2	Absolute optical oscillator strengths for the vibronic bands of the γ ($X^2\Pi \rightarrow A^2\Sigma^+$) transition in nitric oxide.....	314
11.3	Absolute optical oscillator strengths for the vibronic bands of the β ($X^2\Pi \rightarrow B^2\Pi$) transition in nitric oxide.....	316
11.4	Absolute optical oscillator strengths for the vibronic bands of the δ ($X^2\Pi \rightarrow C^2\Pi$) transition in nitric oxide.....	317
11.5	Absolute optical oscillator strengths for the vibronic bands of the ϵ ($X^2\Pi \rightarrow D^2\Sigma^+$) transition in nitric oxide.....	318
11.6	Integrated absolute optical oscillator strengths over the energy region 7.52–9.43 eV in the photoabsorption of nitric oxide.....	322

List of Figures

Figure	Page
2.1	Comparison of the absolute valence shell photoabsorption oscillator strength spectra of molecular nitrogen obtained by photoabsorption and dipole (e,e) experiments in the energy region 12.4–13.2 eV 18
2.2	Diagrammatic representation of the "line saturation" effect occurring in Beer–Lambert law photoabsorption experiments ... 21
2.3	Variation of integrated peak intensity ($N \times A_4$) with column number for different ratios of (incident bandwidth (ΔE))/(natural absorption line-width (ΔL))..... 25
2.4	Variation of the observed integrated cross-section with column number for different $\Delta E/\Delta L$ ratios..... 26
2.5	Variation of the observed integrated cross-section with column number at $\Delta E/\Delta L = 10$ for peaks with true integrated cross-section 27
3.1	Schematic of the dipole (e,e+ion) spectrometer..... 40
3.2	Schematic of the high resolution dipole (e,e) spectrometer 43
3.3	Flow-chart showing the data recording and processing procedures used in determining the absolute dipole oscillator strengths for the discrete electronic excitation transitions ($1^1S \rightarrow n^1P$, $n=2-7$) of helium 50
4.1	Absolute dipole oscillator strengths for helium measured by the low resolution dipole (e,e) spectrometer from 20–180 eV (FWHM=1 eV)..... 57

4.2	Absolute dipole oscillator strengths for helium measured by the high resolution electron energy loss spectrometer from 20–30 eV (FWHM=0.048 eV)	66
4.3	Absolute dipole oscillator strengths for helium in the autoionizing resonance regions measured by the high resolution electron energy loss spectrometer. (a) in the energy region 58–66 eV, (b) in the energy region 69–72 eV....	73
5.1	Absolute oscillator strengths for the photoabsorption of neon measured by the low resolution dipole (e,e) spectrometer (FWHM=1eV). (a) 15.7–250 eV, (b) Expanded view of the 20–60 eV energy region	85
5.2	Absolute oscillator strengths for the photoabsorption of neon measured by the high resolution dipole (e,e) spectrometer (FWHM=0.048 eV). (a) 16–26 eV, (b) 19.5–22 eV.....	93
5.3	Absolute oscillator strengths for the photoabsorption of neon in the autoionizing resonance region 40–55 eV (FWHM=0.098 eV).....	106
6.1	Absolute oscillator strengths for the photoabsorption of argon in the energy region 10–60 eV.....	119
6.2	Absolute oscillator strengths for the photoabsorption of argon in the energy region 40–240 eV.....	120
6.3	Absolute oscillator strengths for the photoabsorption of argon in the energy region 220–500 eV.....	121
6.4	Absolute oscillator strengths for the photoabsorption of krypton in the energy region 5–60 eV.....	134
6.5	Absolute oscillator strengths for the photoabsorption of krypton in the energy region 50–400 eV.....	135

6.6	Absolute oscillator strengths for the photoabsorption of xenon in the energy region 5–60 eV.....	142
6.7	Absolute oscillator strengths for the photoabsorption of xenon in the energy region 40–200 eV.....	143
6.8	Absolute oscillator strengths for the photoabsorption of xenon in the energy region 160–400 eV.....	144
6.9	Absolute oscillator strengths for the photoabsorption of argon obtained using the high resolution dipole (e,e) spectrometer (FWHM=0.048 eV). (a) in the energy region 11–18 eV, (b) Expanded view of the 13.5–16.5 eV energy region.....	153
6.10	Absolute oscillator strengths for the photoabsorption of krypton obtained using the high resolution dipole (e,e) spectrometer (FWHM=0.048 eV) in the energy region 9–16 eV	154
6.11	Absolute oscillator strengths for the photoabsorption of krypton obtained using the high resolution dipole (e,e) spectrometer (FWHM=0.048 eV). (a) Expanded view of the 12.2–13.6 eV energy region, (b) Expanded view of the 13.5–15.0 eV energy region	155
6.12	Absolute oscillator strengths for the photoabsorption of xenon obtained using the high resolution dipole (e,e) spectrometer (FWHM=0.048 eV) in the energy region 8–15 eV	156
6.13	Absolute oscillator strengths for the photoabsorption of xenon obtained using the high resolution dipole (e,e) spectrometer (FWHM=0.048 eV). (a) Expanded view of the 11–12 eV energy region, (b) Expanded view of the 12–13.7 eV energy region.....	157

6.14	Absolute oscillator strengths for the photoabsorption of argon in the autoionizing resonance region 25–30 eV	178
6.15	Absolute oscillator strengths for the photoabsorption of krypton in the autoionizing resonance region 23–28.5 eV	180
6.16	Absolute oscillator strengths for the photoabsorption of krypton in the autoionizing resonance region 20–24 eV	181
7.1	Absolute oscillator strengths for the photoabsorption of molecular hydrogen in the energy region 11–20 eV measured by the high resolution dipole (e,e) spectrometer (FWHM=0.048 eV).....	193
7.2	Absolute oscillator strengths for the photoabsorption of molecular hydrogen in the energy region 11–14 eV.....	194
7.3	The absolute optical oscillator strengths for individual vibronic transitions as a function of the vibrational quantum number v' for the Lyman band	199
7.4	The absolute optical oscillator strengths for individual vibronic transitions as a function of the vibrational quantum number v' for the Werner band.....	200
7.5	The electronic transition moment $ R_e(r_{v'0}) $ in atomic units (a.u.) as a function of the internuclear distance $r_{v'0}$ in Ångstroms (Å) for the Lyman band	207
7.6	The electronic transition moment $ R_e(r_{v'0}) $ in atomic units (a.u.) as a function of the internuclear distance $r_{v'0}$ in Ångstroms (Å) for the Werner band.....	208

8.1	Absolute oscillator strengths for the photoabsorption of molecular nitrogen measured using the low resolution (FWHM=1 eV) dipole (e,e) spectrometer. (a) in the energy region 10–50 eV, (b) in the energy region 50–200 eV	222
8.2	Absolute oscillator strengths for the photoabsorption of molecular nitrogen in the energy region 12–22 eV measured using the high resolution dipole (e,e) spectrometer (FWHM=0.048 eV).....	228
8.3	Expanded view of figure 8.2 for the photoabsorption of molecular nitrogen in the energy region 12.4–13.4 eV.....	229
8.4	Expanded view of figure 8.2 for the photoabsorption of molecular nitrogen in the energy region 13.2–15.0 eV.....	230
8.5	Expanded view of figure 8.2 for the photoabsorption of molecular nitrogen in the energy region 15–19 eV.....	231
9.1	Absolute oscillator strengths for the photoabsorption of molecular oxygen in the energy region 5–30 eV measured using the high resolution dipole (e,e) spectrometer (FWHM=0.048 eV).....	253
9.2	Absolute oscillator strengths for the photoabsorption of molecular oxygen. Expanded view of figure 9.1 in the energy region 6.5–10 eV, showing the Schumann–Runge continuum region.....	255
9.3	Absolute oscillator strengths for the photoabsorption of molecular oxygen. (a) The energy region 9.5–15 eV, (b) The energy region 14–25 eV.....	259

10.1	Absolute oscillator strengths for the photoabsorption of carbon monoxide measured using the low resolution (FWHM=1 eV) dipole (e,e) spectrometer. (a) in the energy region 5–50 eV, (b) in the energy region 50–200 eV.....	277
10.2	Absolute oscillator strengths for the photoabsorption of carbon monoxide in the energy region 7–21 eV measured using the high resolution dipole (e,e) spectrometer (FWHM=0.048 eV)..	282
10.3	Absolute oscillator strengths for the photoabsorption of carbon monoxide in the energy region 7.5–10.5 eV at 0.048 eV FWHM	284
10.4	Absolute oscillator strengths for the photoabsorption of carbon monoxide in the energy region 10.5–12 eV at 0.048 eV FWHM	289
10.5	Absolute oscillator strengths for the photoabsorption of carbon monoxide in the energy region 12–20 eV at 0.048 eV FWHM..	294
10.6	The electronic transition moment $ R_e(r_{v'0}) $ in atomic units (a.u.) as a function of the internuclear distance $r_{v'0}$ in Ångstroms (Å) for the vibronic bands of the $X^1\Sigma^+ \rightarrow A^1\Pi$ transition.....	299
11.1	Absolute oscillator strengths for the photoabsorption of nitric oxide in the energy region 5–30 eV measured using the high resolution dipole (e,e) spectrometer (FWHM=0.048 eV)	308
11.2	Expanded view of figure 11.1 in the energy region 5–8.2 eV ...	309
11.3	Expanded view of figure 11.1. (a) in the energy region 8–10 eV, (b) in the energy region 10–13 eV.....	310
11.4	Expanded view of figure 11.1. (a) in the energy region 13–16 eV, (b) in the energy region 16–22 eV.....	311

Acknowledgements

I would like to express my sincere thanks to my research supervisor, Dr. C. E. Brion for his interest, assistance and encouragement throughout the course of my study. It has been a pleasure to work with him and with other members in his research group. Special thanks are due to Dr. G. Cooper for a lot of help in my research work and for his helpful comments and suggestions on the writing of my thesis. Thanks are due to Dr. K. H. Sze for introducing me to the high resolution spectrometer and to Dr. W. Zhang and G. R. Burton for many helpful discussions.

I would like to thank Professor M. J. Seaton for sending me his calculated data for helium and Professor J. A. R. Samson for sending me his measured data for argon, krypton and xenon. Helpful comments and discussions concerning the present work with Professor M. J. Seaton, Professor J. A. R. Samson, Dr. W. L. Wiese and Dr. M. Inokuti are also acknowledged.

I would like to thank the staff of the mechanical and electronic workshops for their assistance in maintenance the spectrometers, in particular B. Greene and E. Gomm. Thanks are also due to D. Jones and M. Hatton (Electronic workshop) for the design and construction of the fast data buffer.

Financial support in the form of a University of British Columbia Graduate Fellowship is gratefully acknowledged. The research work has been supported by operating grants from the Canadian National Networks of Centres of Excellence Programme (Centres of Excellence in Molecular

and Interfacial Dynamics) and from the Natural Sciences and Engineering Research Council of Canada.

Finally, I wish to thank to my parents and Josanna for their patience and encouragement. This thesis is dedicated to them.

Chapter 1

Introduction

Absolute optical oscillator strength (cross section) information is of importance because of the need to know electronic transition probabilities for both valence and inner shell excitation and ionization processes in many areas of application including plasmas, fusion research, lithography, aeronomy, astrophysics, space chemistry and physics, laser development, radiation biology, dosimetry, health physics and radiation protection. Such information is also a crucial requirement for the development and evaluation of quantum mechanical theoretical methods and for the modelling procedures used for various phenomena involving electronic transitions induced by energetic radiation [1].

However, most spectroscopic studies to date for discrete electronic excitation processes have emphasized the determination of transition energies rather than oscillator strengths, since the former quantities are generally relatively easier to obtain both experimentally and theoretically. In contrast only rather limited information is available for the corresponding absolute optical oscillator strengths (or equivalent quantities reflecting transition probability such as cross section, lifetime, linewidth, extinction coefficient, A value etc.) for atoms. In the case of discrete electronic transitions for molecules such quantities are extremely sparse, while for core (inner shell) processes the available data are even more limited. In particular oscillator strengths are in very short supply for transition energies beyond 10 eV where most valence shell electronic excitation and ionization processes occur. This situation is

partly due to the well known inherent difficulties of quantitative work in the vacuum UV and soft X-ray regions of the electromagnetic spectrum (i.e. beyond the LiF cut-off). These and other limitations provide considerable challenges in both photoabsorption and photoemission studies. The situation also reflects the limitations and application restrictions involved in other types of optical methods such as lifetime, line profile, self absorption and level crossing techniques. Furthermore, the commonly employed direct photoabsorption methods using the Beer-Lambert law transmission measurements are subject to so-called "line saturation" (bandwidth) effects, which can lead to large errors in the derived absolute optical oscillator strengths for discrete transitions. These spurious effects become more severe for transitions with narrow linewidth and high cross section. In such cases the measured oscillator strengths are too small. Detailed discussions of Beer-Lambert law photoabsorption and the associated "line saturation" effects are given in chapter 2 section 3.

From a theoretical standpoint, calculation offers an alternative approach to experimental oscillator strength determination. However, theoretical calculations of oscillator strengths involve computational methods that require extremely sophisticated correlated wavefunctions and reasonable accuracy is at present only feasible for the simplest atoms such as hydrogen [2] and helium [3-9].

Electron energy loss spectroscopy (EELS), utilizing the virtual photon field induced in a target by fast electrons at negligible momentum transfer, provides an alternative and versatile means of measuring optical oscillator strengths for electronic transitions in atoms and molecules in both the discrete and continuum regions. Under such experimental

conditions the electron energy loss spectra are governed by dipole selection rules, and for this reason EELS based methods for optical oscillator strength determination are often referred to as dipole electron impact experiments. The theoretical groundwork showing the quantitative relationship between photoabsorption measurements and electron scattering experiments was laid earlier, in 1930, by Bethe [10], by using the First Born approximation. The Bethe-Born theory has been further discussed by Inokuti [11] and Kim [12] and its application in experimental studies has been reviewed by Lassetre and Skerbele [13] and Brion and Hamnett [14]. Since 1960, there has been growing interest in electron scattering experiments partly due to recognition of the importance of phenomena involving electron-atom and electron-molecule interactions, and partly due to advances in high-vacuum technology, low energy electron optics, and detection techniques such as fast pulse counting using channel electron multipliers (channeltrons). Electron energy loss experiments have been applied to the measurements of absolute optical oscillator strength for discrete transitions following the pioneering work of Lassetre *et al.* [15-18] and of Geiger [19,20]. In other work Van der Wiel and co-workers [21-23] developed a variety of "photon simulation" experiments using high impact energy, small angle electron scattering techniques to determine absolute differential optical oscillator strengths in the continuum region. In recent years, the techniques used by Van der Wiel and his co-workers [21-23] have been modified and further developed here at the University of British Columbia where a variety of low resolution dipole electron impact methods have now provided absolute differential optical oscillator strengths for a wide range of valence-shell [24-27] and inner-shell

[28,29] photoabsorption and photoionization processes. A review and compilation of photoabsorption and photoionization data obtained by direct optical and dipole electron impact methods for small molecules in the continuum region has recently been published by Gallagher *et al.* [30].

In other work, a high impact energy, zero-degree scattering angle, high resolution EELS spectrometer [31] was built in this laboratory for the study of valence-shell [32-34] and inner-shell [32,34,35] electronic excitation spectra of a variety of molecules. In the present work, the operation of this EELS spectrometer [31] has now been modified to provide a new high resolution dipole (e,e) method for the determination of optical oscillator strength for discrete photoabsorption processes in free atoms and molecules. This new method is free of the spurious "line saturation" effects that complicate the measurement of absolute optical oscillator strengths (cross sections) in Beer-Lambert law photoabsorption experiments for discrete transitions. The method is applicable to all transitions throughout the discrete valence shell region of the valence shell spectrum at high energy resolution (0.048 eV FWHM). The Bethe-Born conversion factor for the high resolution dipole (e,e) spectrometer, developed here in the University of British Columbia has been determined by calibration against a previously developed low resolution dipole (e,e) spectrometer. The absolute scales of the present oscillator strength data were obtained from Thomas-Reiche-Kuhn (TRK) sum-rule normalization of the Bethe-Born transformed electron-energy-loss spectra and as such do not involve the difficult determinations of photon (or electron) flux or target density required in photoabsorption and other types of electron scattering experiments.

In chapter 2 of this thesis the photoabsorption and electron impact methods are compared, together with a consideration of other techniques for optical oscillator strength determination. The presently used electron impact based dipole (e,e) methods are discussed in chapter 3. Absolute optical oscillator strengths for photoabsorption in the discrete and continuum regions for five noble gases (helium [36,37], neon [38] and argon, krypton and xenon [39]) and five diatomic gases (hydrogen [40], nitrogen [41], oxygen [42], carbon monoxide [43] and nitric oxide [44]) are presented from chapters 4 through 11. The variations of electronic transition moment with the internuclear distance for the Lyman and Werner bands of molecular hydrogen and for the $X^1\Sigma^+ \rightarrow A^1\Pi$ bands of carbon monoxide are also discussed in chapters 7 and 10 respectively. The present results are compared with previously reported experimental and theoretical data from the literature.

Chapter 2

Measurement of Absolute Optical Oscillator Strengths by Photoabsorption and Electron Impact Methods

2.1 Photoabsorption Cross Section measurements *via* the Beer-Lambert Law

In photoabsorption experiments, quantitative cross section measurements are governed by the Beer-Lambert law. Consider first the reduction in the photon intensity when a light flux I passes through a distance dl containing a sample target of number density n . The loss of intensity dI of the incident photon beam is proportional to the distance travelled dl , the number density n of the target, and the photoabsorption cross section of the target $\sigma_p(E)$. The relationship can be written as

$$dI = - I \sigma_p(E) n dl \quad (2.1)$$

where the photoabsorption cross section $\sigma_p(E)$ is related to the probability that a photon of energy E will be absorbed in passing through the target and has the dimension of area. Integrating equation 2.1 over the path length l , we obtain

$$\begin{aligned} I &= I_o \exp (- \sigma_p(E) n l) \\ &= I_o \exp (- \sigma_p(E) N) \end{aligned} \quad (2.2)$$

Equation 2.2 is the familiar Beer-Lambert law [30,45] where I_o and I are the incident and transmitted light intensities, respectively. The

quantity N is equal to nl and is sometimes referred to as the column number. The Beer–Lambert photoabsorption method can in principle be readily applied to the complete electronic spectrum of a given atomic and molecular target in both the discrete and continuum regions.

Furthermore, the measurement procedure would at first seem to be quite straight forward. Extensive measurements using this technique have been made for atoms and molecules in the continuum region. Reviews and compilations of such cross section (oscillator strength) data can be found in references [30,45–48]. However, in the discrete excitation region, only limited cross section information is available from use of the Beer–Lambert law photoabsorption methods, and most of the measurements performed are for molecules. This situation arises because of the large errors which can occur in Beer–Lambert law cross section measurements for discrete transitions due to "line saturation" (i.e. bandwidth) effects. These spurious effects are particularly severe for discrete transitions with narrow natural linewidths and high cross sections. A comparison of different optical methods for determining absolute oscillator strengths in the discrete excitation region is given in section 2.2, while the perturbing "line saturation" effects in Beer–Lambert law photoabsorption are discussed in detail in section 2.3.

A dimensionless quantity, namely the optical oscillator strength, $f^0(E)$, is also often used in optical absorption spectroscopy. The oscillator strength is related [49] to the integrated photoabsorption cross section σ_n for a discrete transition through the equation (in atomic units):[†]

[†] All equations are in atomic units.

$$\sigma_n = \frac{2\pi^2}{c} f^o(E) \quad (2.3)$$

In quantum mechanics, $f^o(E)$ is defined [14] as:

$$f^o(E) = 2E \left| \langle \Psi_n | \sum_s^N \vec{r}_s | \Psi_o \rangle \right|^2 \quad (2.4)$$

where E is the excitation energy, \vec{r}_s gives the coordinates of the N electron species, and Ψ_o and Ψ_n are the initial and excited state wavefunctions respectively.

At sufficiently high photon energies, ionization occurs and transitions occur from the bound initial state to a continuum final state. Instead of using the integrated photoabsorption cross section, σ_n , and the optical oscillator strength, f^o , equation 2.3 can be rewritten as [50]

$$\sigma_p(E) = \frac{2\pi^2}{c} \frac{df^o(E)}{dE} \quad (2.5)$$

where $\sigma_p(E)$ is the photoabsorption cross section as defined earlier and $df^o(E)/dE$ is the differential optical oscillator strength with the dimension of $(\text{energy})^{-1}$. If the energy E is expressed in electron volts (eV) and $\sigma_p(E)$ is in megabarns ($1 \text{ megabarn} = 10^{-18} \text{ cm}^2$), we have

$$\sigma_p(E) [\text{Mbarns}] = 109.75 \frac{df^o(E)}{dE} [\text{eV}^{-1}] \quad (2.6)$$

Equation 2.6 may be used for the interconversion of cross section and differential oscillator strength data.

The optical oscillator strengths $f^o(E)$ in the discrete region and $df^o(E)/dE$ in the continuum region have an important property that is useful for establishing the absolute intensity scale in the presently developed dipole (e,e) method (see chapter 3). It has been shown that for an N electron species [50,51],

$$\sum f^o(E) + \int \frac{df^o(E)}{dE} dE = N \quad (2.7)$$

This simply means that the total integrated optical oscillator strength (i.e. summing over all discrete transitions and integrating over all continuum states) is equal to the total number of electrons. Equation 2.7 is the famous Thomas-Reiche-Kuhn (TRK) sum-rule which in general holds for any atomic and molecular system. Generally, a valence shell partial sum rule is applied and in this case spectral area (i.e. the total oscillator strength) is normalized to the number of valence shell electrons plus a small correction for the Pauli excluded transitions from the core orbitals to the already occupied ground state valence orbitals [52,53].

2.2 Optical Methods for Determining Absolute Optical Oscillator Strengths for Discrete Transitions

A variety of different optically based methods have traditionally been used for the determination of most of the optical oscillator strength

data available for discrete electronic transitions in the literature. Only a limited amount of data is available for atoms and much of this is to be found in the important compilations published by Wiese and co-workers [54]. Very little information is available for molecules. The oscillator strength data base is extremely limited because such measurements are difficult to perform and also because most available methods suffer from a variety of often serious difficulties and/or limitations which severely restrict their range of application. Wiese and co-workers [54] have discussed various aspects of the optical methods used for atoms and provide useful conversion formulae relating the various quantities produced by the different types of measurements.

The most commonly used optical measurement techniques include (a) Photoabsorption *via* the Beer-Lambert law [55], (b) Lifetime measurements by level crossing techniques (including the Hanle effect) [56,57], (c) Lifetime measurements by beam foil methods [58], (d) Emission profile measurements from plasmas [59] and beams [60], (e) Resonance broadening emission profiles [61], (f) Self absorption [62-64], (g) Total absorption [65] and (h) Optical phase-matching [66]. The strengths and weaknesses of these methods with regard to their widespread general application to atomic and molecular electronic excitation spectra are summarised in Table 2.1. Also shown in table 2.1 are corresponding considerations for theory as well as for electron impact based oscillator strength methods [67-71], including the present work, as discussed in section 2.4 below. Methods (b)-(h) have all been used but only in selected favourable cases involving relatively intense atomic transitions. However such approaches are generally complex and various limitations make them unsuitable for widespread application

Table 2.1

Methods of obtaining optical oscillator strengths for discrete electronic transitions at high resolution

Method [Ref.]	Advantages	Difficulties and Problem Areas	Suitability for General Molecular Studies
Beer-Lambert Law. Photoabsorption [55]	Simple relation, $I_0/I = \exp(n l \sigma_p)$ Very high resolution Wide spectral range	Bandwidth effect (line saturation) due to the resonant nature of discrete excitation and use of logarithmic relation to obtain σ_p . Stray light, order overlapping. Extrapolation to zero column number.	Limited suitability under favourable circumstances
Lifetime Methods [56-58] (i) Level crossing (Hanle effect) [56,57] (ii) Beam foil [58]	No bandwidth problem Good for strong resonances Useful for mean lifetimes of excited state atomic and ionic levels	Branching ratios must be known. Molecular energy states must be known. Slight dependence of line width on background pressure. Cascades from other states. Blending of unresolved spectral lines.	Not generally suitable

Table 2.1 (continued)

Method [Ref.]	Advantages	Difficulties and Problem Areas	Suitability for General Molecular Studies
Plasma emission profile [59]	No bandwidth problem	Only good for optically thick emission. Uncertainties in calculated Stark width.	Difficult and not generally suitable
Beam emission profile [60]	No bandwidth problem	Time variations in Doppler width. Relies on calculated electron collision cross section.	Difficult and not generally suitable
Resonance broadening emission profile [61]	No bandwidth problem	Extrapolation to zero pressure. Different Doppler width corresponding to different excitation to upper levels.	Difficult and not generally suitable
Self absorption [62-64]	No bandwidth problem	Possible departure from Doppler profile. Re-emission from atoms excited by absorption of resonance photons.	Difficult and not generally suitable

Table 2.1 (continued)

Method [Ref.]	Advantages	Difficulties and Problem Areas	Suitability for General Molecular Studies
Total absorption [65]	No bandwidth problem	Only good for optically thick absorption in the absence of collision broadening.	Difficult and not generally suitable
Optical phase-matching [66]	No bandwidth problem	Transition peak must not be perturbed by collision effects. Refractive index of buffer gas at particular wavelength must be known.	Difficult and not generally suitable
Electron scattering (Vary θ at fixed E_0) [67-70]	No bandwidth problem	Extrapolation to $K^2=0$ is problematical. Tedious procedure for each transition. Absolute scale requires external procedures.	Difficult but possible
Electron scattering (Vary E_0 at fixed θ) [71]	No bandwidth problem	Extrapolation to $K^2=0$ is problematical. Tedious procedure for each transition. Electron optical effects and lens ratios. Absolute scale requires external procedures.	Difficult for general application

Table 2.1 (continued)

Method [Ref.]	Advantages	Difficulties and Problem Areas	Suitability for General Molecular Studies
Electron scattering HR Dipole (e.e) [this work] Quantum mechanical calculation [3-9]	No bandwidth problem Absolute scale via TRK sum rule. No pressure or incident flux measurements required. Direct measurement over wide spectral range. Good accuracy. Very accurate for small atoms. No instrumental effects. Infinite energy resolution.	Stray electrons. Accuracy of Bethe Born conversion factor since B(E) in low energy region is dependent on extrapolation. Resolution limited to $\Delta E \approx 0.01\text{eV FWHM}$. Extension to large systems limited by wavefunction accuracy and calculation methods. Lack of sufficiently accurate experimental data for comparison.	Readily applicable over wide spectral range. Most difficulties can be overcome with very careful experiments. Very difficult to obtain good accuracy.

across the complete valence shell spectral range for atomic and in particular molecular targets. Although in principle Beer–Lambert law photoabsorption measurements would seem to offer a straightforward means for routine measurement of absolute optical oscillator strengths for atomic and molecular transitions over a wide spectral range, application of the method may often result in large errors in the measured cross section. Since the limitations of this method are not widely appreciated, the special case of the Beer–Lambert law photoabsorption method will now be discussed in detail.

2.3 "Line Saturation" Effects in Beer–Lambert Law Photoabsorption for Discrete Transitions

Photoabsorption *via* the Beer–Lambert law (method (a) in table 2.1) can in principle be applied readily to the complete valence shell spectrum of atoms and molecules, and the measurement procedure would seem to be quite straightforward in principle. While the method works well for continuum processes, very few accurate determinations of absolute oscillator strengths for discrete electronic transitions have actually been made using the Beer–Lambert law. This is because very serious problems can arise when Beer–Lambert law discrete photoabsorption spectra are used for absolute intensity (oscillator strength) determinations [72] rather than just for indicating the energy levels. These problems, which are not always widely appreciated or well understood, arise from the finite energy resolution of any real optical monochromator and the resonant nature of discrete photoabsorption. In particular, it should be noted that equation 2.2 is only strictly valid for

the unphysical situation of zero bandwidth (i.e. infinite energy resolution) as discussed in references [11,37,46,73,74]. Difficulties arise because a logarithmic transform is required (equation 2.2) in order to obtain the absolute cross-section $\sigma_p(E)$ from the percentage transmission (I/I_0) obtained from the experimental measurements. As a result of this logarithmic transform the measured cross section at the characteristic energy will correspond to a weighted average observed cross section (which is often much less than the true cross section $\sigma_p(E)$) in situations where the bandwidth ($BW=\Delta E$) is a significant fraction of, or greater than, the natural linewidth ($LW=\Delta L$) for a transition [46,73,74]. This limitation and the fact that measured peak cross-sections are often a function of the instrument as much as of the target, has been reviewed in some detail by Hudson [46] and commented on by others [11,75]. The situation is potentially particularly serious for intense narrow lines in the discrete region because of the Bohr frequency condition and the fact that the line profile varies rapidly within the BW unless the latter is very much narrower than the natural LW. Hudson [46] has also discussed the so-called "apparent pressure" effect and shown how the bandwidth effects can be minimised (but never entirely eliminated) by the tedious procedure of extrapolating peak intensities measured at a series of pressures, for each separate transition, to zero column number N. However, even with such procedures, as Hudson [46] correctly points out, I approaches I_0 as this optically thin limit is approached and thus the greatest weight is placed on the least accurate data! The net result is that accurate optical oscillator strengths often cannot be obtained from Beer-Lambert law photoabsorption measurements for very sharp, intense lines (for example compare references [55,76-80]). These problems are

likely to be particularly severe in the vacuum UV and soft X-ray regions of the spectrum where low light fluxes, even from monochromated synchrotron sources, often require the use of wide monochromator exit slits. These bandwidth effects will occur when the monochromator is placed between the continuum light source and the sample cell. This arrangement is the usual situation on synchrotron beam lines (i) because of the ultra high vacuum requirements in the storage ring and the monochromator and (ii) because the monochromator is usually an integral part of the beam line facility feeding different possible experimental arrangements. However, these spurious bandwidth effects would also influence the measured cross sections in the same way if the sample cell was placed between the source and monochromator as occurs in many laboratory-based spectrometer arrangements.

Despite the well documented and serious deficiencies which can complicate the determination of absolute optical oscillator strengths for discrete transitions using the Beer-Lambert Law, it is still sometimes used and it can then often result in spurious results which are not always apparently realised by the experimenters. A particularly drastic example of such "line saturation" BW effects occurs in the vacuum UV absorption spectrum of N_2 [80] illustrated in figure 2.1. The vacuum UV spectrum as reported by Gurtler *et al.* [80] on an absolute scale (figure 2.1(a)) has high enough resolution to show evidence of rotational effects. This optical absorption spectrum [80] is compared with a high impact energy, negligible momentum transfer, high resolution ($\Delta E=0.017$ eV) electron energy loss spectrum placed on an absolute scale [37,41] in figure 2.1(b) over the same energy region. Clearly there are large differences in relative intensity between the two spectra in the 12.6–13.0 eV range, and

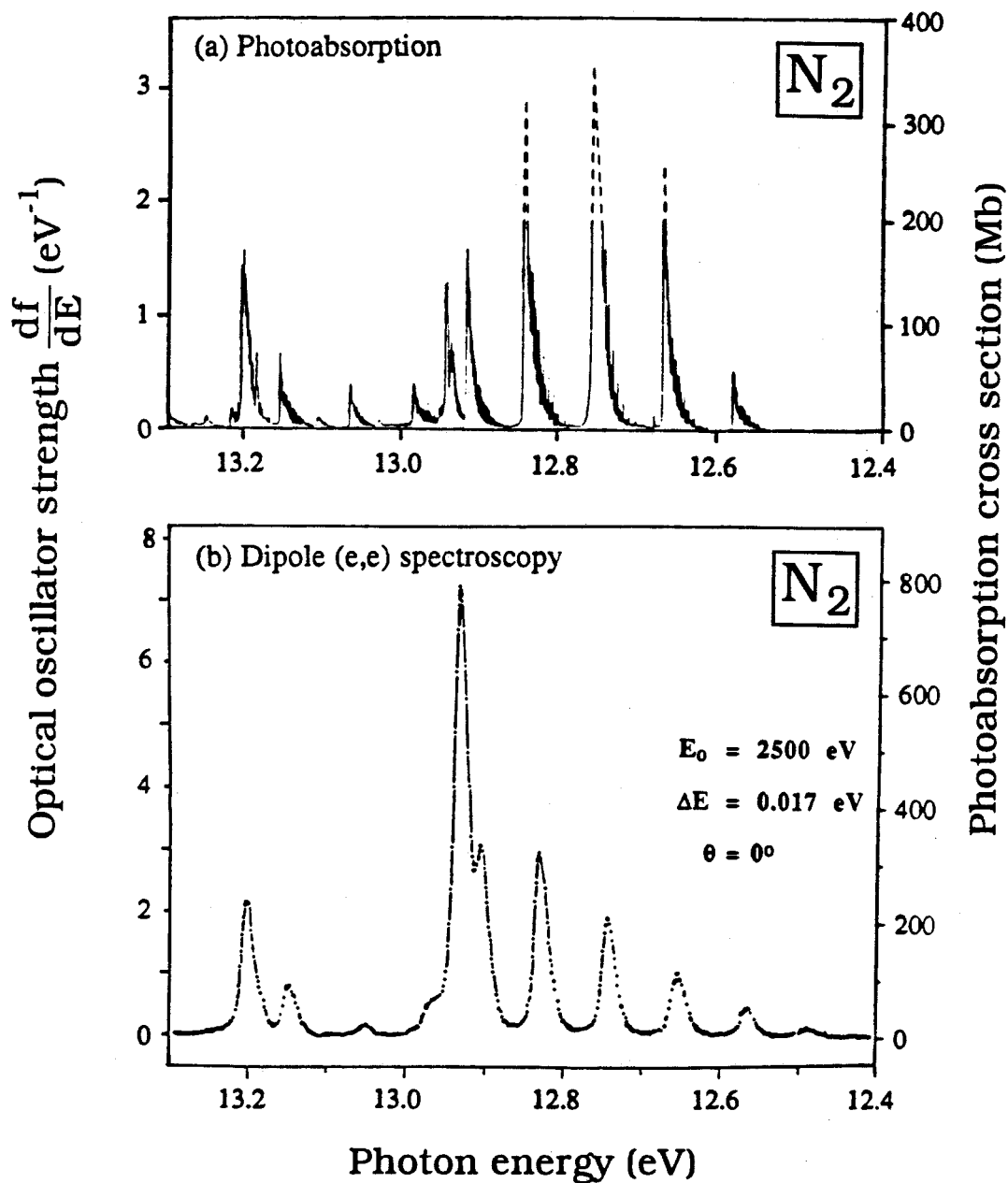


Figure 2.1: Comparison of the absolute valence shell photoabsorption oscillator strength spectra of molecular nitrogen obtained by Beer-Lambert law photoabsorption and dipole (e,e) experiments in the energy region 12.4–13.2 eV. (a) Beer-Lambert law absolute photoabsorption spectrum adapted from figure 1 of reference [80] — the dashed lines have been drawn to show the positions of the maximum cross-sections of the peaks according to the values given in the text of reference [80]. (b) Dipole (e,e) spectrum [37,41] — the electron energy loss spectrum was placed on an absolute optical oscillator strength scale by referencing to the high resolution oscillator strength spectrum reported in the present work (see chapter 8).

particularly in the 12.9–13.0 eV region. These differences reflect serious "line saturation" effects in the optical work in the 12.9–13.0 eV region due to the finite bandwidth of the incident radiation and the extremely narrow natural linewidth of these intense transitions. As can be seen from figure 2.1 these factors have dramatic effects on the derived optical oscillator strengths (cross sections). Clearly not only the peak heights but also the peak areas (and thus the apparent oscillator strengths) are drastically reduced in the optical spectrum. In contrast the corresponding absolute optical oscillator strength spectrum obtained *via* Electron Energy Loss Spectroscopy (EELS) in figure 2.1(b) (see section 2.4 following) shows the correct relative intensities (band areas) even though it is at lower energy resolution than the optical work. This large intensity effect in the electronic spectrum of N₂ was pointed out earlier in electron impact studies by Lassetre [81] and also by Geiger [82]. Subsequently, extrapolation of very carefully controlled optical measurements [78,79], made as a function of column number N, was found to give results much more consistent with the intensities derived from the EELS measurements [81,82].

It is important to note that the earlier treatment of "line saturation" effects by Hudson [46] only emphasized the effects of finite BW on the peak heights of sharp spectral lines (i.e. the cross section at the peak maximum) and how such effects may, hopefully, be minimised by extrapolation to zero column number. As Hudson [46] has shown, a 40% error still exists in a peak height cross section for the situation where LW=BW, even at N=0! However it should be remembered that an accurately measured oscillator strength for a discrete transition should involve an integral over the whole profile of the spectral line and should

not just be assessed from the peak height. The peak area in a photoabsorption experiment is also severely influenced by the BW effects, which results in a significant reduction in both peak height and peak area, as can be seen in figure 2.1. This clearly leads to an integrated optical oscillator strength for the transition which is significantly in error unless the BW is very narrow compared with the narrowest features in the spectrum — regardless of whether or not such features are resolved! Such errors are therefore likely to be particularly serious for molecular spectra because of the vibrational and rotational fine structure — as can be seen in figure 2.1. Since in general different lines in the same spectrum have different natural LW, the cross section perturbations are different for every transition (see again figure 2.1(a) and (b)). Thus the complete spectroscopy (i.e. all line widths and line shapes) must already be known if any meaningful understanding of photoabsorption cross sections for spectral lines is to be obtained from Beer–Lambert law measurements. If such information was available then of course the oscillator strengths would already be known from the linewidths! Clearly then, one can never be sure that the correct oscillator strength has been obtained in a Beer–Lambert law photoabsorption experiment unless either the information is already available in some form from other sources, or unless the absolute integrated spectral intensities can be shown to be effectively independent of the BW as well as the column number N .

Given the above considerations it is necessary to extend the peak height analysis of Hudson [46] to consider the effects of bandwidth on the integrated cross section over the spectral line profile (i.e. peak area) in a discrete photoabsorption experiment. For example, consider (figure 2.2)

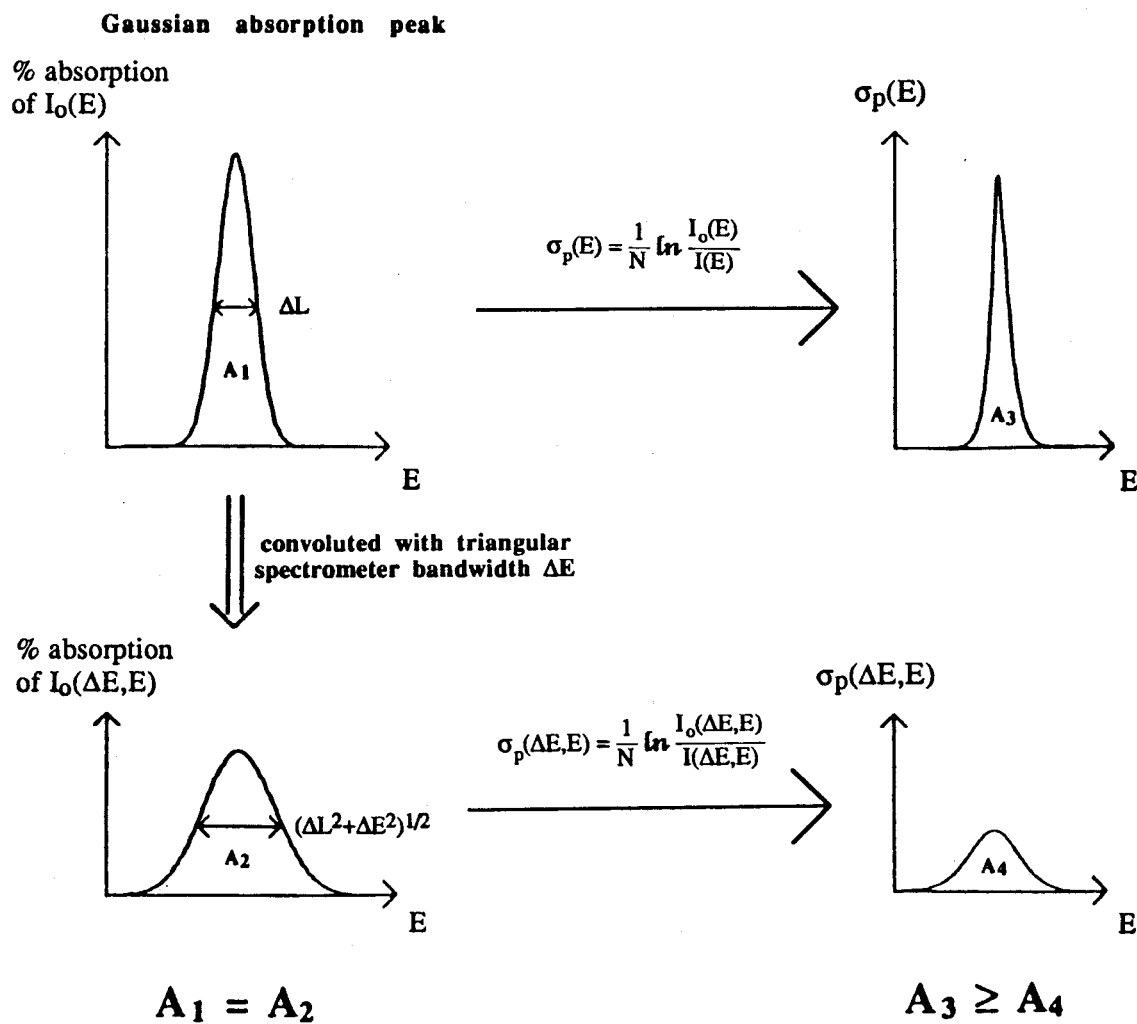


Figure 2.2: Diagrammatic representation of the "line saturation" effects occurring in photoabsorption experiments when the Beer-Lambert law is used to determine the integrated cross-section of a discrete transition.

$$A_3 = \int^{\text{Peak}} \sigma_p(E) dE = \int^{\text{Peak}} \ln \frac{I_o(E)}{I(E)} dE \quad (2.10)$$

$$A_4 = \int^{\text{Peak}} \sigma_p(\Delta E, E) dE = \int^{\text{Peak}} \ln \frac{I_o(\Delta E, E)}{I(\Delta E, E)} dE \quad (2.11)$$

It is found that A_3 is always greater than A_4 unless ΔE is equal to zero, which is only true of course for the hypothetical case of infinitely narrow bandwidth. In more detail mathematically, area A_1 is convoluted by bandwidth ΔE to yield an area A_2 such that $A_1=A_2$. If area A_2 is also a Gaussian distribution with full width at half maximum (FWHM) approximately equal to $(\Delta L^2 + \Delta E^2)^{1/2}$ then under this circumstance, $A_1=A_2(=1/S)$ (where S is a scale factor in order that we may vary the area under the Gaussian peak). After integration of equations 2.10 and 2.11, we obtain

$$A_3 = \frac{1}{N} \left[\sum_{n=1}^{\infty} \frac{C^{n-1}}{\Delta L^{n-1} S^n \sqrt[n]{n}} \right] \quad (2.12)$$

$$A_4 = \frac{1}{N} \left[\sum_{n=1}^{\infty} \frac{C^{n-1}}{(\sqrt{\Delta L^2 + \Delta E^2})^{n-1} S^n \sqrt[n]{n}} \right] \quad (2.13)$$

where

$$C = \frac{2\sqrt{\ln 2}}{\sqrt{\pi}}$$

Comparing each term for equation 2.12 and 2.13, A_3 is always greater than A_4 unless ΔE is zero, and only in this case does $A_3=A_4$.

In figure 2.3, the variation of observed peak area ($N \times A_4$) with column number N for a given transition is shown for different $\Delta E/\Delta L$ ratios. It shows that the area becomes smaller as the ratio $\Delta E/\Delta L$ is increased for the same column number. Figure 2.4 shows the variation of integrated cross section for a given transition obtained by use of the Beer-Lambert law with column number for different values of $\Delta E/\Delta L$. The true integrated cross section (100Mb eV) is only attained at $N=0$ or where $\Delta E=0$ (i.e. infinite resolution). Figure 2.5 ((a)-(e)) shows the variation of observed integrated cross section with column number at $\Delta E/\Delta L=10$, calculated for a series of transitions of different true cross section (given at zero column number). Note that for each cross section the behaviour is different even for a fixed ΔL . Since in general different lines will have different natural linewidths ΔL , it can be seen that the effects and therefore the interpretation of photoabsorption experiments can be very complex indeed. These effects are known as the "line saturation" or "apparent pressure" effects occurring in photoabsorption experiments [46]. With a very narrow natural linewidth (i.e. large $\Delta E/\Delta L$) and a high cross section the problem is obviously more severe. In order to attempt to obtain a result closer to the correct cross section, the only experimental approach is the tedious procedure of performing the measurements for each transition in the spectrum at a series of pressures and extrapolating to zero column number as shown in figures 2.4 and 2.5.

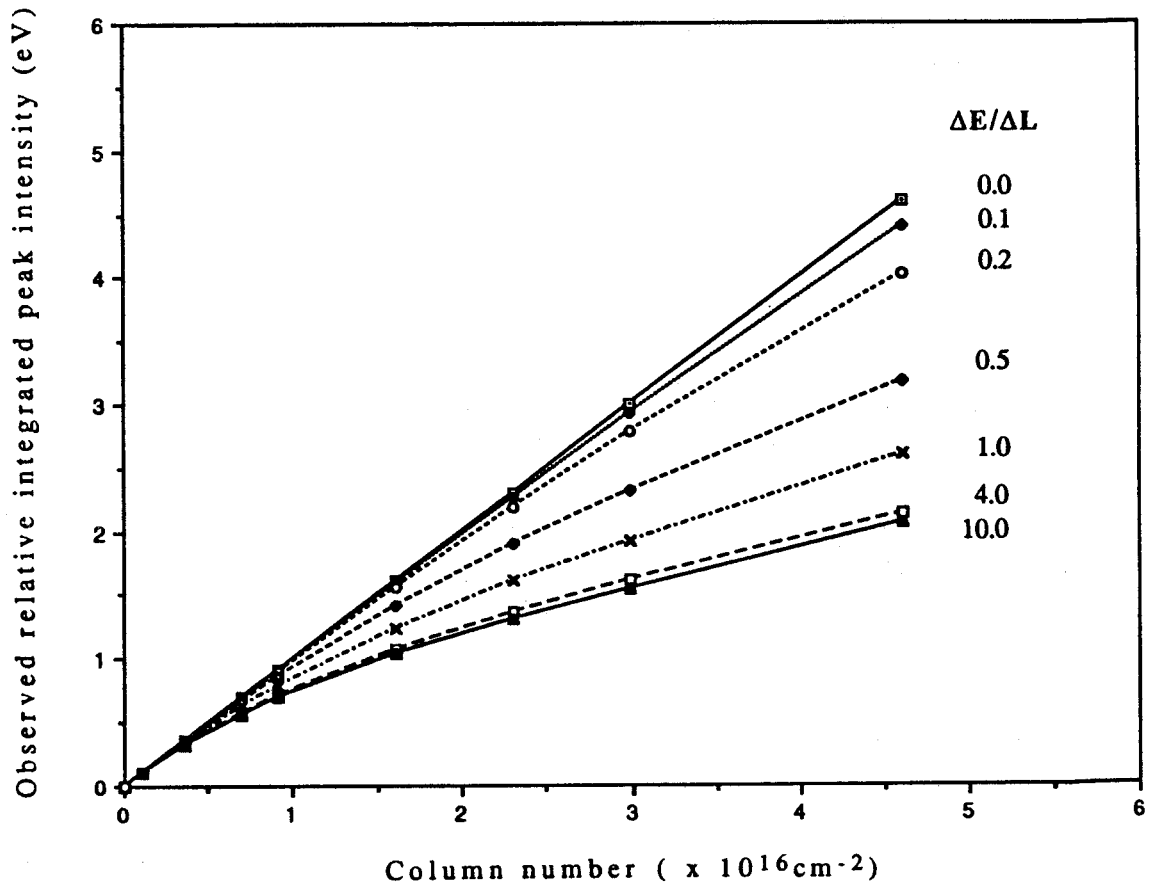


Figure 2.3: Variation of integrated peak intensity ($Nx A_4$) with column number for different ratios of (incident bandwidth (ΔE))/(natural absorption line-width (ΔL)), calculated using equations 2.12 and 2.13.

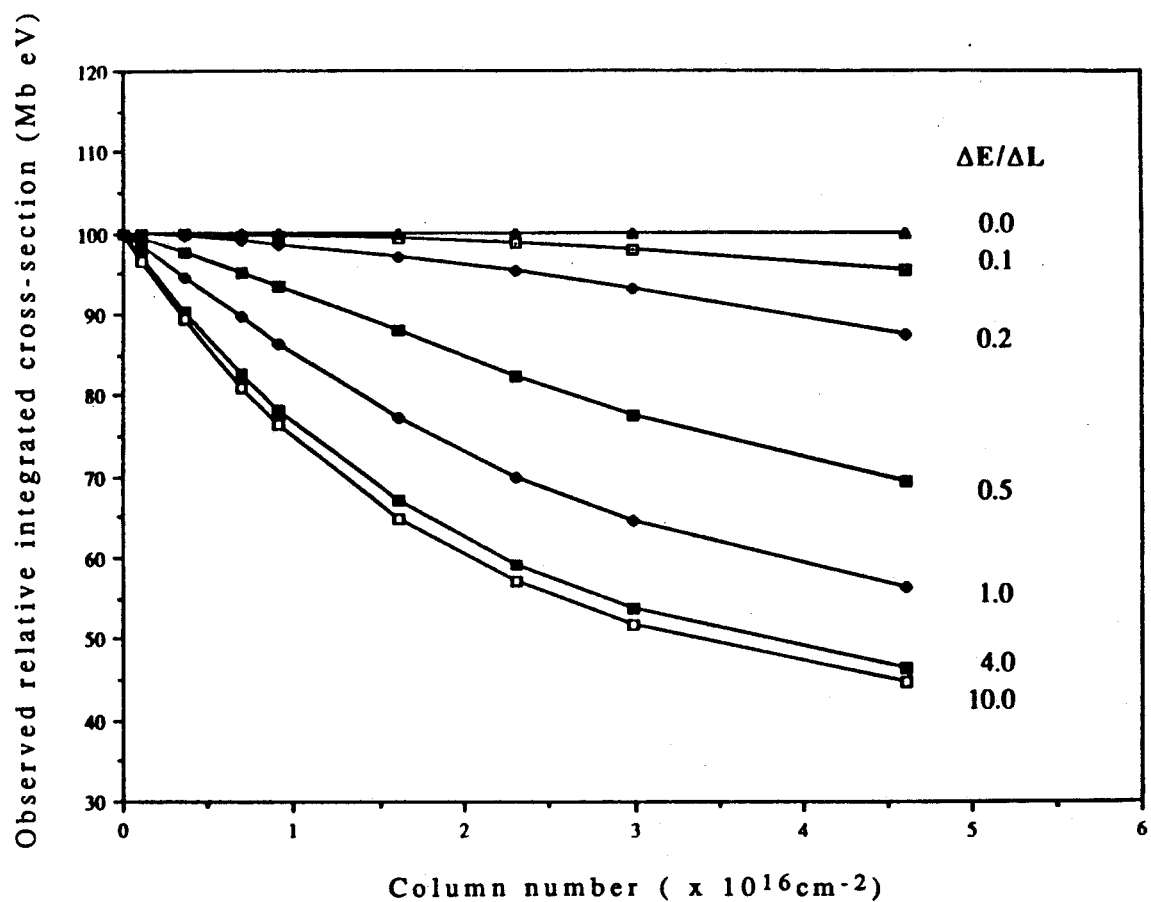


Figure 2.4: Variation of the observed integrated cross-section with column number for different $\Delta E/\Delta L$ ratios, calculated using equations 2.12 and 2.13. The true integrated cross-section is taken to be 100Mb eV.

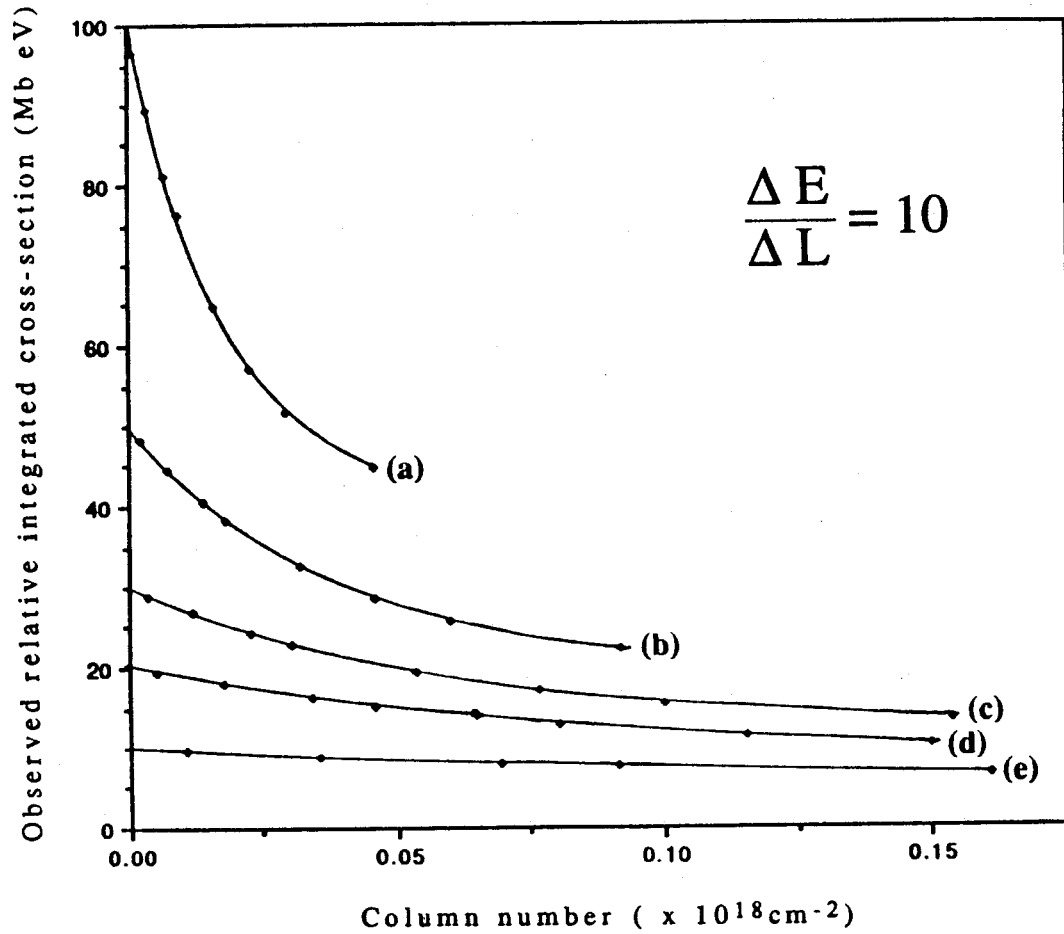


Figure 2.5: Variation of the observed integrated cross-section with column number at $\Delta E/\Delta L=10$ for peaks with true integrated cross-section of (a) 100, (b) 50, (c) 30, (d) 20 and (e) 10 Mb eV. The curves were calculated using equations 2.12 and 2.13.

Such procedures have been used by Lawrence [78] and Carter [79]. In figure 2.5 we can see that for peaks with the same $\Delta E/\Delta L$ value, the higher the true cross section, the greater the error in the optically measured cross section at a given column number. Thus it can be seen that for very narrow peaks of very high cross section, extrapolation to extremely low pressure would be required to obtain the correct cross section experimentally. However, in an actual experiment, the error in measuring $I_o(\Delta E, E)/I(\Delta E, E)$ increases with decrease in pressure. As Hudson [46] has pointed out, extrapolation procedures put the most emphasis on the least accurate data and hence the extrapolated value is likely to be inaccurate. These extrapolation procedures only minimise the BW effect and the resulting cross sections may in some cases still be subject to large errors. In such situations direct photoabsorption measurements are meaningless and for example, Yoshino *et al.* [55] have stated that the (12,0) transition of $^{18}\text{O}_2$ is too narrow to be measured using the Beer-Lambert law photoabsorption method.

In summary then, the above model calculations indicate that it is often extremely difficult to obtain highly accurate optical oscillator strengths for discrete transitions in optical photoabsorption experiments based on the Beer-Lambert law, especially for very sharp peaks with high cross section. As such, absolute photoabsorption cross sections obtained for discrete transitions using the Beer-Lambert law must always be viewed with some caution because of the possibility of significant systematic errors due to finite bandwidth effects which in general will be different for every transition. Therefore, widespread application of Beer-Lambert law photoabsorption methods to the study of discrete atomic and molecular spectra is not practical if accurate cross-sections are desired.

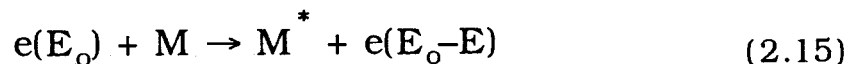
In the following discussion alternative methods of determining optical oscillator strengths are described which do not suffer from these spurious bandwidth effects.

2.4 Electron Impact Methods

An alternative and entirely independent approach to optical oscillator strength determination, free of spurious bandwidth effects, is provided by exploiting the virtual photon field induced in a target by fast electrons. This can be achieved by means of fast electron impact electron energy loss techniques at vanishingly small momentum transfer. The theoretical relation between high energy electron scattering and optical excitation has long been understood [10]. The resonant process of absorption of a photon of energy E



may be compared with the non-resonant process of electron impact excitation



Clearly the electron energy loss (E) is analogous to the photon energy E . The intensity of scattered electrons resulting from the excitation process is measured rather than a percentage absorption. The non-resonant nature of the electron impact excitation process together with avoidance of the logarithmic Beer-Lambert law in determining oscillator strength

(cross section) means that the "line saturation" bandwidth problem which often complicates discrete photoabsorption experiments is eliminated in the EELS method [11].

2.4.1 Theoretical Background for Fast Electron Impact Techniques

The process involving the collision between a fast electron and a target atom or molecule can be considered as a sudden but small perturbation of the target by the incident electron. The sudden transfer of energy and momentum to the target electrons due to the perturbation results in excitations within the target molecule [11]. Under these conditions the perturbation is due to an induced electric field, sharply pulsed in time and therefore corresponding broad in the frequency domain. This provides a "virtual photon field" or dipole excitation of constant flux in the spectral region of interest. A key quantity in the electron impact method for determining optical oscillator strengths is the momentum transfer (\mathbf{K}) in the collision. A momentum transfer dependent, generalised oscillator strength $f(\mathbf{K},E)$, describing the transition probability, can be defined as [10,11,14]

$$f(\mathbf{K},E) = \frac{2E}{\mathbf{K}^2} \left| \langle \Psi_n | \sum_s^N e^{i\vec{\mathbf{K}} \cdot \vec{\mathbf{r}}_s} | \Psi_o \rangle \right|^2 \quad (2.16)$$

where the quantities have the same physical meanings as in equation 2.4. It can be seen that equations 2.4 and 2.16 are very similar in form. It will be shown later that equation 2.4 is a limiting case of equation 2.16. In the continuum region, $f(\mathbf{K},E)$ is replaced by $df(\mathbf{K},E)/dE$, the

differential generalised oscillator strength, which will be used throughout the following discussion. In fact, even for discrete transitions the quantity measured at a given energy in an actual experiment is also $df(\mathbf{K},E)/dE$, and integration over the discrete peak area gives $f(\mathbf{K},E)$. The quantity $df(\mathbf{K},E)/dE$ is related [11] to the differential inelastic electron impact cross-section $d^2\sigma_e(\mathbf{K},E)/dEd\Omega^\#$ (which is proportional to the inelastically scattered current) by the equation

$$\frac{df}{dE}(\mathbf{K},E) = \left[\frac{E}{2} \frac{\mathbf{k}_o \cdot \mathbf{K}}{k_n \cdot \mathbf{K}} \right] \frac{d^2\sigma_e(E)}{dEd\Omega} \quad (2.17)$$

where E is the energy loss and \mathbf{k}_o , \mathbf{k}_n are the incident and scattered momenta respectively. The various momenta are related to the polar scattering angle θ by the cosine rule

$$\mathbf{K}^2 = \mathbf{k}_o^2 + \mathbf{k}_n^2 - 2\mathbf{k}_o \cdot \mathbf{k}_n \cos\theta \quad (2.18)$$

and
$$\vec{\mathbf{K}} = \vec{\mathbf{k}}_o - \vec{\mathbf{k}}_n \quad (2.19)$$

According to the Bethe-Born theory [10], equation 2.16 can be expanded in terms of a power series in \mathbf{K}^2 if $|\mathbf{K}|$ is small

$$\frac{df(\mathbf{K},E)}{dE} = \frac{df^o(E)}{dE} + A\mathbf{K}^2 + B\mathbf{K}^4 + \dots \quad (2.20)$$

$d^2\sigma_e(\mathbf{K},E)/dEd\Omega$ as a function of energy loss E is the electron energy loss spectrum at momentum transfer \mathbf{K} involving scattering into a solid angle element $d\Omega$.

where $A = (\epsilon_2^2 - 2\epsilon_1\epsilon_3)$, $B = (\epsilon_3^2 + 2\epsilon_1\epsilon_5 - 2\epsilon_2\epsilon_4)$ (2.21)

and $\epsilon_m = \frac{1}{m!} \langle \Psi_n | \sum_s \vec{r}_s^m | \Psi_o \rangle$ (2.22)

where $df^\circ(E)/dE$ is the differential optical oscillator strength and ϵ_m is the m^{th} order multipole matrix element with $m=1$ for electric dipole and $m=2$ for electric quadrupole, etc.. As $|\mathbf{K}| \rightarrow 0$, the so-called OPTICAL LIMIT, which corresponds to zero momentum transfer, can be obtained from equation 2.20 [11]

$$\text{Lt}_{\mathbf{K}^2 \rightarrow 0} \frac{df(\mathbf{K}, E)}{dE} = \frac{df^\circ(E)}{dE} \quad (2.23)$$

Under such conditions of negligible momentum transfer dipole selection rules apply and equation 2.17 can be rewritten as

$$\frac{df^\circ(E)}{dE} = \left[\frac{\mathbf{E} \cdot \mathbf{k}_o \cdot \mathbf{K}^2}{2 \mathbf{k}_n} \right] \frac{d^2 \sigma_e(E)}{dE d\Omega} = B(E) \frac{d^2 \sigma_e(E)}{dE d\Omega} \quad (2.24)$$

The quantity $B(E)$ is called the Bethe-Born factor and it can be seen that it depends on kinematic (i.e. instrumental) factors alone. $B(E)$ relates the electron impact differential cross-section at negligible momentum transfer to the differential optical oscillator strength. In an actual experiment the factor $B(E)$ must also take into account the finite

acceptance angle of the spectrometer about the mean scattering angle of 0° . This will be considered in the following section.

2.4.2 Experimental Approach

It is clear from equations 2.17-2.24 that electron impact measurements made under appropriate conditions may be used to make absolute optical oscillator strength measurements if appropriate absolute normalisation procedures can be established. The momentum transfer \mathbf{K} , which depends on the impact energy E_o , the energy loss E and the mean scattering angle θ , can be obtained for a particular experimental condition by substituting $\mathbf{k}_o^2=2E_o$ and $\mathbf{k}_n^2=2(E_o-E)$ into equation 2.18 [14].

$$\mathbf{K}^2 = 2E_o + 2(E_o-E) - 2\sqrt{2E_o}\sqrt{2(E_o-E)} \cos\theta \quad (2.25)$$

Equation 2.25 can be rearranged to become

$$\mathbf{K}^2 = 2E_o \left(2 - \frac{E}{E_o} - 2\sqrt{1 - \frac{E}{E_o}} \cos\theta \right) \quad (2.26)$$

From equation 2.26, it can be seen that if we require $\mathbf{K}^2 \rightarrow 0$, E/E_o and θ should be made as small as possible. Under these conditions, we can expand $(1-E/E_o)^{1/2}$ into a binomial series and neglect the contribution of the higher terms for small E/E_o . In addition, $\cos\theta$ can be made equal to $(1-\theta^2/2)$ for small θ . Equation 2.26 can then be simplified to

$$\mathbf{K}^2 = 2E_o (x^2 + \theta^2) \quad (2.27)$$

where x is a dimensionless quantity and is equal to $E/2E_o$. By substituting equation 2.27 into equation 2.24 and integrating over the finite half angle of acceptance θ_o of the detector, the Bethe-Born conversion factor $B(E)$ can be derived for a particular spectrometer geometry to be [14,83]

$$B(E) = \left[\frac{EE_o}{\pi} \frac{\mathbf{k}_o}{\mathbf{k}_n} \right] \left[\ln \left(1 + \frac{\theta_o^2}{x^2} \right) \right]^{-1} \quad (2.28)$$

Two general approaches have been used for optical oscillator strength determination by electron impact:

- (a) An indirect EELS method, pioneered in the 1960's by E. Lassette and co-workers [67-70], involves measurement of the relative intensity for a given transition as a function of scattering angle (i.e. of \mathbf{K}^2 , see equation 2.25) at a fixed intermediate impact energy (typically ~500 eV). This results in a relative generalized oscillator strength curve (see equations 2.17-2.23) which can be extrapolated to $\mathbf{K}^2=0$ to give an estimate of the relative optical oscillator strength for the transition. The extrapolation procedure is tedious since a series of measurements is required for each transition. In addition the procedure can often be problematical due to unusual behaviour of the functional form of $f(\mathbf{K})$ at low \mathbf{K} [67] and also due to the fact that the minimum experimental value of \mathbf{K}^2 was often still quite large [67-

70] so that a lengthy extrapolation was required. The minimum attainable value of \mathbf{K}^2 was further limited [67–70] by the fact that the spectrometer could not be operated at $\theta=0^\circ$ due to interference from the incident primary electron beam in the electron energy loss analyzer. The relative value of the oscillator strength was usually made absolute by reference to concurrent measurements of the relative elastic scattering intensity which was in turn normalized on a published value of the calculated or experimental absolute elastic scattering cross section. A variation of this extrapolation approach used by Ross *et al.* to study alkali metals [71], involved scanning the impact energy at fixed scattering angle for each transition. However such an approach is even more difficult for general application to quantitative work because of electron optical effects on the scattered electron intensities and as a result its use has been extremely limited.

- (b) A more direct and versatile approach which avoids the need for the undesirable extrapolation procedures is to choose the experimental conditions so that the OPTICAL LIMIT (i.e. $\mathbf{K}^2 \rightarrow 0$) is effectively satisfied directly [21–23]. This can be achieved by measuring at high impact energy E_0 (typically 3000 eV for valence shell processes) and designing the electron analyzer and associated electron optics so that a mean scattering angle of 0° can be used [83–87]. This typically results in $\mathbf{K}^2 < 10^{-2}$ a.u.. Under such conditions equation 2.24 is satisfied to better than 1% accuracy and an entire EELS spectrum covering both the discrete and continuum regions can be scanned directly under dipole (optical) conditions. To obtain a relative optical oscillator strength spectrum it suffices merely to transform the

relative electron impact differential cross section (at $\mathbf{K}^2 \sim 0$) by the known Bethe–Born factor $B(E)$ for the spectrometer. $B(E)$ must take into account the effects caused by the finite acceptance angles of the electron energy loss analyzer (i.e. a spread of \mathbf{K}^2 , see equation 2.28). The relative optical oscillator strength spectrum obtained in this way has the correct relative intensity distribution because of the "flat" nature of the virtual photon field [14,88] associated with inelastically scattered fast electrons at $\mathbf{K}^2 \sim 0$ [10]. This means that no determination of beam flux is required. The relative spectrum can be made absolute by using a known theoretical [85] or experimental [87] value of the photoabsorption cross section at a single photon energy, usually in the photoionization continuum. However, an independent and accurate means of obtaining an absolute scale, frequently used in this laboratory (for some examples see references [24–27,30]), is to obtain the Bethe–Born transformed valence shell EELS spectrum (i.e. $d^2\sigma_e(E)/dEd\Omega$ – see equations 2.24 and 2.28) out to high energy loss. The proportion of valence shell oscillator strength from the limit of the data to $E=\infty$ is estimated by extrapolation of a curve fitted to the higher energy measurements. The total area of the spectrum is then normalised to the number of valence shell electrons. This overall procedure makes use of the valence shell Thomas–Reiche–Kuhn (TRK) sum rule (see equation 2.7). The TRK sum rule normalisation of a Bethe–Born converted EELS spectrum produces an accurate absolute scale without the need for measurements of beam flux and target density which are required in conventional absolute cross section determinations.

In summary, the selection of experimental conditions corresponding directly to the optical limit, together with TRK sum rule normalisation, provides an extremely direct and versatile approach which is the basis of the dipole (e,e), (e,2e) and (e,e+ion) techniques for measuring absolute optical oscillator strengths. These three methods provide quantitative simulations of tunable energy photoabsorption, photoelectron spectroscopy and photoionization mass spectroscopy respectively [14,30,88]. The three dipole electron scattering techniques have been used extensively in recent years for total and partial optical oscillator strength measurements [30] for photoabsorption and photoionization in the continuum at modest energy resolution (1 eV FWHM) for a wide variety of valence shell and inner shell processes (see references [24–30] for some recent examples). The modest energy resolution results from using an unmonochromated incident electron beam of thermal width. At such a low energy resolution the sharp peaks in the valence shell excitation spectra of atoms and molecules are largely unresolved [24–27] but the spectral envelope nevertheless encloses the correct integrated discrete oscillator strength, regardless of the bandwidth, since electron impact excitation (equation 2.15) is non-resonant [11,14,88]. In the high resolution dipole (e,e) method (0.048 eV FWHM) developed in the present work a detailed absolute differential optical oscillator strength spectrum is obtained throughout the valence shell discrete region, free of "line saturation" effects.

Chapter 3

Experimental Methods

The complementary performance characteristics of two different zero degree, high-impact-energy electron-energy-loss spectrometers (or dipole (e,e) spectrometers), one with low resolution and a known Bethe-Born conversion factor, the other with high energy resolution, have been used to obtain the results reported in this thesis. Absolute optical oscillator strengths for the discrete and continuum photoabsorption of five noble gases and five diatomic gases have been obtained. The combined techniques establish a general method suitable for routine application to measurements of absolute optical oscillator strengths for electronic excitation (i.e. photoabsorption) of atoms and molecules at high resolution over a wide spectral range.

3.1 The Low Resolution Dipole (e,e) Spectrometer

The present low resolution dipole (e,e) spectrometer is the non-coincident forward scattering portion of a dipole (e,e+ion) spectrometer that has been extensively used in this laboratory in recent years to obtain highly accurate photoabsorption and photoionization continuum total and partial oscillator strengths for a large number of molecular targets [24-30]. This dipole (e,e+ion) spectrometer was originally built at the FOM institute in Amsterdam [21-23,85-87], but was moved to the University of British Columbia in 1980 where the spectrometer has been further modified [89,90]. Details of the construction and operation of this

spectrometer can be found in references [21–23,85–87,89,90]. A schematic diagram of the dipole (e,e+ion) spectrometer is shown in figure 3.1.

Briefly, a black and white television electron gun with an indirectly heated oxide cathode (Philips 6AW59) at -4 kV potential with respect to ground is employed to produce a narrow (~ 1 mm diameter) beam of fast electrons. The electron beam is collided with the target molecules in a collision chamber which is at potential of $+4$ kV. Thus, the kinetic energy of the incident electrons is 8 keV in the interaction region containing the target molecules. The inelastically scattered electrons are collected in a small cone of 1.4×10^{-4} steradians about the zero degree mean scattering angle, defined by an angular selection aperture. After passing through Einzel lenses and a decelerating lens, the electrons are energy-analyzed by a hemispherical electron analyzer and finally are detected by a channel electron multiplier (Mullard B419AL) used in the pulse counting mode. The resolution of this electron energy loss spectrometer is ~ 1 eV FWHM. The time-of-flight mass spectrometer, consisting of extraction plates, ion lenses and an ion multiplier, capable of detecting the positive ions produced in the collision chamber is arranged at 90 degrees to the incident electron beam but this arrangement (dipole (e,e+ion) spectroscopy) was not used in the present work. Helmholtz coils and high permeability mumetal are employed to shield the scattering regions from external magnetic fields. The use of turbo molecular pumps provides a clean vacuum environment suitable for quantitative electron spectroscopy. Recently, some modifications have been made to this dipole (e,e+ion) spectrometer [27,29]. A differential pumping chamber pumped by a Seiko–Seiki (STP300) magnetic levitation

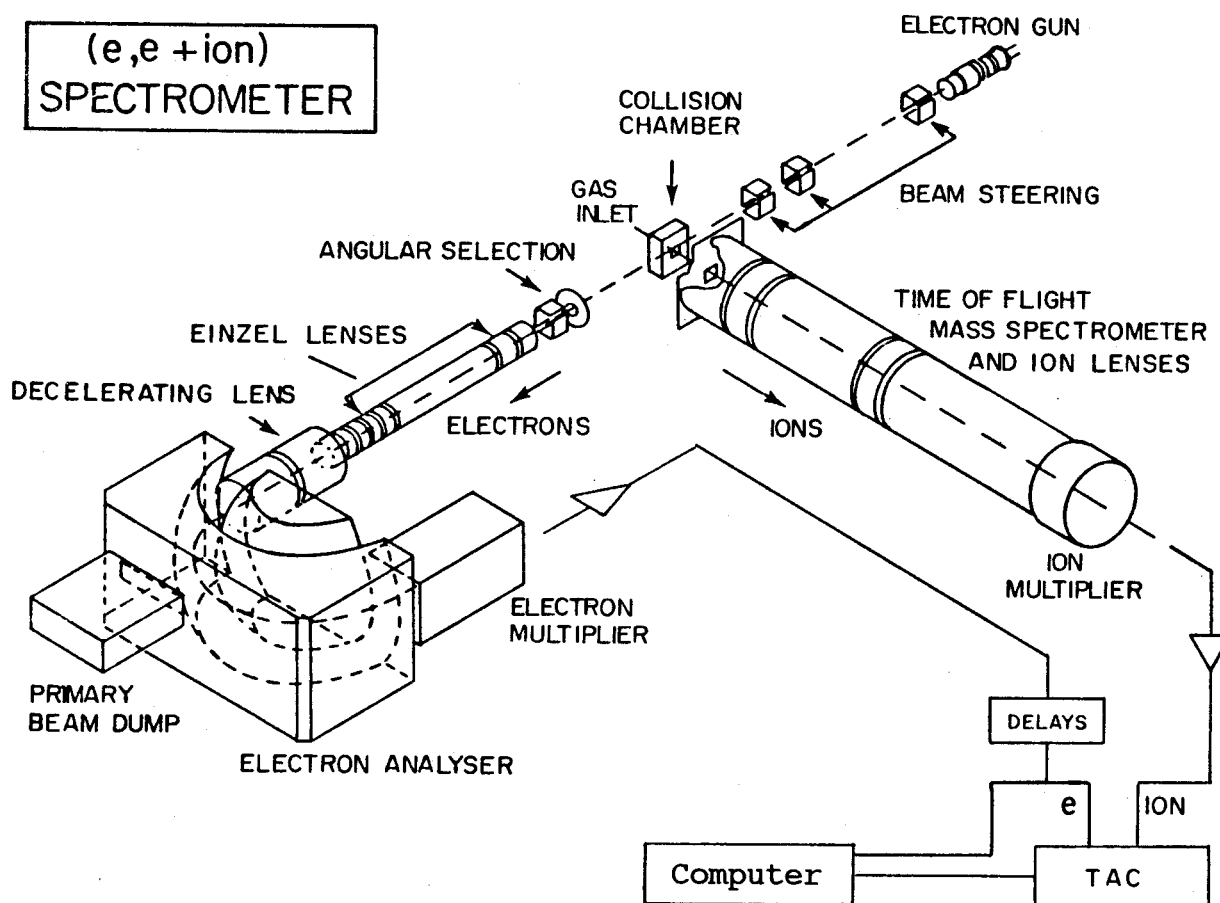


Figure 3.1: Schematic of the dipole (e,e+ion) spectrometer

In the present work, this instrument has been used only in the dipole (e,e) mode (i.e. the forward electron energy loss spectrometer has been employed without the time-of-flight spectrometer).

turbo-molecular pump, was added to the existing spectrometer between the electron gun vacuum chamber and the collision chamber in order to effectively isolate the electron gun from the sample gas such that the oxide cathode of the electron gun will have a longer life. In addition, the extra differential pumping chamber also stabilizes the electron beam and only slight retuning of the beam is necessary when the sample is introduced into the system. The modifications above involved adding a further set of quadrupole electrostatic deflectors and a new electron beam monitoring aperture (~1 mm diameter). The electron gun was moved back from the target region by ~7 cm. A vacuum isolation valve was also added between the electron gun and the differential pumping chamber and with this device in place maintenance work can be performed on either the gun chamber or the main system without letting the whole system up to atmospheric pressure.

The experimental conditions ($E_0=8$ keV and half-angle of acceptance $\theta_0=6.7\times 10^{-3}$ radians) of this low resolution dipole (e,e) spectrometer satisfy the small momentum transfer (\mathbf{K}) condition when the energy loss $E \leq 500$ eV according to the Bethe-Born theory (see chapter 2). The electron energy loss spectrum is then converted to a relative optical spectrum from the known scattering geometry (E_0 , E and θ_0) of the spectrometer using the equation 2.28. The absolute differential oscillator strength scale for the relative optical spectrum can then be established by using the (partial) TRK sum-rule or by normalizing at a single point in the smooth continuum to published optical data. The latter procedure has only been used when the sum-rule normalization procedures are not tractable because of closely spaced inner shells

adjacent to the valence shell (see results for argon, krypton and xenon, chapter 6).

3.2 The High Resolution Dipole (e,e) Spectrometer

All the high resolution spectra reported in this thesis were measured using the high resolution dipole (e,e) spectrometer which was built earlier by Daviel, Brion and Hitchcock [31] to record EELS spectra. The design and construction of this spectrometer have been described in detail in reference [31]. Figure 3.2 shows a schematic diagram of the high resolution dipole (e,e) spectrometer. The following features of the spectrometer provide improved performance in terms of resolution, sensitivity and stability, compared with older designs:

- (a) Differential pumping of the four vacuum chambers including the electron gun, the monochromator, the collision region and the analyzer, alleviates the problems of surface contamination, retuning and frequent cleaning of the system. This arrangement ensures long term stability as well as high sensitivity and good resolution of the spectrometer. The vacuum isolation of the electron gun also enhances the study of thermally unstable compounds.
- (b) Advanced electron optics were designed [31] to improve the beam currents and also minimize the effects of scattering of the incident beam from slit edges and the surfaces of the analyzers into the detector. The large background originating from the primary electron beam is strongly suppressed and operation at zero-degree mean scattering angle is possible with minimal background effects.

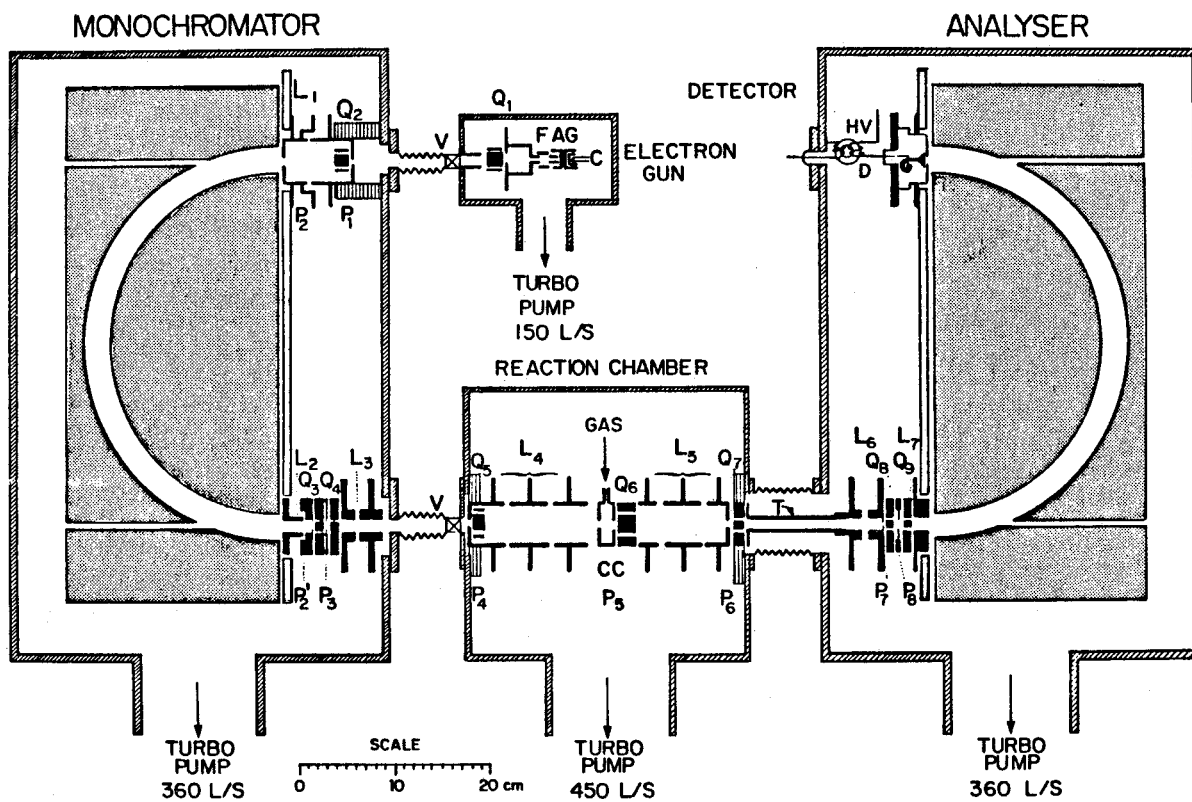


Figure 3.2: Schematic of the high resolution dipole (e,e) spectrometer

Legend: A anode	G grid	P ₁ - P ₈ apertures
C cathode	F focusing lens	Q ₁ - Q ₉ deflectors
CC collision chamber	V valve	L ₁ - L ₇ lenses
T tube	HV high voltage	GAS gas inlet
L/S liter per second	D decoupling transformer	

(c) Large hemispherical electron energy analyzers (mean radius $R_0 = 19 \text{ cm} = 7.5 \text{ in}$) are employed. As a result, high transmission and high resolution at relatively high pass energy can be attained. The high pass energy in turn permits the required high impact energy while retaining reasonable lens voltage ratios.

Briefly, a thoriated tungsten filament, spot welded onto an externally adjustable mount and located just in front of the grid of an oscilloscope electron gun body (Cliftronics CE5AH), is heated by a direct current to produce thermal electrons. Except for the grounded first and third elements of the focussing Einzel lens F, the filament cathode (C), grid (G), anode (A) and the second element of the focussing lens F are all floated on top of -3 kV in the present design. A two element lens (L_1) is used to retard the 3 keV electron beam ($\sim 1 \text{ mm}$ diameter) to the required pass energy of the monochromator before being energy-selected by a hemispherical electron energy analyzer. A virtual slit generated by the accelerating (voltage ratio 1:20) lens (L_2) is located at the monochromator exit. The monochromated beam is further accelerated ($\times 5$) by lens (L_3) and then focussed onto the entrance of the reaction chamber. After passing through the Einzel lens (L_4), the electron beam collides with the sample molecules in the collision chamber which is at ground potential. The kinetic energy of the incident electrons is 3 keV in the collision region. The electron beam then passes through a zoom, energy-add, lens (L_5). The design of the analyzer entrance lenses (L_6 and L_7) is similar to that of the monochromator exit lenses (L_2 and L_3) and a virtual slit is employed. In the present work, the pass energy of the

analyzer was always set to be equal to that of the monochromator. The inelastically scattered electrons are energy analyzed before being detected by the channel electron multiplier (Mullard B419AL) which is mounted just behind the analyzer exit aperture. Hydrogen-annealed mumetal enclosures located outside the vacuum housing provide magnetic shielding in various regions of the spectrometer. Seiko-Seiki (STP 300 and 400) magnetic levitation turbo molecular pumps have been used to establish a clean vacuum environment.

The spectrometer is tuned up by using the primary (unscattered) electron beam which is directed to the cone of the channeltron with energy analyzer deflection voltages, lens voltages (L_1 to L_7) and the quadrupole deflectors (Q_1 to Q_9). The quadrupole deflectors each consist of two pairs of electrostatic plates in the x and y directions. Electrometers are connected to the apertures (P_1 to P_8) to monitor the collimation and direction of the electron beam, while a floated vibrating reed electrometer (Cary, model 401) is used to measure the small currents on the cone of the channeltron. In the present work, the lens voltages (L_1 to L_7) were recorded after the initial tuning of the spectrometer for a given resolution (which is set by pass energy of the energy analyzers). The same lens voltages were then used for subsequent measurements performed at the same energy resolution. This procedure was used in order to ensure the same half-angle of acceptance θ_0 of the analyzer/detection system (which may be changed by different lens voltages) at a given resolution. To obtain an energy loss spectrum, a voltage corresponding to the energy loss of the inelastically scattered electrons is added to the lens L_5 and to the complete analyzer and detection system. The inelastically scattered electrons thus regain their

energy loss and are transmitted to the detector. At the same time, the primary (incident) electron beam gains the same energy and is strongly defocused by the advanced electron optics at the input of the analyzer. This results in a strong suppression of the primary, unscattered, beam and permits operation at zero degree scattering angle. High gain pre-amplifier and amplifier/discriminator units (PRA models 1762 and 1763 respectively) are employed to process the signals coming from the channeltron. The signals are collected using a Nicolet 1073 signal averager operated in a multichannel scaling mode. The data are then transmitted to the PDP 11/23 computer which is also used to control the scanning voltages on L_5 and the analyzer of the spectrometer as well as the channel advance of the signal averager.

The energy resolution ΔE (FWHM) of the spectrometer depends on the selected pass energies E for both the monochromator (E_m) and analyzer (E_a). The theoretical resolution (neglecting angular effects) for a hemispherical analyzer is given [91] by

$$\frac{\Delta E}{E} = \frac{\omega}{2r} \quad (3.1)$$

where ω is the slitwidth and r is the mean radius. For the combining monochromator and analyzer the individual resolution functions must be added quadrature. The observed halfwidth of the monochromated and analyzed primary beam at a pass energy of 10 eV is 0.036 eV in excellent agreement with equation 3.1. Under these conditions the halfwidth of the inelastically scattered beam originating in the collision chamber, is somewhat larger (0.048 eV FWHM) due to the additional angular spread.

3.3 Experimental Considerations and Procedures

The high resolution dipole (e,e) spectrometer had been used extensively in recent years for the measurement of high resolution valence shell [32–34], and inner shell [32,34,35] excitation spectra. However, prior to the present work no attempt had been made to quantitative measurements of absolute oscillator strengths because the Bethe–Born factor of the spectrometer was not known. In order to obtain absolute optical oscillator strengths from the high resolution EELS spectra, an absolute scale must be established, and in addition the energy dependent Bethe–Born conversion factor for this high resolution spectrometer (B_{HR}) must be determined. The conversion factor is in practice more complex than that given by the single expression in equation 2.24 because it must account for integration over the finite spectrometer acceptance angles about $\theta=0^\circ$ (see equation 2.28). A sufficiently exact knowledge of the effective acceptance angles would require a very accurate and detailed understanding of the complex electron optical functions of the lenses in all regions of the high resolution dipole (e,e) spectrometer as a function of energy loss. Furthermore, this detailed information would be required for each analyser/monochromator pass energy combination selected to provide a given energy resolution. Such detailed information is difficult to obtain with sufficient precision by model calculations for the complex electron optics in this type of instrument.

A better and more feasible approach [37] is to calibrate the intensity response of the high resolution instrument and obtain an

empirically determined, relative, Bethe–Born factor by referencing the high resolution EELS signal to the known optical cross section in the smooth photoionization continuum spectral region of a suitable gas. This could be achieved by taking the ratio of the high resolution EELS intensity to that of an independently measured absolute photoabsorption cross section, as a function of energy loss (photon energy). An obvious choice for this calibration is helium gas. Recommended experimental values of absolute photoabsorption cross section for the helium continuum have been tabulated by Marr and West [47] from a consideration of a large number of published optical experiments. We have, however, chosen an alternative and entirely independent approach, in which the high sensitivity low resolution (~ 1 eV FWHM) dipole (e,e) spectrometer (described in section 3.1), with no monochromator, simpler optics and collision geometry, and a well characterised Bethe–Born factor (B_{LR}) [24–30], has been used to obtain a new wide range measurement of the helium discrete and continuum absolute photoabsorption oscillator strengths, entirely independent of any optical measurement. It has been found [14,30] that TRK sum rule normalization of Bethe–Born converted EELS spectra obtained on this low resolution dipole (e,e) spectrometer provides a highly accurate absolute photoabsorption oscillator strength scale, without the need for any measurement of beam flux or target density. Helium is a particularly suitable choice for the calibration measurements since it has only a single ($1s^2$) shell and thus no shell separation or corrections for Pauli excluded transitions are required for the TRK sum rule procedure, in contrast to the situation for more complex targets.

The absolute photoabsorption oscillator strengths obtained on the low resolution dipole (e,e) spectrometer may then be used to generate the relative Bethe–Born factor for the high resolution instrument by taking the ratio of the signals in the smooth continuum region above the first ionization energy of helium, as described above. The relative Bethe–Born factor for the high resolution spectrometer can then be obtained at lower energies by extrapolation of a suitable function (see chapter 4) fitted to the measured factor in the region above 25 eV. Finally, the Bethe–Born converted high resolution EELS spectrum of helium was placed on an absolute scale by single point normalization in the continuum (at 30 eV) to the absolute optical oscillator strength determined using the low resolution dipole (e,e) instrument. Employing these procedures, both the Bethe–Born calibration and the measurement of absolute optical oscillator strengths is achieved entirely independently of any optical techniques. Furthermore, exploitation of the TRK sum rule avoids the difficulties and limitations of conventional methods of absolute scale determination. The resulting absolute measurements can thus be independently compared with published values of measured and calculated optical oscillator strengths for helium. The sequence of measurements and procedures used in the present work are summarised by the flow chart shown in figure 3.3.

Similar procedures have been performed using the measurements for neon [38], and the values obtained for B_{HR} are in excellent agreement with those using helium. The average of the two determinations provides further statistical precision, and this average value has been used in the high resolution absolute oscillator strength work performed with the high resolution dipole (e,e) spectrometer. The averaged B_{HR} also

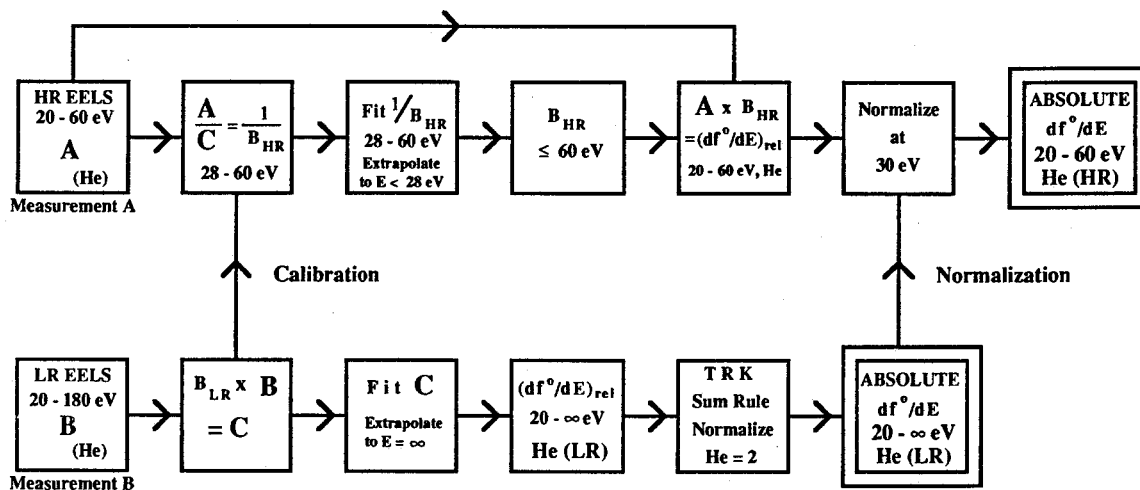


Figure 3.3: Flow-chart showing the data recording and processing procedures used in determining the absolute dipole oscillator strengths for the discrete electronic excitation transitions ($1^1S \rightarrow n^1P$, $n=2-7$) of helium.

provides increased reliability when the curve above 25 eV is fitted and extrapolated down to equivalent photon energies as low as 5 eV. The high resolution electron energy loss spectra of the three heavier noble gases (Ar, Kr and Xe) and five diatomic gases (H₂, N₂, O₂, CO and NO) have been converted to relative oscillator strength spectra using the B_{HR} factor obtained as described above. The absolute scales were then obtained by normalizing in the smooth continuum to the data determined using the low resolution dipole (e,e) spectrometer. Low resolution dipole (e,e) measurements have been made in the present work for the argon, krypton and xenon. However, the TRK partial valence shell sum rule normalization procedures used to establish the absolute scales for helium and neon could not be used for the heavier noble gases since the successive atomic inner subshell energy separations are relatively small and thus a good fit to the valence shell tail is not possible. In these circumstances the extrapolation procedures used to estimate the amount of valence shell oscillator strength above a certain energy become unreliable. Therefore, the alternative procedure of single point normalization to a previously published photoabsorption measurement has been used to establish the absolute scale for argon, krypton and xenon. For the five diatomic gases, low resolution dipole (e,e) oscillator strength measurements have been previously reported [86,87,92,93]. The TRK sum rule normalization procedures were used to establish the absolute scale for the measurements of hydrogen [86], oxygen [92] and nitric oxide [93]. In contrast, single point normalization procedures were used for the earlier reported measurements for nitrogen and carbon monoxide [87] since the data were only obtained up to 70 eV energy and hence sufficiently accurate extrapolation procedures could not be carried

out. Therefore in the present work, new wide ranging low resolution dipole (e,e) measurements of nitrogen and carbon monoxide have been performed up to an equivalent photon energy of 200 eV. The TRK partial valence shell sum rule has now been employed in order to establish the absolute oscillator strength scale for these new measurements for nitrogen and carbon monoxide. Thus, the presently determined absolute optical oscillator strength data for all five diatomic gases at both high and low resolution are completely independent of any directly obtained optical data.

For quantitative measurements it is essential to ensure that saturated count rates are obtained in the channeltron detectors of both spectrometers over the full dynamic range of the signals. In order to avoid dead-time errors it was also necessary to use a fast data buffer between the output of the high resolution spectrometer and the PDP 11/23 computer. Since for the high resolution instrument no fast MCA compatible with the PDP 11/23 computer was available, a specially adapted Nicolet 1073 signal averager was used as the data buffer in the present work. Maximum count rates were restricted to a maximum of 20000 per second in order to ensure linearity over the full dynamic range of the spectra.

3.4 Energy Calibration

The absolute energy scale of the electron energy loss spectrum of helium measured using the high resolution dipole (e,e) spectrometer was obtained by referencing to the $2^1S \rightarrow 2^1P$ transition of helium at 21.218 eV. For the other gases, the absolute scale was established in separate

experiments by simultaneous admission of helium and referencing the sample spectrum to the $2^1S \rightarrow 2^1P$ transition of helium at 21.218 eV [54]. In practice, the calibration corrections were found to be ≤ 0.015 eV. The energy scale for the low resolution dipole (e,e) measurements was obtained by referencing the energy position of a prominent spectral feature to the corresponding peak in the high resolution electron energy loss spectrum.

3.5 Sample Handling and Background Subtraction

The sample gases studied in the present work were obtained commercially. Their sources and stated minimum purities are summarized in table 3.1. No impurities were apparent in the high resolution electron energy loss spectra. Appropriate gas regulators were used to establish a steady gas flowrate and sample introduction to the spectrometers was achieved using Granville-Phillips series 203 stainless steel leak valves. Ambient gas pressures were adjusted to be in the range $0.5\text{--}2.0 \times 10^{-5}$ torr and $0.1\text{--}1.0 \times 10^{-5}$ torr for the high resolution and low resolution spectrometers, respectively, by using the Granville-Phillips leak valves. It is important to maintain single collision conditions and no evidence for double scattering was found in the energy loss spectrum under the selected conditions.

Contributions to the electron energy loss spectra from background gases remaining at the base pressures (2×10^{-7} torr) of the turbo molecular pumped spectrometers and/or non-spectral electrons were removed by subtracting the signals obtained when the sample pressures were quartered. Such procedures were used because complete removal

of the sample gas was found to influence slightly the tuning of the energy loss spectrometers.

Table 3.1: Sources and stated minimum purity of samples

Sample	Source	Stated minimum purity (%)
He	Linde	99.995
Ne	Matheson	99.99
Ar	Linde	99.998
Kr	Linde	99.995
Xe	Matheson	99.995
H ₂	Linde	99.95
N ₂	Medigas	99.0
O ₂	Medigas	99.0
CO	Matheson	99.5
NO	Linde	98.5

Chapter 4

Absolute Optical Oscillator Strengths for the Electronic Excitation of Helium

4.1 Introduction

The availability of very accurate quantum mechanical calculations, together with the fact that helium has only a K shell and thus a total oscillator strength of exactly 2, with no corrections needed for Pauli excluded transitions [52,53], makes the dipole excitation of ground state helium an ideal test case for the high resolution dipole (e,e) method. In addition further consistency checks can be made involving oscillator strength sums in appropriate regions of the discrete and continuum spectrum. In the present work, test measurements, involving a completely independent determination of the absolute optical oscillator strengths for the $1^1S \rightarrow n^1P$ series ($n=2-7$) for helium, are compared with previously published experimental data for $n=2$ and 3 obtained using a range of optical [56-64] and electron impact [19,68,84] methods. The measured results $n=2-7$ are also compared for with high level quantum mechanical calculations employing correlated wavefunctions [3-9,54]. The present measurements represent the first absolute experimental results for $n=4-7$ and very few previous measurements for $n=3$ have been reported. Measurements of the absolute continuum photoabsorption oscillator strengths up to 180 eV photon energy, including the Fano profile resonance regions of double excitations around 60 eV and 70 eV, were also obtained and are compared with existing direct optical

measurements [94–97] and calculations [9,98–100]. The results for helium are used to establish the viability of the high resolution dipole (e,e) method for general application to measurements of absolute optical oscillator strengths in the discrete valence shell spectral regions of electronic excitation for atoms and molecules.

4.2 Results and Discussion

4.2.1 Low Resolution Optical Oscillator Strength Measurements for Helium

Using the low resolution dipole (e,e) spectrometer, electron energy loss measurements were performed in the energy ranges 20–25.5, 25.5–50, 50–110 and 110–180 eV at intervals of 0.1, 0.5, 1, and 2 eV respectively. The energy resolution was ~1 eV FWHM. Absolute optical oscillator strengths for helium were obtained by Bethe–Born conversion (using B_{LR} , see figure 3.3) and TRK sum rule normalization (to a value of two) of the electron energy loss data as described above. The portion of the relative oscillator strength from 180 eV to infinity was first estimated by extrapolation of a least squares fit to the measured data in the 72–180 eV region using a function of the form AE^{-B} (E =energy and A and B are best fit parameters). The fit gives $B=2.5583$ and the fraction of the total oscillator strength above 180 eV was estimated to be 4.65%. The helium $1^1S \rightarrow 2^1P$ transition (21.218 eV) was used for calibration of the energy scale of the spectrum and is the only discrete structure resolved at the resolution of this spectrometer. The measured data is recorded in table 4.1 and illustrated in figure 4.1 (solid circles). Also shown on figure 4.1

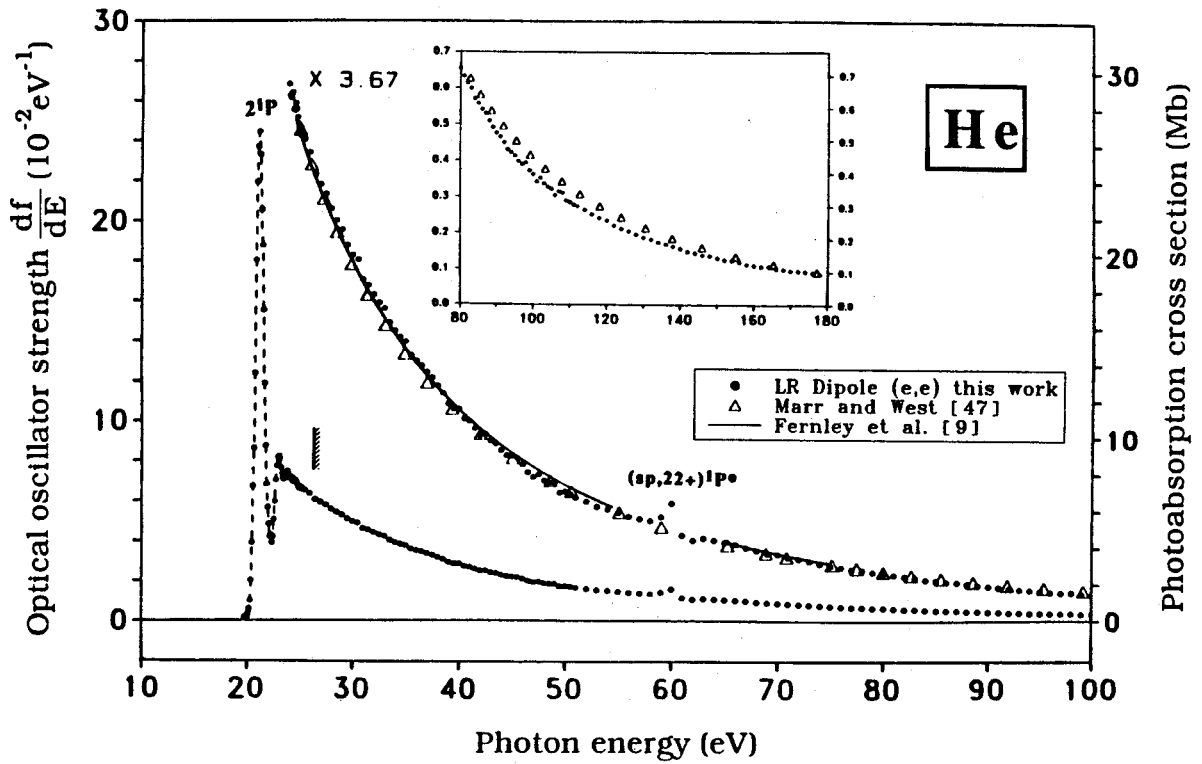


Figure 4.1: Absolute dipole oscillator strengths for helium measured by the low resolution dipole (e,e) spectrometer from 20–180 eV (FWHM=1 eV). Solid circles are this work, open triangles are photoabsorption data of Marr and West [47], solid line is theory, Fernley *et al.* [9].

Table 4.1

Absolute differential optical oscillator strengths for helium obtained using the low resolution (1 eV FWHM) dipole (e,e) spectrometer (24.6-180 eV)

Energy (eV)	Oscillator Strength (10^{-2}eV^{-1})	Energy (eV)	Oscillator Strength (10^{-2}eV^{-1})	Energy (eV)	Oscillator Strength (10^{-2}eV^{-1})
24.6	7.05	29.5	5.12	38.0	3.21
24.7	6.96	30.0	4.98	38.5	3.11
24.8	6.85	30.5	4.92	39.0	2.97
24.9	6.76	31.0	4.65	39.5	2.89
25.0	6.62	31.5	4.57	40.0	2.90
25.1	6.71	32.0	4.45	40.5	2.76
25.2	6.66	32.5	4.34	41.0	2.73
25.3	6.58	33.0	4.26	41.5	2.63
25.4	6.58	33.5	4.07	42.0	2.54
25.5	6.55	34.0	3.95	42.5	2.56
26.0	6.37	34.5	3.87	43.0	2.46
26.5	6.08	35.0	3.81	43.5	2.42
27.0	5.94	35.5	3.63	44.0	2.33
27.5	5.81	36.0	3.55	44.5	2.26
28.0	5.61	36.5	3.49	45.0	2.25
28.5	5.45	37.0	3.40	45.5	2.23
29.0	5.33	37.5	3.32	46.0	2.14

Table 4.1 (continued)

Energy (eV)	Oscillator Strength (10^{-2}eV^{-1})	Energy (eV)	Oscillator Strength (10^{-2}eV^{-1})	Energy (eV)	Oscillator Strength (10^{-2}eV^{-1})
46.5	2.04	63.0	1.14	83.0	0.598
47.0	1.97	64.0	1.11	84.0	0.569
47.5	2.00	65.0	1.08	85.0	0.557
48.0	1.92	66.0	1.05	86.0	0.540
48.5	1.90	67.0	1.01	87.0	0.529
49.0	1.89	68.0	0.968	88.0	0.508
49.5	1.75	69.0	0.926	89.0	0.491
50.0	1.77	70.0	0.912	90.0	0.475
51.0	1.68	71.0	0.869	91.0	0.464
52.0	1.63	72.0	0.850	92.0	0.448
53.0	1.56	73.0	0.822	93.0	0.429
54.0	1.52	74.0	0.785	94.0	0.421
55.0	1.48	75.0	0.757	95.0	0.412
56.0	1.43	76.0	0.735	96.0	0.397
57.0	1.40	77.0	0.708	97.0	0.388
58.0	1.37	78.0	0.698	98.0	0.393
59.0	1.43	79.0	0.669	99.0	0.370
60.0	1.61	80.0	0.652	100.0	0.360
61.0	1.18	81.0	0.632	101.0	0.341
62.0	1.11	82.0	0.612	102.0	0.350

Table 4.1 (continued)

Energy (eV)	Oscillator Strength (10 ⁻² eV ⁻¹)	Energy (eV)	Oscillator Strength (10 ⁻² eV ⁻¹)	Energy (eV)	Oscillator Strength (10 ⁻² eV ⁻¹)
103.0	0.335	136.0	0.168	178.0	0.0856
104.0	0.326	138.0	0.162	180.0	0.0824
105.0	0.321	140.0	0.155		
106.0	0.302	142.0	0.147		
107.0	0.314	144.0	0.144		
108.0	0.310	146.0	0.138		
109.0	0.288	148.0	0.136		
110.0	0.284	150.0	0.130		
112.0	0.273	152.0	0.125		
114.0	0.262	154.0	0.123		
116.0	0.250	156.0	0.118		
118.0	0.240	158.0	0.112		
120.0	0.232	160.0	0.109		
122.0	0.219	162.0	0.106		
124.0	0.211	164.0	0.106		
126.0	0.204	168.0	0.0998		
128.0	0.194	170.0	0.0980		
130.0	0.187	172.0	0.0932		
132.0	0.181	174.0	0.0916		
134.0	0.173	176.0	0.0893		

$$\sigma \text{ (Mb)} = 1.0975 \times 10^2 \frac{df}{dE} \text{ eV}^{-1}$$

are "recommended values" of the absolute photoabsorption (photoionization) oscillator strengths of helium (open triangles) reported in the compilation by Marr and West [47]. The values compiled in reference [47] were obtained by Marr and West as follows: Various optical measurements of the photoionization cross sections of helium in different energy ranges have been reported by different groups using optical methods [45,101,102]. West and Marr [103] have also themselves measured the photoionization of helium in the $340 \rightarrow 40 \text{ \AA}$ ($35 \rightarrow 310 \text{ eV}$) range using synchrotron radiation. There are some slight discrepancies between the different data sets in some energy ranges. A critical evaluation of the various cross section measurements was carried out [103] by giving a weight to the various data sets according to criteria such as the scatter of data points, performance and quality of the monochromator usedetc. Then all the data was combined and the "best values" were obtained by fitting polynomials to the weighed data points. The resulting absolute photoionization cross section data for helium and also for other noble gases in the vacuum UV and soft x-ray regions were then tabulated [47].

It can be seen from figure 4.1 that the presently reported Bethe-Born converted, TRK sum rule normalised, low resolution dipole (e,e) results are generally in good quantitative agreement with the absolute photoabsorption data recommended by Marr and West [47], from a consideration of a range of published results. It should be noted that the dipole (e,e) and direct photoabsorption techniques are physically different and also that the associated methods of obtaining the absolute scales are completely different. The good agreement therefore provides convincing proof of the validity of the Bethe-Born theory and the

quantitative equivalence of the dipole (e,e) and photoabsorption (photoionization) methods at least in the continuum region. In the region near 60 eV the dipole (e,e) data show evidence of the well known double excitation resonances of helium whereas the Marr and West data [47] were obtained by fitting a smooth curve through the resonance region. Notwithstanding the excellent overall quantitative agreement some small differences in shape are apparent. In particular, the Marr and West data [47] are slightly below and slightly above the present data in the 30–40 eV and 80–180 eV regions respectively.

Also shown on figure 4.1 are the very accurate photoionization (equivalent to photoabsorption for helium) oscillator strength (cross section) calculations for helium recently reported by Fernley *et al.* [9] (solid line). The calculated data [9] have been shifted up in energy by 0.280 eV as the first ionization energy of helium calculated by Fernley *et al.* [9] is 0.280 eV lower than the accurately known spectroscopic value (24.59 eV). It can be seen that the oscillator strength calculations [9] are in excellent agreement with the present dipole (e,e) measurements. Similar calculations were reported earlier by Cooper [104] and by Bell and Kingston [105].

The presently obtained low resolution dipole (e,e) measurements (table 4.1, figure 4.1) have been used to obtain the Bethe–Born conversion factor (B_{HR}) for the high resolution spectrometer and for normalization of the high resolution spectrum of helium (at 30 eV). The high resolution oscillator strength results are presented in the following section.

4.2.2 High Resolution Optical Oscillator Strength Measurements for Helium

4.2.2.1 The Discrete Transitions $1^1S \rightarrow n^1P$ ($n=2$ to 7)

Using the high resolution electron energy loss spectrometer, electron energy loss spectra of helium were obtained at an impact energy of 3000 eV in the energy loss range 20–60 eV at a resolution of 0.048 eV FWHM and in the range 20–100 eV at resolutions of 0.072, 0.098, 0.155 and 0.270 eV FWHM. The data have been processed using the procedures outlined in section 3.3. The intensity of the high resolution electron spectrum at each energy loss in the smooth continuum region above 25 eV was divided by the absolute optical oscillator strengths measured by the LR dipole (e,e) spectrometer (see section 4.2.1, table 4.1 and figure 4.1). This quotient provided a relative Bethe–Born conversion factor (B_{HR} , see figure 3.3) for the high resolution instrument in the energy range above 25 eV. In order to extend this Bethe–Born factor to the excitation region below 25 eV, the quotient has been fitted to a suitable function (which effectively represents the Bethe–Born correction factor for the HR spectrometer) over the energy range 28–60 eV, which can then be extrapolated to lower energy. This fitting and the extrapolation must be done very carefully if correct experimental dipole oscillator strengths are to be obtained in the discrete excitation region down to 21 eV for helium and to even lower energies (5 eV) for other atoms and molecules. In particular the effects of finite angular resolution about the forward scattering direction must be properly accounted for in the Bethe–Born conversion factor if it is to be accurate over the long

extrapolation down to 5 eV. Therefore the effects of angular resolution must be accounted for in some way in the fitting function [14]. In the real situation of finite acceptance angles, the Bethe-Born conversion factor has been derived as shown in equation 2.28. At sufficiently high impact energy and $\mathbf{k}_o \sim \mathbf{k}_n$, equations 2.24 and 2.28 can be combined to give

$$F(E) = \frac{d^2\sigma_e(E)/dEd\Omega}{df^o(E)/dE} = \frac{a}{E} \ln \left(1 + \frac{\theta_o^2}{x^2} \right) \quad (4.1)$$

where $F(E)$ is equal to $1/B(E)$ and a is a constant. Thus we might expect a function of the form of the right hand side of equation 4.1 to fit the ratio of the high resolution electron energy loss spectrum to the absolute optical oscillator strength. While the use of equation 4.1 gave a quite reasonable fit, in practice a further improved fit to the ratio $F(E)$ in the continuum (28–60 eV) was obtained by adding an energy dependent term to the constant a on the right hand side of equation 4.1 to give

$$F(E) = \frac{d^2\sigma_e(E)/dEd\Omega}{df^o(E)/dE} = \frac{a + cE}{E} \ln \left(1 + \frac{\theta_o^2}{x^2} \right) \quad (4.2)$$

In this equation a and c are constants. ($F(E)$ is equal to $1/B_{HR}$ — see figure 3.3). Values of a , c and θ_o were determined from a least squares best fit. The value of the half angle θ_o was found to be approximately 0.17 degrees. At each resolution a function of this form

fitted the data very well over the range 28→60 eV and was extrapolated to lower energies in order to convert $d^2\sigma_e(E)/dEd\Omega$ for the discrete transitions in helium to a relative optical oscillator strength scale. The effectiveness of the extrapolation method employed has been examined by comparing the shapes of the photoabsorption oscillator strength curves down to 5 eV for a range of molecules (O_2 [42], NO [44] and also N_2O , CO_2 and H_2O [106]), obtained using the high resolution dipole (e,e) method, with those obtained earlier using the low resolution dipole (e,e) method [30]. The oscillator strength distributions of the high and low resolution dipole (e,e) spectra are consistent for each molecule for energies down to 5 eV when the differences in energy resolution are considered. Further confirmation of the accuracy of the high resolution Bethe–Born conversion factor at low energies is provided by the very good agreement between the high resolution dipole (e,e) and photoabsorption measurements for O_2 [42] and NO [44]. It should be noted that the exact form of B_{HR} changes for the different resolution settings of the spectrometer. These B_{HR} factors will be used for future oscillator strength measurements of other atoms and molecules.

The high resolution energy loss spectra of helium were multiplied by the appropriate B_{HR} function in order to obtain relative optical oscillator strength spectra which were then normalised in the continuum region at 30 eV using the absolute data of table 4.1, as determined using the low resolution spectrometer. A typical result at an energy resolution of 0.048 eV FWHM is shown in figure 4.2, which is the first reported absolute optical oscillator strength spectrum of helium covering the range $n=2-7$ of the optically allowed discrete transitions ($1^1S \rightarrow n^1P$) preceding the first ionization threshold. Over the near threshold

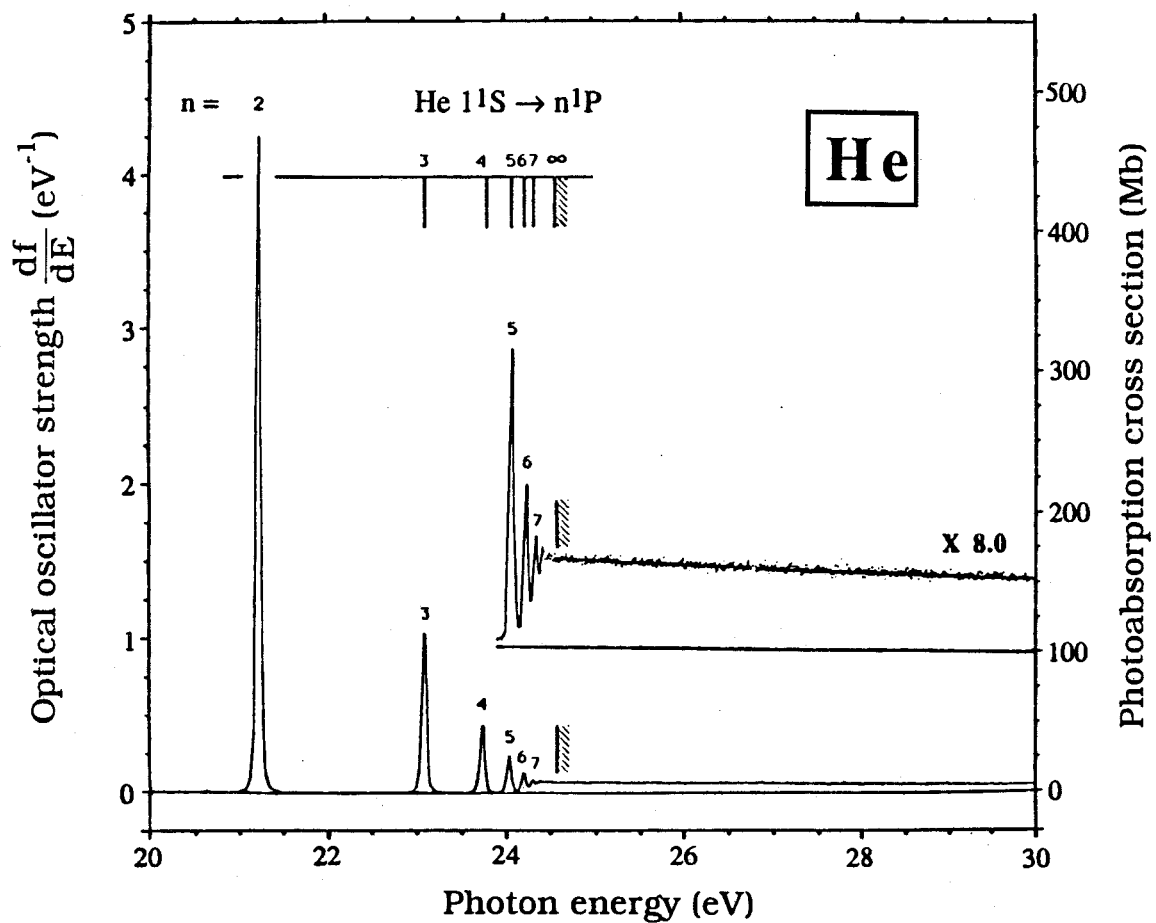


Figure 4.2: Absolute dipole oscillator strengths for helium measured by the high resolution electron energy loss spectrometer from 20–30 eV (FWHM=0.048 eV). Solid line above the ionization edge on X8 spectrum is photoabsorption data from Marr and West [47] and Fernley *et al.* [9].

continuum region (24.6–30 eV) there is excellent quantitative agreement (see insert to figure 4.2) between the present work and the photoabsorption measurements compiled by Marr and West [47] and also the continuum calculations reported by Fernley *et al.* [9] (the data of references [9,47] are both represented by the same solid line).

Transitions up to $n=7$ for the n^1P series are resolved. A very small peak barely visible at 20.6 eV represents a contribution from the dipole forbidden $1^1S \rightarrow 2^1S$ transition due to the finite (but very small) momentum transfer of the dipole (e,e) experiment. This non-dipole contribution is less than 0.5 percent of the 2^1P peak.

Integration of the peak areas in each spectrum, such as that in figure 4.2, provides a measure of the absolute oscillator strengths for each discrete transition in the $1^1S \rightarrow n^1P$ series. An analysis of the spectra obtained at a series of different energy resolutions results in the values shown in table 4.2. The uncertainties quoted represent the scatter in the measurements made at different resolutions. The absolute uncertainty is estimated to be ~5%. Other than the relative values for $n=3$ and 4 reported by Jongh and Eck [62], previously reported work (see table 4.2) has been confined to absolute values for $n=2$ and a few measurements [19,57,64,85] for $n=3$. The present data which extend to $n=7$ represent the first measured values above $n=3$. Various other calculated and measured values for the helium $1^1S \rightarrow n^1P$ series are shown in table 4.2. Immediately it can be seen that the present high resolution dipole (e,e) measurements are in excellent agreement across the range of n values with the calculations for helium reported by Schiff and Pekeris [4], Fernley *et al.* [9] and others [3,5–8,54] (see table 4.2). The earlier electron impact measurements of Lassetre *et al.* [68] for $n=2$ and of

Table 4.2

Theoretical and experimental determinations of the absolute optical oscillator strengths for the $(1^1S \rightarrow n^1P, n = 2 \text{ to } 7)$ transitions in helium[†]

	Oscillator Strength for Transition from 1^1S to							Total to Ionization Threshold
	2^1P	3^1P	4^1P	5^1P	6^1P	7^1P		
A. Theory :								
Fernley, Taylor and Seaton(1987) [9]	0.2811	0.07434	0.03028	0.01524	0.008734	0.005469		
Schiff, Pekeris and Accad(1971) [8]	0.2762	0.073	0.030	0.015				
Weiss(1967) [7]	0.2760	0.0732	0.0303					
Green <i>et al.</i> (1966) [5]	0.27562	0.07294	0.02959	0.01484	0.00846	0.00525		
Dalgarno and Parkinson(1966) [6]	0.276	0.0734	0.0299	0.0151	0.0086	0.0054		0.424
Wiese, Smith and Glennon(1966) [54]	0.2762	0.0734	0.0302	0.0153	0.00848	0.00593		
Schiff and Pekeris(1964) [4]	0.02762	0.00734						
Dalgarno and Stewart(1960) [3]	0.270	0.0746	0.0304	0.0153	0.00878			

Table 4.2 (continued)

	Oscillator Strength for Transition from 1 ¹ S to							Total to Ionization Threshold
	2 ¹ P	3 ¹ P	4 ¹ P	5 ¹ P	6 ¹ P	7 ¹ P		
B. Experiment :								
Present work (HR dipole (e,e))	0.280 (0.007)	0.0741 (0.0007)	0.0303 (0.0007)	0.0152 (0.0003)	0.00892 (0.0005)	0.00587 (0.0003)	0.431 (0.006)	
Tsurubuchi <i>et al.</i> (1989) [64] (Self absorption)	0.273 (0.008)	0.071 (0.003)						
Westerveld and Eck(1977) [63] (Self absorption)	0.262 (0.018)							
Backx <i>et al.</i> (1975) [85] (Electron impact)*	0.276	0.073					0.421	
Burger and Lurio(1971) [57] (Lifetime: Level-crossing)	0.275 (0.007)	0.073 (0.005)						
Jongh and Eck(1971) [62] (Self absorption)#	0.276	0.076 (0.004)	0.029 (0.002)					
Lassette <i>et al.</i> (1970) [68] (Electron impact)	0.269 (0.01)							
Martinson and Bickel(1969) [58] (Lifetime: Beam foil)	0.27 (0.01)							

Table 4.2 (continued)

	Oscillator Strength for Transition from 1 ¹ S to						Total to Ionization Threshold
	2 ¹ P	3 ¹ P	4 ¹ P	5 ¹ P	6 ¹ P	7 ¹ P	
B. Experiment : (continued)							
Fry and Williams(1969) [56] (Lifetime: Hanle effect)	0.273 (0.011)						
Lincke and Griem(1966) [59] (Plasmas emission profile)	0.26 (0.07)						
Korolyov and Odintsov(1964) [60] (Beam emission profile)	0.28 (0.02)						
	0.26 (0.012)						
Kuhn and Vaughan(1964) [61] (Resonance broadening emission profile)	0.37 (0.03)						
Geiger(1963) [19] (Electron impact)	0.312 (0.04)	0.0898 (0.006)					

† Estimated uncertainties in experimental measurements are shown in brackets.

* Relative measurements normalized to the theoretical value for n=2 reported by Schiff and Pekeris (1964) [4].

Relative measurements normalized to the theoretical value for n=2 reported by Weiss (1967) [7].

Backx *et al.* [85] for $n=3$ respectively, are reasonably consistent with the present more comprehensive work. The slightly lower value obtained for $n=2$ by Lassette *et al.* [68] may reflect the difficulties of extrapolation to $K^2=0$ (see section 1.4). The electron impact data for $n=2$ and 3 reported by Geiger [19] show large departures from the present data and also from the calculations [3-9,54]. This could partly be due to the normalization procedure used by Geiger [19], which was based on elastic scattering values, but as Lassette [68] has pointed out the ratio of the values for $n=2$ and 3 reported by Geiger shows a significant departure from the ratio of the calculated oscillator strength values [3-9,54]. The various optical measurements are in almost all cases restricted to $n=2$ [56,58-61,63] and in general are reasonably consistent with the present measurements and with theory [3-9,54]. The Hanle effect measurement for $n=2$ reported by Fry and Williams [56] and the level crossing lifetime measurements reported for $n=2$ and 3 by Burger and Lurio [57] would seem to be the most accurate optical determinations. To the best of our knowledge, no Beer-Lambert law photoabsorption measurements have been reported for the helium discrete transitions, probably due to the bandwidth/linewidth difficulties or "line-saturation" effects discussed in section 2.3. Such effects would be particularly difficult to avoid for the intense and extremely narrow lines in the helium resonance series. The self-absorption method used by Jongh and Eck [62], Westerveld and Eck [63] and Tsurubuchi *et al.* [64] is not subject to "line saturation" effects but unfortunately like most other optical methods it is restricted in its application to the lower n values. A further interesting check on the presently reported data is the integrated oscillator strength for the discrete region up to the first ionization threshold. The value of 0.431

obtained in the present work is in good agreement with earlier estimates of 0.424 [6], 0.421 [85] and 0.427 [85].

4.2.2.2 The Autoionizing Excited State Resonances

The energies and profiles of the well-known autoionizing doubly excited state resonances of helium in the 59–72 eV energy region have been previously studied in some detail both experimentally [94–97,107] and theoretically [98–100,108]. In the present work, this region containing the autoionizing resonances was remeasured using the HR dipole (e,e) spectrometer at medium resolution. By dividing the HR electron energy loss spectrum at each energy loss in the smooth regions of the continuum by the absolute optical oscillator strength measured by the LR dipole (e,e) spectrometer (see section 4.2.1, table 4.1 and figure 4.1) values of B_{HR} in the energy region of the autoionizing resonances were obtained. A fitted curve through these points permitted interpolated values of B_{HR} to be obtained in a continuous form throughout the resonance region. The Bethe–Born converted relative optical oscillator strength spectrum was normalised in the smooth continuum region at 75 eV using the absolute photoabsorption oscillator strength data from table 4.1, as determined by the LR dipole (e,e) spectrometer. The present results for the absolute optical oscillator strengths throughout the region of the autoionizing doubly excited state resonances below the $He^+(2s)$ and $He^+(3s)$ thresholds are shown in figures 4.3(a) and (b) respectively.

In figure 4.3(a) the absolute oscillator strengths for the autoionizing resonances below the $He^+(2s)$ threshold calculated by Fernley *et al.* [9]

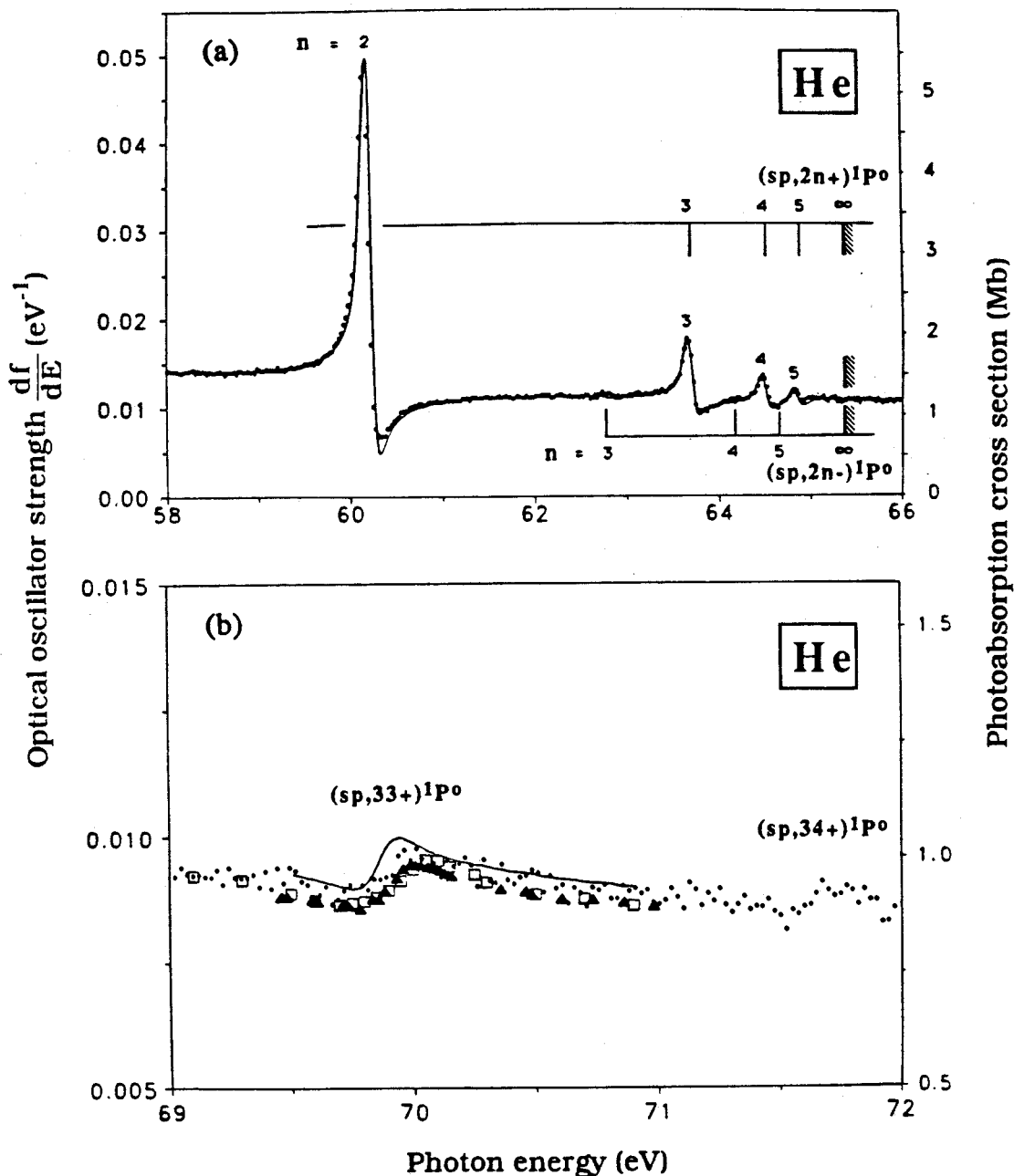


Figure 4.3: Absolute dipole oscillator strengths for helium in the autoionizing resonance regions measured by the high resolution electron energy loss spectrometer. (a) in the energy region 58–66 eV; solid circles are this work, solid line is data from Fernley *et al.* [9] (convoluted with the present experimental bandwidth of 0.115 eV), (b) in the energy region 69–72 eV; solid circles are this work, solid triangles are data of Kossmann *et al.* [97], open squares are data of Lindle *et al.* [96], solid line is theory, Gersbachber *et al.* [99].

(solid line) have been convoluted with a Gaussian of 0.115 eV FWHM, which was used to represent the experimental energy resolution. The energy scale of the data calculated by Fernley *et al.* [9] has been shifted by +0.280 eV to give a correct energy scale. It can be seen that there is generally excellent agreement in both the shapes and magnitudes of the resonances between the convoluted calculations of Fernley *et al.* [9] (solid line) and the present experimental work (dots) except for the minimum of the (sp,22+) $^1P^o$ state. Slight differences in the energies of the maxima of the resonances are also observed. The energies of the maxima of the (sp,2n+) $^1P^o$ resonances for n=2 to 5 have been determined in the present work to be 60.150, 63.655, 64.465 and 64.820 eV respectively. These values are in good agreement with previous experimental determinations [94,95,97,98,100].

The autoionizing resonances (sp,33+) and (sp,34+) $^1P^o$ were also observed in the present work. In figure 4.3(b), the present data (dots) is compared with other experimental results by Lindle *et al.* [96] (open squares) and by Kossmann *et al.* [97] (solid triangles) both of whom normalised their results at 68.9 eV using the Marr and West tabulated data [47]. The solid line on figure 4.3(b) represents theoretical values calculated by Gersbacher *et al.* [99].

4.3 Conclusions

The present high resolution dipole (e,e) measurements of optical oscillator strengths for the discrete excitation transitions ($1^1S \rightarrow n^1P$, n=2-7), the autoionizing doubly excited state resonances and also the photoionization continuum have considerably extended the range of

measured absolute oscillator strength data for the photoabsorption of helium. The presently reported results are all in excellent quantitative agreement with state of the art quantum mechanical calculations carried out using correlated wavefunctions [4–9] and are consistent with most optical and other measurements for those few transitions where previous experimental data were available. These findings confirm the validity of the Bethe–Born approximation and the suitability of the high resolution dipole (e,e) method using TRK sum rule normalization for general application to the measurement of optical oscillator strengths for discrete electronic excitations and ionization in atoms and molecules. The dipole (e,e) method therefore provides a versatile and accurate means of oscillator strength measurement across the entire valence shell region at high resolution and does not suffer from the problems of "line-saturation" (bandwidth) effects that can complicate Beer–Lambert law photoabsorption studies for discrete transitions.

Chapter 5

Absolute Optical Oscillator Strengths for the Electronic Excitation of Neon

5.1 Introduction

Absolute optical oscillator strengths for discrete and continuum electronic excitation of neon are important quantities in areas such as radiation physics, plasma physics and astrophysics. For instance, Auer and Mihalas [109] have used Ne I oscillator strength data to re-evaluate the abundances of neon in the B stars. Recently there has also been strong interest in the energy levels and oscillator strengths of neon-like systems because of their application in the development of soft X-ray lasers [110]. Discrete oscillator strengths also provide a sensitive test for atomic structure calculations, since the simple LS and j-j coupling schemes are not strictly applicable for neon and some sort of intermediate coupling scheme must be used instead [111]. In contrast to the situation for helium, the photoionization cross section maximum of neon is not at threshold, showing a significant departure from hydrogenic behavior due to more prominent electron correlations. Cooper [104] has calculated the oscillator strength distribution for the outer atomic subshell of neon by assuming an electron moving in an effective central potential similar to the Hartree-Fock potential. McGuire [112], approximating the Herman-Skillman central field with a series of straight lines, has computed the photoionization cross section of neon with the continuum orbitals calculated from the approximate potential. Kennedy

and Manson [113], utilizing Hartree-Fock wave functions with complete exchange, Luke [114], employing a multi-configuration close coupling method for the wavefunctions, Burke and Taylor [115], using the R-matrix theory, and Amus'ya *et al.* [116] applying the RPAE (random-phase approximate with exchange) method have also calculated photoionization cross sections for neon. Relativistic random-phase approximation (RRPA) calculations carried out by Johnson and Cheng [117] showed that relativistic effects are small in neon and gave results in good agreement with the non-relativistic RPAE results of Amus'ya *et al.* [116]. Parpia *et al.* [118] have also reported the photoionization cross sections of the outer shells of neon using the relativistic time-dependent local-density approximation (RTDLDA) method, which is closely related to the RRPA method of Johnson and Cheng [117]. Although the calculated values are much improved with the inclusion of electron correlation, some discrepancies (>15%) still exist between the experimental [21,23,45,47,102,103,119-123] and theoretical [104-118] photoionization cross sections in certain energy ranges.

Experimental total photoabsorption and photoionization measurements for neon in the continuum performed using the Beer-Lambert law [45,47,102,103,119-122] show good agreement with each other in terms of the shape (i.e. relative cross section). However, the various reported values of the absolute cross sections in the continuum show substantial differences (~10%), probably due to difficulties in obtaining sufficiently precise measurements of the sample target density in a 'windowless' far UV system. In addition, inadequately accounted for contributions from stray light and/or higher order radiation will affect measured cross sections. Lee and Weissler [119], and Ederer and

Tomboulian [120] have measured the photoabsorption cross section of neon using discharge lamp line sources in the energy ranges 15.5–54, and 20–155 eV respectively. Lee and Weissler [119] recorded the absorption photometrically in a grazing incidence vacuum spectrograph. Ederer and Tomboulian [120] have made measurements combining the conventional photographic recording method with a Geiger–Müller counter for selected wavelengths. Samson [45,121,122] has designed an extremely effective double ion chamber technique which is capable of measuring very accurate photoionization cross sections using either line or continuum sources. Using this apparatus Samson [45,121,122] has reported measurements for neon in the range 21.6–310 eV. Saxon [124] reviewed the limited neon photoabsorption data available in 1973 and provided a sum rule analysis which suggested that the measured cross sections were reasonably accurate. Wuilleumier and Krause [125] derived 2p, 2s and 1s subshell partial photoionization cross sections by combining photoelectron branching ratio studies using x-ray line sources with existing total photoabsorption measurements. In addition contributions from multiple ionization were estimated [125]. With the advance of synchrotron radiation (SR), an intense and continuous light source became available for measuring the photoionization cross sections of atoms and molecules up to high energies. However with SR sources very careful work is required to correct for the effects of contributions from stray light and higher order radiation on absolute cross section measurements [126–128]. Watson [102] obtained photoionization cross sections for neon in the 60–230 eV photon energy range. West and Marr [103] not only used synchrotron radiation to make absolute absorption measurements for neon over the range 36–310 eV, but also gave a critical

evaluation of existing published cross section data and obtained recommended weighted-average values [47] throughout the vacuum ultraviolet and X-ray region. Electron impact based techniques [21,23,123] have also been employed to obtain photoionization cross sections of neon. By approximating the generalized oscillator strength ($f(\mathbf{K},E)$ where \mathbf{K} =momentum transfer and E =energy) as the optical oscillator strength ($f^o(E)$) using an impact energy 500–1000 eV and collecting the inelastically scattered electrons at small angles, Kuyatt and Simpson [123] converted the electron energy loss spectrum of neon (up to 100 eV energy loss) to a *relative* photoabsorption cross section curve. Using high electron impact energy (10 keV) and the calculated scattering geometry of the beam to obtain the relative Bethe–Born factor, electron energy loss results at small momentum transfer have been converted to relative photoionization cross sections for neon by Van der Wiel [21]. Van der Wiel and Wiebes [23] have also studied multiple photoionization of neon using the same method. The relative optical oscillator strength data obtained by the electron impact methods described above were normalized using a literature value of the absolute photoabsorption cross section at a single energy.

Apart from the difficulty of measuring an accurate sample density, Beer–Lambert law photoabsorption measurements for the discrete excitation region of neon may also be subject to serious errors due to so-called "line-saturation" (i.e. bandwidth) effects [36,37,46,72] (see chapter 2) since the neon valence shell (2p) electronic transitions have extremely narrow natural line-widths [65,129–137]. These effects are most significant when the cross section is large and where the bandwidth of the incident radiation is greater than the natural line-widths of the

spectral lines being measured. In such situations the oscillator strengths (cross sections) may be much smaller (by as much as an order of magnitude) than the true values unless careful measurements are made as a function of pressure [37,46]. Detailed discussions and quantitative assessments of "line saturation" effects have been given in refs. [37,46]. Other experimental methods for optical oscillator strength determination which avoid the "line saturation" problems include profile analysis [129,138], self absorption [62,139,140], total absorption [65], and lifetime measurements [130–137], as well as the completely independent approach afforded by electron impact based methods using electron energy loss spectroscopy [20,36,37,141,142]. These various optical and electron impact methods have been used in earlier reported work to obtain absolute optical oscillator strengths for neon in the discrete region, but the measurements have been mainly restricted to the 16.671 eV (f_1) and 16.848 eV (f_2) resonance lines corresponding to the ($2s^22p^6 \rightarrow 2s^22p^5(2P_{3/2,1/2})3s$) transitions. Korolev *et al.* [129] measured the transition probability of the f_2 line from the natural broadening profile, while Lewis [138] studied the pressure broadening profile and gave the oscillator strengths for both the f_1 and f_2 resonance lines. The relative self-absorption method was used by Jongh and Eck [62] to measure the oscillator strength of the f_2 resonance line using the calculated oscillator strength of the helium $1^1S \rightarrow 2^1P$ line as a reference. Westerveld *et al.* [139] and Tsurubuchi *et al.* [140] used the absolute self-absorption method to determine the oscillator strengths of the f_1 and f_2 resonance lines. Aleksandrov *et al.* [65] employed the total-absorption method to obtain oscillator strengths for various lines in the 20–80nm (15.5–62 eV) range. Radiative lifetimes for some of the resonance

transitions of neon have been determined using: a) a pulsed electron source for excitation and studying the resulting photon decay curve [130,131]; b) the beam foil method [132,133]; c) the level-crossing technique [134]; d) the phenomena of hidden alignment [135]; e) relaxation upon polarized laser irradiation in a magnetic field [136,137]. Knowing the branching ratios for the resonance lines, the obtained lifetimes can then be converted to the optical oscillator strengths for the respective transitions. In electron impact based studies, Geiger [20] obtained the sum of the absolute photoabsorption oscillator strengths for the f_1 and f_2 resonance lines at low resolution by measuring both the electron elastic scattering cross section and the small-angle inelastic scattering cross section at very high impact energy (25 keV) and normalising on known absolute values of the elastic scattering cross section. Later, Geiger [141] obtained the ratio (f_2/f_1) of the oscillator strengths of the resonance lines using a high resolution electron energy loss spectrometer, and by combining the values obtained from the low resolution spectrometer with this ratio he obtained values for the individual oscillator strengths for the two resonance lines. The electron impact method has also been employed by Natali *et al.* [142] to measure discrete optical oscillator strengths of neon. The unpublished results of Natali *et al.* [142] are quoted in refs. [139,143].

A variety of discrete oscillator strength calculations have been reported for neon. Cooper [104], employing a one electron central potential model, Kelly [144], using the Slater approximation to the Hartree-Fock method, and Amus'ya *et al.* [145], applying the RPAE method, have calculated the oscillator strengths for the transitions from the ground state of neon to the $2s^2 2p^5 ({}^2P_{3/2,1/2})ns$ and nd states. Other

calculations of the oscillator strengths for individual transitions from the ground state to various $2s^2 2p^5(2P_{3/2})ns$ and nd states, and also to $2s^2 2p^5(2P_{1/2})ns'$ and nd' states, have likewise been reported, but in most cases these are only for the transitions to the $2s^2 2p^5(2P_{3/2})3s$ (f_1) and $2s^2 2p^5(2P_{1/2})3s'$ (f_2) states. The oscillator strengths of the f_1 and f_2 resonance lines were calculated by Gold and Knox [146] using the Hartree Fock equation based on experimental energies and dipole matrix elements computed from theoretical atomic wavefunctions. Gruzdev [111], using the techniques of intermediate coupling and values of the transition integral obtained from the Coulomb approximation, has reported the oscillator strengths for the f_1 and f_2 resonance lines. Aymar *et al.* [147] calculated Ne I transition probabilities and lifetimes with the introduction of an effective operator for the angular part of the wavefunctions and a parametrized central potential for the radial part of the wavefunctions. Gruzdev and Loginov [148] carried out a calculation of the radiative lifetimes of several levels of neon with a many-configuration approximation using Hartree-Fock self-consistent field wavefunctions. Albat and Gruen [149] have reported the excitation cross section of the lowest resonance level of neon using a CI calculation based on the orthogonal set of orbitals obtained from a ground state Hartree-Fock calculation. The time dependent Hartree-Fock equations were also employed by Stewart [150,151] to study the excitation energies and bound-bound oscillator strengths for atoms isoelectronic with neon over a wide range of energies. Aleksandrov *et al.* [65] not only reported measurements for the discrete oscillator strengths of neon by the total-absorption method, but have also calculated oscillator strengths for the same discrete lines of neon based on an intermediate-coupling scheme

with the electrostatic, spin-orbit, and effective interactions included in the energy matrices. An examination of the various experimental [62,65,129–140] and theoretical [104,111,144–151] studies reveals a considerable spread in oscillator strength values for a given transition, even in the case of the intense f_1 and f_2 resonance lines of neon.

Recently, we have reported a new, highly accurate, electron impact method [36,37] (see chapters 2–4) for obtaining absolute photoabsorption oscillator strengths for discrete excitation processes over a wide spectral range at high resolution. In chapter 4, helium was used to check the accuracy of the new high resolution method [37]. Excellent agreement was found between experiment and theory for the He $1^1S \rightarrow n^1P$ ($n=2-7$) series as well as in the photoionization continuum and doubly excited state resonance regions [36,37]. The new high resolution dipole (e,e) method is now applied to the electronic transitions for neon. In this chapter, we also report measurements of the absolute photoabsorption continuum oscillator strengths up to 250 eV. The absolute scale has been obtained by TRK sum rule normalization and is thus completely independent of any direct optical measurement. The absolute (photoabsorption) oscillator strengths for the dipole-allowed electronic transitions of neon from the $2p^6$ subshell to lower members of the $2s^2 2p^5 ns$ and $2s^2 2p^5 nd$ ($^2P_{3/2,1/2}$) manifolds have been obtained from high resolution dipole (e,e) spectra of neon normalised on the low resolution results in the smooth continuum region. The present measurements are compared with other published experimental and theoretical data. Absolute optical oscillator strengths have also been obtained in the energy range 43–55 eV in the region of the Beutler-Fano autoionization resonance profiles arising from processes involving single

excitation of a valence 2s electron as well as processes due to double excitation of 2p electrons.

5.2 Results and Discussions

5.2.1 Low Resolution Measurements of the Photoabsorption

Oscillator Strengths for Neon up to 250 eV

A relative photoabsorption spectrum of neon was obtained by Bethe-Born conversion of an electron energy loss spectrum measured with the low resolution dipole (e,e) spectrometer from 15.7 to 250 eV. This was then least squares fitted to the function AE^{-B} over the energy range 120–250 eV, and extrapolation of the formula gave the relative photoabsorption oscillator strength for the valence shell from 250 eV to infinity. The fit gave $B=1.959$ and the fraction of the total valence shell oscillator strength above 250 eV was estimated to be 17.6%. The total area was then TRK sum rule normalized to a value of 8.34, corresponding to the number of valence electrons of neon (eight) plus a small correction (0.34) for Pauli excluded transitions [52,53]. Figure 5.1(a) shows the resulting absolute optical differential oscillator strengths for the photoabsorption of neon below 250 eV. Also shown in figure 5.1(a) are previously reported theoretical and experimental data from the literature [23,45,102,103,112,113,116,118,121,152]. Figure 5.1(b) is an expanded view (on an offset vertical scale) of the spectrum in the energy region 20–60 eV, where in addition to previous experimental data [23,45,47,103,121,152], theoretical oscillator strengths from refs. [112–116,118] are also shown for comparison. Numerical values of the

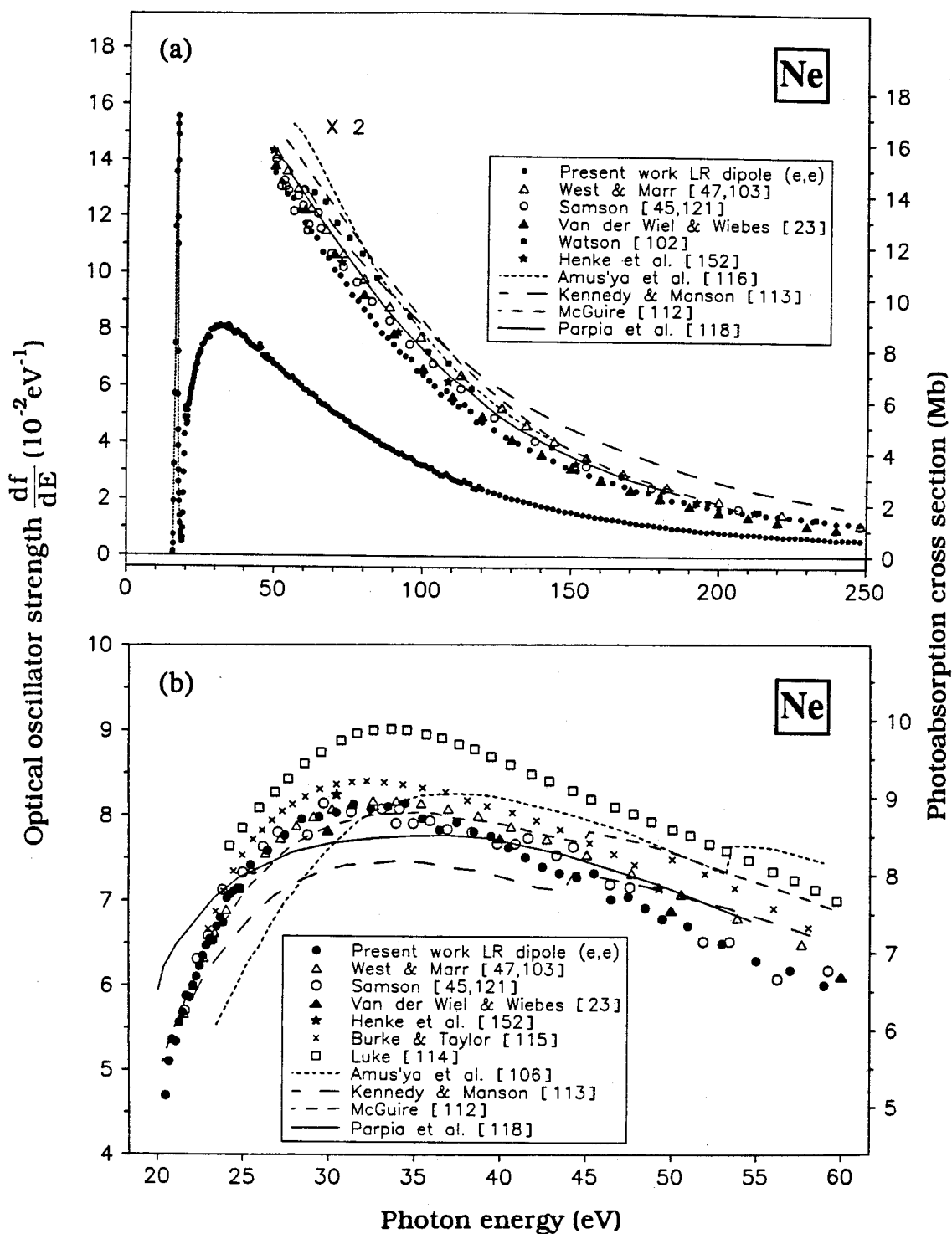


Figure 5.1: Absolute oscillator strengths for the photoabsorption of neon measured by the low resolution dipole (e,e) spectrometer (FWHM=1 eV). (a) 15.7–250 eV compared with other experimental [23,45,47,102,103,121,152] and theoretical [112,113,116,118] data. (b) Expanded view of the 20–60 eV energy region compared with other experimental [23,45,47,103,121,152] and theoretical [112–116,118] values. Note offset vertical scale.

absolute photoabsorption oscillator strengths for neon obtained in the present work from 21.6 to 250 eV are summarised in table 5.1.

From figures 5.1(a) and (b), it can be seen that the presently reported Bethe–Born converted, TRK sum rule normalized results obtained from the low resolution spectrometer are generally in quite good quantitative agreement with the measurements of Samson [45,121], the compilation data of Henke *et al.* [152] and the earlier electron impact based measurements by Van der Wiel and Wiebes [23]. The data of Samson [45,121] and Henke *et al.* [152] are slightly higher than the present work in the energy region 60–150 eV, while the results reported by Van der Wiel and Wiebes [23] are lower at energies above 180 eV. The photoionization oscillator strengths for neon measured by Watson [102] in the energy range 60–230 eV are larger than all other reported experimental data below ~200 eV but are in better agreement at higher energies. West and Marr [103] measured photoionization cross sections for neon in the energy range 36–310 eV using synchrotron radiation and gave a critical evaluation of several published cross section data (including the data of Samson [45,121] and Watson [102]) which they used to obtain "best weighted–average" values [47] throughout the vacuum ultraviolet and X–ray spectral regions. However the West and Marr measured and compiled values [47,103] are significantly higher than the present data and than the other experimental data from Samson [45,121], Henke *et al.* [152], and Van der Wiel and Wiebes [23] in the energy range 35–200 eV.

The calculated photoionization cross sections for neon generally show great differences in absolute values between calculations using the dipole–length and dipole–velocity forms. The dipole–length data have

Table 5.1

Absolute differential optical oscillator strengths for neon obtained using the low resolution (1 eV FWHM) dipole (e,e) spectrometer (21.6–250 eV)

Energy (eV)	Oscillator Strength (10^{-2}eV^{-1})	Energy (eV)	Oscillator Strength (10^{-2}eV^{-1})	Energy (eV)	Oscillator Strength (10^{-2}eV^{-1})
21.6	5.75	23.3	6.52	25.0	7.22
21.7	5.88	23.4	6.73	25.5	7.42
21.8	5.82	23.5	6.69	26.0	7.46
21.9	5.86	23.6	6.77	26.5	7.58
22.0	5.98	23.7	6.80	27.0	7.67
22.1	6.00	23.8	6.82	27.5	7.76
22.2	6.05	23.9	6.74	28.0	7.69
22.3	6.10	24.0	6.97	28.5	7.95
22.4	6.15	24.1	7.02	29.0	7.99
22.5	6.22	24.2	7.05	29.5	7.98
22.6	6.25	24.3	7.07	30.0	8.09
22.7	6.35	24.4	7.07	30.5	8.03
22.8	6.40	24.5	7.11	31.0	8.05
22.9	6.47	24.6	7.13	31.5	8.13
23.0	6.60	24.7	7.14	32.0	8.08
23.1	6.55	24.8	7.18	32.5	8.08
23.2	6.55	24.9	7.14	33.0	8.06

Table 5.1 (continued)

Energy (eV)	Oscillator Strength (10^{-2}eV^{-1})	Energy (eV)	Oscillator Strength (10^{-2}eV^{-1})	Energy (eV)	Oscillator Strength (10^{-2}eV^{-1})
33.5	8.10	43.5	7.32	57.0	6.17
34.0	8.00	44.0	7.29	58.0	6.08
34.5	8.14	44.5	7.27	59.0	5.99
35.0	8.08	45.0	7.45	60.0	5.86
35.5	7.96	45.5	7.32	61.0	5.83
36.0	7.88	46.0	7.06	62.0	5.71
36.5	7.83	46.5	7.01	63.0	5.69
37.0	7.90	47.0	6.96	64.0	5.59
37.5	7.92	47.5	7.04	65.0	5.43
38.0	7.86	48.0	6.91	66.0	5.35
38.5	7.80	48.5	6.91	67.0	5.31
39.0	7.73	49.0	6.89	68.0	5.24
39.5	7.76	49.5	6.78	69.0	5.13
40.0	7.72	50.0	6.75	70.0	5.03
40.5	7.62	51.0	6.70	71.0	4.99
41.0	7.52	52.0	6.59	72.0	4.93
41.5	7.50	53.0	6.49	73.0	4.88
42.0	7.42	54.0	6.37	74.0	4.78
42.5	7.39	55.0	6.29	75.0	4.73
43.0	7.35	56.0	6.30	76.0	4.59

Table 5.1 (continued)

Energy (eV)	Oscillator Strength (10^{-2}eV^{-1})	Energy (eV)	Oscillator Strength (10^{-2}eV^{-1})	Energy (eV)	Oscillator Strength (10^{-2}eV^{-1})
77.0	4.52	97.0	3.37	117.0	2.39
78.0	4.48	98.0	3.25	118.0	2.36
79.0	4.41	99.0	3.22	119.0	2.46
80.0	4.33	100.0	3.19	120.0	2.36
81.0	4.28	101.0	3.18	122.0	2.28
82.0	4.22	102.0	3.09	124.0	2.23
83.0	4.16	103.0	3.10	126.0	2.17
84.0	4.07	104.0	2.99	128.0	2.09
85.0	4.06	105.0	2.94	130.0	2.02
86.0	3.92	106.0	2.84	132.0	1.99
87.0	3.89	107.0	2.83	134.0	1.93
88.0	3.84	108.0	2.90	136.0	1.88
89.0	3.78	109.0	2.81	138.0	1.82
90.0	3.72	110.0	2.71	140.0	1.77
91.0	3.65	111.0	2.67	142.0	1.73
92.0	3.59	112.0	2.63	144.0	1.69
93.0	3.60	113.0	2.59	146.0	1.62
94.0	3.51	114.0	2.67	148.0	1.58
95.0	3.44	115.0	2.58	150.0	1.57
96.0	3.46	116.0	2.55	152.0	1.52

Table 5.1 (continued)

Energy (eV)	Oscillator Strength (10 ⁻² eV ⁻¹)	Energy (eV)	Oscillator Strength (10 ⁻² eV ⁻¹)	Energy (eV)	Oscillator Strength (10 ⁻² eV ⁻¹)
154.0	1.46	194.0	0.915	234.0	0.649
156.0	1.44	196.0	0.887	236.0	0.635
158.0	1.39	198.0	0.906	238.0	0.614
160.0	1.38	200.0	0.857	240.0	0.596
162.0	1.32	202.0	0.848	242.0	0.612
164.0	1.31	204.0	0.826	244.0	0.595
166.0	1.29	206.0	0.823	246.0	0.607
168.0	1.25	208.0	0.786	248.0	0.581
170.0	1.21	210.0	0.792	250.0	0.572
172.0	1.16	212.0	0.791		
174.0	1.14	214.0	0.771		
176.0	1.13	216.0	0.736		
178.0	1.11	218.0	0.740		
180.0	1.08	220.0	0.724		
182.0	1.06	222.0	0.700		
184.0	1.00	224.0	0.703		
186.0	1.00	226.0	0.706		
188.0	0.981	228.0	0.678		
190.0	0.971	230.0	0.684		
192.0	0.929	232.0	0.649		

$$\sigma \text{ (Mb)} = 1.0975 \times 10^2 \frac{df}{dE} \text{ eV}^{-1}$$

better agreement with the experimental values than the dipole-velocity data. The dipole-length data of McGuire [112], obtained using the Hartree-Fock-Slater approach with the Herman-Skillman central field, show good agreement with the present experimental values from the 2p ionization threshold to 35 eV, but are significantly higher in the region 35-210 eV. Kennedy and Manson [113], employing Hartree-Fock functions with complete exchange, have also reported calculations of the photoionization cross sections of neon from the 2p ionization threshold up to 400 eV. Their dipole-length data [113] give lower results below the 2s threshold and become much higher at higher energies when compared with the present experimental values. Both the McGuire [112] and Kennedy and Manson [113] data show a lower calculated 2s threshold energy than other theoretical [115] and experimental [153,154] work. The dipole-length data calculated using a Hartree-Fock core as reported by Luke [114] (see figure 5.1(b)) are considerably higher than all other reported experimental and theoretical data. The R-matrix theory dipole-length results of Burke and Taylor [115] show good agreement with the experimental values at the 2p ionization threshold but agreement becomes worse at higher energies, although below the 2s ionization threshold there is less than 10% difference with the experimental values (note offset intensity scale in figure 5.1(b)). Amus'ya *et al.* [116], using the RPAE method, report very close agreement between the dipole-length and dipole-velocity results. However the RPAE calculation [116] shows a shift of several electron-volts from experiment in the photoionization cross section maximum and also the energy of the 2s ionization threshold for neon. The predicted oscillator strengths [116] are also considerably larger than experiment in the energy region 40-100

eV. Since the values calculated by Johnson and Cheng [117] using the RRPA method show good agreement with those calculated by Amus'ya *et al.* [116] using the non-relativistic RPAE method, only values from Amus'ya *et al.* [116] are shown on figure 5.1. Except in the region near the maximum, the values calculated by Parpia *et al.* [118] using the RTDLDA method show better agreement with experiment than the other theoretical data [112–117].

5.2.2 High Resolution Measurements of the Photoabsorption Oscillator Strengths for the Discrete Transitions of Neon Below the 2p Ionization Threshold

High resolution electron energy loss spectra of neon at resolutions of 0.048, 0.072 and 0.098 eV FWHM in the energy range 16–26 eV were multiplied by the appropriate B_{HR} functions for the high resolution dipole (e,e) spectrometer (see section 3.3) to obtain relative optical oscillator strength spectra which were then normalized in the smooth continuum region at 25 eV using the absolute data of table 5.1, as determined in the present work with the low resolution spectrometer. Figure 5.2(a) shows the typical absolute differential optical oscillator strength spectrum of neon over the range 16–26 eV at an energy resolution of 0.048 eV FWHM. Figure 5.2(b) is an expanded view of the spectrum in the energy region 19.5–22 eV showing the dipole-allowed electronic transitions from the $2s^2 2p^6$ configuration of neon to members of the $2s^2 2p^5 ({}^2P_{3/2,1/2}) ns$ and nd manifolds. Very small peaks, barely visible at 18.96 and 20.38 eV, represent contributions from the dipole forbidden $2s^2 2p^6 \rightarrow 2s^2 2p^5 ({}^2P_{3/2,1/2}) 3p$ and $4p$ transitions respectively. These non-

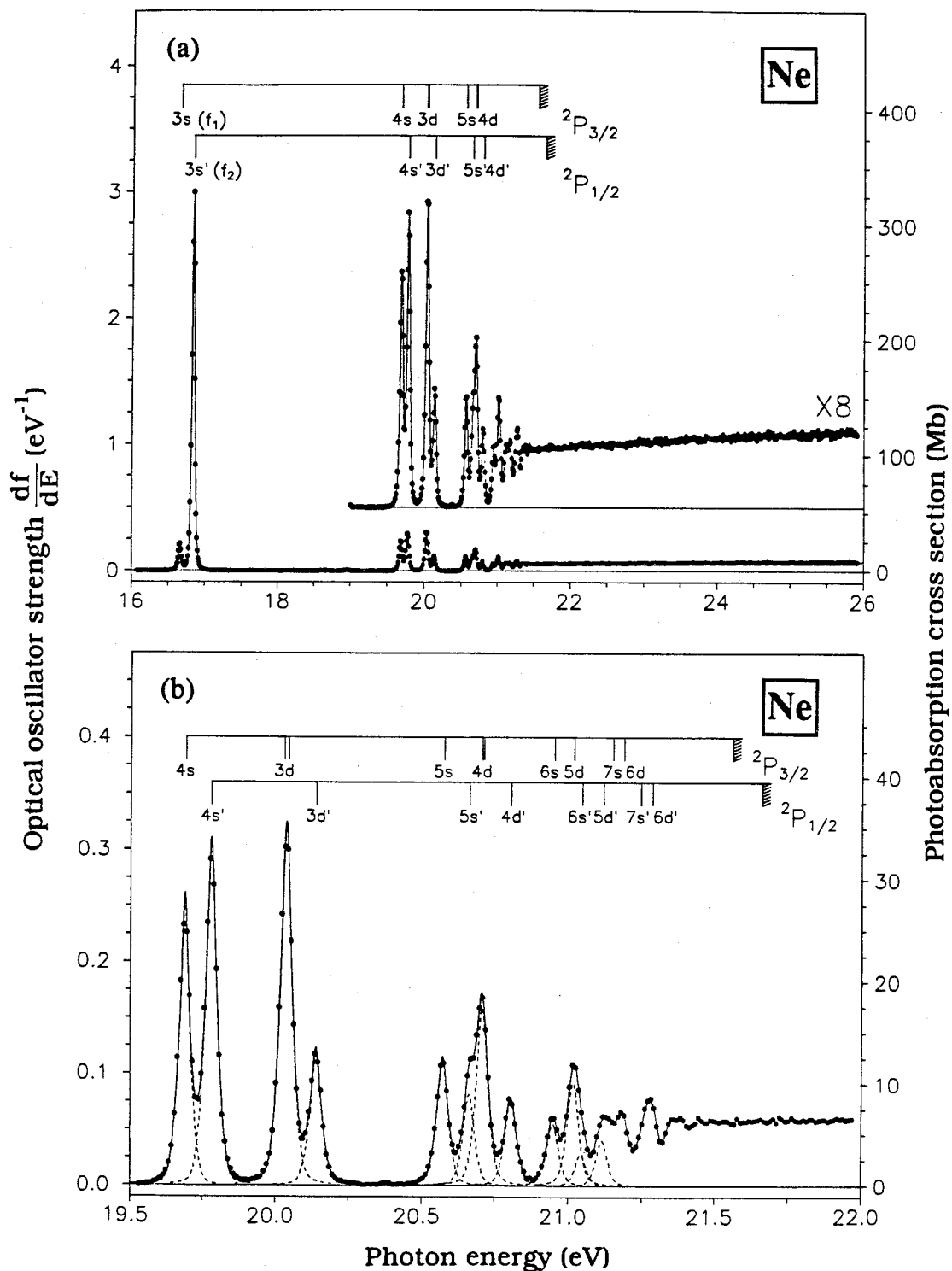


Figure 5.2: Absolute oscillator strengths for the photoabsorption of neon measured by the high resolution dipole (e,e) spectrometer (FWHM=0.048 eV). Assignments are from reference [155]. (a) 16–26 eV. (b) 19.5–22 eV with deconvoluted peaks shown as dashed lines.

dipole transitions which occur because of the finite but very small momentum transfer ($K^2 < 0.01 \text{ a.u.}$) of the dipole (e,e) experiment, are all less than 0.3 percent of the f_2 peak. The positions and assignments [155] of the various members of the nl and nl' series are indicated on figure 5.2. Above 19 eV the peaks have been deconvoluted as indicated (figure 5.2(b)) to obtain the separate oscillator strengths for the various transitions. Since the peak energies of the $nd[1/2]$ and $nd[3/2]$ states which converge to the same ${}^2P_{3/2}$ limit are very close, especially at higher n values, the two transitions have been treated as single peak in the deconvolution.

For peaks in the experimental spectrum which can be completely resolved such as the f_1 and f_2 resonance lines (i.e. the $3s, 3s'$ lines, figure 5.2(a)), integration of the peak areas provides a direct measure of the absolute optical oscillator strengths for the individual discrete electronic transitions. For the higher energy peaks which cannot be completely resolved, absolute oscillator strengths have been obtained from the deconvoluted peak areas as shown in figure 5.2(b). The accuracy of the presently developed method is confirmed by the consistency of the oscillator strengths determined for given transitions at the three different resolutions. The results obtained from the analysis of the spectrum at the highest resolution (0.048 eV FWHM) are given in tables 5.2, 5.3 and 5.4. The uncertainties are estimated to be $\sim 5\%$ for the lower energy resolved transitions and $\leq 10\%$ for those such as $6s, 6s', 5d$ and $5d'$ at higher energies due to additional errors involved in deconvoluting the peaks. Also shown in tables 5.2, 5.3 and 5.4 are the absolute oscillator strength values for several discrete electronic

Table 5.2

Theoretical and experimental determinations of the absolute optical oscillator strengths for the $2s^22p^6 \rightarrow 2s^22p^5(^2P_{3/2,1/2})3s$ discrete transitions of neon†

	Oscillator strength for transition from $2s^22p^6 \rightarrow 2s^22p^5m$ where $m =$	
	$[^2P_{3/2}]3s$ (f_1)	$[^2P_{1/2}]3s'$ (f_2)
A. Theory:		
Amus'ya (1990) [145]	0.163*	
Kelly (1964) [144]	0.188*	
Cooper (1962) [104]	0.163*	
Aleksandrov <i>et al.</i> (1983) [65]	0.0106	0.141
Stewart (1975) [150]		0.159
Albat and Gruen (1974) [149]	0.0113	0.149
Gruzdev and Loginov (1973) [148]	0.0106	0.139
Aymar <i>et al.</i> (1970) [147]		
(a) dipole length	0.0121	0.161
(b) dipole velocity	0.0100	0.130
Gruzdev (1967) [111]	0.035	0.160
Gold and Knox (1959) [146]		
(a) wavefunction	0.011	0.110
(b) semi-empirical	0.012	0.121
B. Experiment:		
Present work (HR dipole(e,e))	0.0118	0.159
	(0.0006)	(0.008)
Tsurubuchi <i>et al.</i> (1990) [140]	0.0122	0.123
(Absolute self-absorption)	(0.0006)	(0.006)
Aleksandrov <i>et al.</i> (1983) [65]	0.012	0.144
(Total absorption)	(0.003)	(0.024)

Table 5.2 (continued)

	Oscillator strength for transition from $2s^2 2p^6 \rightarrow 2s^2 2p^5 m$ where $m =$	
	$[^2P_{3/2}]3s (f_1)$	$[^2P_{1/2}]3s' (f_2)$
B: Experiment: (continued)		
Westerveld <i>et al.</i> (1979) [139]	0.0109	0.147
(Absolute self-absorption)	(0.0008)	(0.012)
Bhaskar and Luro (1976) [134]	0.0122	0.148
(Lifetime: Hanle effect)	(0.0009)	(0.014)
Knystautas and Drouin (1974) [132]	0.0078	0.161
(Lifetime: Beam foil)	(0.0008)	(0.011)
Irwin <i>et al.</i> (1973) [133]		0.158
(Lifetime: Beam foil)		(0.006)
Natali <i>et al.</i> (1973) [142]	0.012	0.158
(Electron impact)		
Jongh and Eck (1971) [62]		0.134
(Relative self-absorption)		(0.010)
Kazantsev and Chaika (1971) [135]	0.0138	
(Lifetime: Hidden alignment)	(0.0008)	
Geiger (1970) [20,141]	0.009	0.131
(Electron impact)	(0.002)	(0.026)
Lawrence and Liszt (1969) [130]	0.0078	0.130
(Lifetime: Delay coincidence)	(0.0004)	(0.013)
Lewis (1967) [138]	0.012	0.168
(Pressure broadening profile)	(0.002)	(0.002)
Korolev <i>et al.</i> (1964) [129]		0.160
(Natural broadening profile)		(0.014)

†Estimated uncertainties in experimental measurements are shown in brackets.

*Total oscillator strength (f_1+f_2).

Table 5.3

Theoretical and experimental determinations of the absolute optical oscillator strengths for discrete transitions of neon (19.5–20.9 eV)[†]

	Oscillator strength from $2s^2 2p^6 \rightarrow 2s^2 2p^5 m$ where m is							
	($2P_{3/2}$)4s	($2P_{1/2}$)4s'	($2P_{3/2}$)3d	($2P_{1/2}$)3d'	($2P_{3/2}$)5s	($2P_{1/2}$)5s'	($2P_{3/2}$)4d	($2P_{1/2}$)4d'
A: Theory:								
Amus'ya (1990) [145]*	0.028		0.021					
Kelly (1964) [144]*	0.029		0.036		0.008		0.025	
Cooper (1962) [104]*	0.026		0.037		0.009		0.020	
Aleksandrov <i>et al.</i> (1983) [65]	0.0124	0.0160	0.0176	0.0064	0.0060	0.0043	0.0091	0.0041
Stewart (1975) [150]		0.0260	0.0238					
Gruzdev and Loginov (1973) [148]#	0.0121	0.0164		0.0081	0.0058	0.0046		
Klose (1969) [131]								
(i) IC and HFS						0.0032		
(ii) IC and CF						0.0037		
Klose (1969) [158]								
(i) IC and HFS		0.0156						
B: Experiment:								
Present work (HR dipole (e,e))	0.0129 (0.0006)	0.0165 (0.0008)	0.0186 (0.0009)	0.00665 (0.00033)	0.00637 (0.00032)	0.00461 (0.00023)	0.00944 (0.00047)	0.00439 (0.00022)
Aleksandrov <i>et al.</i> (1983) [65]	0.0145	0.0185	0.0222	0.0082	0.0083	0.0049	0.0147	0.005
(Total absorption)	(0.0035)	(0.006)	(0.0046)	(0.0029)	(0.0031)	(0.0017)	(0.0036)	(0.002)

Table 5.3 (continued)

	Oscillator strength from $2s^2 2p^6 \rightarrow 2s^2 2p^5 m$ where m is							
	$(2P_{3/2})4s$	$(2P_{1/2})4s'$	$(2P_{3/2})3d$	$(2P_{1/2})3d'$	$(2P_{3/2})5s$	$(2P_{1/2})5s'$	$(2P_{3/2})4d$	$(2P_{1/2})4d'$
B: Experiment: (continued)								
Westerveld <i>et al.</i> (1979) [139]	0.0128	0.0153		0.0064	0.0061	0.0042		
(Absolute self-absorption)	(0.0010)	(0.0012)		(0.0005)	(0.0005)	(0.0003)		
Ducloy (1973-74) [137]		0.0153						
(Lifetime: Laser irradiation)		(0.0030)						
Natali <i>et al.</i> (1973) [142]	0.013	0.016	0.017	0.006	0.006	0.0043	0.0085	0.0043
(Electron impact)								
Klose (1970) [131]						0.0040		
(Lifetime: Delay coincidence)						(0.0003)		
Lawrence and Liszt (1969) [130]								
(Lifetime: Delay coincidence) (1)	0.0086	0.0130	0.0217	0.0064	0.0057	0.0042		
	(0.0010)	(0.0020)	(0.0022)	(0.0010)	(0.0010)	(0.0010)		
(2)@	0.0134	0.0178		0.0068	0.0062	0.0048		
	(0.0010)	(0.0025)		(0.0010)	(0.0010)	(0.0010)		
Decomps and Dumont (1968) [136]		0.0164				0.00598		
(Lifetime: Laser irradiation)		(0.0020)				(0.00023)		

†Estimated uncertainties in experimental measurements are shown in brackets

*summed oscillator strength as indicated

#Lifetime data converted by Westerveld *et al.* [139] to oscillator strengths using transition probabilities reported in refs. [156] and [157]

@Recalculated by Westerveld *et al.* [139] using branching ratios reported in refs. [148], [156], and [157]

Table 5.4
Theoretical and experimental determinations of the absolute optical oscillator strengths for discrete transitions of neon (20.9–21.2 eV)[†]

	Oscillator strength from $2s^2 2p^6 \rightarrow 2s^2 2p^5 m$				Total to Ionization
	where m is				
	$(^2P_{3/2})6s$	$(^2P_{1/2})6s$	$(^2P_{3/2})5d$	$(^2P_{1/2})5d'$	
A: Theory:					
Kelly (1964) [144]*	0.003		0.018		
Cooper (1962) [104]*	0.004		0.011		
Aleksandrov <i>et al.</i> (1983) [65]	0.0031	0.0018	0.0050	0.0024	
B: Experiment:					
Present work (HR dipole (e,e))	0.00330 (0.00030)	0.00156 (0.00016)	0.00543 (0.00054)	0.00229 (0.00023)	0.292 (0.015)
Aleksandrov <i>et al.</i> (1983) [65] (Total absorption)	0.0045 (0.0019)	0.003 (0.001)			
Natali <i>et al.</i> (1973) [142] (Electron impact)					0.277

[†] Estimated uncertainties in experimental measurements are shown in brackets

*summed oscillator strength as indicated

transitions of neon reported in various other experimental [20,62,65,129–142] and theoretical [65,104,144–150] studies.

It can be seen (table 5.2) that there is very little variation in the oscillator strength values for the f_1 resonance line calculated by different theoretical approaches (0.010–0.012) and these results [65,111,146–149] correspond closely with the presently reported experimental value (0.0118). However, for the f_2 resonance line there is substantial variation in the calculated oscillator strengths (0.110 to 0.161). The dipole-length result reported by Aymar *et al.* [147], the result of Gruzdev [111] and the calculation by Stewart [150] all show good agreement with the presently reported experimental value (0.159) for f_2 . Other theoretical calculations [65,146–149] for the f_2 resonance line give lower oscillator strengths. Cooper [104], Kelly [144] and Amus'ya [145] have reported calculated summed ($f_1 + f_2$) oscillator strengths for transitions from $2s^2 2p^6$ to several $2s^2 2p^5 (2P_{3/2,1/2}) ns$ or nd states. For the $2p \rightarrow (3s+3s')$ transitions (table 5.2), the summed absolute optical oscillator strengths (i.e. $f_1 + f_2$) calculated by Cooper [104] and Amus'ya [145] are slightly lower while the value of Kelly [144] is slightly higher than the presently reported summed result (0.171). For the higher energy transitions (tables 5.3 and 5.4) such as $2p \rightarrow (4s+4s')$, all three calculations [104,144,145] give good agreement with the present work, while for the $2p \rightarrow (5s+5s')$ and $2p \rightarrow (6s+6s')$ transitions the data of Cooper [104] and Kelly [144] are slightly lower. For the $2p \rightarrow (3d+3d')$, $2p \rightarrow (4d+4d')$ and $2p \rightarrow (5d+5d')$ transitions the Cooper [104] and Kelly [144] data are significantly higher while the Amus'ya [145] data for the $2p \rightarrow (3d+3d')$ transitions are slightly lower when compared with the present experimental results. The calculated f_2 value reported by Gruzdev [111]

using intermediate coupling techniques is consistent with the presently reported value while the f_1 value is much higher than all the other values quoted in table 5.2. The calculated data reported by Aleksandrov *et al.* [65] using an intermediate-coupling scheme are more comprehensive and comparison with the presently reported experimental data is possible for individual transitions up to the 6s, 6s', 5d and 5d' states as shown in tables 5.2, 5.3 and 5.4. Immediately it can be seen that the calculated data of Aleksandrov *et al.* [65] are in good agreement with the presently reported values except for the f_1 and f_2 values for which their data are slightly lower. Gruzdev and Loginov [148] have calculated the radiative lifetimes of several transitions of neon using an intermediate type coupling and the Hartree-Fock self-consistent field method. Westerveld *et al.* [139] have converted the lifetime data of Gruzdev and Loginov [148] to oscillator strength values using transition probabilities reported by Gruzdev and Loginov in refs [156,157] and these values show good agreement with the present work for oscillator strength values of the 4s, 4s', 5s and 5s' lines, while their value for the 3d' line is slightly higher. Stewart [150], using fully-coupled time dependent Hartree-Fock equations, has reported calculated oscillator strength values for the 4s' and 3d lines which are considerably higher than the present experimental results. Klose [131], using intermediate coupling and a Hartree-Fock-Slater calculation (IC-HFS), and intermediate coupling and the central field approximation (IC-CF), has reported two oscillator strength values for the 5s' line but both values are considerably lower than the presently reported experimental values. In a second paper, Klose [158] reported an oscillator strength for the 4s' line from an IC-

HFS calculation which is slightly lower than the present experimental result.

Turning now to a consideration of the various experimental results, it can be seen from tables 5.2, 5.3 and 5.4 that the presently reported data are in very good agreement over the whole discrete region with the earlier electron impact based results of Natali *et al.* [142]. The latter unpublished results [142] have been quoted in references [139] and [143]. The high resolution data reported by Aleksandrov *et al.* [65], using the total absorption method, have rather large uncertainties and agreement with the present data is good for the f_1 and f_2 resonance lines but generally poorer for the higher transitions. The measured absolute oscillator strengths [65] for the discrete transitions at higher energy are significantly higher than those determined in the present work (see tables 5.3 and 5.4). The self-absorption method was used by three groups [62, 139, 140] and the reported values range from 0.123 to 0.147 for the absolute oscillator strength of the f_2 resonance line. All these values are lower than the present value of 0.159. Agreement between different groups using the self-absorption method is generally better for the f_1 resonance line where the value of Tsurubuchi *et al.* [140] is consistent with the present work, and that obtained by Westerveld *et al.* [139] is slightly lower but still within the quoted uncertainty. Westerveld *et al.* [139] have also measured oscillator strengths for the transitions from the ground state to the $2s^2 2p^5(2P_{3/2})4s$ and $5s$ states, and also to the $2s^2 2p^5(2P_{1/2})4s'$, $5s'$ and $3d'$ states. Their results [139] for these transitions all show very good agreement with the present work.

Lifetime measurements using various experimental procedures [130–137] show good agreement for the absolute oscillator strength of

the f_2 resonance line with the present data, with the exception of ref. [130] which is ~20% lower. For the f_1 resonance line the result of Kazantsev and Chaika [135] is somewhat higher and the values reported by Knystautas and Drouin [132], and by Lawrence and Liszt [130] are much lower than most other reported values which are in close agreement with the present work. In the case of discrete transitions at high energy (table 5.3), the Lawrence and Liszt [130] values are slightly lower than the present work except for the transitions to the $2s^2 2p^5(2P_{3/2})3d$ and $2s^2 2p^5(2P_{1/2})3d'$ states. Westerveld *et al.* [139] have re-evaluated the lifetime data of Lawrence and Liszt [130] using the transition probabilities calculated by Gruzdev and Loginov [148,156,157] and it is note-worthy that the re-evaluated oscillator strength values are in all cases in better agreement with the present work. The absolute oscillator strength for the $5s'$ line determined by Klose [131] using a delayed coincidence method is slightly lower than the present value while that determined by Decomps and Dumont [136] is ~33% higher. For the $4s'$ line, the values of Decomps and Dumont [136] and Ducloy [137] are both consistent with the presently reported experimental measurement.

With the use of a high resolution electron impact spectrometer, Geiger [141] measured the intensity ratio of the f_2/f_1 resonance lines giving a value consistent with the ratio derived from the present data. However, the total absolute optical oscillator strength sum for the two resonance lines obtained [141] in Geiger's earlier work [20], which was normalized on the elastic electron scattering cross section, is about 20% lower than the presently reported value. The absolute oscillator strengths obtained from line profile analysis for f_1 and f_2 by Lewis [138] and for f_2 by

Korolev *et al.* [129] are in good agreement (see table 5.2) with the present work. Finally, the total discrete oscillator strength sum up to 21.616 eV, which is the middle point between the $2P_{3/2}$ and $2P_{1/2}$ ionization thresholds of neon, has been determined in the present work to be 0.292 compared with estimates of 0.277 reported by Natali *et al.* [142] and 0.4 reported by West and Marr [103]. The latter value would seem to be too high.

5.2.3 High Resolution Photoabsorption Oscillator Strengths for Neon in the 40–55 eV Region of the Autoionizing Excited State Resonances

The spectroscopy (i.e. the energy levels) of the autoionizing excited state resonances of neon involving excitation of a 2s electron and also double excitation of 2p electrons, has been studied in some detail experimentally [65,154,159]. However, prior to the present quantitative work no detailed high resolution absolute intensity measurements have been reported for neon in this region. Similar absolute intensity measurements in the double excitation region for helium in excellent agreement with theory [9] have recently been reported from this laboratory for helium [37] (see section 4.2.2.2). In the present study, the electron energy loss spectrum in the 40–55 eV energy region of neon was measured with the use of the high resolution dipole (e,e) spectrometer at a resolution of 0.098 eV FWHM. This was then converted to a relative optical oscillator strength spectrum by multiplying with the B_{HR} function (see section 3.3). Normalization was performed in the smooth continuum region at 55 eV using the absolute optical oscillator strength

data given in table 5.1, as determined by the low resolution dipole (e,e) spectrometer. The present high resolution absolute dipole oscillator strengths (solid circles) are shown in figure 5.3. The few photoabsorption (absolute) data points earlier reported by Samson [45,121] in this region are seen from figure 5.3 (open circles) to be reasonably consistent with the present high resolution dipole (e,e) results.

As shown in figure 5.3, the energies (± 0.005 eV) of the maxima of the transitions corresponding to excitation of the 2s electrons to np subshells with $n=3$ to 6, and the double excitation transition of 2p electrons to the 3s3p configuration of neon have been determined in the present work to be 45.550, 47.127, 47.677 and 47.975, and 44.999 eV respectively. These energies are in good agreement with the high resolution experimental studies reported by Codling *et al.* [154] and by Aleksandrov *et al.* [65], as well as with the multi-configuration close coupling calculations of Luke [114]. For peaks observed at higher energies in the present work, the assignments and energy positions of the excited state resonances shown in figure 5.3 are taken from the photoabsorption data reported by Codling *et al.* [154]. A small peak (X) at 43.735 eV has not been reported in previous photoabsorption measurements [65,154,159], but it should be noted that the published spectra in all of these measurements did not extend below 44 eV. However, a threshold electron impact study by Brion and Olsen [160] and a lower electron impact energy (400 eV) study of the ionization continuum of neon by Simpson *et al.* [161] also detected a peak at ~ 43.7 eV and it was suggested that this was probably due to excitation to the $2s2p^63s$ state which had earlier been reported [162] to be at 43.65 eV.

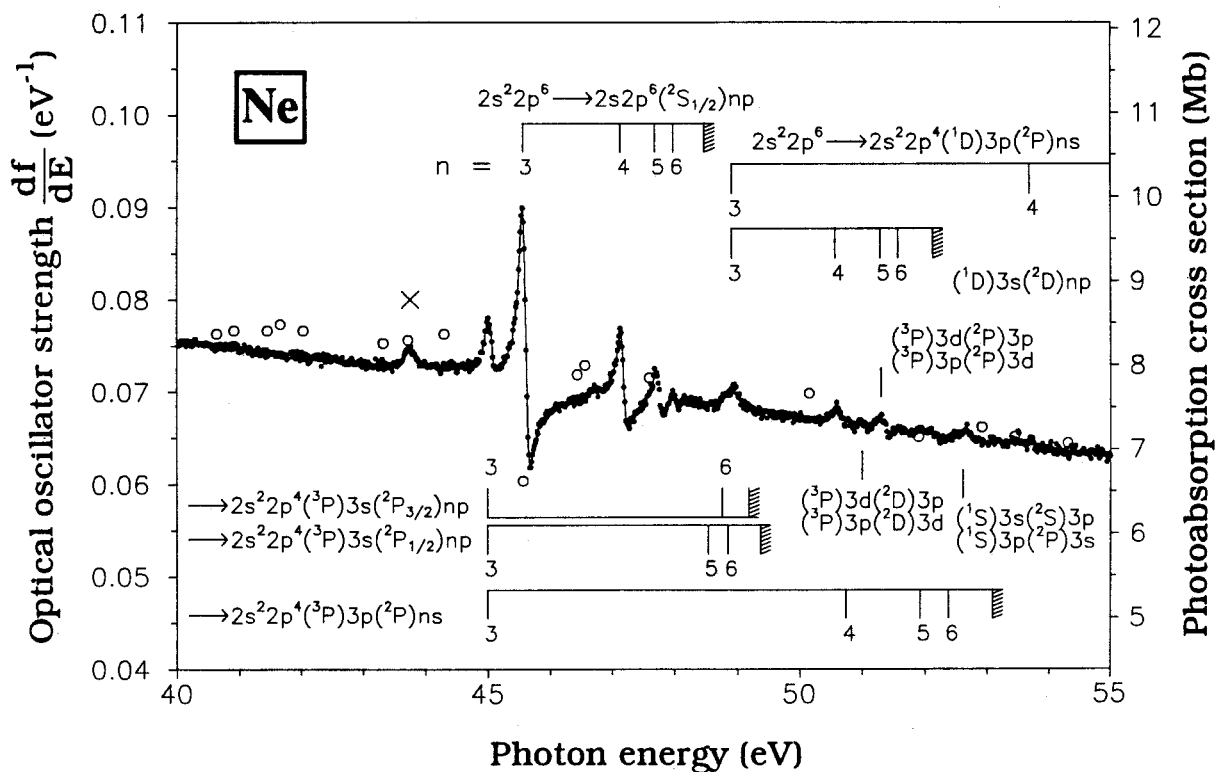


Figure 5.3: Absolute oscillator strengths for the photoabsorption of neon in the autoionizing resonance region 40–55 eV (FWHM=0.098 eV) measured by the high resolution dipole (e,e) spectrometer. Solid circles are this work and open circles are photoabsorption data reported by Samson [45,121]. Assignments are from reference [154]. Note offset vertical scale.

However, it seems unlikely that the formally dipole forbidden transition $2s^22p^6 \rightarrow 2s2p^63s$ would be so prominent at the very low momentum transfer ($K^2 \approx 0.014$ a.u.) corresponding to the present experimental conditions of high impact energy (3 keV) and zero degree mean scattering angle. This peak at 43.735 eV is also too high in energy to be due to any double scattering processes involving below edge outer valence processes.

5.3 Conclusions

The present absolute oscillator strength data for neon, unlike the optical measurements, are subject to the stringent constraints of the TRK sum rule and are considered to be of high accuracy. Optical oscillator strengths for the discrete transitions involving valence 2p electrons and also for the photoionization continuum up to 250 eV have been measured for neon. The presently reported results were compared with theory and also with earlier reported experimental data, all of which are less comprehensive than the present work. The accuracy of the earlier unpublished electron impact data of Natali *et al.* [142] at lower impact energy (i.e. large momentum transfer) in the discrete region is confirmed. Unlike the situation for helium, theoretical calculations for the absolute oscillator strengths of neon in both the discrete and continuum regions show a wide spread of values. The present data provide a critical test for these quantum mechanical calculations throughout the spectrum and especially for the valence 2p discrete electronic excitations such as the f_1 and f_2 resonance lines. The first high resolution absolute optical oscillator strengths have been obtained

for the autoionizing excited state and doubly excited state resonance region (40–55 eV) involving 2s excitation and double excitation, and it is hoped that these measurements will stimulate calculation in this region.

Chapter 6

Absolute Optical Oscillator Strengths for the Electronic Excitation of Argon, Krypton and Xenon

6.1 Introduction

Similar to the situation for neon [104,112,113,115–118,163] (see chapter 5), the photoionization cross section maxima of argon and krypton [112,113,115–118,163,164] are shifted to energies above the ionization threshold, showing significant departure from the hydrogenic model. While this departure is not so obvious for xenon [113,116–118,163] it does nevertheless show significant non-hydrogenic behaviour. In addition minima (sometimes called Cooper minima) have been observed in the photoionization cross sections of argon, krypton and xenon [104,112,113,115–118,163–165]. Instead of using a pure Coulomb nuclear potential, Cooper [104], employing a more realistic potential similar to the Hartree-Fock potential for the outer subshell of each atom, and also both Manson and Cooper [165] and McGuire [112], starting with Herman-Skillman central potentials, have been able to theoretically reproduce the maxima above the threshold and also the existence of the minima in the photoionization cross sections starting from one-electron approximations. However the above calculations give narrower peaks shifted in energy relative to the experimental cross sections, with the cross sections at the peak maxima two or three times higher than the experimental values. The 4d shell in xenon is an example where significant discrepancies between experimental and

theoretical results have been observed. It has been found that electron correlation is important in many cases [113,115–118,163,164,166]. Starace [164] has computed the photoionization cross sections of argon and xenon starting from a local Herman–Skillman central field and including final–state correlation. Amus'ya *et al.* [116], employing the random–phase approximation with exchange (RPAE), Kennedy and Manson [113], using Hartree–Fock functions with exchange, Burke and Taylor [115], applying the R–matrix theory, and Zangwill and Soven [163], using density–functional theory, have also calculated the photoionization cross sections of the noble gas atoms. The relativistic random–phase approximation (RRPA) [117] and the relativistic time–dependent local–density approximation (RTDLDA) [118], two methods which are closely related, have also been applied to calculation of the photoionization cross sections of the outer shells of argon, krypton and xenon. Recently, Rozsnyai [166] has reported the photoionization cross sections of the 3p and 3d electrons in krypton and the 4d electrons in xenon based on a self–consistent Dirac–Slater model including the effect of the hole in the ionized shell. With the inclusion of electron correlation, the calculated photoionization cross sections [115–118,163] are generally in better agreement with experiment, however some discrepancies (>20%) still remain between the experimental and theoretical values in certain energy ranges.

Experimentally, photoabsorption and photoionization cross section measurements in the ionization continuum regions of argon, krypton and xenon have been widely performed using Beer–Lambert law photoabsorption and the double ion chamber methods [45,47,48,102,103,167–179]. Line–emitting light sources [45,167,169–

172,175,178,179] have most commonly been used. The Hopfield continuum [168,173], generated by a repetitive, condensed discharge through helium, provides a useful continuum source in the energy region 11.3–21.4 eV. With the advance of synchrotron radiation an intense and continuous light source has become available for measuring the photoionization cross sections of atoms and molecules up to high energies [47,48,102,103,174,176,177]. However, contributions from stray light and higher order radiation have to be carefully assessed and the measurements appropriately corrected if synchrotron radiation is to be used as the light source for accurate absolute cross section measurements [126–128]. Photographic plates [167,172], Geiger counters [172] (used at high energy), photomultiplier tubes [47,48,103,168,171,174] and channel electron multipliers [102,176,177] have been employed as detectors. Ionization chambers of different geometries have been constructed [45,173,176,178,179] and photoionization cross sections of the sample gases have been obtained from the length of the ion collector plates, the sample target density and the current flowing from the collector plates. These Beer–Lambert law measurements give good agreement for the individual noble gases in terms of the shapes of the continua. However the absolute values of the photoabsorption cross sections in the continua typically show substantial differences (~10%), especially at higher energies, due to difficulties in obtaining precise measurements of the sample target density in a 'windowless' far UV system and also due to contributions from stray light and/or higher order radiation. By using the dipole excitation associated with inelastic scattering of electron beams of high impact energy (10 keV) and small scattering angle, the single and multiple photoionization

of argon [22], krypton and xenon [180] has been studied using electron/ion coincidence techniques. Relative optical oscillator strengths were obtained [22,180] by Bethe–Born conversion of electron scattering data and absolute scales were established by normalizing at a single energy to previously published [45] absolute photoabsorption cross sections.

For the excitation of the heavier noble gas atoms in the discrete region, several theoretical oscillator strength calculations have been reported. Cooper [104], employing a one electron central potential model, and Amus'ya [145], applying the RPAE method, have calculated oscillator strengths for the transitions from the ground states to the $ms^2mp^5(2P_{3/2,1/2})ns$ and nd states where $n>m$ and m is 3, 4 and 5 for argon, krypton and xenon respectively. Calculations of the oscillator strengths for the separate transitions from the ground state to the $ms^2mp^5(2P_{3/2})ns$ and nd states, and the $ms^2mp^5(2P_{1/2})ns'$ and nd' states have also been reported [111,147,151,181–189], but mostly these calculations only give oscillator strengths for the $ms^2mp^5(2P_{3/2})(m+1)s$ and $ms^2mp^5(2P_{1/2})(m+1)s'$ states [111,147,181–183,151,186–189]. Theoretical discrete oscillator strength values have been reported by Knox [181] for argon, and Dow and Knox [182] for krypton and xenon. The first [181] set of data is based solely on solving the Hartree–Fock equations while the second [182] is based on experimental energies with the dipole matrix elements computed from the Hartree–Fock wavefunctions. Gruzdev [111] has reported the oscillator strengths of resonance lines in the spectra of Ar I, Kr I and Xe I atoms using the technique of intermediate coupling with the transition integral obtained from the Coulomb approximation. Kim *et al.* [183], using Hartree–Fock

wavefunctions without freezing of the core orbitals, have calculated the generalized oscillator strengths of the Xe I resonance lines, which in the optical limit gave optical oscillator strengths for these transitions. Aymar *et al.* [147] calculated Ar I, Kr I and Xe I transition probabilities and lifetimes using a least-squares fit procedure on energy levels for the angular part of the wavefunctions and a parametrized central potential for the radial part of the wavefunctions. Lee and Lu [184], who have determined three sets of parameters: eigen-quantum defects, transformation matrices and excitation dipole moments by fitting to experimental data, have reported a semi-empirical calculation of discrete oscillator strengths for argon. Later, Lee [185] calculated the same parameters by solving the many-electron Schrodinger equation for an atom within a limited spherical volume. The radiative lifetimes of the levels of Ar I [186] and Kr I [187] have been calculated by Gruzdev and Loginov using an intermediate coupling scheme with radial integrals obtained from Hartree-Fock functions. Albat *et al.* [188], carrying out Born and four-state "close coupling" calculations, have reported oscillator strengths for the low lying argon levels while Stewart [151], using simplified time-dependent Hartree-Fock calculations, has reported the oscillator strength for the ($3p^6\ ^1S \rightarrow 3p^5 4s\ ^1P$) transition of argon. Aymar and Coulombe [189] have computed the transition probabilities and lifetimes for Kr I and Xe I spectra using a central field model which takes into account intermediate coupling and configuration mixing.

Since the valence shell electronic transitions of noble gas atoms have extremely narrow natural line-widths, absolute oscillator strength measurements for the discrete regions of the argon, krypton and xenon photoabsorption spectra *via* the Beer-Lambert law are not viable since

significant errors may arise due to so-called "line-saturation" (i.e. bandwidth) effects. Detailed discussions of "line-saturation" effects and their implications for absolute photoabsorption oscillator strength (cross section) measurements have been given in refs. [36,37,46,72] (see chapter 2). Several alternative experimental methods for determining discrete optical oscillator strengths which avoid "line-saturation" problems have been reported. However, in most cases these methods are somewhat complex and also are often severely restricted in their range of application so that only a very few transitions can be studied for a given target [37]. In the cases of argon, krypton and xenon, other techniques which have been used include the self-absorption method [62,64,139,140], the total (optical) absorption method [190-192], the linear absorption method [193], refraction index determination [194], lifetime measurements [195-202], pressure-broadening profile analysis [138,203-206], phase-matching techniques [66,207], study of the electron excitation function [208] and electron impact methods [20,141,209-216]. The relative self-absorption method has been used by Jongh and Eck [62], while the absolute self-absorption method has been used by Westerveld *et al.* [139] and Tsurubuchi *et al.* [64,140]. Oscillator strengths for the resonance lines of krypton and xenon have been determined by Wilkinson [190,191], and Griffin and Hutcherson [192] using the total (optical) absorption method. Chashchina and Shreider [193] used the method of linear absorption and reported oscillator strengths for the resonance lines of krypton, while in a further paper they reported the oscillator strength for one resonance line (8.434 eV) of xenon by determining the refractive index of xenon using the spectral line-shift method [194]. The radiative lifetimes of the resonance

transitions of the noble gases have been determined using: a) the beam-foil method [199]; b) the zero-field level-crossing technique (Hanle effect) [195]; (c) study of the photon decay curve using a pulsed electron excitation source [196–198,200] or pulsed light source [201]; (d) electron-photon delayed coincidence techniques [202]. By studying the pressure-broadening profiles of the noble gas resonance lines, several groups [138,203–206] have reported their oscillator strengths. With the development of lasers, a phase-matching technique involving focused beams for optical wave-mixing became possible and oscillator strengths for the resonance lines in the noble gases have been determined using these techniques by Kramer *et al.* [207] for xenon and by Ferrell *et al.* [66] for krypton and xenon. By analyzing the electron excitation function, McConkey and Donaldson [208] have reported optical oscillator strengths for the resonance lines of argon. Electron impact based methods have also been employed for measuring the discrete optical oscillator strengths of argon, krypton and xenon. By using very high impact energy (25–32 keV) and very small scattering angle ($\sim 1 \times 10^{-4}$ rad), Geiger [20,141,210,212,213] obtained optical oscillator strengths for the resonance lines of the noble gases by converting electron energy loss spectra to relative optical spectra and normalizing on the elastic differential cross section. In other electron impact work Li *et al.* [214] for argon, Takayanagi *et al.* [215] for krypton, and Delage and Carette [211] and also Suzuki *et al.* [216] for xenon, have reported optical oscillator strengths for resonance lines in the heavier noble gases by extrapolating the generalized oscillator strengths of lines, measured at different scattering angles and at low electron impact energy, to zero momentum transfer. Delage and Carette [211] normalized their data on

one of the transition peaks of xenon that was measured by Geiger [210], while Li *et al.* [214], Takayanagi *et al.* [215] and Suzuki *et al.* [216] normalized their data on the elastic scattering cross section. The unpublished electron impact work of Natali *et al.* [142] for the optical oscillator strengths of the noble gases has been quoted in references [139,212,143].

Consideration of the various experimental and theoretical oscillator strength values published to date for argon, krypton and xenon shows that there is a large body of existing information for the continuum regions. In contrast there is relative little information available in the valence shell discrete region. For the *discrete* spectra of argon, krypton and xenon only the transitions to the $ms^2mp^5(2P_{3/2})(m+1)s$ and $ms^2mp^5(2P_{1/2})(m+1)s'$ states, where m is 3, 4 and 5 respectively, have been studied in any detail and even for these considerable variations in oscillator strength values have been reported. In the case of argon the optical oscillator strength data available in 1975 was reviewed by Eggarter [217] for both the discrete and continuum regions up to 3202 eV. On the basis of the information available Eggarter [217] listed recommended optical oscillator strength values for argon.

In chapters 4 and 5, we have reported detailed and comprehensive measurements for helium [37] and neon [38] respectively. These results were obtained using a recently developed highly accurate high resolution electron impact based method for obtaining absolute optical oscillator strengths for the discrete, continuum and autoionizing resonance regions in atoms and molecules. This method [37,38] is not subject to the "line saturation" effects which can cause serious errors in Beer-Lambert law photoabsorption experiments when the bandwidth is comparable to or

larger than the natural linewidth. The method involves combining measurements obtained using a high resolution (0.048 eV FWHM) dipole (e,e) spectrometer in conjunction with a lower resolution (~1 eV FWHM) dipole (e,e) instrument. The absolute oscillator strength scales for helium and neon were obtained by TRK sum rule normalization and were thus completely independent of any direct optical measurement. The same general method is now applied to provide independent and wide-ranging measurements of the absolute photoabsorption oscillator strengths for the discrete, continuum and autoionizing resonance regions of argon, krypton and xenon. However, in practice the TRK sum rule normalization procedures which were employed for helium [37] and neon [38] are difficult to apply for the heavier noble gases due to difficulties in carrying out the necessary lengthy valence shell extrapolations. These difficulties arise because of the smaller energy separations between the different subshells of the argon, krypton and xenon atoms compared with the relatively simple electronic configurations of helium and neon. The absolute scales of the presently reported data have therefore been obtained by normalizing on recently reported high precision photoabsorption oscillator strengths measured at helium and neon resonance line photon energies by Samson and Yin [178]. In this chapter, we now report measurements of (i) absolute photoabsorption continuum oscillator strengths for argon, krypton and xenon up to 500, 380 and 398 eV respectively, (ii) absolute photoabsorption oscillator strengths for the discrete dipole allowed electronic transitions from the mp^6 subshells to levels of the lower members of the ms^2mp^5ns and ms^2mp^5nd ($^2P_{3/2,1/2}$) manifolds where $n > m$ and m is 3, 4 and 5 for argon, krypton and xenon respectively, and (iii) absolute photoabsorption

oscillator strengths in the regions of the Beutler–Fano autoionization resonance profiles involving excitation of the inner valence ms electrons. The results are compared with previously published experimental and theoretical data in regions where such data are available.

6.2 Results and Discussion

6.2.1 Low Resolution Measurements of the Photoabsorption Oscillator Strengths for Argon, Krypton and Xenon

Relative photoabsorption spectra of argon, krypton and xenon were obtained by Bethe–Born conversion of electron energy loss spectra measured with the low resolution dipole (e,e) spectrometer (see chapter 3) from 10–500 eV, 8–380 eV and 7–398 eV for argon, krypton and xenon respectively. The relative spectra were normalized at 21.218 eV for argon and krypton and at 16.848 eV for xenon using the recently published photoionization data of Samson and Yin [178]. The uncertainties of the present low resolution dipole (e,e) work are estimated to be ~5%. The results for argon, krypton and xenon are presented in the following separate sections.

6.2.1.1 Low Resolution Measurements for Argon

Figures 6.1–6.3 show the presently measured absolute optical oscillator strengths for the photoabsorption of argon. The corresponding numerical values in the energy region 16–500 eV are summarized in table 6.1. Of the three noble gases (argon, krypton and xenon) studied in the present work, the photoionization cross sections of argon have been

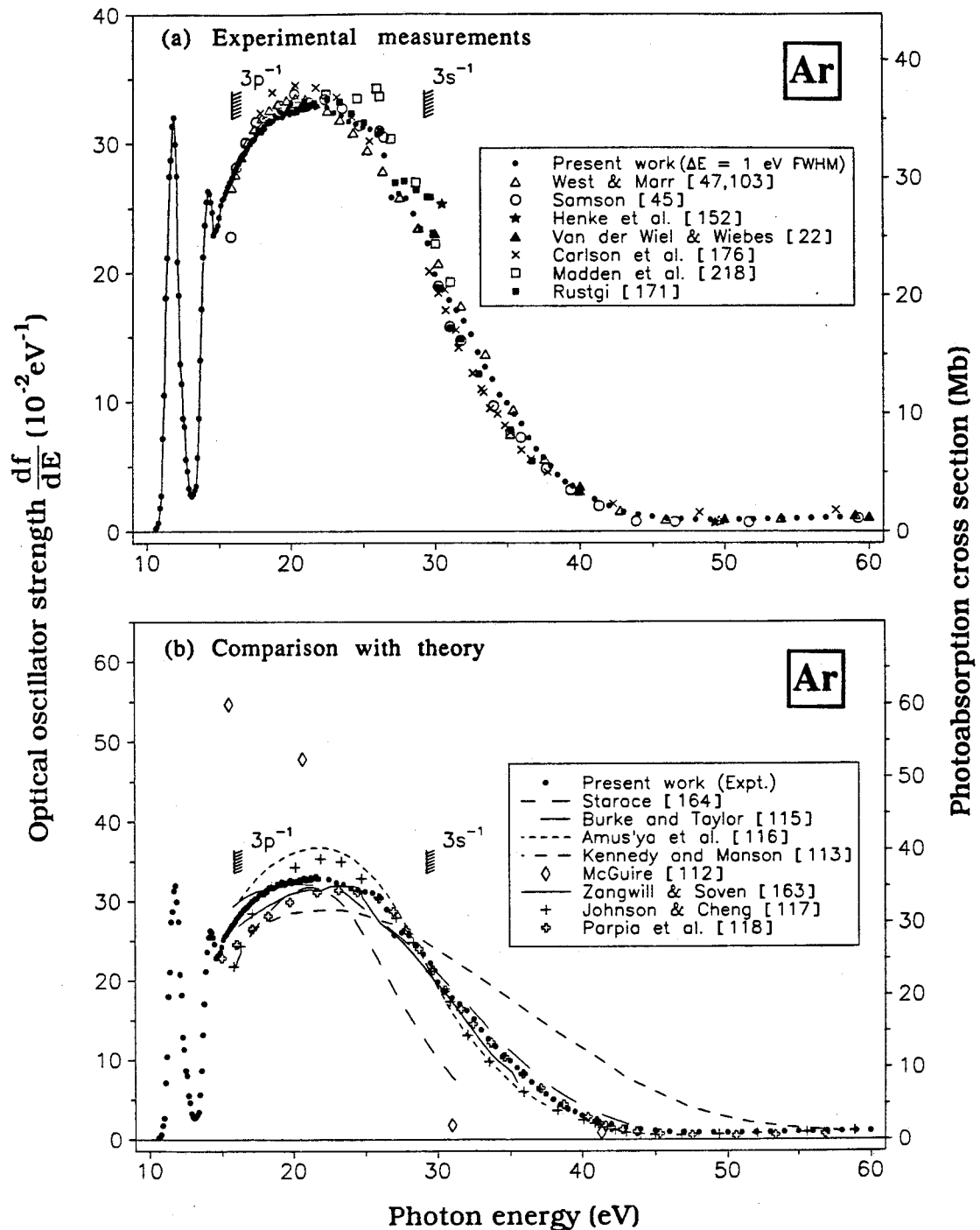


Figure 6.1: Absolute oscillator strengths for the photoabsorption of argon in the energy region 10-60 eV. (a) comparison with other experimental data [22,45,47,103,152,171,176,218]. The discrete region below 16 eV is shown at high resolution in figure 6.9. The resonances in the region 26–29.2 eV preceding the $3s^{-1}$ edge are shown at high resolution in figure 6.14. (b) comparison with theory [112,113,115–118,163,164].

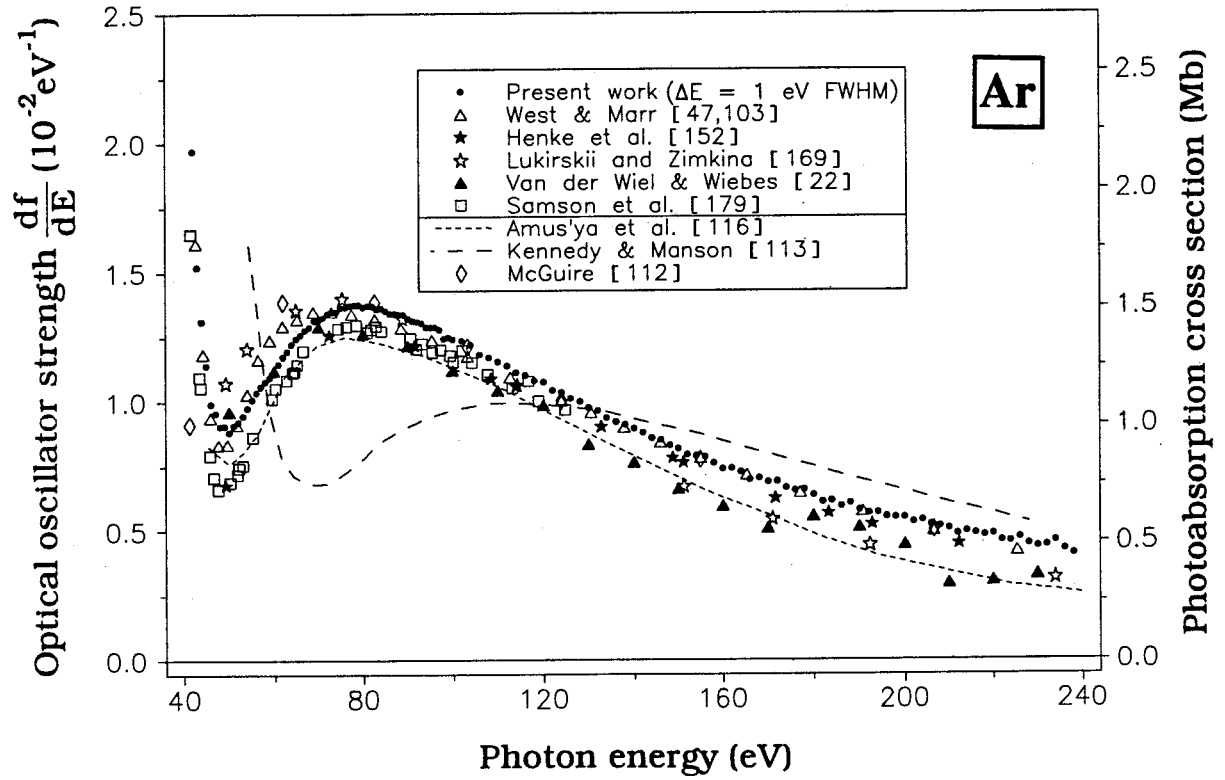


Figure 6.2: Absolute oscillator strengths for the photoabsorption of argon in the energy region 40–240 eV compared with other experimental [22,47,103,152,169,179] and theoretical [112,113,116] data.

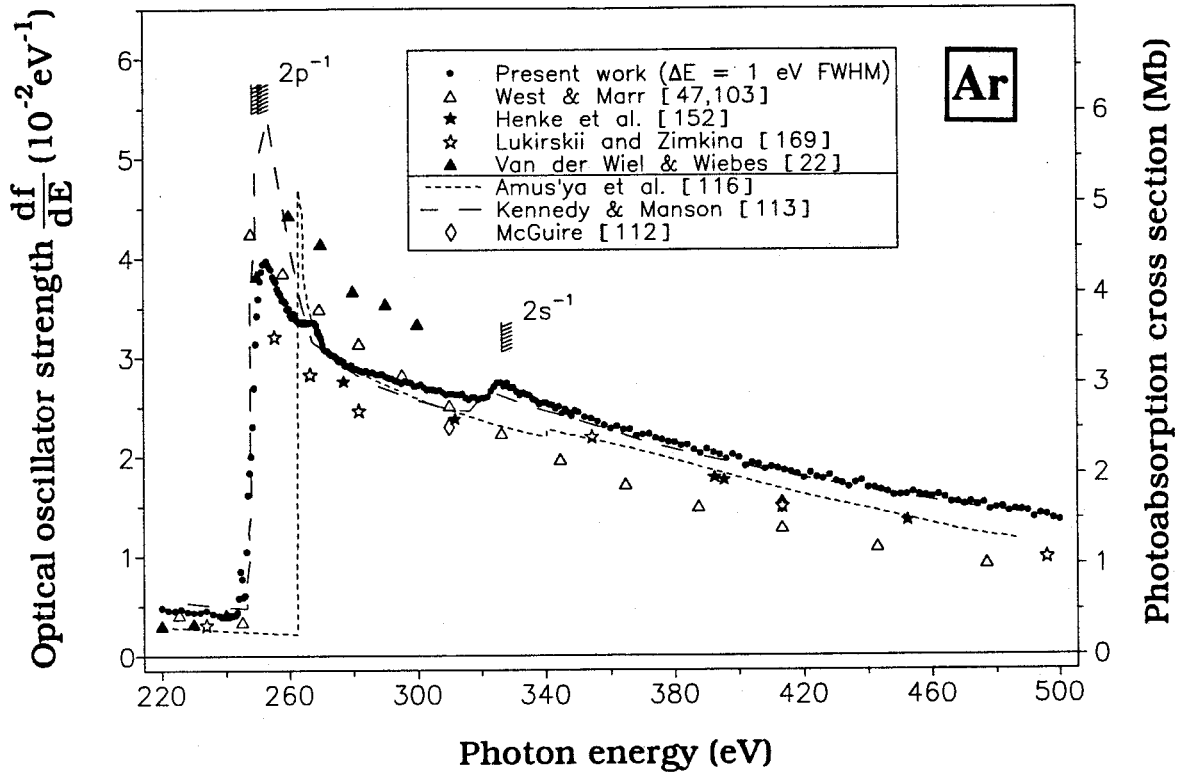


Figure 6.3: Absolute oscillator strengths for the photoabsorption of argon in the energy region 220–500 eV compared with other experimental [22,47,103,152,169] and theoretical [112,113,116] data.

Table 6.1

Absolute differential optical oscillator strengths for the photoabsorption of argon above the first ionization potential obtained using the low resolution (1 eV FWHM) dipole (e,e) spectrometer (16–500 eV)

Energy (eV)	Oscillator Strength (10^{-2}eV^{-1})	Energy (eV)	Oscillator Strength (10^{-2}eV^{-1})	Energy (eV)	Oscillator Strength (10^{-2}eV^{-1})
16.0	27.74	17.7	31.05	19.4	32.02
16.1	27.96	17.8	31.09	19.5	32.19
16.2	28.16	17.9	30.86	19.6	32.35
16.3	28.48	18.0	30.87	19.7	32.52
16.4	28.55	18.1	31.33	19.8	32.71
16.5	28.94	18.2	31.15	19.9	32.23
16.6	28.95	18.3	31.57	20.0	32.49
16.7	29.25	18.4	31.67	20.1	32.51
16.8	29.25	18.5	31.81	20.2	32.36
16.9	29.52	18.6	31.61	20.3	32.38
17.0	29.71	18.7	31.73	20.4	32.71
17.1	29.99	18.8	31.78	20.5	32.40
17.2	29.97	18.9	32.19	20.6	32.58
17.3	30.30	19.0	32.03	20.7	32.91
17.4	30.25	19.1	32.02	20.8	32.94
17.5	30.39	19.2	32.51	20.9	32.57
17.6	30.73	19.3	32.41	21.0	32.75

Table 6.1 (continued)

Energy (eV)	Oscillator Strength (10^{-2}eV^{-1})	Energy (eV)	Oscillator Strength (10^{-2}eV^{-1})	Energy (eV)	Oscillator Strength (10^{-2}eV^{-1})
21.1	32.62	28.5	24.50	38.5	4.38
21.2 [†]	33.00	29.0	23.37	39.0	3.84
21.3	32.72	29.5	22.24	39.5	3.51
21.4	32.89	30.0	19.84	40.0	3.03
21.5	33.09	30.5	18.66	41.0	2.48
21.6	33.16	31.0	17.85	42.0	1.970
21.7	32.80	31.5	17.08	43.0	1.521
21.8	32.86	32.0	16.25	44.0	1.312
22.5	32.90	32.5	15.19	45.0	1.141
23.0	32.36	33.0	13.81	46.0	0.991
23.5	32.16	33.5	12.69	47.0	0.956
24.0	31.66	34.0	11.73	48.0	0.905
24.5	31.49	34.5	10.50	49.0	0.906
25.0	31.24	35.0	9.89	50.0	0.883
25.5	31.08	35.5	9.02	51.0	0.909
26.0	30.63	36.0	8.28	52.0	0.923
26.5	29.02	36.5	7.20	53.0	0.946
27.0	25.76	37.0	6.34	54.0	0.977
27.5	26.06	37.5	5.71	55.0	1.009
28.0	25.71	38.0	5.04	56.0	1.036

Table 6.1 (continued)

Energy (eV)	Oscillator Strength (10^{-2}eV^{-1})	Energy (eV)	Oscillator Strength (10^{-2}eV^{-1})	Energy (eV)	Oscillator Strength (10^{-2}eV^{-1})
57.0	1.059	77.0	1.373	97.0	1.278
58.0	1.078	78.0	1.374	98.0	1.244
59.0	1.094	79.0	1.376	99.0	1.248
60.0	1.110	80.0	1.366	100.0	1.241
61.0	1.146	81.0	1.371	102.0	1.236
62.0	1.175	82.0	1.371	104.0	1.219
63.0	1.196	83.0	1.359	106.0	1.182
64.0	1.223	84.0	1.363	108.0	1.171
65.0	1.245	85.0	1.353	110.0	1.154
66.0	1.259	86.0	1.341	112.0	1.139
67.0	1.278	87.0	1.340	114.0	1.112
68.0	1.290	88.0	1.338	116.0	1.101
69.0	1.314	89.0	1.337	118.0	1.081
70.0	1.316	90.0	1.322	120.0	1.074
71.0	1.325	91.0	1.312	122.0	1.043
72.0	1.341	92.0	1.310	124.0	1.035
73.0	1.347	93.0	1.304	126.0	1.011
74.0	1.348	94.0	1.288	128.0	0.999
75.0	1.364	95.0	1.288	130.0	0.975
76.0	1.365	96.0	1.288	132.0	0.963

Table 6.1 (continued)

Energy (eV)	Oscillator Strength (10^{-2}eV^{-1})	Energy (eV)	Oscillator Strength (10^{-2}eV^{-1})	Energy (eV)	Oscillator Strength (10^{-2}eV^{-1})
134.0	0.936	174.0	0.665	214.0	0.495
136.0	0.920	176.0	0.654	216.0	0.487
138.0	0.910	178.0	0.658	218.0	0.480
140.0	0.895	180.0	0.636	220.0	0.484
142.0	0.879	182.0	0.609	222.0	0.459
144.0	0.857	184.0	0.614	224.0	0.455
146.0	0.851	186.0	0.593	226.0	0.470
148.0	0.829	188.0	0.606	228.0	0.446
150.0	0.816	190.0	0.579	230.0	0.436
152.0	0.793	192.0	0.566	232.0	0.439
154.0	0.789	194.0	0.569	234.0	0.457
156.0	0.784	196.0	0.552	236.0	0.425
158.0	0.762	198.0	0.550	238.0	0.408
160.0	0.737	200.0	0.548	240.0	0.405
162.0	0.740	202.0	0.530	240.5	0.412
164.0	0.726	204.0	0.538	241.0	0.404
166.0	0.696	206.0	0.521	241.5	0.402
168.0	0.701	208.0	0.514	242.0	0.409
170.0	0.687	210.0	0.506	242.5	0.406
172.0	0.689	212.0	0.485	243.0	0.416

Table 6.1 (continued)

Energy (eV)	Oscillator Strength (10^{-2}eV^{-1})	Energy (eV)	Oscillator Strength (10^{-2}eV^{-1})	Energy (eV)	Oscillator Strength (10^{-2}eV^{-1})
243.5	0.439	253.5	3.93	263.5	3.35
244.0	0.578	254.0	3.90	264.0	3.36
244.5	0.849	254.5	3.89	264.5	3.34
245.0	0.774	255.0	3.81	265.0	3.36
245.5	0.593	255.5	3.78	265.5	3.34
246.0	0.609	256.0	3.76	266.0	3.34
246.5	1.049	256.5	3.69	266.5	3.35
247.0	1.615	257.0	3.65	267.0	3.35
247.5	1.838	257.5	3.63	267.5	3.36
248.0	2.00	258.0	3.58	268.0	3.34
248.5	2.30	258.5	3.57	268.5	3.33
249.0	2.69	259.0	3.55	269.0	3.27
249.5	3.13	259.5	3.48	269.5	3.22
250.0	3.42	260.0	3.49	270.0	3.19
250.5	3.59	260.5	3.43	270.5	3.14
251.0	3.77	261.0	3.40	271.0	3.08
251.5	3.86	261.5	3.44	271.5	3.07
252.0	3.94	262.0	3.39	272.0	3.07
252.5	3.94	262.5	3.38	272.5	3.04
253.0	3.97	263.0	3.36	273.0	3.03

Table 6.1 (continued)

Energy (eV)	Oscillator Strength (10^{-2}eV^{-1})	Energy (eV)	Oscillator Strength (10^{-2}eV^{-1})	Energy (eV)	Oscillator Strength (10^{-2}eV^{-1})
273.5	3.02	287.0	2.83	307.0	2.67
274.0	3.02	288.0	2.83	308.0	2.64
274.5	3.01	289.0	2.83	309.0	2.62
275.0	2.99	290.0	2.81	310.0	2.63
275.5	2.96	291.0	2.79	311.0	2.63
276.0	2.97	292.0	2.79	312.0	2.62
276.5	2.96	293.0	2.77	313.0	2.62
277.0	2.96	294.0	2.76	314.0	2.63
277.5	2.91	295.0	2.74	315.0	2.59
278.0	2.92	296.0	2.76	316.0	2.57
278.5	2.91	297.0	2.75	317.0	2.59
279.0	2.90	298.0	2.74	318.0	2.59
279.5	2.92	299.0	2.71	319.0	2.57
280.0	2.89	300.0	2.71	320.0	2.59
281.0	2.88	301.0	2.73	321.0	2.59
282.0	2.87	302.0	2.70	322.0	2.60
283.0	2.85	303.0	2.67	323.0	2.66
284.0	2.87	304.0	2.67	324.0	2.70
285.0	2.84	305.0	2.67	325.0	2.74
286.0	2.85	306.0	2.66	326.0	2.74

Table 6.1 (continued)

Energy (eV)	Oscillator Strength (10^{-2}eV^{-1})	Energy (eV)	Oscillator Strength (10^{-2}eV^{-1})	Energy (eV)	Oscillator Strength (10^{-2}eV^{-1})
327.0	2.70	347.0	2.44	384.0	2.11
328.0	2.74	348.0	2.41	386.0	2.06
329.0	2.69	349.0	2.46	388.0	2.03
330.0	2.69	350.0	2.44	390.0	2.07
331.0	2.65	352.0	2.40	392.0	2.03
332.0	2.61	354.0	2.38	394.0	2.01
333.0	2.64	356.0	2.35	396.0	1.971
334.0	2.62	358.0	2.31	398.0	2.01
335.0	2.61	360.0	2.28	400.0	1.983
336.0	2.58	362.0	2.30	402.0	1.898
337.0	2.56	364.0	2.27	404.0	1.931
338.0	2.52	366.0	2.27	406.0	1.917
339.0	2.54	368.0	2.21	408.0	1.869
340.0	2.54	370.0	2.22	410.0	1.891
341.0	2.52	372.0	2.22	412.0	1.875
342.0	2.52	374.0	2.18	414.0	1.854
343.0	2.48	376.0	2.17	416.0	1.839
344.0	2.50	378.0	2.14	418.0	1.820
345.0	2.43	380.0	2.14	420.0	1.778
346.0	2.47	382.0	2.11	422.0	1.827

Table 6.1 (continued)

Energy (eV)	Oscillator Strength (10 ⁻² eV ⁻¹)	Energy (eV)	Oscillator Strength (10 ⁻² eV ⁻¹)	Energy (eV)	Oscillator Strength (10 ⁻² eV ⁻¹)
424.0	1.784	458.0	1.597	492.0	1.374
426.0	1.769	460.0	1.587	494.0	1.411
428.0	1.805	462.0	1.605	496.0	1.400
430.0	1.743	464.0	1.578	498.0	1.364
732.0	1.724	466.0	1.528	500.0	1.346
434.0	1.686	468.0	1.532		
436.0	1.728	470.0	1.507		
438.0	1.751	472.0	1.532		
440.0	1.677	474.0	1.501		
442.0	1.675	476.0	1.523		
444.0	1.655	478.0	1.453		
446.0	1.637	480.0	1.471		
448.0	1.601	482.0	1.482		
450.0	1.604	484.0	1.436		
452.0	1.606	486.0	1.454		
454.0	1.635	488.0	1.452		
456.0	1.608	490.0	1.437		

† normalized to ref. [178] at 21.218 eV

$$\sigma \text{ (Mb)} = 1.0975 \times 10^2 \frac{df}{dE} \text{ eV}^{-1}$$

previously studied in the greatest detail. Figures 6.1(a) and 6.1(b) show the presently measured absolute optical oscillator strengths for the valence shell photoabsorption of argon in the energy region 10–60 eV along with previously reported experimental [22,45,47,103,152,171,176,218,152] and theoretical [112–118,163,164] data, respectively. In figure 6.1(a), the higher resolution data from Samson [45] and Carlson *et al.* [176] in the 26–29 eV autoionizing region have been omitted to permit clearer comparison with the present low resolution data. The data reported by Samson [45] and Carlson *et al.* [176] in the continuum autoionization regions will be compared with the present data obtained from the high resolution dipole (e,e) spectrometer in section 3.3 below. West and Marr [103] have made absolute photoabsorption measurements for argon over the range 36–310 eV and have given a critical evaluation of existing published cross section data to obtain recommended (weighted-average) values throughout the vacuum ultraviolet and x-ray regions. These values [47,103] did not take into account previously published data in the autoionizing region (26–29 eV) and simply reported interpolated smooth cross sections throughout the autoionizing region. From figure 6.1(a) it can be seen that all the experimental data including the present low resolution results show a similar shape for the continuum and are in generally good quantitative agreement. The data from Madden *et al.* [218] are slightly higher than other experimental values in the vicinity of 25 eV. In contrast to the experimental data, the theoretical values for argon show substantial differences in terms of both the shape and the absolute values of the cross sections when compared with the present results (see figure 6.1(b)). The one-electron calculation by McGuire [112] gives much

higher cross sections just above the 3p threshold and the cross sections drop very quickly to a very low value before reaching the Cooper minimum at ~50 eV. Even with the inclusion of electron correlation, the calculations reported by Starace [164] and by Kennedy and Manson [113] still show large discrepancies with the present and other measured values. Since relativistic effects in argon are small, the RPAE calculation of Amus'ya *et al.* [116] and the relativistic RPAE of Johnson and Cheng [117] agree very closely with each other. However, these calculations [116,117] are considerably higher than the present and other experimental values below 30 eV and are somewhat lower in the energy region 30–50 eV. The values reported by Parpia *et al.* [118] using the RTDLDA method give excellent agreement with the presently reported experimental values above 25 eV, but in common with most of the other theoretical work there still exist some discrepancies with the experimental data in the energy region between the 3p threshold and the cross section maximum.

Figure 6.2 shows the presently measured absolute photoabsorption oscillator strengths for argon from 40 to 240 eV just below the inner shell 2p excitations of argon. Other previously reported experimental and theoretical data that are available in this energy region are also shown for comparison. The present data are in generally good agreement with the compilation data reported by Henke *et al.* [152] and West and Marr [47,103]. The photoabsorption data of Lukirskii and Zimkina [169] and the earlier electron impact data of Van der Wiel and Wiebes [22] give lower values at energies above 120 eV. The values measured recently by Samson *et al.* [179] using a double ionization chamber in the energy region 40–120 eV are slightly lower than the present work. In

theoretical work, the one-electron calculation of McGuire [112], which shows very high cross sections just above the 3p threshold (figure 6.1(b)) gives very good agreement with the present results from an energy just above the Cooper minimum to 240 eV (figure 6.2). The RPAE calculations reported by Amus'ya *et al.* [116] show a similar shape in the continuum to the present measurements, but the theoretical values are slightly lower from 40 to 150 eV and become increasingly lower above 150 eV. The photoionization cross sections calculated by Kennedy and Manson [113] show large discrepancies with the present and all other experimental data and furthermore the predicted position of the Cooper minimum is ~15 eV too high in energy.

Figure 6.3 shows the presently measured absolute photoabsorption oscillator strengths for argon in the energy region from 220 to 500 eV where excitation and ionization of the argon 2s and 2p electrons take place on top of the valence shell continuum. The limited previously published experimental and theoretical data in this energy region are also shown in figure 6.3 for comparison. Unlike the situation below 240 eV, the agreement between the available experimental data is poor in this energy region. It can be seen in figure 6.3 that the data reported by Lukirskii and Zimkina [169] and the compilation data of Henke *et al.* [152] are ~10–25% lower than the present results. The data of West and Marr [47,103], which are slightly higher than the presently reported values in the energy region 250–290 eV, are lower by more than 30% at energies above 320 eV. The theoretical calculations reported by Kennedy and Manson [113], which show considerable discrepancies with the experimental data below 240 eV, exhibit very good agreement with the presently measured values in the energy region 270–500 eV, while the

calculations of Amus'ya *et al.* [116] and of McGuire [112] are (~10–15%) lower than the present results in this energy region.

6.2.1.2 Low Resolution Measurements for Krypton

Figures 6.4 and 6.5 show the presently measured absolute optical oscillator strengths for the photoabsorption of krypton. Table 6.2 summarizes the numerical absolute oscillator strength values in the energy region 14.7–380 eV. In figures 6.4(a) and 6.4(b), the presently measured valence shell photoabsorption oscillator strengths for krypton in the energy region 5–60 eV are compared with the previously reported experimental and theoretical values, respectively. The earlier reported photoionization data of Samson [45] are slightly lower than the present work in the energy region from the 4p threshold to 30 eV. The weighted-average values reported in the West and Marr compilation [47,103], which included the data from Samson [45], show similar behavior to the original Samson data [45]. In contrast, the most recent data reported by Samson *et al.* [179] show excellent agreement with the presently reported values. As shown in figure 6.4(b), the situation for the theoretical cross sections of krypton when compared with the experimental data is similar to that for argon (in figure 6.1(b)). Even though agreement between theoretical and experimental values is better at higher energies, difficulties still remain in describing the behavior of the photoionization cross sections just above the 4p threshold and in the region around the cross section maximum.

Ionization from the 3d sub-shell of krypton takes place at ~90 eV. The ejection of the d-electrons is delayed due to the angular momentum

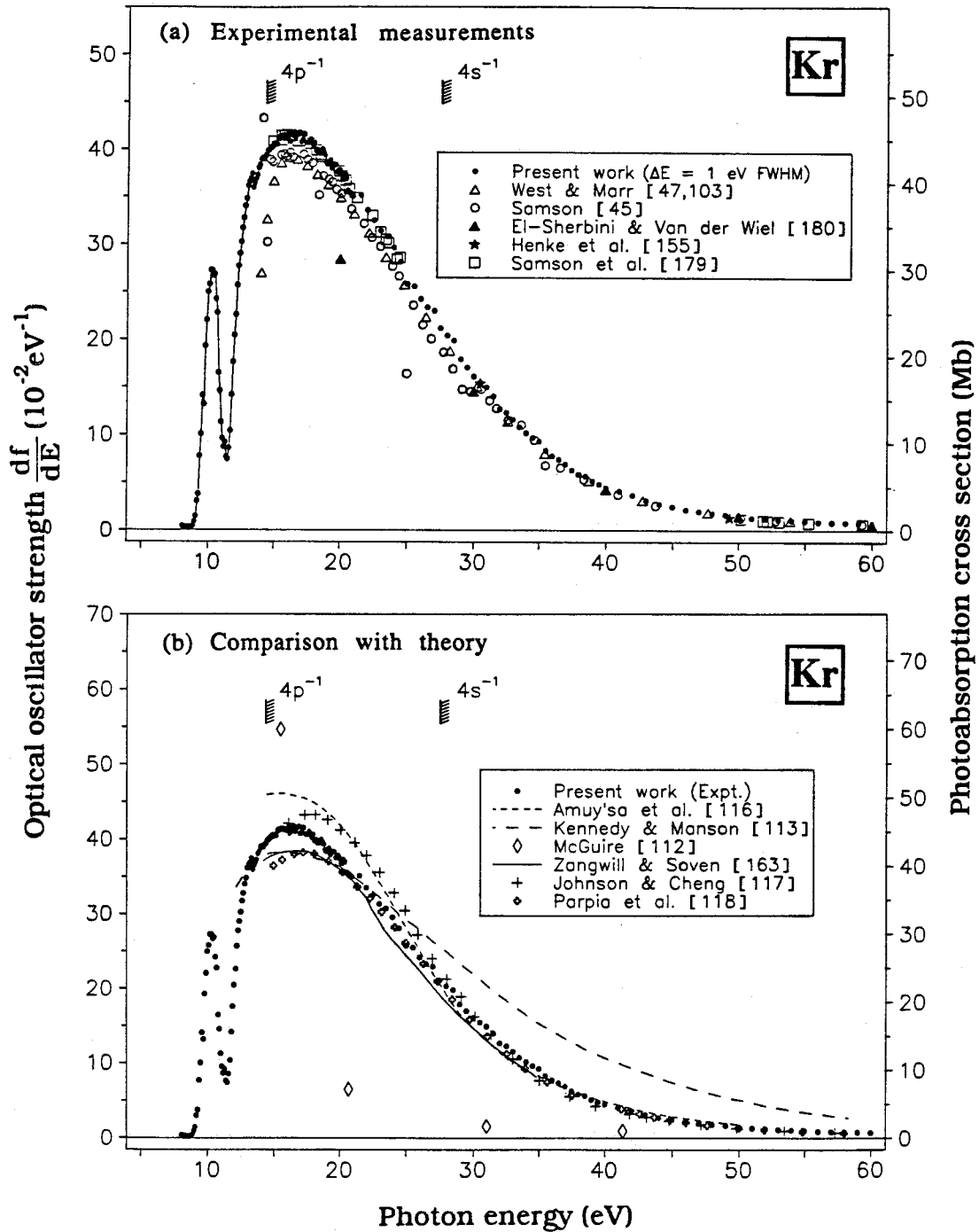


Figure 6.4: Absolute oscillator strengths for the photoabsorption of krypton in the energy region 5–60 eV. (a) comparison with other experimental data [45,47,103,152,180]. The discrete region below 15 eV is shown at high resolution in figure 6.10. The resonances in the region 24.5–27.5 eV preceding the $4s^{-1}$ edge are shown at high resolution in figure 6.15. (b) comparison with theory [112,113,116–118,163].

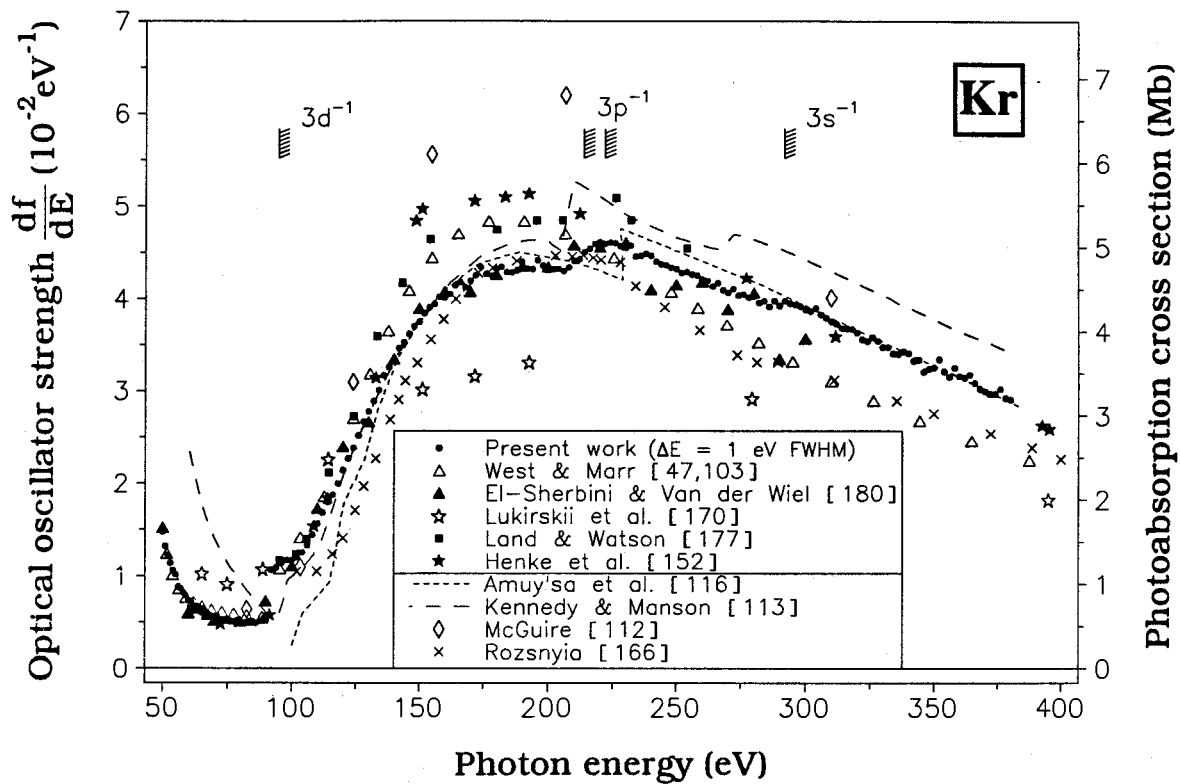


Figure 6.5: Absolute oscillator strengths for the photoabsorption of krypton in the energy region 50–400 eV compared with other experimental [47,103,152,170,177,180] and theoretical [112,113,116,166] data.

Table 6.2

Absolute differential optical oscillator strengths for the photoabsorption of krypton above the first ionization potential obtained using the low resolution (1 eV FWHM) dipole (e,e) spectrometer (14.7–380 eV)

Energy (eV)	Oscillator Strength (10^{-2}eV^{-1})	Energy (eV)	Oscillator Strength (10^{-2}eV^{-1})	Energy (eV)	Oscillator Strength (10^{-2}eV^{-1})
14.7	40.22	16.4	41.41	18.1	39.82
14.8	40.16	16.5	41.81	18.2	39.96
14.9	40.56	16.6	41.04	18.3	39.55
15.0	40.42	16.7	41.46	18.4	39.65
15.1	40.64	16.8	41.62	18.5	39.58
15.2	40.50	16.9	41.76	18.6	40.00
15.3	41.25	17.0	40.77	18.7	39.64
15.4	41.13	17.1	41.02	18.8	39.35
15.5	41.41	17.2	41.63	18.9	38.59
15.6	41.46	17.3	41.53	19.0	38.40
15.7	41.49	17.4	40.70	19.1	38.53
15.8	41.22	17.5	40.67	19.2	38.83
15.9	41.28	17.6	40.65	19.3	37.98
16.0	41.20	17.7	41.07	19.4	38.41
16.1	41.73	17.8	40.70	19.5	38.32
16.2	40.78	17.9	40.26	19.6	38.38
16.3	41.57	18.0	40.70	19.7	37.57

Table 6.2 (continued)

Energy (eV)	Oscillator Strength (10^{-2}eV^{-1})	Energy (eV)	Oscillator Strength (10^{-2}eV^{-1})	Energy (eV)	Oscillator Strength (10^{-2}eV^{-1})
19.8	37.76	25.0	25.81	35.0	9.30
19.9	37.85	25.5	25.57	35.5	8.33
20.0	37.46	26.0	24.22	36.0	7.77
20.1	36.80	26.5	23.37	36.5	7.39
20.2	36.79	27.0	22.99	37.0	6.92
20.3	37.33	27.5	21.14	37.5	6.28
20.4	36.98	28.0	20.38	38.0	5.85
20.5	35.65	28.5	19.85	38.5	5.65
20.6	35.42	29.0	17.92	39.0	5.15
20.7	35.39	29.5	17.04	39.5	4.81
20.8	35.09	30.0	16.08	40.0	4.47
20.9	35.03	30.5	15.47	41.0	4.10
21.0 [†]	34.90	31.0	14.96	42.0	3.66
21.5	35.15	31.5	14.01	43.0	3.12
22.0	33.57	32.0	12.69	44.0	2.74
22.5	32.49	32.5	12.30	45.0	2.49
23.0	31.38	33.0	11.58	46.0	2.17
23.5	30.79	33.5	10.78	47.0	1.983
24.0	29.62	34.0	10.20	48.0	1.787
24.5	28.12	34.5	9.69	49.0	1.675

Table 6.2 (continued)

Energy (eV)	Oscillator Strength (10^{-2}eV^{-1})	Energy (eV)	Oscillator Strength (10^{-2}eV^{-1})	Energy (eV)	Oscillator Strength (10^{-2}eV^{-1})
50.0	1.475	70.0	0.551	110.0	1.566
51.0	1.319	72.0	0.527	112.0	1.684
52.0	1.220	74.0	0.528	114.0	1.797
53.0	1.135	76.0	0.505	116.0	1.878
54.0	1.057	78.0	0.499	118.0	2.00
55.0	1.014	80.0	0.494	120.0	2.14
56.0	0.880	82.0	0.497	122.0	2.27
57.0	0.862	84.0	0.494	124.0	2.38
58.0	0.818	86.0	0.489	126.0	2.52
59.0	0.788	88.0	0.508	128.0	2.67
60.0	0.737	90.0	0.565	130.0	2.78
61.0	0.722	92.0	1.064	132.0	2.89
62.0	0.679	94.0	1.088	134.0	3.01
63.0	0.657	96.0	1.138	136.0	3.17
64.0	0.667	98.0	1.170	138.0	3.26
65.0	0.599	100.0	1.171	140.0	3.33
66.0	0.645	102.0	1.199	142.0	3.47
67.0	0.605	104.0	1.252	144.0	3.53
68.0	0.582	106.0	1.327	146.0	3.62
69.0	0.553	108.0	1.444	148.0	3.70

Table 6.2 (continued)

Energy (eV)	Oscillator Strength (10^{-2}eV^{-1})	Energy (eV)	Oscillator Strength (10^{-2}eV^{-1})	Energy (eV)	Oscillator Strength (10^{-2}eV^{-1})
150.0	3.75	190.0	4.40	230.0	4.55
152.0	3.84	192.0	4.33	232.0	4.57
154.0	3.91	194.0	4.32	234.0	4.46
156.0	3.94	196.0	4.41	236.0	4.46
158.0	4.02	198.0	4.36	238.0	4.49
160.0	4.01	200.0	4.31	240.0	4.46
162.0	4.05	202.0	4.32	242.0	4.40
164.0	4.14	204.0	4.32	244.0	4.37
166.0	4.18	206.0	4.30	246.0	4.36
168.0	4.12	208.0	4.34	248.0	4.34
170.0	4.19	210.0	4.41	250.0	4.32
172.0	4.25	212.0	4.43	252.0	4.28
174.0	4.35	214.0	4.50	254.0	4.29
176.0	4.27	216.0	4.54	256.0	4.26
178.0	4.25	218.0	4.59	258.0	4.25
180.0	4.32	220.0	4.61	260.0	4.21
182.0	4.35	222.0	4.59	262.0	4.20
184.0	4.29	224.0	4.61	264.0	4.14
186.0	4.28	226.0	4.60	266.0	4.17
188.0	4.31	228.0	4.57	268.0	4.09

Table 6.2 (continued)

Energy (eV)	Oscillator Strength (10^{-2}eV^{-1})	Energy (eV)	Oscillator Strength (10^{-2}eV^{-1})	Energy (eV)	Oscillator Strength (10^{-2}eV^{-1})
270.0	4.07	308.0	3.79	346.0	3.21
272.0	4.11	310.0	3.75	348.0	3.24
274.0	4.04	312.0	3.73	350.0	3.25
276.0	4.05	314.0	3.68	352.0	3.34
278.0	4.01	316.0	3.68	354.0	3.21
280.0	4.03	318.0	3.67	356.0	3.15
282.0	3.96	320.0	3.63	358.0	3.25
284.0	3.97	322.0	3.56	360.0	3.16
286.0	3.91	324.0	3.54	362.0	3.14
288.0	3.98	326.0	3.58	364.0	3.17
290.0	3.92	328.0	3.54	366.0	3.09
292.0	3.98	330.0	3.48	368.0	3.02
294.0	3.95	332.0	3.48	370.0	3.00
296.0	3.94	334.0	3.41	372.0	2.97
298.0	3.92	336.0	3.40	374.0	2.97
300.0	3.88	338.0	3.43	376.0	3.02
302.0	3.86	340.0	3.41	378.0	2.93
304.0	3.90	342.0	3.33	380.0	2.91
306.0	3.83	344.0	3.34		

† normalized to ref. [178] at 21.218 eV

$$\sigma \text{ (Mb)} = 1.0975 \times 10^2 \frac{df}{dE} \text{ eV}^{-1}$$

barrier which separates the inner well and outer well states. The photoionization cross sections reach a maximum value at ~ 180 eV which is ~ 90 eV above threshold. Figure 6.5 shows the presently measured photoionization cross sections of krypton in the energy region 50–400 eV which includes not only the 3d ionization threshold but also the 3s (~ 290 eV) and 3p (~ 220 eV) thresholds as well. The optical data of West and Marr [47,103], Land and Watson [177], and Henke *et al.* [152] show 10–15% higher values than the present work around the 3d cross section maximum, while the values of Lukirskii *et al.* [170] are lower by more than 25%. The electron impact data of El-Sherbini and Van der Wiel [180] agree very well with the present work. The one-electron calculation of McGuire [112] gives cross sections which are too high. In contrast all theoretical calculations which include electron correlation [113,116,166] adequately describe the behavior of the photoionization oscillator strength of the 3d-electrons. In particular the RPAE data of Amus'ya *et al.* [116] show extremely good agreement with the present data.

6.2.1.3 Low Resolution Measurements for Xenon

Figures 6.6–6.8 show the presently measured absolute optical oscillator strengths for the photoabsorption of xenon and table 6.3 summarizes the corresponding absolute oscillator strength values in the energy region 13.5–398 eV. Figures 6.6(a) and 6.6(b) show the presently measured photoabsorption oscillator strengths for xenon in the energy region 5–60 eV along with previously reported experimental and theoretical data respectively. It can be seen from figure 6.6(a) that the

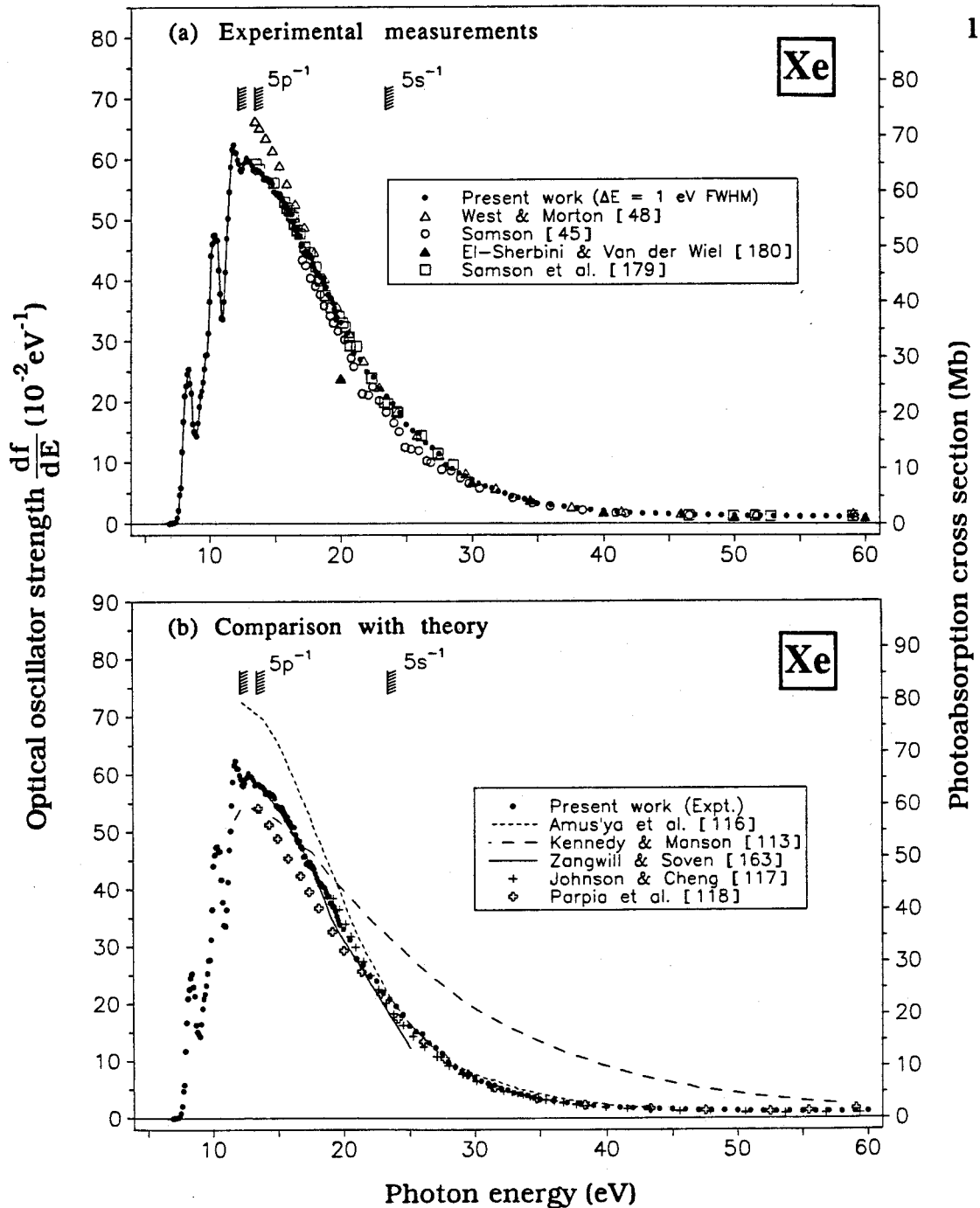


Figure 6.6: Absolute oscillator strengths for the photoabsorption of xenon in the energy region 5–60 eV. (a) comparison with other experimental data [45,48,179,180]. The discrete region below 13.5 eV is shown at high resolution in figure 6.12. The resonances in the region 20.5–27.4 eV preceding the $5s^{-1}$ edge are shown at high resolution in figure 6.16. (b) compared with theory [113,116–118,163].

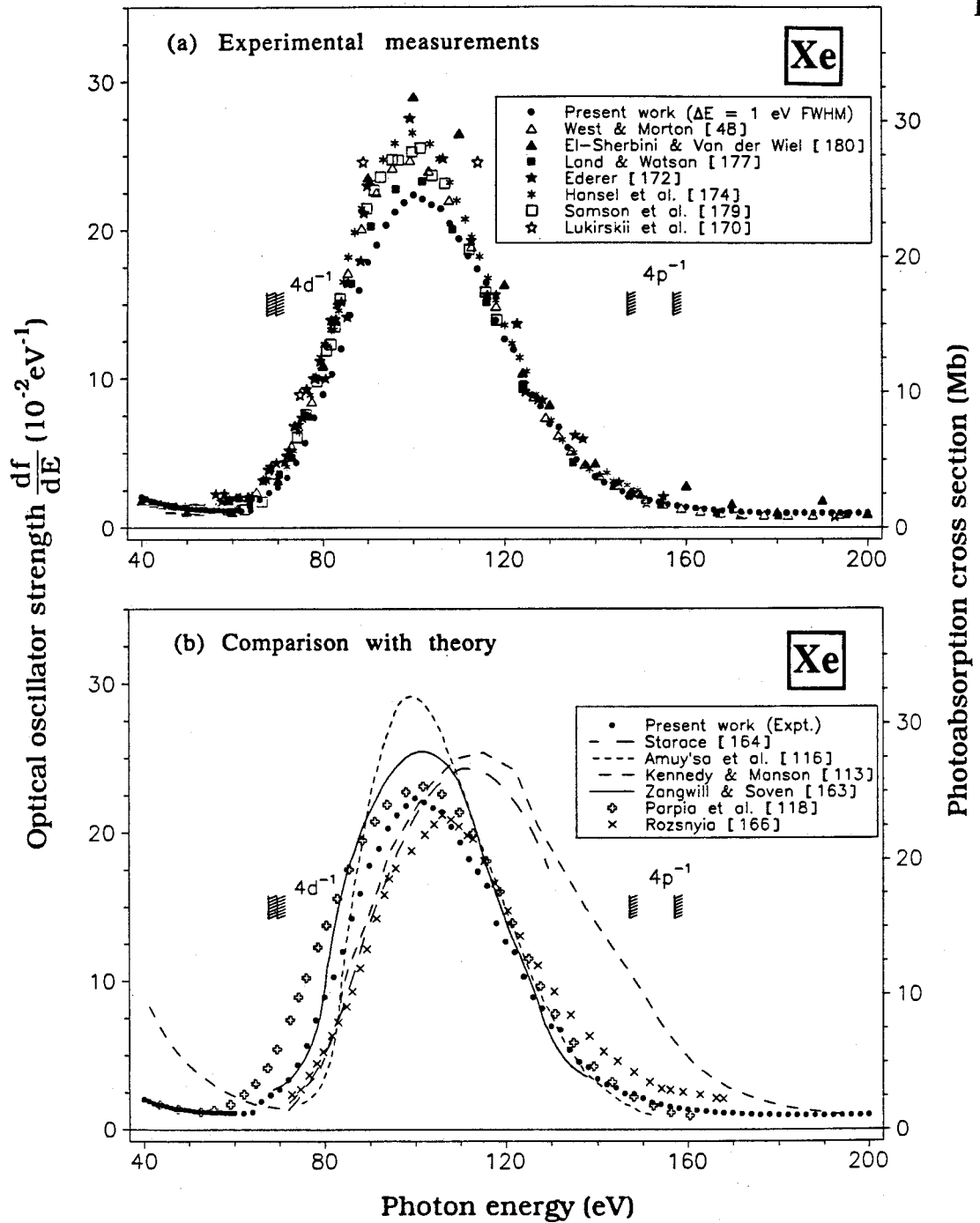


Figure 6.7: Absolute oscillator strengths for the photoabsorption of xenon in the energy region 40–200 eV. (a) comparison with other experimental data [48,170,,172,174,179,,180,]. (b) comparison with theory [113,116,118,163,164,166].

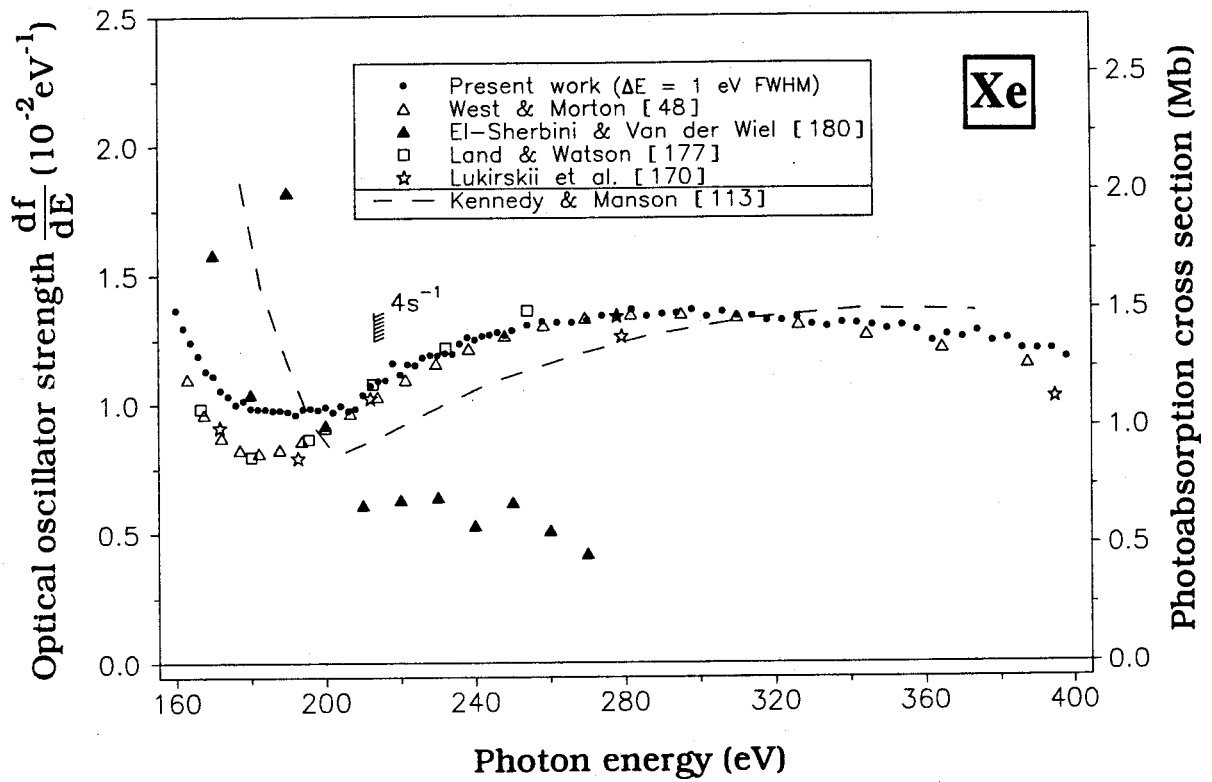


Figure 6.8: Absolute oscillator strengths for the photoabsorption of xenon in the energy region 160–400 eV compared with other experimental [48,17,0,177,180] and theoretical [113] data.

Table 6.3

Absolute differential optical oscillator strengths for the photoabsorption of xenon above the first ionization potential obtained using the low resolution (1 eV FWHM) dipole (e,e) spectrometer (13.5–398 eV)

Energy (eV)	Oscillator Strength (10^{-2}eV^{-1})	Energy (eV)	Oscillator Strength (10^{-2}eV^{-1})	Energy (eV)	Oscillator Strength (10^{-2}eV^{-1})
13.5	58.35	15.2	54.37	16.9	47.11
13.6	58.29	15.3	53.74	17.0	45.63
13.7	57.96	15.4	54.25	17.1	45.82
13.8	57.98	15.5	53.62	17.2	44.48
13.9	57.80	15.6	53.16	17.3	44.70
14.0	57.53	15.7	52.20	17.4	44.16
14.1	56.71	15.8	52.65	17.5	44.74
14.2	56.95	15.9	51.86	17.6	43.80
14.3	56.62	16.0	51.64	17.7	44.09
14.4	56.86	16.1	51.07	17.8	43.58
14.5	56.34	16.2	50.88	17.9	42.73
14.6	56.58	16.3	50.84	18.0	42.01
14.7	56.34	16.4	49.54	18.1	41.44
14.8	55.87	16.5	48.68	18.2	40.88
14.9	54.59	16.6	48.20	18.3	41.07
15.0	54.47	16.7	48.41	18.4	40.62
15.1	54.16	16.8 [†]	47.44	18.5	40.43

Table 6.3 (continued)

Energy (eV)	Oscillator Strength (10^{-2}eV^{-1})	Energy (eV)	Oscillator Strength (10^{-2}eV^{-1})	Energy (eV)	Oscillator Strength (10^{-2}eV^{-1})
18.6	40.28	24.0	19.62	34.0	4.02
18.7	39.55	24.5	18.13	34.5	3.69
18.8	38.70	25.0	16.17	35.0	3.28
18.9	38.84	25.5	15.22	36.0	3.11
19.0	37.61	26.0	14.78	37.0	2.77
19.1	37.49	26.5	13.20	38.0	2.49
19.2	37.00	27.0	12.39	39.0	2.23
19.3	36.96	27.5	11.39	40.0	2.05
19.4	36.19	28.0	9.59	41.0	1.944
19.5	35.28	28.5	8.97	42.0	1.789
19.6	34.60	29.0	8.27	43.0	1.696
19.7	33.83	29.5	7.72	44.0	1.664
20.0	33.04	30.0	7.17	45.0	1.578
20.5	31.21	30.5	6.54	46.0	1.493
21.0	27.93	31.0	6.12	47.0	1.407
21.5	26.88	31.5	5.80	48.0	1.398
22.0	24.88	32.0	5.28	49.0	1.341
22.5	24.01	32.5	4.95	50.0	1.314
23.0	22.08	33.0	4.48	51.0	1.243
23.5	20.84	33.5	4.26	52.0	1.219

Table 6.3 (continued)

Energy (eV)	Oscillator Strength (10^{-2}eV^{-1})	Energy (eV)	Oscillator Strength (10^{-2}eV^{-1})	Energy (eV)	Oscillator Strength (10^{-2}eV^{-1})
53.0	1.203	86.0	14.25	126.0	8.90
54.0	1.201	88.0	15.91	128.0	8.15
55.0	1.160	90.0	17.80	130.0	6.94
56.0	1.153	92.0	18.96	132.0	6.73
57.0	1.178	94.0	20.30	134.0	5.36
58.0	1.145	96.0	21.19	136.0	4.55
59.0	1.137	98.0	21.83	138.0	4.19
60.0	1.148	100.0	22.33	140.0	3.41
62.0	1.124	102.0	22.05	142.0	3.03
64.0	1.177	104.0	21.67	144.0	2.82
66.0	1.900	106.0	21.41	146.0	2.43
68.0	2.33	108.0	20.40	148.0	2.41
70.0	2.71	110.0	19.37	150.0	2.11
72.0	3.36	112.0	18.23	152.0	1.838
74.0	4.36	114.0	17.39	154.0	1.702
76.0	5.66	116.0	16.45	156.0	1.554
78.0	7.38	118.0	13.91	158.0	1.454
80.0	8.92	120.00	12.66	160.0	1.366
82.0	10.29	122.0	11.96	162.0	1.297
84.0	11.99	124.0	10.29	164.0	1.241

Table 6.3 (continued)

Energy (eV)	Oscillator Strength (10^{-2}eV^{-1})	Energy (eV)	Oscillator Strength (10^{-2}eV^{-1})	Energy (eV)	Oscillator Strength (10^{-2}eV^{-1})
166.0	1.189	206.0	0.974	246.0	1.277
168.0	1.130	208.0	0.983	248.0	1.265
170.0	1.111	210.0	1.037	250.0	1.284
172.0	1.056	212.0	1.072	254.0	1.305
174.0	1.031	214.0	10.90	258.0	1.319
176.0	0.999	216.0	1.092	262.0	1.315
178.0	1.015	218.0	1.159	266.0	1.315
180.0	0.986	220.0	1.114	270.0	1.323
182.0	0.983	222.0	1.154	274.0	1.342
184.0	0.982	224.0	1.151	278.0	1.341
186.0	0.977	226.0	1.181	282.0	1.365
188.0	0.977	228.0	1.190	286.0	1.339
190.0	0.972	230.0	1.188	290.0	1.347
192.0	0.960	232.0	1.197	294.0	1.350
194.0	0.981	234.0	1.194	298.0	1.363
196.0	0.984	236.0	1.235	302.0	1.337
198.0	0.979	238.0	1.258	306.0	1.356
200.0	0.990	240.0	1.248	310.0	1.340
202.0	0.969	242.0	1.263	314.0	1.338
204.0	0.995	244.0	1.267	318.0	1.321

Table 6.3 (continued)

Energy (eV)	Oscillator Strength ($10^{-2}eV^{-1}$)	Energy (eV)	Oscillator Strength ($10^{-2}eV^{-1}$)	Energy (eV)	Oscillator Strength ($10^{-2}eV^{-1}$)
322.0	1.322	382.0	1.249		
326.0	1.332	386.0	1.208		
330.0	1.306	390.0	1.207		
334.0	1.297	394.0	1.208		
338.0	1.313	398.0	1.175		
342.0	1.309				
346.0	1.302				
350.0	1.288				
354.0	1.300				
358.0	1.283				
362.0	1.241				
366.0	1.264				
370.0	1.254				
374.0	1.279				
378.0	1.237				

† normalized to ref. [178] at 16.848 eV

$$\sigma (\text{Mb}) = 1.0975 \times 10^2 \frac{df}{dE} eV^{-1}$$

present data are in excellent agreement with the recent work of Samson *et al.* [179] over the entire energy range shown. The data from the West and Morton compilation [48] are much higher than the present work just above the 5p threshold but are very close to the present data at 20 eV. The earlier reported Samson data [45] is slightly lower in the region 16–30 eV. In theoretical work, the relativistic RPAE data of Johnson and Cheng [117] show better agreement with the present work than do the non-relativistic RPAE data of Amus'ya *et al.* [116], which give much higher cross sections just above the 5p threshold. The calculations reported by Zangwill and Soven [163] in the 15–25 eV region using density-functional theory show very good agreement with the present work. In contrast other theoretical calculations yield less satisfactory results particularly below 20 eV.

Photoionization cross sections for the 4d-subshell of xenon have been studied extensively both experimentally and theoretically. Figures 6.7(a) and 6.7(b) show the presently measured photoabsorption oscillator strengths of xenon in the energy region 40–200 eV. It can be seen from figure 6.7(a) that the values obtained in the present work are slightly lower than other experimental data in the energy region around the 4d ionization cross section maximum. The data from Lukirskii *et al.* [170], Ederer [172] and El-Sherbini and Van der Wiel [180] give the highest oscillator strengths in this region. All one-electron calculations [112,165] are in severe disagreement with experiment and are not shown in figure 6.7(b). This disagreement is not surprising in view of the many-electron effects which influence the 4d cross sections. The more complex calculations [113,116,118,163,164,166] which include electron correlation achieve closer agreement with experimental values.

In figure 6.7(b) it can be seen that the theoretical calculations including electron correlation give photoionization cross sections reasonably similar in shape to the present experimental work. However, the cross section maxima reported by Starace [164], Kennedy and Manson [113] and Rozsnyai [166] are shifted to higher energy. The calculations reported by Zangwill and Soven [163] and Parpia *et al.* [118] show reasonable agreement with the present work, although the calculated values are slightly higher.

Figure 6.8 shows the presently determined photoabsorption oscillator strengths for xenon in the energy region 160–398 eV. There are few previously reported data in this energy region. The data from the West and Morton compilation [48] are lower than the present values in the energy region 160–200 eV but show good agreement with the present work at higher energies. Similar to the results obtained from the data reported by Lukirskii and Zimkina [169] for argon and by Lukirskii *et al.* [170] for krypton, the data reported by Lukirskii *et al.* [170] for xenon are lower than the present values at energies higher than 160 eV. The earlier dipole electron impact data of El-Sherbini and Van der Wiel [180] show large statistical errors in this energy region, and are much lower than the present work above 200 eV. The calculation by Kennedy and Manson [113], also shown in figure 6.8, shows fair agreement with experiment above 200 eV.

6.2.2 High Resolution Measurements of the Photoabsorption Oscillator Strengths for the Discrete Transitions Below the mp Ionization Thresholds for Argon (m=3), Krypton (m=4) and Xenon (m=5)

High resolution electron energy loss spectra at resolutions of 0.048, 0.072 and 0.098 eV FWHM in the energy range 11–22 eV for argon, 9–22 eV for krypton and 8–22 eV for xenon were multiplied by the appropriate Bethe–Born factors for the high resolution dipole (e,e) spectrometer (see refs. [37,38] and chapter 3) to obtain relative optical oscillator strength spectra which were then normalized in the smooth continuum regions at 21.218 eV for argon and krypton, and at 16.848 eV for xenon using the absolute data determined by Samson and Yin [178]. Figures 6.9–6.13 show the resulting absolute differential optical oscillator strength spectra of argon, krypton and xenon at a resolution of 0.048 eV FWHM. The dipole–allowed electronic transitions from the ms^2mp^6 configurations of argon, krypton and xenon with $m=3, 4$ and 5 respectively, to members of the $ms^2mp^5(2P_{3/2,1/2})ns$ and nd manifolds (where $n>m$) were observed. The positions and assignments [155] of the various members of the nl and nl' series are indicated in the figures where the $nd[1/2]$ and $nd[3/2]$ states which converge to the same $2P_{3/2}$ limit are labelled as nd and \underline{nd} respectively. For peaks in the experimental spectrum which are completely resolved such as the $4s$ and $4s'$ resonance lines of argon, integration of the peak areas provides a direct measure of the absolute optical oscillator strengths for the respective individual discrete electronic transitions. For states at higher energies which cannot be completely resolved, absolute oscillator

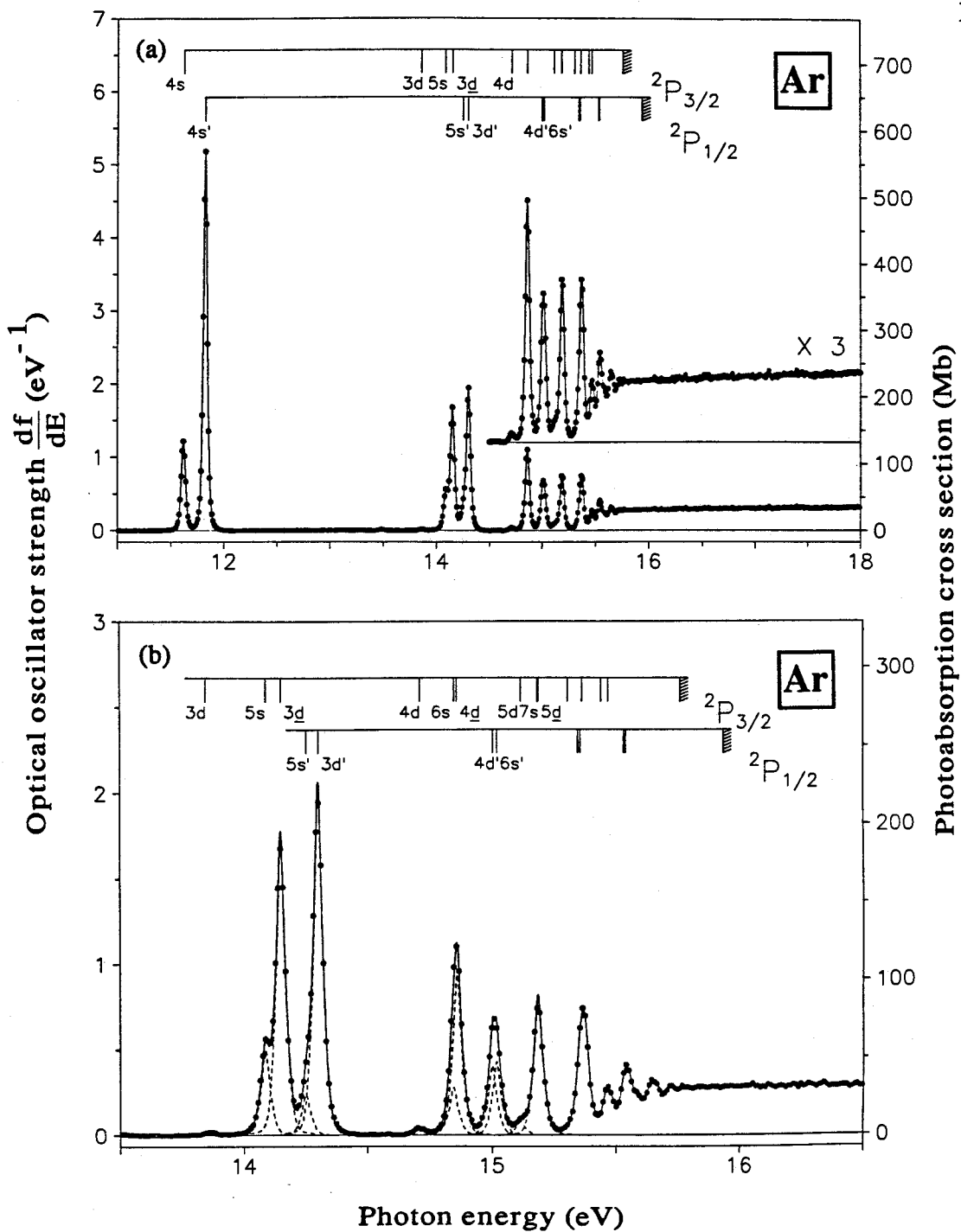


Figure 6.9: Absolute oscillator strengths for the photoabsorption of argon obtained using the high resolution dipole (e,e) spectrometer (FWHM=0.048 eV). The assignments and energy positions are taken from reference [155]. (a) 11–18 eV. (b) Expanded view of the 13.5–16.5 eV energy region. The deconvoluted peaks are shown as dashed lines.

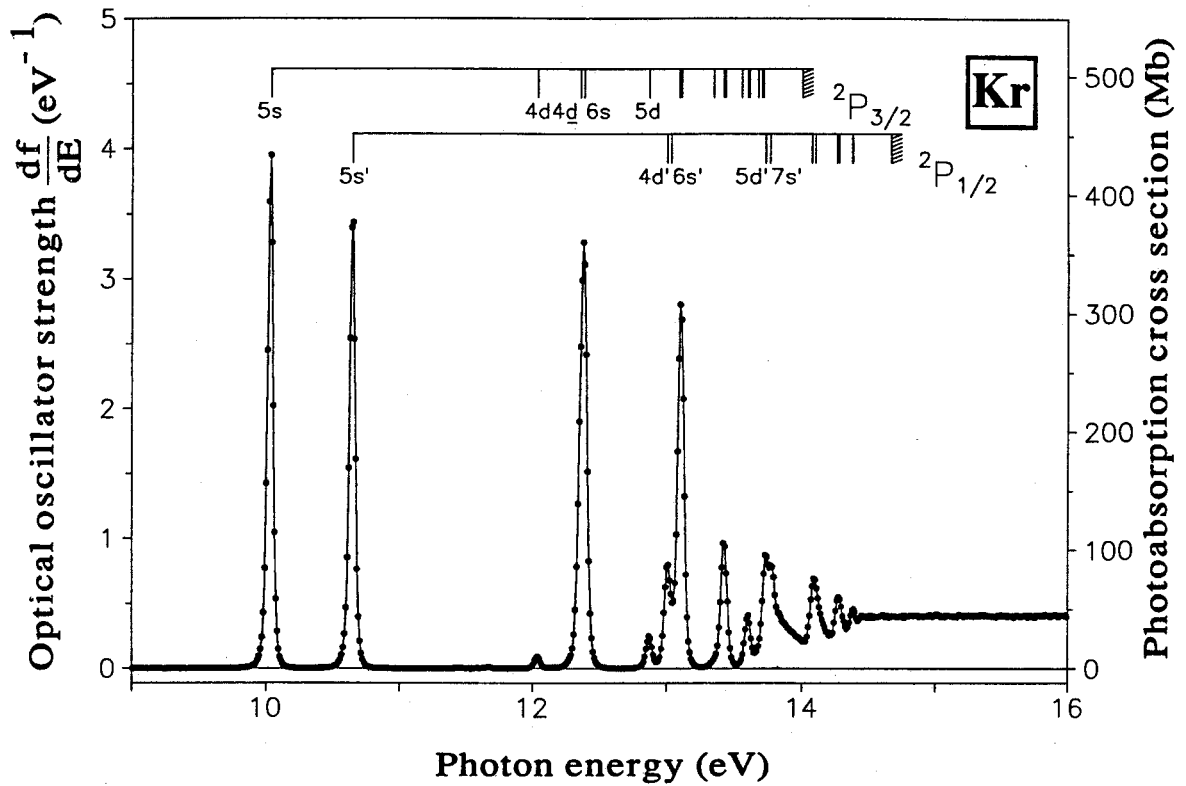


Figure 6.10: Absolute oscillator strengths for the photoabsorption of krypton obtained using the high resolution dipole (e,e) spectrometer (FWHM=0.048 eV) in the energy region 9–16 eV. The assignments and energy positions are taken from reference [155].

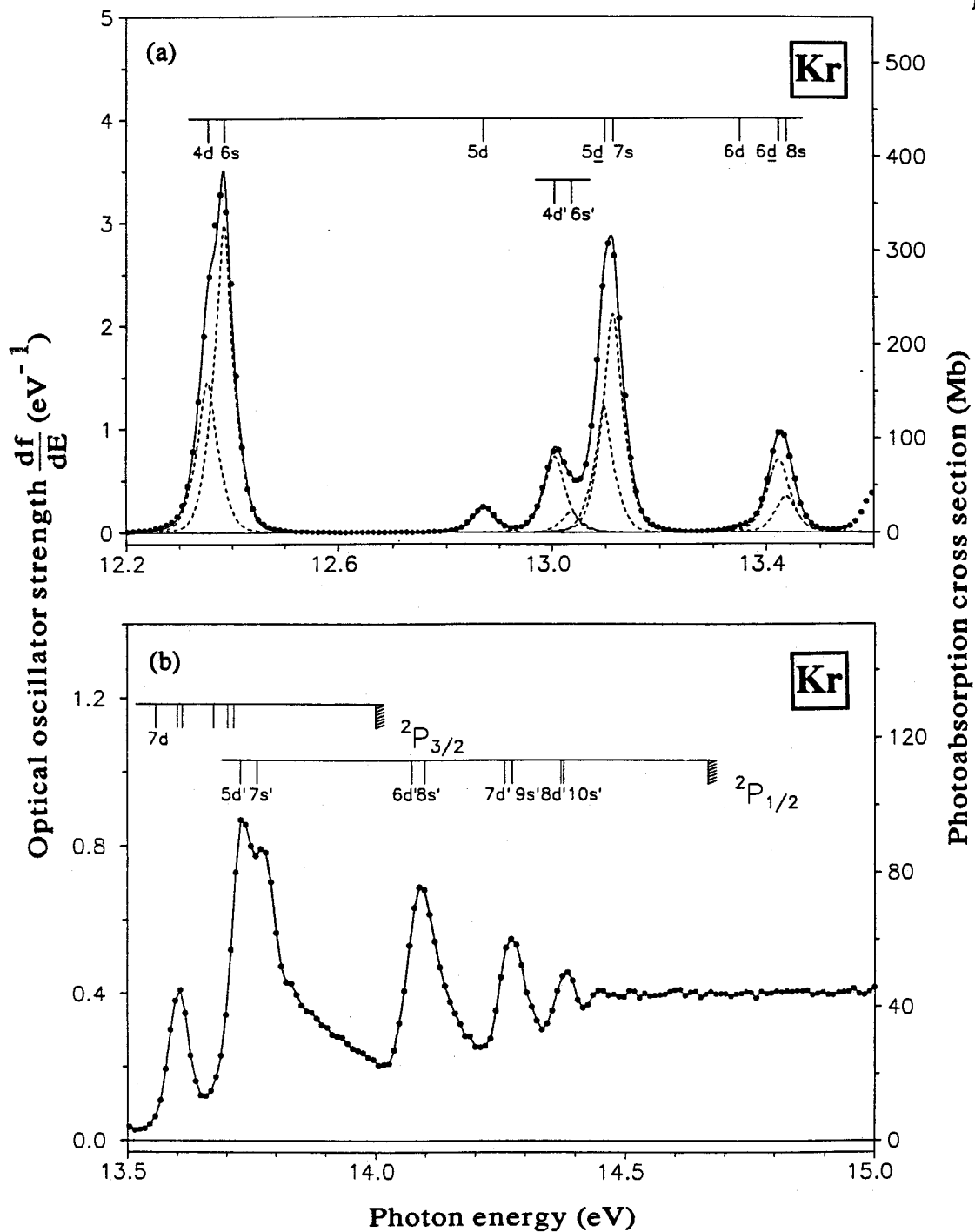


Figure 6.11: Absolute oscillator strengths for the photoabsorption of krypton obtained using the high resolution dipole (e,e) spectrometer (FWHM=0.048 eV). The assignments and energy positions are taken from reference [155]. (a) Expanded view of the 12.2–13.6 eV energy region. The deconvoluted peaks are shown as dashed lines. (b) Expanded view of the 13.5–15.0 eV energy region.

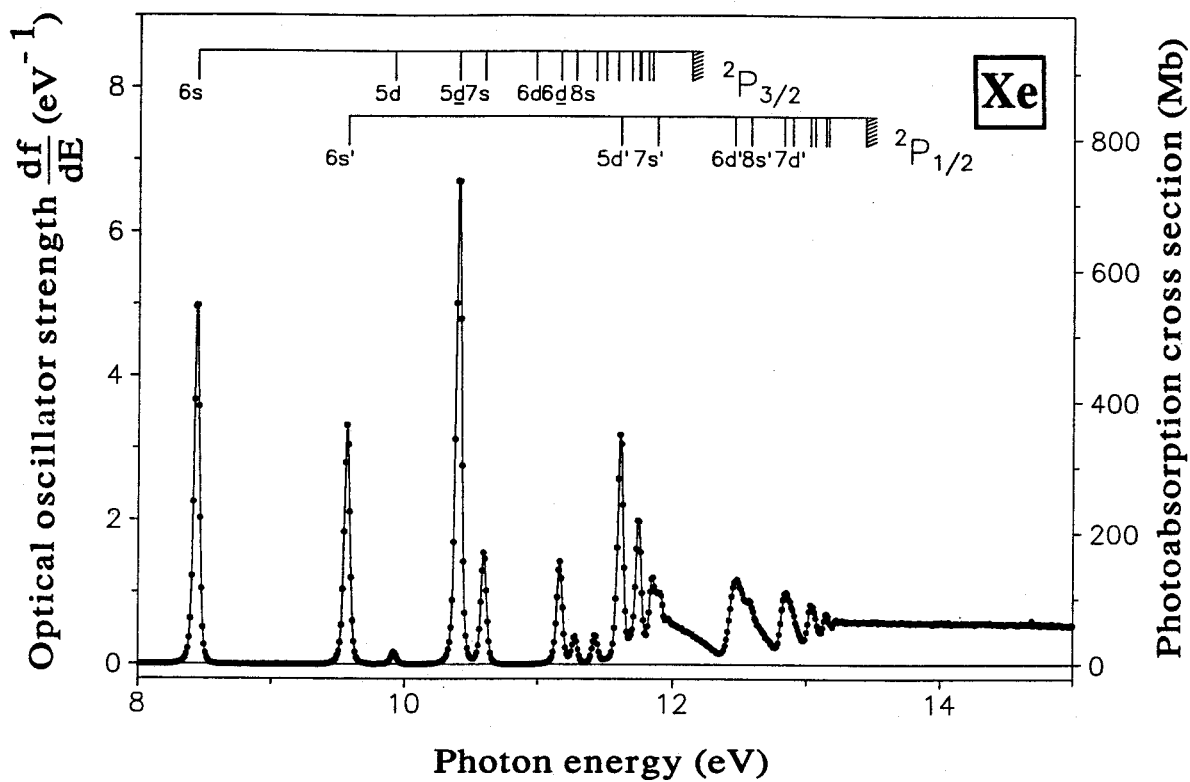


Figure 6.12: Absolute oscillator strengths for the photoabsorption of xenon obtained using the high resolution dipole (e,e) spectrometer (FWHM=0.048 eV) in the energy region 8–15 eV. The assignments and energy positions are taken from reference [155].

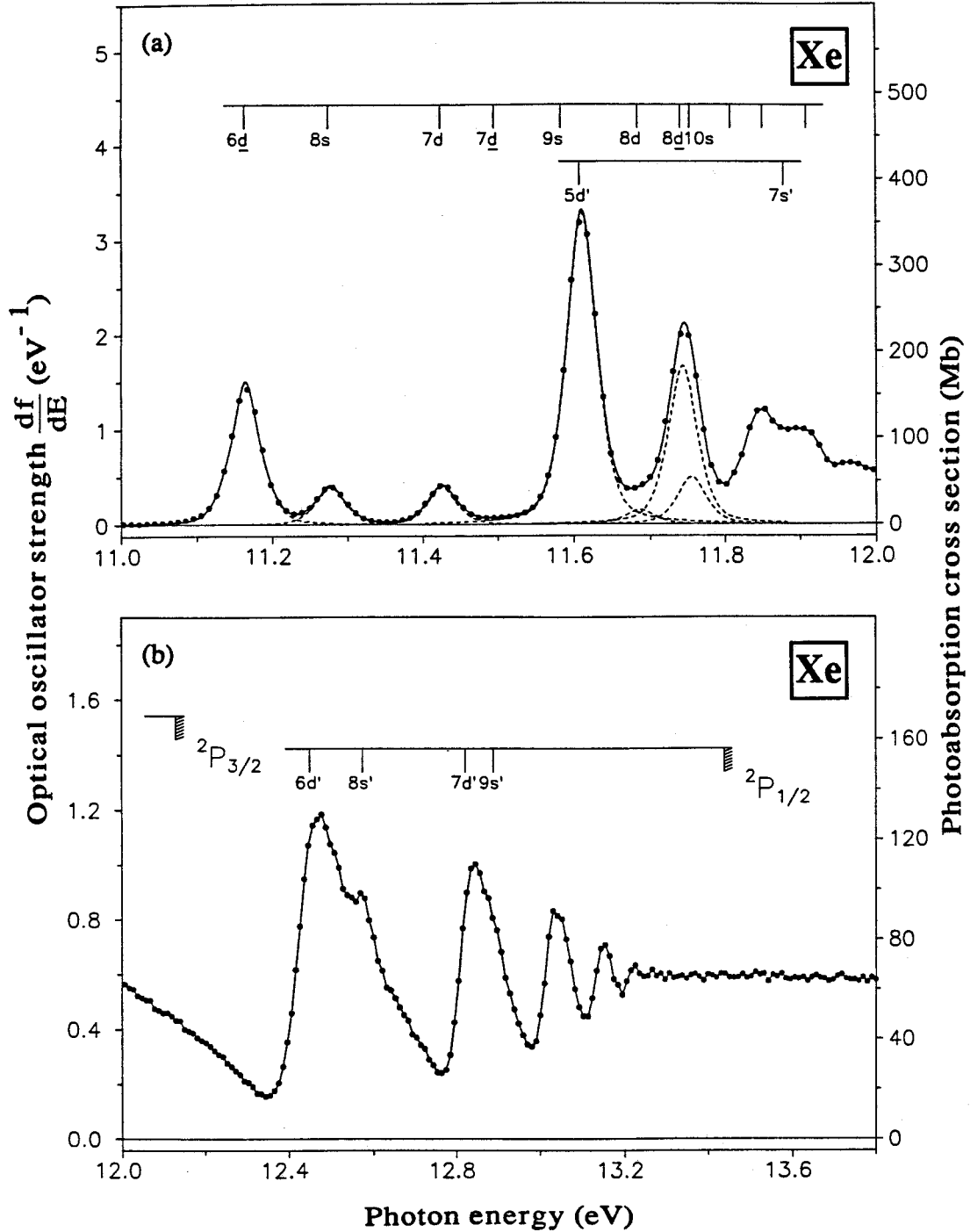


Figure 6.13: Absolute oscillator strengths for the photoabsorption of xenon obtained using the high resolution dipole (e,e) spectrometer (FWHM=0.048 eV). The assignments and energy positions are taken from reference [155]. (a) Expanded view of the 11–12 eV energy region. The deconvoluted peaks are shown as dashed lines. (b) Expanded view of the 12–13.7 eV energy region.

strengths have been obtained from fitted peak areas as shown in the figures, according to least squares fits of the experimental data. The same fitting procedures have been applied to the spectra obtained at the three different experimental resolutions. The consistency of the oscillator strength values obtained for given transitions at the different resolutions confirms the accuracy of the fitting procedures and the respective Bethe–Born factors determined as described in refs. [37,38] and chapter 3. Tables 6.4–6.9 summarize the optical oscillator strengths for the discrete transitions of the three noble gases obtained from the analyses of the spectra (figures 6.9–6.13) at the highest resolution (0.048 eV FWHM). The uncertainties are estimated to be ~5% for resolved transitions and $\leq 10\%$ for unresolved peaks such as the 5s, 5s', 3d and 3d' excited states of argon due to the additional errors involved in deconvoluting the peaks. Other previously reported experimental and theoretical oscillator strengths for the discrete electronic transitions of the three noble gases are also shown in the tables for comparison.

Figure 6.9(a) shows a typical absolute differential optical oscillator strength spectrum of argon obtained at a resolution of 0.048 eV FWHM over the energy range 11–18 eV. Figure 6.9(b) shows an expanded view of the spectrum in the 13.5–16.5 eV energy region including the fitted peaks corresponding to partially resolved or unresolved states. Since most of the previously reported experimental [62,138,139,141,197,199,202,205,206,208,209,214] and theoretical [111,147,151,181,186,188] data are restricted mainly to the 4s (a_1) and

Theoretical and experimental determinations of the absolute optical oscillator strengths for the $3s^23p^6 \rightarrow 3s^23p^5(2P_{3/2,1/2})4s$ discrete transitions of argon[†]

	Oscillator strength for transition from $3s^23p^6 \rightarrow 3s^23p^5m$ where m is		Oscillator strength ratio (a_1/a_2)
	$(2P_{3/2})4s$ (a_1) (11.614 eV) [#]	$(2P_{1/2})4s'$ (a_2) (11.828 eV)	
A. Theory:			
Amus'ya (1990) [145]	0.298 [*]		
Cooper (1962) [104]	0.33 [*]		
Stewart (1975) [151]		0.270	
Albat <i>et al.</i> (1975) [188]	0.048	0.188	0.255
Gruzdev and Loginov (1975) [186]	0.061	0.231	0.264
Lee (1974) [185]	0.059	0.30	0.197
Lee and Lu (1973) [184]	0.080	0.210	0.381
Aymar <i>et al.</i> (1970) [147]			
(a) dipole length	0.071	0.286	0.248
(b) dipole velocity	0.065	0.252	0.258
Gruzdev (1967) [111]	0.075	0.15	0.500
Knox (1958) [181]			
(a) wavefunction	0.052	0.170	0.306
(b) semi-empirical	0.049	0.200	0.245
B. Experiment:			
Present work (HR dipole(e,e))	0.0662 (0.0033)	0.265 (0.013)	0.250
Tsurubuchi <i>et al.</i> (1990) [140] (Absolute self-absorption)	0.057 (0.003)	0.213 (0.011)	0.268
Li <i>et al.</i> (1988) [143] (Electron impact)	0.058 (0.003)	0.222 (0.02)	0.261
Chornay <i>et al.</i> (1984) [202] (Lifetime: electron-photon coincidence)	0.065 (0.005)		
Westerveld <i>et al.</i> (1979) [139] (Absolute self-absorption)	0.063 (0.005)	0.240 (0.02)	0.263
Geiger (1978) [213] (Electron impact)	0.066	0.255	0.259

Table 6.4 (continued)

	Oscillator strength for transition from $3s^23p^6 \rightarrow 3s^23p^5m$ where m is		Oscillator strength ratio (a_1/a_2)
	($^2P_{3/2}$)4s (a_1)	($^2P_{1/2}$)4s' (a_2)	
	(11.614 eV) [#]	(11.828 eV)	
B: Experiment: (continued)			
Vallee <i>et al.</i> (1976) [206]	0.051	0.210	0.243
(Pressure broadening profile)	(0.007)	(0.030)	
Kuyatt (1975) [219]	0.067	0.267	0.251
(Electron impact)			
Copley and Camm (1974) [205]	0.076	0.283	0.269
(Pressure broadening profile)	(0.008)	(0.024)	
Irwin <i>et al.</i> (1973) [199]	0.083	0.35	0.237
(Lifetime: beam foil)	(0.027)	(0.130)	
Natali <i>et al.</i> (1973) [142]	0.070	0.278	0.252
(Electron impact)			
McConkey and Donaldson (1973) [208]	0.096		
(Electron excitation function)	(0.02)		
Jongh and Eck (1971) [62]		0.22	
(Relative self-absorption)		(0.02)	
Geiger (1970) [141]	0.047	0.186	0.253
(Electron impact)	(0.009)	(0.037)	
Lawrence (1968) [198]	0.059	0.228	0.259
(Lifetime: Delay coincidence)	(0.003)	(0.021)	
Morack and Fairchild (1967) [197]	0.024		
(Lifetime: delayed coincidence)	(0.003)		
Lewis (1967) [138]	0.063	0.278	0.227
(Pressure broadening profile)	(0.004)	(0.002)	
Chamberlain <i>et al.</i> (1965) [209]	0.049	0.181	0.271
(Electron impact)			

[†] Estimated uncertainties in the experimental measurements are shown in parentheses.

^{*} Summed oscillator strength (a_1+a_2).

Table 6.5(a)
Theoretical and experimental determinations of the absolute optical oscillator strengths for discrete transitions of argon in the energy region 13.80–14.85 eV†

	Oscillator strength from $3s^23p^6 \rightarrow 3s^23p^5m$ where m, l, s						
	$(^2P_{3/2})3d^*$ (13.864 eV)‡	$(^2P_{3/2})5s$ (14.090 eV)	$(^2P_{3/2})3d$ (14.153 eV)	$(^2P_{1/2})5s'$ (14.255 eV)	$(^2P_{1/2})3d'$ (14.304 eV)	$(^2P_{3/2})4d$ (14.711 eV)	$(^2P_{3/2})6s$ (14.848 eV)
A: Theory:							
Lee (1974) [185]	0.0016	0.045	0.045	0.039	0.128	0.0026	0.023
Lee and Lu (1973) [184]	0.0011	0.034	0.053	0.025	0.11	0.0031	0.014
B: Experiment:							
Present work (HR dipole (e.e))	0.0013 (0.0001)	0.0264 (0.0026)	0.0914 (0.0091)	0.0126 (0.0013)	0.106 (0.011)	0.0019 (0.0002)	0.0144 (0.0014)
Westerveld <i>et al.</i> (1979) [139] (Absolute self-absorption)	0.00089 (0.00007)	0.025 (0.002)	0.079 (0.006)	0.0106 (0.0008)	0.086 (0.007)		
Geiger (1978) [213] (Electron impact)	<0.0025	0.032	0.108	0.0108	0.097		
Natali <i>et al.</i> (1973) [142] (Electron impact)	0.0010	0.028	0.092	0.0124	0.110	0.004	0.0094
Wiese <i>et al.</i> (1969) [54]@ (Lifetime data from ref. [198])		0.0268	0.093	0.0119	0.0106		
Lawrence (1968) [198] (Lifetime: delayed coincidence)		0.028 (0.002)	0.093 (0.006)	0.013 (0.003)	0.107 (0.015)		

† Estimated uncertainties in the experimental measurements are shown in parentheses.

* nd and nd refer to the $nd(1/2)$ and $nd(3/2)$ states respectively which converge to the same $2p\ 3/2$ limit.

‡ The transition energies were obtained from ref. [155].

@ Values obtained by reanalyzing the lifetime data of Lawrence (1968) [198].

Table 6.5(b)
Theoretical and experimental determinations of the absolute optical oscillator strengths for discrete transitions of argon in the energy region 14.85–15.30 eV†

	Oscillator strength from $3s^23p^6 \rightarrow 3s^23p^5m$ where m is						Total to ionization
	$(2P_{3/2})4d^*$ (14.859 eV)‡	$(2P_{1/2})4d'$ (15.004 eV)	$(2P_{1/2})6s'$ (15.022 eV)	$(2P_{3/2})5d$ (15.118 eV)	$(2P_{3/2})7s$ (15.186 eV)	$(2P_{3/2})5d$ (15.190 eV)	
A: Theory:							
Lee (1974) [185]	0.036						0.82
Lee and Lu (1973) [184]	0.039	0.032	0.013				
B: Experiment:							
Present work (HR dipole (e,e))	0.0484 (0.0048)	0.0209 (0.0021)	0.0221 (0.0022)	0.0041 (0.0004)	0.0426 (0.0043)		0.859 (0.0043)
Natali <i>et al.</i> (1973) [142] (Electron impact)	0.048	0.015	0.0224	0.0032	0.0139	0.0234	0.827

† Estimated uncertainties in the experimental measurements are shown in parentheses.

* nd and nd refer to the nd(1/2) and nd(3/2) states respectively which converge to the same $2P_{3/2}$ limit.

The transition energies were obtained from ref. [155].

Table 6.6

Theoretical and experimental determinations of the absolute optical oscillator strengths for the $4s^2 4p^6 \rightarrow 4s^2 4p^5 ({}^2P_{3/2,1/2}) 5s$ discrete transitions of krypton⁺

	Oscillator strength for transition from $4s^2 4p^6 \rightarrow 4s^2 4p^5 m$ where m is		Oscillator strength ratio (b_1/b_2)
	(${}^2P_{3/2}$)5s (b_1) (10.033 eV) [#]	(${}^2P_{1/2}$)5s' (b_2) (10.644 eV)	
A. Theory:			
Amus'ya (1990) [145]	0.353 [*]		
Cooper (1962) [104]	0.405 [*]		
Aymar and Coulombe (1978) [189]			
(a) dipole length	0.176	0.177	0.99
(b) dipole velocity	0.193	0.172	1.12
Geiger (1977) [212]	0.250	0.143	1.748
Gruzdev and Loginov (1975) [187]	0.190	0.177	1.073
Aymar <i>et al.</i> (1970) [147]			
(a) dipole length	0.215	0.215	1.000
(b) dipole velocity	0.185	0.164	1.128
Gruzdev (1967) [111]	0.20	0.20	1.000
Dow and Knox (1966) [182]			
(a) wavefunction	0.138	0.136	1.015
(b) semi-empirical	0.152	0.153	0.993
B. Experiment:			
Present work (HR dipole(e.e))	0.214 (0.011)	0.193 (0.010)	1.109
Tsurubuchi <i>et al.</i> (1990) [140]	0.155 (0.011)	0.139 (0.010)	1.115
(Absolute self-absorption)			
Takayanagi <i>et al.</i> (1990) [215]	0.143 (0.015)	0.127 (0.015)	1.126
(Electron impact)			

Table 6.6 (continued)

	Oscillator strength for transition from $4s^{24}p^6 \rightarrow 4s^{24}p^5m$ where m is		Oscillator strength ratio (b_1/b_2)
	($^2P_{3/2}$)5s (b_1) (10.033 eV) [#]	($^2P_{1/2}$)5s' (b_2) (10.644 eV)	
B: Experiment: (continued)			
Ferrell <i>et al.</i> (1987) [66] (Phase-matching)		0.180 (0.027)	
Matthias <i>et al.</i> (1977) [201] (Lifetime: resonance fluorescence)	0.208 (0.006)	0.197 (0.006)	1.056
Geiger (1977) [212] (Electron impact)	0.195	0.173	1.127
Natali <i>et al.</i> (1973) [142] (Electron impact)	0.212	0.191	1.110
Jongh and Eck (1971) [62] (Relative self absorption)		0.142 (0.015)	
Geiger (1970) [141] (Electron impact)	0.173 (0.035)	0.173 (0.035)	1.000
Griffin and Hutchison (1969) [192] (Total absorption)	0.187 (0.006)	0.193 (0.009)	0.969
Chashchina and Shrieder (1967) [193] (Linear absorption)	0.21 (0.05)	0.21 (0.05)	1.000
Lewis (1967) [138] (Pressure broadening profile)	0.204 (0.02)	0.184 (0.02)	1.109
Wilkinson (1965) [190] (Total absorption)	0.159	0.135	1.178
Turner (1965) [196] (Lifetime: resonance imprisonment)	0.166		

† Estimated uncertainties in the experimental measurements are shown in parentheses.

The transition energies were obtained from ref. [155].

* Summed oscillator strength (b_1+b_2).

Table 6.7(a)
Theoretical and experimental determinations of the absolute optical oscillator strengths for discrete transitions of krypton in the energy region 11.90–13.05 eV[†]

	Oscillator strength from $4s^2 4p^6 \rightarrow 4s 2 4p^5 m$ where m is					
	$(2P_{3/2})4d^*$ (12.037 eV) [#]	$(2P_{3/2})4d$ (12.355 eV)	$(2P_{3/2})6s$ (12.385 eV)	$(2P_{3/2})5d$ (12.870 eV)	$(2P_{1/2})4d'$ (13.005 eV)	$(2P_{1/2})6s'$ (13.037 eV)
A: Theory:						
Geiger (1977) [212]	0.0144	0.0973	0.108	0.0114	0.0438	0.0065
B: Experiment:						
Present work (HR dipole (e,e))	0.0053 (0.0003)	0.0824 (0.0082)	0.154 (0.015)	0.0140 (0.0014)	0.0435 (0.0044)	0.0105 (0.0011)
Geiger (1977) [212] (Electron impact)	0.0055	0.0649	0.142	0.014	0.0439	0.015
Natali <i>et al.</i> (1973) [142] (Electron impact)	0.0044	0.0817	0.152	0.0138	0.0420	0.0056

[†] Estimated uncertainties in the experimental measurements are shown in parentheses.

* nd and nd refer to the $nd[1/2]$ and $nd[3/2]$ states respectively which converge to the same $2P_{3/2}$ limit.

[#] The transition energies were obtained from ref. [155].

Table 6.7(b)

Theoretical and experimental determinations of the absolute optical oscillator strengths for discrete transitions of krypton in the energy region 13.05–13.50 eV[†]

	Oscillator strength from $4s^2 4p^6 \rightarrow 4s^2 4p^5 m$ where m is					Total to ionization
	$(2P_{3/2})5d^*$ (13.099 eV) [#]	$(2P_{3/2})7s$ (13.114 eV)	$(2P_{3/2})6d$ (13.350 eV)	$(2P_{3/2})6d$ (13.423 eV)	$(2P_{3/2})8s$ (13.437 eV)	
A: Theory:						
Geiger (1977) [212]	0.0960	0.0436	0.0025	0.0307	0.0163	
B: Experiment:						
Present work (HR dipole (e,e))	0.0610 (0.0061)	0.113 (0.011)	0.0015 (0.0002)	0.0439 (0.0044)	0.0203 (0.0020)	1.126 (0.056)
Geiger (1977) [212] (Electron impact)	0.187		0.0042	0.054		
Natali <i>et al.</i> (1973) [142] (Electron impact)	0.119	0.048	0.0024	0.0295	0.0290	1.10

[†] Estimated uncertainties in the experimental measurements are shown in parentheses.

* nd and nd refer to the $nd[1/2]$ and $nd[3/2]$ states respectively which converge to the same $2P_{3/2}$ limit.

[#] The transition energies were obtained from ref. [155].

Table 6.8

Theoretical and experimental determinations of the absolute optical oscillator strengths for the $5s^25p^6 \rightarrow 5s^25p^5(^2P_{3/2,1/2})6s$ discrete transitions of xenon*

	Oscillator strength for transition from $5s^25p^6 \rightarrow 5s^25p^5m$ where m is		Oscillator strength ratio (c_1/c_2)
	$(^2P_{3/2})6s$ (c_1) (8.437 eV)#	$(^2P_{1/2})6s'$ (c_2) (9.570 eV)	
A. Theory:	0.403*		
Amus'ya (1990) [145]			
Aymar and Coulombe (1978) [189]			
(a) dipole length	0.282	0.306	0.922
(b) dipole velocity	0.294	0.270	1.089
Geiger (1977) [212]	0.28	0.365	0.767
Aymar <i>et al.</i> (1970) [147]			
(a) dipole length	0.273	0.235	1.162
(b) dipole velocity	0.176	0.118	1.492
Kim <i>et al.</i> (1968) [183]	0.212	0.189	1.122
Gruzdev (1967) [111]	0.28	0.25	1.120
Dow and Knox (1966) [182]			
(a) wavefunction	0.194	0.147	1.320
(b) semi-empirical	0.190	0.170	1.118
B. Experiment:			
Present work (HR dipole(e.e))	0.273 (0.014)	0.186 (0.009)	1.468
Suzuki <i>et al.</i> (1991) [216]	0.222 (0.027)	0.158 (0.019)	1.405
(Electron impact)			
Ferrell <i>et al.</i> (1987) [66]	0.260 (0.05)	0.19 (0.04)	1.368
(Phase-matching)			

Table 6.8 (continued)

	Oscillator strength for transition from $5s^25p^6 \rightarrow 5s^25p^5m$ where m is		Oscillator strength ratio (c_1/c_2)
	$(^2P_{3/2})6s$ (c_1)	$(^2P_{1/2})6s'$ (c_2)	
	(8.437 eV) [#]	(9.570 eV)	
B: Experiment: (continued)			
Matthias <i>et al.</i> (1977) [201] (Lifetime: resonance fluorescence)	0.263 (0.007)	0.229 (0.007)	1.148
Geiger (1977) [212] (Electron impact)	0.26	0.19	1.368
Delage and Carette (1976) [211] (Electron impact)	0.183	0.169	1.083
Natali <i>et al.</i> (1973) [142] (Electron impact)	0.272	0.189	1.439
Wieme and Mortier (1973) [200] (Lifetime: resonance imprisonment)	0.213 (0.020)	0.180 (0.040)	1.183
Geiger (1970) [141] (Electron impact)	0.26	0.19	1.368
Griffin and Hutchison (1969) [192] (Total absorption)		0.194 (0.005)	
Lewis (1967) [138] (Pressure broadening profile)	0.256 (0.008)	0.238 (0.015)	1.071
Wilkinson (1966) [191] (Total absorption)	0.260 (0.020)	0.270 (0.020)	0.963
Anderson (1965) [195] (Lifetime: level-crossing)	0.256 (0.008)	0.238 (0.015)	1.076

[†] Estimated uncertainties in the experimental measurements are shown in parentheses.

[#] The transition energies were obtained from ref. [155].

* Summed oscillator strength (c_1+c_2).

Table 6.9(a)
Theoretical and experimental determinations of the absolute optical oscillator strengths for discrete transitions of xenon in the energy region 9.80–11.45 eV[†]

	Oscillator strength from $5s^25p^6 \rightarrow 5s25p^5m$ where m is							
	$(^2P_{3/2})5d^*$ (9.917 eV) [#]	$(^2P_{3/2})5d$ (10.401 eV)	$(^2P_{3/2})7s$ (10.593 eV)	$(^2P_{3/2})6d$ (10.979 eV)	$(^2P_{1/2})6d$ (11.163 eV)	$(^2P_{3/2})8s$ (11.274 eV)	$(^2P_{3/2})7d$ (11.423 eV)	
A: Theory:								
Geiger (1977) [212]	0.0237	0.550	0.0769	0.0025	0.0940	0.0126	0.0190	
B: Experiment:								
Present work (HR dipole (e,e))	0.0105 (0.0005)	0.379 (0.019)	0.0859 (0.0043)	<0.001	0.0835 (0.0084)	0.0222 (0.0022)	0.0227 (0.0023)	
Ferrell <i>et al.</i> (1987) [66] (Phase-matching)		0.370 (0.07)	0.088 (0.01)					
Kramer <i>et al.</i> (1984) [207] (Phase-matching)			0.098					
Geiger (1977) [212] (Electron impact)	0.0095	0.395	0.0968	0.0025	0.0862	0.0236	0.0217	
Delage and Carrette (1976) [211] (Electron impact)	0.019	0.395 [@]	0.110		0.123	0.032	0.027	
Natall <i>et al.</i> (1973) [142] (Electron impact)	0.012	0.381	0.09	0.002	0.082	0.021	0.021	

[†] Estimated uncertainties in the experimental measurements are shown in parentheses.

^{*} nd and nd refer to the nd|1/2| and nd|3/2| states respectively which converge to the same $^2P_{3/2}$ limit.

[#] The transition energies were obtained from ref. [155].

[@] This value was normalized to the experimental value of Geiger (1977) [212].

Table 6.9(b)
Theoretical and experimental determinations of the absolute optical oscillator strengths for discrete transitions of xenon in the energy region 11.45–11.80 eV[†]

	Oscillator strength from $5s^25p^6 \rightarrow 5s^25p^5m$ where m is						Total to ionization
	$(^2P_{3/2})7d^*$ (11.495 eV) [#]	$(^2P_{3/2})9s$ (11.583 eV)	$(^2P_{1/2})5d'$ (11.607 eV)	$(^2P_{3/2})8d$ (11.683 eV)	$(^2P_{3/2})8d$ (11.740 eV)	$(^2P_{3/2})10s$ (11.752 eV)	
A: Theory: Gelger (1977) [212]	0.0024	0.0009	0.206	0.0155	0.123	0.0169	
B: Experiment: Present work (HR dipole (e,e))	<0.001	<0.001	0.191 (0.019)	0.0088 (0.0009)	0.0967 (0.0097)	0.0288 (0.0029)	1.606 (0.080)
Gelger (1977) [212] (Electron Impact)	0.004	0.006	0.205	0.0096	0.123	0.0204	1.640 [⊗]
Delage and Carrette (1976) [211] (Electron Impact)			0.251		0.171		
Natail et al. (1973) [142] (Electron Impact)	0.0003	0.001	0.186	0.006	0.109	0.015	

[†] Estimated uncertainties in the experimental measurements are shown in parentheses.

^{*} nd and nd refer to the nd|1/2| and nd|3/2| states respectively which converge to the same $^2P_{3/2}$ limit.

[#] The transition energies were obtained from ref. [155].

[⊗] This value is quoted in ref. [143].

4s' (a_2) resonance lines[#], the results for these two lines are presented separately in table 6.4. Immediately it can be seen that there are great variations in the oscillator strength values reported for the 4s and 4s' lines in both experimental work and also in the theoretical calculations. However, experimental work gives a reasonably consistent result (~0.25) for the oscillator strength ratio (a_1/a_2) as shown in the fourth column of table 6.4. This suggests that systematic errors, such as uncertainties in measuring the target density or errors in normalizing the data, may be the cause of the large variations in the absolute values. The summed absolute optical oscillator strength (i.e. a_1+a_2) calculated by Cooper [104], using a one-electron approximation, (value of Cooper) agrees very well with the sum of the presently measured values (0.331) while the value (0.298) reported by Amus'ya [145] using the RPAE method is slightly lower. The calculated data reported by Aymar *et al.* [147] for a_1 and a_2 , and the value reported by Stewart [151] for a_2 are consistent with the present work. The calculations by Knox [181] and by Albat *et al.* [188] give very low values. Experimentally, the oscillator strength values reported by three groups [62,139,140] using the self-absorption method are all lower than the present values by 5–20%. Lifetime measurements performed by Irwin *et al.* [199] using the beam foil method show values for a_1 and a_2 much higher than the present work, while the value of a_1 reported by Morack and Fairchild [197], who used a delayed coincidence method, is much lower than all other experimental values. The values measured by Copley and Camm [205] and by Lewis [138] from analyses of

[#] The designations a_1, a_2 ; b_1, b_2 ; and c_1, c_2 ; are used for convenience in the present work for the respective ns, ns' resonance lines of argon, krypton and xenon, respectively.

the pressure broadening profiles are consistent with the present work. Several electron impact based experimental methods have been employed for deriving the absolute oscillator strengths for a_1 and a_2 . The values reported by Chamberlain *et al.* [209], Geiger in his earlier work [141] and Li *et al.* [214], are all lower than those measured in the present work. However the unpublished data of Natali *et al.* [142], the data of Kuyatt [219] which are quoted in the compilation of Eggarter [217], and the later work of Geiger [213] which has been quoted in refs. [139,143], show quite good agreement with the presently measured values. In a compilation published by Wiese *et al.* [54] values of a_1 and a_2 (not shown in table 6.4) were obtained from averaging the data reported by Lawrence [198] and Lewis [138].

A summary of the absolute optical oscillator strengths for the discrete transitions of argon at higher energies is given in tables 6.5(a) and 6.5(b). Two sets of theoretical results [184,185] have been published, but both show substantial differences with the presently reported and most other experimental data. The lifetime measurements of Lawrence [198], obtained using a pulsed electron source, show good agreement with the present values for the $5s$, $3d$, $5s'$ and $3d'$ transition lines. A reanalysis of the lifetime data of Lawrence [198] by Wiese *et al.* [54] gave absolute oscillator strength values for the above four transition lines which are also consistent with the present work. Similar to the situation for the $4s$ and $4s'$ resonance lines, the self-absorption data for other lines at higher energies measured by Westerveld *et al.* [139] are lower than the present values. A more comprehensive data set was reported in the electron impact based work of Natali *et al.* [142], and the oscillator strength values for most of the more intense lines are

consistent with the present work. The total discrete oscillator strength sum up to the $2P_{3/2}$ ionization threshold of argon has been determined in the present work to be 0.859, a value which agrees within 5% with estimates of 0.82 calculated by Lee [185] and 0.827 measured by Natali *et al.* [142]. In the earlier compilation reported by Eggarter [217], the total discrete oscillator strength of argon was estimated to be 0.793 on the basis of the more limited data available at that time.

Figure 6.10 shows the presently determined absolute differential optical oscillator strength spectrum for krypton over the energy range 9–16 eV. Figures 6.11(a) and 6.11(b) show expanded views of the spectrum in the energy regions 12.2–13.6 eV and 13.5–15 eV, respectively. Since higher members of the ns' and nd' series which converge to the $2P_{1/2}$ ionization threshold are above the $2P_{3/2}$ ionization threshold, autoionizing resonance profiles are observed as shown in figure 6.11(b) due to the interaction between the discrete and continuum states. The absolute optical oscillator strengths for the individual discrete electronic transitions of krypton determined in the present work are summarized in tables 6.6 and 6.7. There are considerable variations between the various experimental and theoretical oscillator strength values for both the $5s$ (b_1) and the $5s'$ (b_2) resonance lines as can be seen in table 6.6. However, on the basis of the oscillator strength ratio (b_1/b_2) the reported data can be divided into two groups. For one group the ratio is close to 1 while for the other it is ~ 1.1 . The summed absolute optical oscillator strength (i.e. 0.405 for b_1+b_2) computed by Cooper [104] is consistent with the present value (0.407). The values of b_1 and b_2 calculated by Dow and Knox [182] are too low compared with the present and most other experimental work. Similar to the situation

for argon the self-absorption data reported by Tsurubuchi *et al.* [140] for b_1 and b_2 and Jongh and Eck [62] for b_2 are lower than the presently reported values. The experimental data of Ferrell *et al.* [66] obtained using the phase-matching method, that of Matthias *et al.* [201], which was determined by measuring the lifetimes of the radiative fluorescence, the data of Natali *et al.* [142], who applied the electron impact based method and the data of Lewis [138], which were obtained by studying the pressure broadening profiles, are all in good agreement with the presently reported oscillator strength values for b_1 and b_2 . The absolute optical oscillator strength values for transitions at higher energies are shown in tables 6.7(a) and 6.7(b). The theoretical data available are limited to the semi-empirical calculations reported by Geiger [212]. Only the value for the $4d'$ resonance line computed by Geiger [212] agrees with the present results. Previously published data obtained by application of electron impact based methods [142,212] together with the present dipole (e,e) work provide the only available optical oscillator strength data for the discrete transitions of krypton at higher energies. Generally quite good agreement for the absolute optical oscillator strength values is observed among the different electron impact methods for most of the transition lines. The total discrete oscillator strength up to the $2P_{3/2}$ ionization threshold is determined to be 1.126 in the present work compared with an estimate of 1.10 reported by Natali *et al.* [142].

Figure 6.12 shows the high resolution absolute differential oscillator strength spectrum of xenon obtained in the present work over the energy region 8–15 eV. Figures 6.13(a) and 6.13(b) show expanded views of the spectrum in the energy regions 11–12 eV and 12–13.7 eV

respectively. Broad autoionizing resonance profiles of higher members of the ns' and nd' series above the $2P_{3/2}$ limit are observed as can be seen in figure 6.13(b). Tables 6.8 and 6.9 summarize all the discrete absolute optical oscillator strengths values for xenon determined in the present work along with various previously reported theoretical and experimental data. It can be seen from table 6.8 that there are large variations in the oscillator strengths reported for the $6s$ (c_1) and $6s'$ (c_2) resonance lines. The oscillator strength ratio of c_1/c_2 also shows considerable variation from 0.767–1.492 for theory and 0.963–1.468 for experiment. Some theoretical data show agreement of either c_1 [111,147,189,212] or c_2 [183] with the present work. However, no single set of theoretical data are consistent with the present work for both the c_1 and c_2 values. Experimentally, the phase-matching data of Ferrell *et al.* [66], and the electron impact data of Geiger [141,212] and Natali *et al.* [142] show good agreement with the presently reported c_1 and c_2 values. The recently reported data of Suzuki *et al.* [216] are ~20% lower than the present values. Similar discrepancies were observed in the cases of the a_1 and a_2 transitions of argon and the b_1 and b_2 transitions of krypton between the present work and absolute oscillator strengths reported by the same group [214,215] (see above). The absolute data for the discrete transitions at higher energies are shown in tables 6.9(a) and 6.9(b). The phase-matching data of Ferrell *et al.* [66] show excellent agreement for the $5\bar{d}$ and $7s$ lines with the present values while the earlier phase-matching value reported by Kramer *et al.* [207] for the $7s$ line is slightly higher. Other more comprehensive data for the discrete transitions of xenon at higher energies have all been measured by electron impact based methods [142,211,212]. It can be seen that the oscillator

strengths determined in the present work are in excellent agreement over the whole energy range with the data reported by Natali *et al.* [142], except for the 10s line. This discrepancy may be caused by errors in deconvoluting the peak. The data of Geiger [212] are consistent with the present work for most of the transitions, while the data of Delage and Carette [211], which have been normalized on the 5d line from the data of Geiger [212], show considerable variations compared with the presently reported values. Finally, the total oscillator strength sum up to the $2P_{3/2}$ ionization threshold of xenon was determined to be 1.606 in the present work, which is in good agreement with the estimate of 1.640 reported by Geiger [212].

6.2.3 High Resolution Measurements of the Photoabsorption Oscillator Strengths in the Autoionizing Resonance Regions due to Excitation of the Inner Valence s Electrons

The profiles and relative cross sections of the autoionizing excited state resonances of argon, krypton and xenon involving the excitation of an inner valence ms electron have been previously studied in some detail experimentally [45,176,218,220–226]. Although double excitation processes have also been reported in these energy regions [218,221–223], these transitions are extremely weak and they are not specifically identified in the present work. Absolute intensity measurements [45,176,220,226] have also been reported. In the present study Bethe-Born converted electron energy loss spectra of the three noble gases were obtained in these regions with the use of the high resolution dipole (e,e) spectrometer at a resolution of 0.048 eV FWHM. The resulting

relative optical oscillator strength spectra were then normalized in the respective smooth continua at 21.218 eV for argon and krypton, and at 16.848 eV for xenon using the absolute data determined by Samson and Yin [178].

Figure 6.14 shows the resulting absolute optical oscillator strength spectrum of argon in the energy region 25–30 eV. The absolute data reported by Carlson *et al.* [176] (crosses) using synchrotron radiation and Samson [45,220] (open circles) employing a double ionization chamber are also shown in figure 6.14. Only the assignments for the transitions involving excitation of a 3s electron to an np states are shown. The energy positions of the resonances as indicated in the manifold on figure 6.14 are taken from the high resolution photoabsorption data reported by Madden *et al.* [218]. The data of Carlson *et al.* [176] show a slight shift in energy scale with respect to the present work, which may be due to errors in digitizing the data from the small figure in the original paper. The absolute data reported by Samson [45,220] and Carlson *et al.* [176] are in good agreement with the present work in the energy region 25–26 eV. However, the Samson data are higher than the present work above 29 eV while the data of Carlson *et al.* [176] are lower. It seems likely that "line saturation" effects, which have been discussed in detail in refs. [36,37,46,72] are observed in the direct optical data reported by Samson [45,220] for the 3s→np transitions. Since the widths of the 3s→np transition peaks became much narrower as n increases, "line saturation" effects are expected to be more severe for the peaks at higher n values. It can be seen from figure 6.14 that for the relatively broad 3s→4p transition, the data of Samson [45,220] show a lower minimum than the present data, which is consistent with the higher experimental

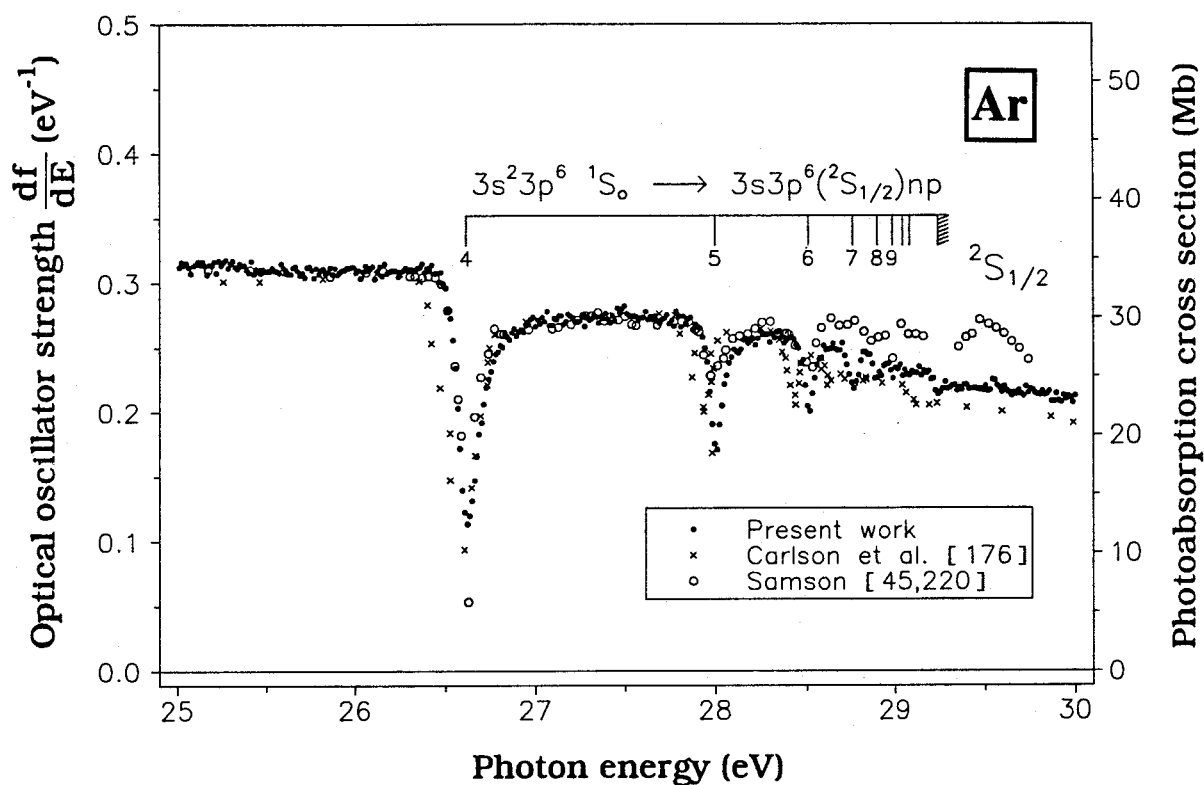


Figure 6.14: Absolute oscillator strengths for the photoabsorption of argon in the autoionizing resonance region 25–30 eV. The solid circles represent the present work (FWHM=0.048 eV), the open circles and crosses represent the photoabsorption data reported by Samson [45,220] and Carlson *et al.* [176], respectively. The assignments and energy positions are taken from reference [218].

resolution of Samson [45,220]. However, for the narrower $3s \rightarrow 5p$ transition, the present work (which cannot show "line saturation" effects) gives a lower minimum than the Samson data [45,220]. This observation strongly suggests the presence of "line-saturation" effects at larger n due to the finite bandwidth of the optical experiments [45,220]. The same phenomenon is observed for the transitions to the higher np states.

Figure 6.15 shows the presently determined high resolution absolute optical oscillator strength spectrum of krypton in the energy region 23–28.5 eV along with the reported absolute data of Samson [45,220]. The assignments and energy positions for the $4s \rightarrow np$ transitions are taken from Codling and Madden [221,223]. There are two $J=1$ components for the transition $4s^2 4p^6 \ ^1S_0 \rightarrow 4s 4p^6 ({}^2S_{1/2}) np$, where one Rydberg series is labelled as n and the other one is labelled as \underline{n} as shown in figure 6.15. Only $\underline{n}=5$ and $\underline{6}$ for the latter series are unambiguously assigned [221–223]. The "line-saturation" effects that are observed in the optical data reported by Samson [45,220] for argon are also seen in the corresponding direct optical data for krypton. The effect is especially severe for the $4s \rightarrow 7p$ transition. Samson [45,220] and other workers, using direct optical methods [221–223,226], have reported a peak (Q) at 24.735 eV which was not observed in the present work.

The presently determined high resolution absolute optical oscillator strength spectrum of xenon in the energy region 20–24 eV is shown in figure 6.16. The figure also shows the photoionization cross sections for xenon in this energy range reported by Samson [45], which are significantly lower than those determined in the present work. The assignments and energy positions for the $5s \rightarrow np$ transitions are taken from the data reported by Codling and Madden [221,223]. Only one

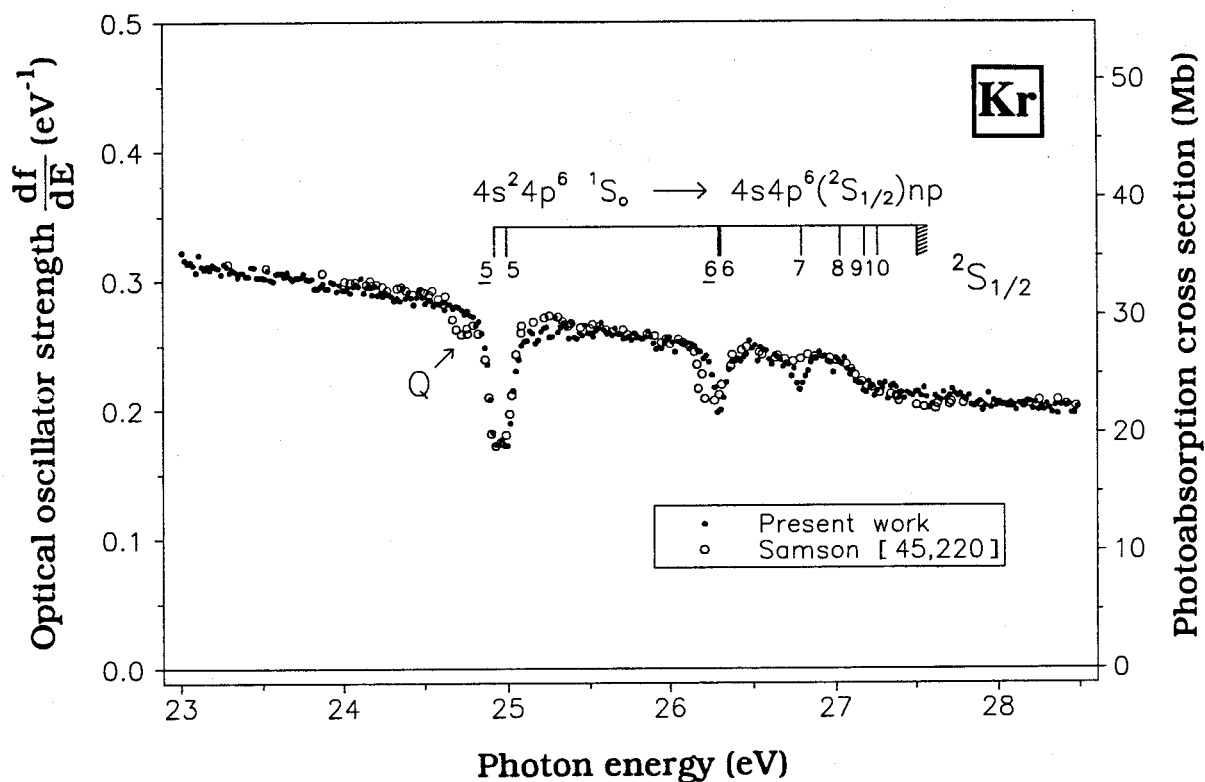


Figure 6.15: Absolute oscillator strengths for the photoabsorption of krypton in the autoionizing resonance region 23–28.5 eV. The solid circles represent the present work (FWHM=0.048 eV), the open circles represent the photoabsorption data reported by Samson [45,220]. The assignments and energy positions are taken from references [221,223].

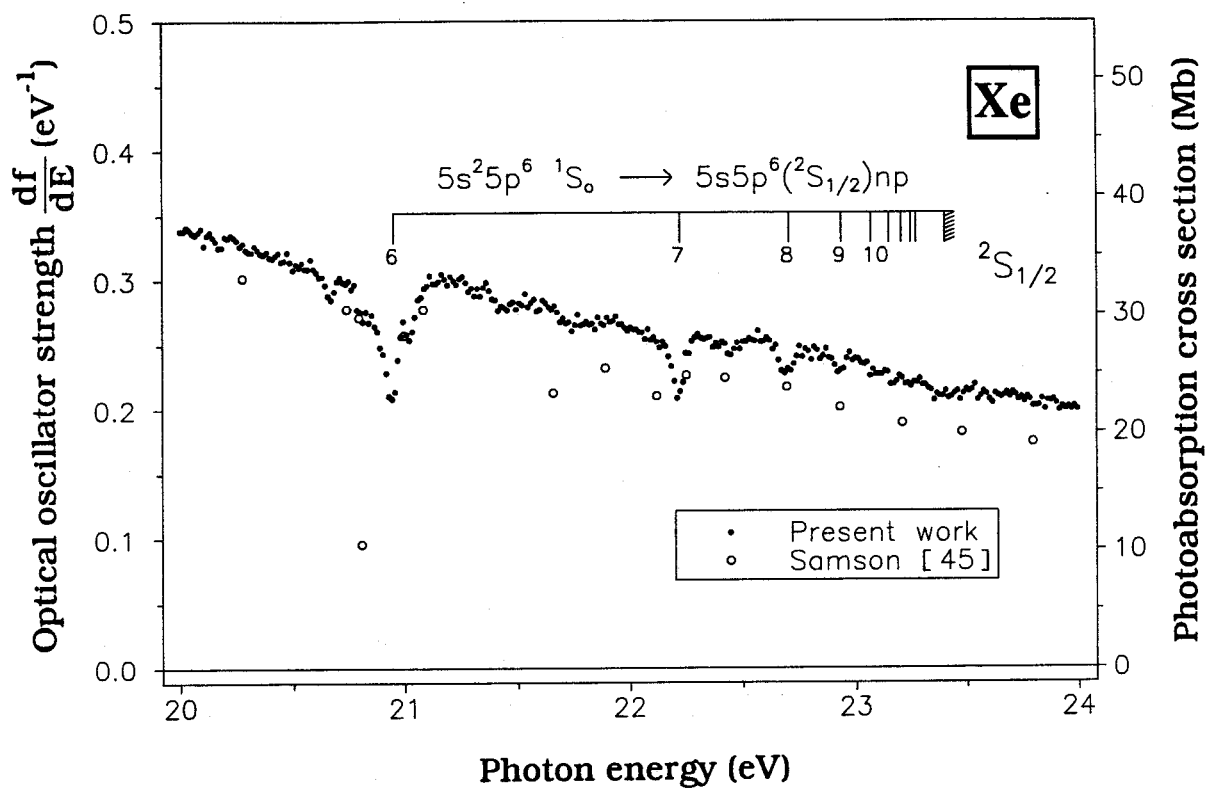


Figure 6.16: Absolute oscillator strengths for the photoabsorption of krypton in the autoionizing resonance region 20–24 eV. The solid circles represent the present work (FWHM=0.048 eV), the open circles represent the photoabsorption data reported by Samson [45]. The assignments and energy positions are taken from references [221,223].

Rydberg series of the two $J=1$ components of the $5s \rightarrow np$ transitions converging to the $2S_{1/2}$ ionization threshold has been assigned [221–223].

6.3 Conclusions

Comprehensive absolute differential optical oscillator strength data for argon, krypton and xenon in both the discrete and continuum regions have been reported, including measurements at high resolution. The present work represents the completion of the measurements for the noble gas series using the high resolution dipole (e,e) method recently developed for measuring absolute optical oscillator strengths for a wide range of transitions in atoms and molecules. The TRK sum-rule normalization method which was used for helium and neon could not be used for argon, krypton and xenon due to the smaller energy separations between the different subshells of the atoms. Therefore, single point normalization on very accurate photoabsorption measurements has been used. The presently reported results are compared with theory and also other earlier reported experimental data. In the continuum regions the various experimental values generally show reasonable agreement at low energy while there are certain variations at high energy. With the inclusion of more electron correlations and more sophisticated calculations, the theoretical data are in better agreement with experimental values. In the discrete region a wide spread of values is seen for the resonance line oscillator strengths a_1 and a_2 of argon, b_1 and b_2 of krypton and c_1 and c_2 of xenon in both experiment and theory. For discrete transitions at higher energies there is a shortage of theoretical

data. Electron impact based methods have thus far provided most of the absolute optical oscillator strength data for the valence shell discrete spectra. Generally, the present measurements are in quite good agreement with the earlier unpublished electron impact based data of Natali *et al.* [142] which were obtained at lower impact energy. Absolute optical oscillator strengths for the autoionizing excited state regions involving mainly the inner valence s-electrons of the three noble gases have also been obtained. The previously published photoionization data of Samson [45,220] in this energy range show evidence of substantial "line saturation" effects.

Chapter 7

Absolute Optical Oscillator Strengths (11–20 eV) and Transition Moments for the Lyman and Werner Bands of Molecular Hydrogen

7.1 Introduction

An accurate knowledge of absolute transition probabilities for electronic excitation is essential for a quantitative understanding of the interaction of energetic radiation with matter. Very few accurate absolute optical oscillator strength (cross section) measurements have been reported for molecular photoabsorption processes at high resolution particularly in the discrete excitation region, below the first ionization potential. Even in the case of the simplest molecule, molecular hydrogen, such information is quite limited for discrete transitions. Absolute oscillator strength measurements require extremely precise and carefully controlled techniques and in particular direct optical methods using the Beer–Lambert law can be subject to serious quantitative errors. However a much larger body of absolute oscillator strength information exists for the photoionization continuum since experimental methods in these energy regions are generally more straightforward in their application [30]. In terms of theoretical work there are few calculations of absolute oscillator strengths. Such calculations are limited by the lack of a sufficiently accurate knowledge of molecular wavefunctions and also by the shortage of precise absolute experimental data for the evaluation and testing of the theoretical methods. Both of these concerns are

addressed by recent advances made in electron impact based spectroscopies. Firstly, electron momentum spectroscopy [227] has provided detailed measurements of electron momentum distributions which have led to the evaluation and design of new molecular wavefunctions of unprecedented accuracy (for example see refs. [228–231]). The growing availability of improved molecular wavefunctions should lead to greater accuracy in calculated oscillator strengths. Secondly, high resolution dipole (e,e) spectroscopy [37–39] has been demonstrated to provide a versatile experimental method for the accurate determination of optical oscillator strengths for atomic and molecular discrete photoabsorption processes over broad ranges of excitation energy (see chapters 4–6 and refs. [27,36–39]).

Hydrogen is an important constituent of the solar and planetary atmospheres and therefore a quantitative understanding of the interaction of molecular hydrogen with energetic radiation is of great interest in astrophysics, astronomy and space sciences [232,233]. For example, the absolute oscillator strength for photoabsorption is an essential quantity in the determination of molecular abundances from interstellar molecular absorption lines [232]. Furthermore, absolute optical oscillator strengths can be used to provide an absolute scale for relative measurements of electron impact cross sections. For instance, the theoretical absolute optical oscillator strengths for hydrogen reported by Allison and Dalgarno [234] were employed by De Heer and Carriere [235] to normalize their measured relative emission cross sections for molecular hydrogen, while Shemansky *et al.* [236] established absolute cross sections for the Lyman and Werner bands from absolute oscillator strengths derived from the lifetime measurements of Schmoranzner *et al.*

[237] and the relative transition probabilities calculated by Allison and Dalgarno [234]. The photoabsorption of molecular hydrogen below the first ionization potential is dominated by the Lyman and Werner bands. However, only a very few rather incomplete experimental studies of their absolute oscillator strengths for excitation from the ground state have been reported in the literature. Furthermore, the available oscillator strength measurements show some discrepancies with each other and with theory, although the energy levels of these bands are well known [238].

Molecular hydrogen is the simplest neutral molecule and it is thus of fundamental interest since quantum mechanical calculations are possible with greater accuracy than for other molecular systems. The Lyman and Werner bands, which correspond to the transitions from the ground $X \ ^1\Sigma_g^+$ state to the $2p\sigma$, $B \ ^1\Sigma_u^+$ and $2p\pi$, $C \ ^1\Pi_u$ states respectively, have been the subject of several theoretical investigations. Mulliken and Rieke [239], employing the LCAO-MO method, have reported calculated oscillator strengths for the Lyman and Werner bands using the dipole length operator. Shull [240] repeated the same computation using the dipole velocity operator. A theoretical investigation of the oscillator strengths of the Lyman band was carried out by Ehrenson and Phillipson [241] with several improved ground state wavefunctions using dipole length, velocity and acceleration operators. By solving a one-electron Schrodinger equation, Peek and Lassetre [242] constructed a correlation diagram for hydrogen for several states and reported the oscillator strength values corresponding to the Lyman and the sum of the Lyman and Werner bands. Miller and Krauss [243] approximated the Hartree-Fock orbitals by a linear combination of Gaussian-type atomic

orbitals and calculated the inelastic electron scattering differential cross sections and oscillator strengths of the Lyman, Werner and several other bands in hydrogen. The theoretical Franck–Condon factors for the hydrogen Lyman band system have been computed by Geiger and Topschowsky [244] employing the Wentzel–Kramers–Brillouin (WKB) approximation, by Nicholls [245] using the Morse potential function, and by Halmann and Laulicht [246] and Spindler [247,248] based on Rydberg–Klein–Rees (RKR) potential functions. From a consideration of previously published experimental electron energy loss data [244,249,250] and lifetime measurements [251], it has been suggested [252] that the electronic transition moment for the Lyman band varies considerably with internuclear separation (r). Using the wavefunctions of Matsen and Browne [253] and Browne and Matsen [254], Browne [252] has computed the electronic transition moment as a function of r for the Lyman band, while Rothenberg and Davidson [255], employing the highly accurate wavefunctions of Kolos and Wolniewicz [256], have also reported the variation of electronic transition moment with r for several transitions of molecular hydrogen. In an earlier paper Dalgarno and Allison [257] reported calculations of the vibronic band oscillator strengths for the Lyman system. These calculations used the potentials developed by Kolos and Wolniewicz [256,258] in conjunction with the asymptotic formulae of Kolos [259] and Chan and Dalgarno [260]. Dalgarno and Allison [257] also adopted transition moments reported by Schiff and Pekeris [4] at $r=0$, by Rothenberg and Davidson [255] at $r=1.4a_0$ and $r=2.0a_0$, and by Browne [252] at large values of r . Using the more accurate transition moments reported by Wolniewicz [261] for both the Lyman and Werner systems, Allison and Dalgarno [262] later repeated calculations similar to those

reported earlier by Dalgarno and Allison [257]. More comprehensive calculated data, including the transition probabilities for the Lyman and Werner bands, were further reported by Allison and Dalgarno [234]. The dependence of electronic transition moment on internuclear distance was investigated at large r values experimentally by Schmoranzler [263] for the Lyman band and by Schmoranzler and Geiger [264] for the Werner band based on measurements of the optical emission intensity from electron impact excited hydrogen molecules. These results are in good agreement with the theoretical predictions by Wolniewicz [261]. Dressler and Wolniewicz [265] have recomputed the transition moments for the Lyman and Werner bands using the most accurate wavefunctions available after 1969 and the results are in excellent agreement with the earlier work of Wolniewicz [261]. In other work Arrighini *et al.* [266] computed the inelastic scattering of fast electrons from the ground state of hydrogen and reported the total integrated absolute dipole oscillator strengths for the Lyman and Werner bands and also for some other higher Rydberg states within the random-phase approximation (RPA) and Tamm-Dancoff approximation (TDA). The transition probabilities for the individual bands of the transitions from the ground state $X\ ^1\Sigma_g^+$ to the higher lying $3p\sigma$, $B\ ^1\Sigma_u^+$ and $3p\pi$, $D\ ^1\Pi_u$ states were also calculated by Glass-Maujean [267]. In 1975 Gerhart [268] reviewed the existing optical oscillator strength and photoabsorption data for molecular hydrogen and recommended some revisions on the basis of sum rule considerations.

Much less information on discrete optical oscillator strengths for molecular hydrogen is available from experiment due to the difficulties of conducting absolute optical cross section determinations. For example,

direct Beer-Lambert law photoabsorption experiments have apparently not been used for absolute optical oscillator strength measurements for molecular hydrogen because, even at high experimental resolution (narrow incident band-width), the extremely narrow natural line-widths of the transitions can result in severe "line-saturation" effects as discussed for example in refs. [37,46] (see chapter 2). Experimentally the discrete valence transitions of hydrogen have been studied quite extensively by photo-emission [269-271] and also by photoabsorption and photoionization [272-278] methods. However, the optical photoabsorption and photoionization studies have been mostly limited to determinations of the energy positions of the discrete transitions rather than of the absolute optical oscillator strengths (i.e. transition probabilities), presumably because of the possibility of "line-saturation" effects. In an attempt to allow for such effects photoabsorption measurements with a "curve of growth analysis", which relates the measured equivalent width to the line oscillator strength, have been employed by Haddad *et al.* [279] and by Hesser *et al.* [280,281] to measure the oscillator strengths for a few vibrational levels of the Lyman band. The same approach has been used by Fabian and Lewis [282] to measure the oscillator strengths of the Lyman and Werner bands below 13.8 eV. In the same way Lewis [283] has measured the oscillator strengths of the Lyman and Werner bands for the higher vibrational levels above 13.8 eV and also the B'-X and the D-X bands. In other photoabsorption experiments Glass-Maujean, Breton and Guyon [284-286] attempted to take into account the effects of the bandwidth of the monochromator on the measured linewidths of the discrete transitions by using Doppler profiles and they reported the photoabsorption

probabilities for several discrete transition peaks. However the results are restricted to very high vibrational levels of the Lyman and Werner bands close to the dissociation limit. Integrated (total) absolute oscillator strengths for the Lyman and Werner bands have also been reported by Hesser [251] using the phase-shift technique to measure the radiative lifetimes of hydrogen.

Electron impact based methods have been previously applied to the study of the discrete transitions of molecular hydrogen [244,249,250,288–291]. Lassetre and Jones [288] obtained absolute optical oscillator strengths in the continuum region of hydrogen by extrapolating the generalized oscillator strengths, determined at a range of different scattering angles, to zero momentum transfer. Direct, forward scattering, electron impact studies of hydrogen at very high impact energy and with very high resolution (0.007–0.040 eV FWHM) have been reported in the discrete region by Geiger [249], Geiger and Topschowsky [244] and Geiger and Schmoranzler [250]. These relative intensity measurements [244,249,250] were subsequently placed on an absolute scale using calculated and measured elastic cross sections [249]. By measuring the elastic and inelastic differential cross sections at different scattering angles with a resolution of ~ 1 eV FWHM, Geiger [249] has also reported the sum of the total integrated oscillator strengths for the Lyman and Werner bands. These integrated values [249] were then used for normalization of the high resolution electron energy loss spectra [244,249,250]. However it should be noted that the elastic relative differential cross sections measured by Geiger [249] were normalized on theoretical values. In addition the relative intensities produced by the Wien filter type of EELS spectrometer used by Geiger and co-workers

[244,249,250] have, in some cases, proved to be significantly in error (see for example the discussion in ref. [37] and chapter 4 for helium, where results including those of Geiger *et al.*, are compared). Such discrepancies may be due to intensity perturbations caused by fringe magnetic fields from the Wien filters. In this regard the three sets of electron impact data reported by Geiger *et al.* for hydrogen [244,249,250] show differences in the (relative) intensities determined for the Lyman and for the Werner bands. These results [244,249,250] are also in serious disagreement with some of the optical work [251,279,281,282] and also, in the case of the Werner bands, with theory [234,262].

The HR dipole (e,e) method [37,38] (described in this thesis in chapter 3) is particularly useful for studying discrete electronic transitions over a wide (photon) energy range and therefore, in view of the existing discrepancies and uncertainties outlined above, it has been used in the present work to make an independent absolute determination of the optical oscillator strengths for the Lyman and Werner band (discrete) transitions and also in the ionization continuum in the electronic spectrum of molecular hydrogen. The absolute scale was obtained by normalizing to earlier reported absolute optical oscillator strengths in the continuum region, as determined using a low resolution (LR) dipole (e,e) spectrometer and TRK sum rule considerations [86]. These LR dipole (e,e) measurements in the continuum [86] are in excellent agreement with direct photoabsorption results [292] obtained with the double ion chamber method.

7.2 Results and Discussion

7.2.1 Absolute Oscillator Strengths

Figure 7.1 shows the absolute differential optical oscillator strength (photoabsorption) spectrum of molecular hydrogen in the (photon) energy region 11–20 eV obtained in the present work at a resolution of 0.048 eV FWHM. The entire spectrum has been placed on an absolute scale by normalization at 18 eV to the previously reported absolute photoabsorption data of hydrogen obtained by Backx *et al.* [86] using low resolution dipole (e,e) spectroscopy. It can be seen from figure 7.1 that both the shape and magnitude of the present oscillator strength distribution in the ionization continuum are highly consistent with the earlier reported low resolution dipole (e,e) work of Backx *et al.* [86] and also with the direct photoabsorption measurements reported by Samson and Haddad [292] over the continuum region shown (see also ref. [30]). Furthermore, in the discrete region the present high resolution and earlier low resolution [86] dipole (e,e) measurements are mutually consistent when the large difference in energy resolution (i.e. 0.048 eV FWHM and 1 eV FWHM respectively) is taken into account.

Figure 7.2 which shows an expanded view of figure 7.1 in the 11–14 eV energy region comprising mainly the absolute differential optical oscillator strength spectrum for the Lyman and Werner bands in more detail. The Lyman and Werner bands are the two strongest electronic transitions of molecular hydrogen and correspond to transitions from the $X^1\Sigma_g^+$ ground state to the $2p\sigma$, $B^1\Sigma_u^+$ and $2p\pi$, $C^1\Pi_u$ states respectively. The positions of the vibrational levels shown in figures 7.1 and 7.2 are

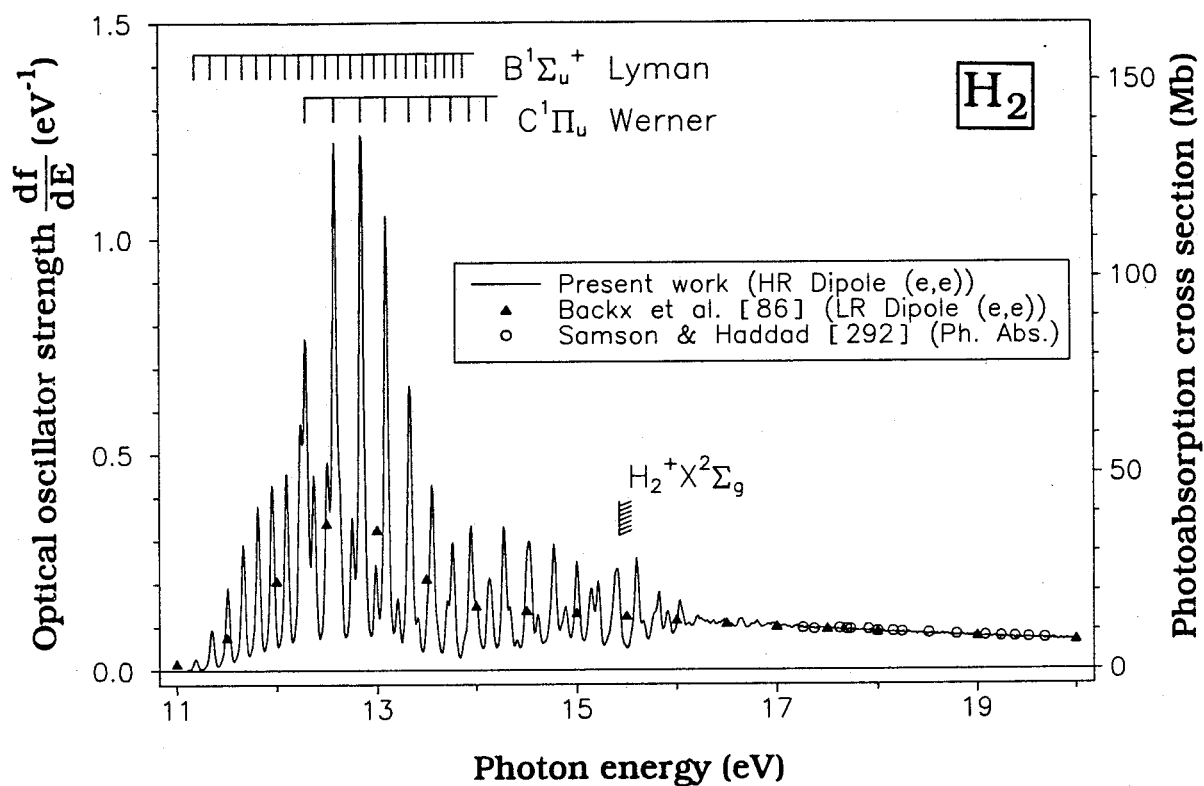


Figure 7.1: Absolute oscillator strengths for the photoabsorption of molecular hydrogen in the energy region 11–20 eV measured by the high resolution dipole (e,e) spectrometer (FWHM=0.048 eV). The assignments are taken from references [270,272–274].

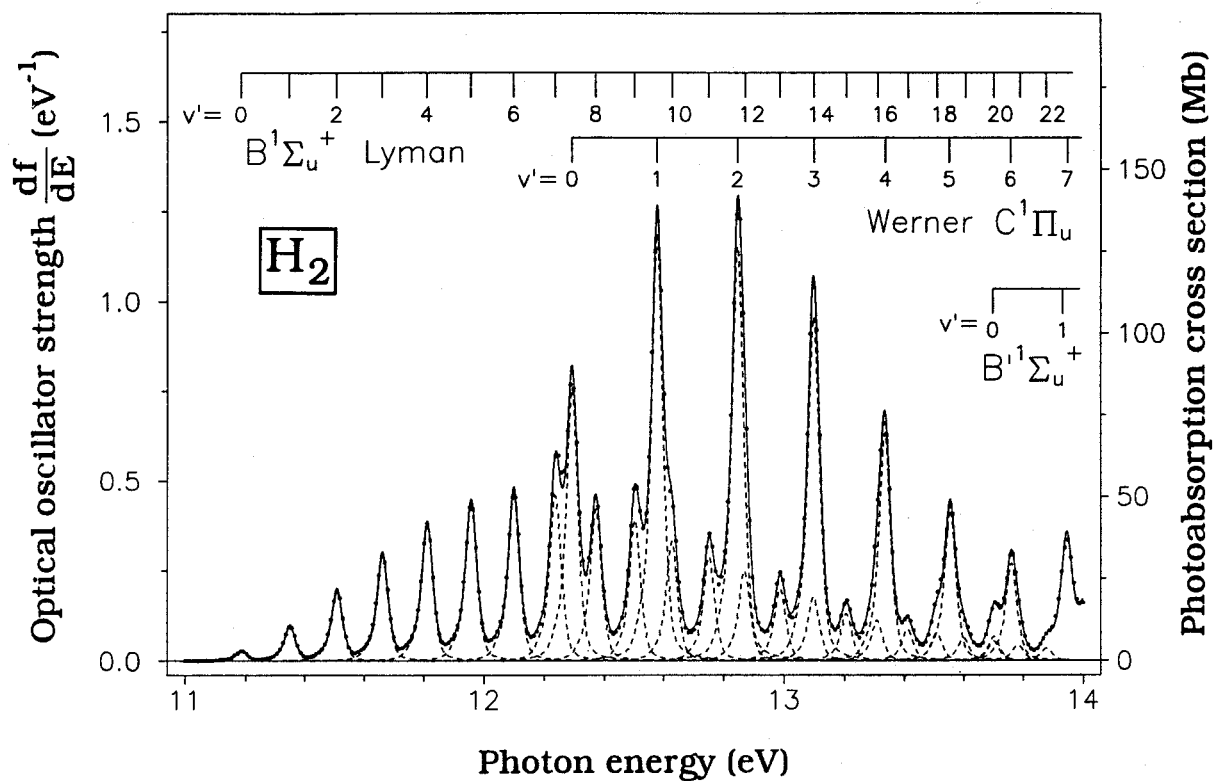


Figure 7.2: Absolute oscillator strengths for the photoabsorption of molecular hydrogen in the energy region 11–14 eV. The assignments are taken from references [270,272,273]. Deconvoluted peaks are shown as dashed lines and the solid line represents the total fit to the experimental data.

taken from the earlier reported optical spectroscopic data of Dieke [270] for $v'=0-17$ of the Lyman band and for $v'=0-4$ of the Werner band, and from the photoabsorption data of Namioka [272,273] for $v'=18-22$ of the Lyman band, for $v'=5,6$ of the Werner band and for $v'=0,1$ of the $B' \ ^1\Sigma_u^+$ band. It can clearly be seen that the shapes of the vibronic peaks ($v'=0-6$) of the Lyman band are slightly asymmetric due to rotational fine structure as observed in the very high resolution electron energy loss spectra reported by Geiger and Topschowsky [244] and by Geiger and Schmoranzler [250]. In the present work, integration of the peak area corresponding to a particular discrete vibronic transition will give directly the absolute optical oscillator strength for that transition. Since all the peaks are expected to be asymmetric because of rotational broadening, asymmetric peak profiles were used to fit the spectrum in figure 7.2. The fitted peaks also incorporate the instrumental energy resolution (0.048 eV FWHM). The resulting deconvoluted peaks and total fitted spectrum are shown as the dashed and solid lines respectively in figure 7.2. The present absolute optical oscillator strength values obtained by deconvoluting the (asymmetric) peak areas for individual vibronic transitions of the Lyman and Werner bands are summarized in tables 7.1 and 7.2 respectively. Previously reported experimental oscillator strength values [250,279,281,282] and the more accurate calculated data of Allison and Dalgarno [234,262], which included the dependence of electronic transition moment on internuclear distance r are also shown for comparison. For the three sets of electron impact data reported by Geiger and co-workers [244,249,250], the absolute scales of the data were obtained by normalizing to the sum of the total integrated oscillator strength of the Lyman and Werner bands [244] as

Table 7.1

Absolute oscillator strengths for the vibronic transitions of the Lyman band of molecular hydrogen

Excited state vibrational level (v')	Absolute optical oscillator strengths for transitions from $v''=0$ of X $1\Sigma_g^+$ to v' of B $1\Sigma_u^+$ (Lyman band)					
	Dipole (e,e) experiments		Direct optical measurements			Theory
	Present work	Gelger and Schmoranzner [250]	Fabian and Lewis [282]	Hesser <i>et al.</i> [281]	Haddad <i>et al.</i> [279]	Allison and Dalgarno [234,262]
0	0.00154		0.00175		0.0019	0.001689
1	0.00575	0.00545	0.00519		0.013	0.005790
2	0.0114	0.00994	0.0115		0.024	0.01156
3	0.0177	0.0165	0.0176		0.037	0.01755
4	0.0228	0.0210	0.0245	0.03		0.02250
5	0.0263	0.0238	0.0258			0.02571
6	0.0276	0.0264				0.02704
7	0.0276	0.0267				0.02673
8	0.0254	0.0232				0.02523
9	0.0236	0.0222				0.02298
10	0.0200	0.0203				0.02035
11	0.0174	0.0181				0.01764
12	0.0153	0.0155				0.01504
13	0.0122	0.0128	0.0114	0.012		0.01266
14	(0.0101)*	0.0104				0.01055
15	0.00794	0.00825	0.0101	0.0073		0.008730
16	0.00687	0.00703	0.00787	0.005		0.007185
17	0.00531	0.00612	0.00575	0.0042		0.005891
18	0.00468	0.00552				0.004820
19	0.00384	0.00425	0.00344	0.0023		0.003939
20	(0.00308)*	0.00329				0.003219
21	0.00267					0.002632
22	0.00209					0.002154

* Interpolated values.

Table 7.2
Absolute oscillator strengths for the vibronic transitions of the Werner band of molecular hydrogen

Excited state vibrational level (v')	Absolute optical oscillator strengths for transitions from $v''=0$ of X $1\Sigma_g^+$ to v' of C $1\Pi_u$ (Werner band)			
	Dipole (e,e) experiments		Direct optical measurement	Theory
	Present work	Geiger and Schmoranzner [250]		
0	0.0454	0.0348		0.04760
1	0.0718	0.0592	0.0592	0.07482
2	0.0695	0.0555	0.0642	0.06982
3	0.0544 [#]	0.0437	0.0442	0.05472
4	0.0387	0.0337	0.0317	0.03874
5	0.0255	0.0210	0.0224	0.02598
6	0.0165	0.0153	0.017	0.01700

[#] The contribution from the overlying v'=14 component of the Lyman band has been subtracted.

determined in separate low resolution experiments, which were in turn normalized on calculated elastic cross sections. Of these three experiments [244,249,250] only the highest resolution data reported by Geiger and Schmoranzler [250] are shown in tables 7.1 and 7.2. It should be noted that the data of refs. [244] and [249] show much more scatter than those of ref. [250]. The uncertainties of the present results are estimated to be $\pm 5\%$ for fully resolved peaks, and $\pm 7-15\%$ for the partially resolved peaks because of the additional errors in the deconvolution procedures. Due to overlapping bands the values of $v'=14$ and 20 for the Lyman band as shown in table 7.1 were obtained in the present work by interpolation. Also the value for $v'=3$ for the Werner band shown in table 7.2 was obtained by subtracting the contribution from the underlying $v'=14$ component of the Lyman band. These peaks (i.e. for $v'=14$ and 20 of the Lyman band and $v'=3$ for the Werner band) were then generated using a computer program and are shown along with the directly fitted peaks as dashed lines in figure 7.2.

A direct comparison of oscillator strength values as a function of vibrational quantum numbers, given by the different experimental studies [250,279,281,282] and the theoretical data reported by Allison and Dalgarno [234,262], is shown in graphical form for the Lyman and Werner bands in figures 7.3 and 7.4 respectively. For the Lyman band it can be seen immediately from figure 7.3 that the presently obtained experimental absolute oscillator strength results are in excellent quantitative agreement with the theoretical work reported by Allison and Dalgarno [234,262] over the entire range of vibrational quantum numbers shown. The calculated data reported by Allison and Dalgarno [234,262] are slightly lower at $v'=5-7$ and become slightly higher for $v'=13-18$ but

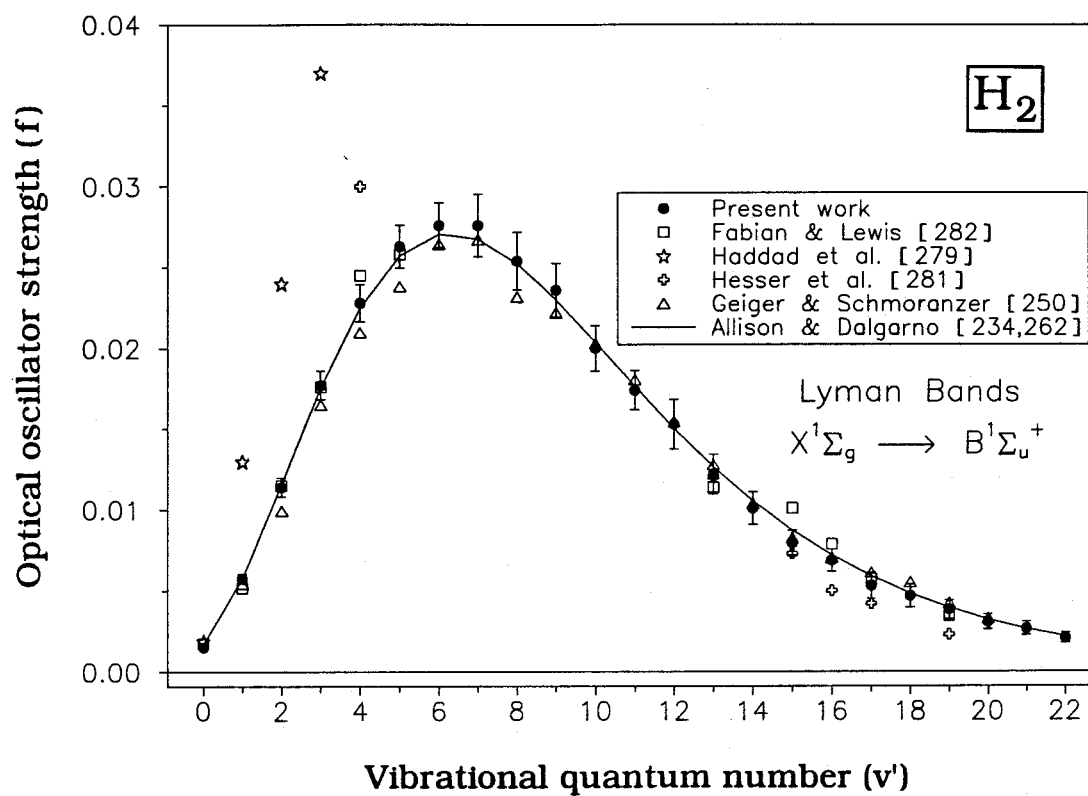


Figure 7.3: The absolute optical oscillator strengths for individual vibronic transitions as a function of the vibrational quantum number v' for the Lyman band.

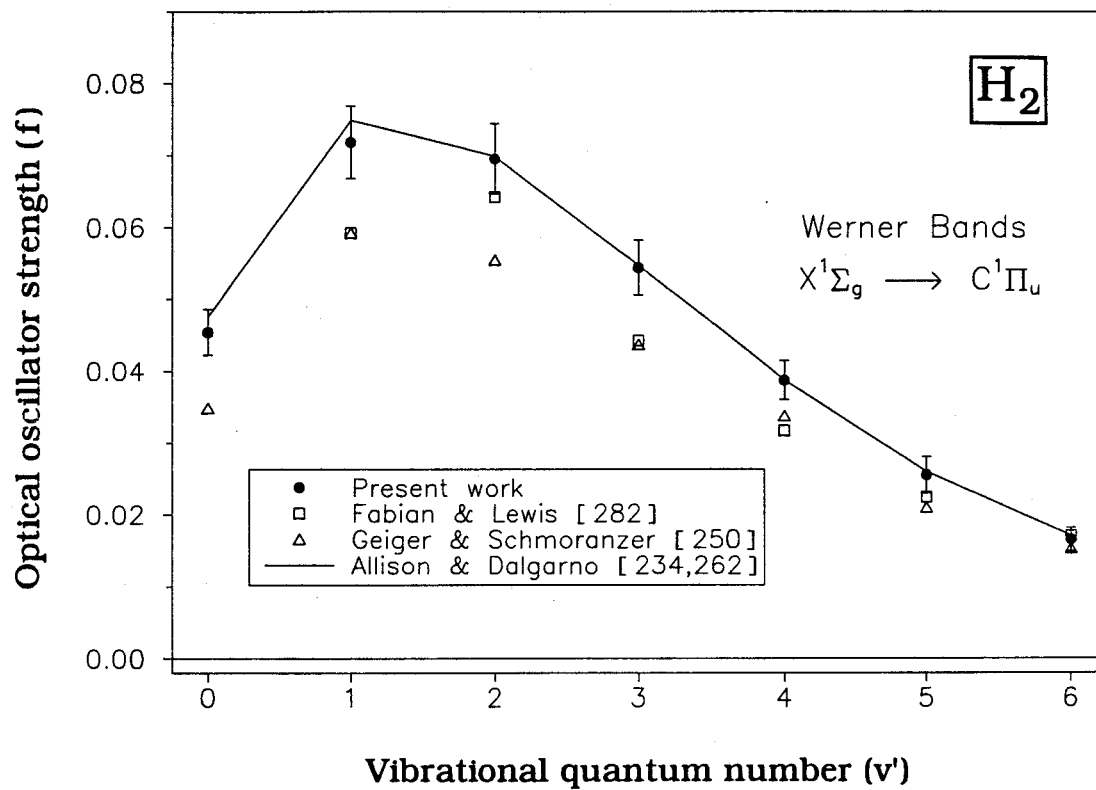


Figure 7.4: The absolute optical oscillator strengths for individual vibronic transitions as a function of the vibrational quantum number v' for the Werner band.

are still within the estimated experimental uncertainties of the present work. The electron impact data of Geiger and Schmoranzner [250] are slightly lower than the present work for $v'=2-5$ and $v'=8$ but are in good agreement for higher v' values. Apart from the electron impact based work of Geiger and Schmoranzner [250], three sets of data (see figure 7.3) obtained from photoabsorption measurements using a curve of growth analysis [279,281,282] provided the only other source of absolute vibronic oscillator strengths for the Lyman band prior to the present work. However, these three sets of optical data [279,281,282] only encompass a few of the vibrational levels and give rather inconsistent results (see figure 7.3). Of these studies only the work reported by Fabian and Lewis [282] is in reasonable agreement with theory [234,262] as seen in figure 7.3. The Fabian and Lewis [282] data are also generally consistent with the presently reported values but the data are much less comprehensive than the present work which covers the entire range of the vibrational numbers from $v'=0$ to 22. Haddad *et al.* [279] and Hesser *et al.* [281] report only a few values mostly at low and high vibrational number respectively, and these show large discrepancies with the present data and with theory [234,262]. It has been suggested [282] that the apparently high values observed by Haddad *et al.* [279] above $v'=0$ may be due to errors in the pressure measurements.

Absolute optical oscillator strengths for the Werner band are shown in figure 7.4. It can be seen that the presently obtained experimental oscillator strength values are again in excellent agreement with the theoretical predictions by Allison and Dalgarno [234,262] except possibly for $v'=0$ and 1 where the calculated values are slightly higher but nevertheless still well within the estimated uncertainties of the present

experiment. The only other absolute experimental data available for the Werner band of hydrogen prior to the present work are from the electron impact work of Geiger and Schmoranzner [250] and the optical work by Fabian and Lewis [282] respectively. However it can be seen from figure 7.4 that for $v'=0$ to 5, both sets of data [250,282] are much lower than the present results and only for $v'=6$ are their values in reasonable agreement with the present work and with theory.

The absolute oscillator strength value for the $v'=0$ component of the $B' \ ^1\Sigma_u^+$ band at 13.702 eV (see figure 7.2) is estimated to be 0.00384 in the present work. The transition probability for this vibronic band has been calculated by Glass-Maujean [267] to be $0.238 \times 10^8 \text{ sec}^{-1}$ and this corresponds to an absolute oscillator strength of 0.00292 which is ~25% lower than the present value of 0.00384.

The total integrated absolute oscillator strengths for the Lyman and Werner bands are estimated in the present work to be 0.301 and 0.341 respectively. These estimates were obtained as follows: For the Lyman band the value was obtained from the summation of the absolute oscillator strength values for $v'=0-22$ as shown in table 7.1. The total absolute oscillator strength for the Werner band was obtained from the summation of the absolute oscillator strength values for $v'=0-6$ determined from the present experimental work (0.322), plus the sum for $v'=7-13$ as calculated [234,262] by Allison and Dalgarno (0.019) to give a total of 0.341. Table 7.3 summarizes the present results along with all the previously reported total absolute oscillator strengths for the Lyman and Werner bands. The present data are in good agreement with the theoretical estimates of Allison and Dalgarno [234,262] and also with those of Arrighini *et al.* [266] which were obtained using the TDA and

Total integrated absolute oscillator strengths for the Lyman and Werner bands of molecular hydrogen

Reference	Total integrated absolute oscillator strengths	
	Lyman band	Werner band
Theory:		
Arrighini <i>et al.</i> [266]		
(i) TDA	0.3090	0.3615
(ii) RPA	0.2863	0.3451
Allison and Dalgarno [234,262]	0.311	0.356
Browne [252]	0.28	
Rothenberg and Davidson [255]		
(i) dipole length	0.286	0.343
(ii) dipole velocity	0.287	0.380
Miller and Krauss [243]	0.279	0.330
Peek and Lassettre [242]	0.28	0.276
Ehrenson and Phillipson [241]	0.27	
Shull [240]	0.18	0.42
Mulliken and Rieke [239]	0.24	0.38
Experiment:		
Present work	0.301	0.341
(dipole (e,e))		
Geiger and Schmoranzner [250]	0.29	0.28
(electron impact)		
Hesser <i>et al.</i> [281]	0.29	
(optical: curve of growth)		
Hesser [251]	0.51	0.71
(lifetimes)		

RPA methods. Only three other sets of measurements have reported for the total integrated absolute oscillator strengths. The integrated value reported in the electron impact work of Geiger and Schmoranzner [250] is slightly lower than the present value while their value for the Werner band is ~20% lower. The total integrated value for the Lyman band as estimated by Hesser *et al.* [281], using the curve of growth analysis, is also just slightly lower than the present work. However, values obtained from the lifetime data reported by Hesser [251] are much higher than all the other reported experimental and theoretical values for both the Lyman and the Werner bands, which is likely caused by the variation of electronic transition moment with internuclear distance r , since the emission observed by Hesser [251] occurs at large r .

In the present work, the total integrated oscillator strength sum for all transitions below the first ionization potential (15.43 eV [274]) of hydrogen is estimated to be 0.836. Arrighini *et al.* [266] have reported oscillator strength values for the Lyman and Werner bands, and also several higher members of the Rydberg $^1\Sigma_u^+$ and $^1\Pi_u$ states. By adding up the oscillator strengths for all those states below the first ionization potential of hydrogen that were calculated by Arrighini *et al.* [266], values of 0.926 and 0.862 were obtained for the TDA and RPA computational methods respectively. The value reported using the RPA method is consistent with the present result (0.836) while that reported using the TDA method is appreciably higher.

7.2.2 The Variation of Transition Moment with the Internuclear Distance for the Lyman and Werner Bands

The vibronic band oscillator strengths ($f_{v'v''}$) for the Lyman and Werner systems of molecular hydrogen can be written as [262];

$$f_{v'v''} = \frac{2G}{3} (E_{v'} - E_{v''}) P_{v'v''} \quad (7.1)$$

$$\text{where } P_{v'v''} = \left| \langle \varphi_{v'} | R_e(r) | \varphi_{v''} \rangle \right|^2 \quad (7.2)$$

In these equations G is the statistical weighting factor which is equal to one for the Lyman bands and two for the Werner bands, $E_{v'} - E_{v''}$ is the transition energy in atomic units and $P_{v'v''}$ is the band strength. The quantity $R_e(r)$ is the electronic transition moment which is a function of the internuclear distance r , and $\varphi_{v'}$ and $\varphi_{v''}$ are the vibrational eigenfunctions of the excited and ground states respectively.

The dependence of the electronic transition moment on the internuclear distance for both the Lyman and the Werner bands can be obtained from the presently reported absolute vibronic oscillator strengths. Equation 7.2 can be rewritten as [250,282]

$$P_{v'v''} = \left| R_e(r_{v'v''}) \right|^2 q_{v'v''} \quad (7.3)$$

$$\text{where } q_{v'v''} = \left| \langle \varphi_{v'} | \varphi_{v''} \rangle \right|^2 \quad (7.4)$$

In equation 7.3, $r_{v'v''}$ is the internuclear distance at which the transition $v'' \rightarrow v'$ takes place and $q_{v'v''}$ is the Franck-Condon factor. Combining equations 7.1 and 7.3, we obtain

$$f_{v'v''} = \frac{2G}{3} (E_{v'} - E_{v''}) |R_e(r_{v'v''})|^2 q_{v'v''} \quad (7.5)$$

In the present work, the $f_{v'0}$ values have been measured directly (see tables 7.1 and 7.2) for both the Lyman and the Werner bands so that if we take Franck-Condon factors (i.e. $q_{v'0}$ values) from the calculated data of Allison and Dalgarno [262], $|R_e(r_{v'0})|$ may be derived. The energies ($E_{v'} - E_{v''}$) have been taken from the optical data of Dieke [270] and Namioka [272,273]. The $r_{v'0}$ values have been obtained by digitizing the data of Allison [293], which are shown in analog form as a private communication in the article by Fabian and Lewis [282]. The resulting values of $|R_e(r_{v'0})|$ are plotted as a function of $r_{v'0}$ in figures 7.5 and 7.6 for the Lyman and Werner bands respectively. These figures therefore show the variation of electronic transition moment with internuclear distance in hydrogen for the Lyman and Werner bands. Previously reported experimental work [250,282] and theoretical calculations [243,252,255,261] are also shown for comparison. The data of Miller and Krauss [243] and Wolniewicz [261] were obtained by digitizing the data from the figures reported in their paper. It can be seen from figure 7.5 that the presently determined variation of the electronic transition moment $|R_e(r_{v'0})|$ with the internuclear distance $r_{v'0}$ is in generally good agreement with the theoretical work of Wolniewicz [261], except at $r_{v'0} = 0.96 \text{ \AA}$ ($v'=0$), where the present value is slightly lower. The

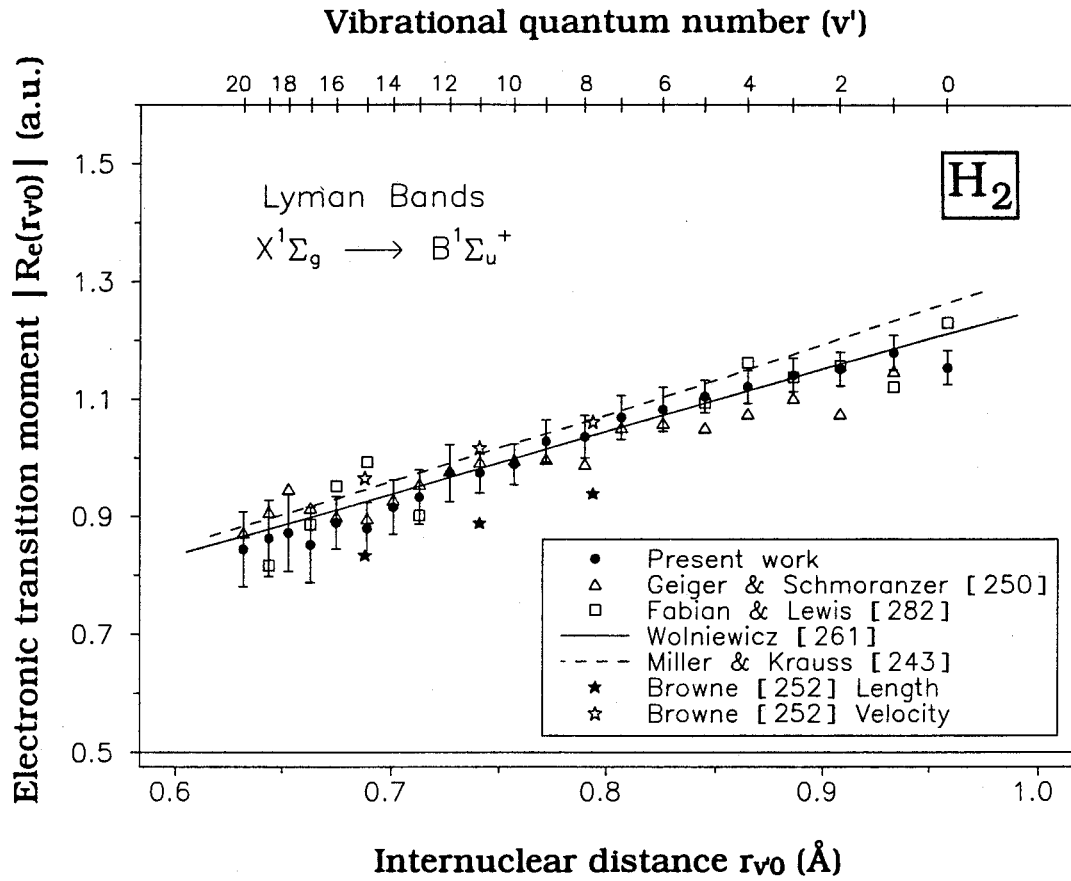


Figure 7.5: The electronic transition moment $|Re(r_{v0})|$ in atomic units (a.u.) as a function of the internuclear distance r_{v0} in Angstroms (Å) for the Lyman band.

calculated data reported by Miller and Krauss [243] are somewhat higher than the present work. The dipole length data reported by Browne [252] are lower than the present results while their dipole velocity data are slightly higher. The electron impact work of Geiger and Schmoranzler [250] and the optical work of Fabian and Lewis [282] are also consistent with the present work but both sets of data exhibit more scatter. From a least-squares fit of a straight line to the present data, the dependence of electronic transition moment with internuclear distance in the range 0.63–0.96Å for the Lyman band is found to be:

$$|R_e(r_{v'0})| = 0.142 + 1.117 r_{v'0} \quad (7.6)$$

In figure 7.6 the present results for the Werner band are also seen to be generally in rather good agreement with the theoretical values calculated by Miller and Krauss [243] and Wolniewicz [261]. The dipole length data calculated by Rothenberg and Davidson [255] are also consistent with the present work while their reported dipole velocity data are slightly higher. The results derived from the electron impact work of Geiger and Schmoranzler [250] are considerably lower than both the present work and theory [243,261]. Except for the value at $r_{v'0} \sim 0.66\text{Å}$, the data for the Werner band reported in the optical work of Fabian and Lewis [282] are also much lower than the presently reported values. A linear least-squares fit of the presently obtained data in the range 0.66–0.89Å gives

$$|R_e(r_{v'0})| = 0.456 + 0.378 r_{v'0} \quad (7.7)$$

The dipole strengths $D_e(r_o)$ at equilibrium internuclear separation r_o have been investigated both experimentally [244,249,250,282] and theoretically [239–243,252,255,261] by several groups. This quantity is defined as [250,282]:

$$D_e(r_o) = G |R_e(r_o)|^2 \quad (7.8)$$

where G is the statistical weighting factor as defined above.

In the present work, the transition moment at the equilibrium internuclear distance r_o for the Lyman and Werner bands can be calculated from equations 7.6 and 7.7 respectively by setting $r_{v'0}=r_o=0.741\text{\AA}$. From equation 7.8 the dipole strengths are determined to be 0.94 for the Lyman band and 1.08 for the Werner band. Table 7.4 summarizes the present results and shows a comparison with other previously reported experimental [244,249,250,282] and theoretical data [239–243,252,255,261]. For the Lyman band the previously published experimental results [244,249,250] and the present work show good agreement with each other except for the value reported by Geiger [249] which is ~10% lower. For the Werner band all the previously reported experimental values [244,249,250,282] are lower than the present work. Of the theoretical studies only the values reported by Wolniewicz [261] and the calculated data of Rothenberg and Davidson [255] are in good agreement with the present values for both the Lyman and the Werner bands. The other calculated values show significant differences from the present results.

Finally it should be noted that the dependence of the electronic transition moment on the internuclear distance and also the dipole

Table 7.4**Dipole strengths $D_e(r_0)$ for the Lyman and Werner bands of molecular hydrogen**

Reference	Dipole strengths $D_e(r_0)$ in a.u.	
	Lyman band	Werner band
Theory:		
Wolniewicz [261]	0.96	1.10
Browne [252]		
(i) dipole length	0.78	
(ii) dipole velocity	1.04	
Rothenberg and Davidson [255]		
(i) dipole length	0.91	1.06
(ii) dipole velocity	0.92	1.18
Miller and Krauss [243]	1.00	1.08
Peek and Lassetre [242]	0.97	0.81
Ehrenson and Phillipson [241]	0.85	
Skull [240]	0.60	1.33
Milliken and Rieke [239]	0.77	1.21
Experiment:		
Present work	0.94	1.08
(dipole (e, e))		
Fabian and Lewis [282]	0.96	0.92
(optical: curve of growth)		
Geiger and Schmoranzner [250]	0.98	0.89
(electron impact)		
Geiger and Topschowsky [244]	0.95	0.92
(electron impact)		
Geiger [249]	0.84	1.03
(electron impact)		

strength at the equilibrium internuclear distance determined in the present work for both the Lyman and Werner bands are consistent with the theoretical work by Rothenberg and Davidson [255], by Wolniewicz [261] and by Miller and Krauss [243]. It should be pointed out that some of these calculations [255,261] were used by Allison and Dalgarno [234,262] in their calculation of the absolute oscillator strengths for the Lyman and Werner bands.

7.3 Conclusions

Absolute optical oscillator strengths for molecular hydrogen have been measured in the energy region 11–20 eV. The absolute scale was obtained by normalizing in the photoabsorption continuum region at 18 eV to the absolute value determined by Backx *et al.* [86] using low resolution dipole (e,e) spectroscopy and TRK sum rule normalization. Absolute optical oscillator strengths for the vibronic transitions of the Lyman and Werner bands have been determined. The presently reported experimental oscillator strength data are in very good agreement with the theoretical values reported by Allison and Dalgarno [234,262] for the Lyman and Werner bands. The optical data of Fabian and Lewis [282] agree with the present results for the Lyman band but are more than 10% lower for the Werner band. The variations of the electronic transition moments of the Lyman and Werner bands of hydrogen with internuclear distance derived from the present measurements are found to be in very good agreement with theoretical calculations [243,255,261].

Chapter 8

Absolute Optical Oscillator Strengths for the Discrete and Continuum Photoabsorption of Molecular Nitrogen (11–200 eV)

8.1 Introduction

Nitrogen is the most abundant molecule in the earth's atmosphere and photoabsorption, photodissociation and photoionization processes resulting from its interaction with solar UV radiation play an important role in the energy balance of the earth's upper atmosphere. In addition the predissociation of electronically excited states of nitrogen is the principle process by which molecular nitrogen is dissociated in the atmosphere by solar radiation and by electron impact. Absolute optical oscillator strengths for nitrogen in the discrete valence region provide information on the excitation cross sections, and these together with emission cross section data can be used to determine the predissociation cross sections and emission yields [294–297] of electronically excited states of nitrogen.

Transition energies and absolute optical oscillator strengths for excitation from the ground state of nitrogen to various Rydberg states have been calculated by a number of authors [298–303]. However, these calculations are at the level of electronic but not vibrational resolution. Duzy and Berry [298] based their calculation on a Hartree–Fock wavefunction for the ground state of nitrogen and excited state wavefunctions derived from an irreducible–tensorial one–center representation of the effective potential of the nitrogen ion core.

Calculations have also been reported by Rescigno *et al.* [299] using the Stieltjes–Tchebycheff moment–theory technique and by Kosman and Wallace [300] using the multiple scattering model. Absolute optical oscillator strength calculations for the transitions from the ground state to the valence $b^1\Pi_u$ and $b^1\Sigma_u^+$ states and some low–lying Rydberg states have been performed by Rose *et al.* [301] using the equation–of–motion method, by Hazi [302] using the semi–classical impact–parameter method and by Bielschowsky *et al.* [303] using extensive *ab initio* calculations with highly correlated configuration interaction wavefunctions.

Irregularities in the vibronic energy levels and intensity distributions associated with the $b^1\Pi_u$ and $b^1\Sigma_u^+$ excited valence states have been observed experimentally [304,305], which has been attributed to homogeneous configuration interaction of the $b^1\Pi_u$ and $b^1\Sigma_u^+$ states with the first two members of the $c^1\Pi_u$ and $c^1\Sigma_u^+$ Rydberg states, respectively. By first fitting the eigenvalues of a vibronic interaction matrix to the observations, Stahel *et al.* [306] have reported vibronic energies, eigenvectors, B values and relative oscillator strengths for the $b^1\Pi_u$ and $b^1\Sigma_u^+$ excited valence states and the $c^1\Pi_u$, $c^1\Sigma_u^+$ and $o^1\Pi_u$ Rydberg states, based on a matrix optimization with direct solutions of coupled oscillator equations. The effects of configuration interaction on the nitrogen spectrum have been discussed in detail by Lefebvre–Brion and Field [307] and also by Carroll and Hagim [308].

The photoabsorption of molecular nitrogen in the valence discrete region has been the focus of many experimental studies and a large amount of spectroscopic data has been reported in the literature [76–80,305,309–320]. Numerous studies using the Beer–Lambert law [76–80,312,313,315,316] have reported absolute optical oscillator strength

(cross section) values in the valence discrete region. However, very large differences in the relative peak intensities for the discrete transitions of nitrogen in the energy region 12.5–13.2 eV were observed between different Beer–Lambert law photoabsorption measurements [76–80,313,316] and also with optical oscillator strength determinations based on a variety of electron energy loss experiments [11,37,81,82,304]. At first it was thought that the discrepancies were due to the failure of the Born approximation used to interpret the electron impact based experiments. However, Lawrence *et al.* [78] subsequently remeasured the absolute oscillator strengths for several discrete excitations of molecular nitrogen using Beer–Lambert law photoabsorption techniques in the same energy region at several different sample pressures, and found that the measured oscillator strengths showed large variations with sample pressure. Extrapolating to small values of the column number (i.e. low pressure), the resulting oscillator strength values [78] were found to be much more consistent with the relative intensities of the peaks obtained earlier by Lassetre *et al.* [81] and by Geiger *et al.* [82,304] from electron energy loss experiments. Following these observations the difficulties involved in using Beer–Lambert law photoabsorption for studies of discrete excitations were realised [11,46]. A detailed quantitative analysis and theoretical investigation of the bandwidth effects and associated errors in Beer–Lambert law photoabsorption has been given by Chan *et al.* [37] (see chapter 2). Chan *et al.* [37] also demonstrate that the bandwidth effects will be manifest in the peak areas as well as the peak heights in oscillator strength determinations for discrete transitions. These difficulties with the Beer–Lambert law, which can lead to very large errors in measured oscillator

strengths, are caused by the finite bandwidth of the optical spectrometer. Severe "line saturation" effects are likely to occur particularly when the measured discrete transition has a very narrow natural line-width and high cross section. In such cases the measured optical oscillator strengths are likely to be too small even when very careful Beer-Lambert law studies are made as a function of pressure. These difficulties could also be minimised in principle if extremely high optical resolution could be obtained [321], but it should be noted that this requires in practice that the spectrometer bandwidth be very much narrower than the natural linewidth of any spectral line being studied. Since electron impact excitation is non-resonant, such "line saturation" or bandwidth effects cannot occur in optical oscillator strength determinations based on electron energy loss measurements [11,30,37]. In particular, the dipole (e,e) method is ideally suited for the accurate determination of photoabsorption oscillator strengths throughout the discrete and continuum spectral regions [37]. In contrast, the Beer-Lambert law optical absorption spectrum can exhibit a very variable relative intensity profile throughout the discrete region depending on the experimental resolution (bandwidth) since different electronic transitions in general have different natural line-widths. These spurious effects are particularly well illustrated by a comparison of the optical oscillator strength spectra obtained by the electron energy loss [37] and Beer-Lambert law photoabsorption [80] methods for molecular nitrogen in the VUV region as shown in figure 2.1 (see chapter 2). It can be seen that both the relative band strengths and the absolute intensities are dramatically different in the two spectra in the 12.4 to 13.0 eV region. The intensities are essentially correct in the electron energy loss spectrum in

figure 2.1(b), whereas bandwidth/linewidth interactions result in severe intensity perturbations in the synchrotron radiation Beer–Lambert law photoabsorption intensities of reference [80] shown in figure 2.1(a). It is instructive to note that it was in this specific spectral region that Lawrence *et al.* [78] made photoabsorption studies as a function of pressure [37,46] in an attempt to avoid the bandwidth effects. It can be seen from figure 3 of reference [78] that the relative intensities of the four transitions at 958 Å (12.942 eV), 960 Å (12.915 eV), 965 Å (12.848 eV) and 972 Å (12.756 eV) are drastically altered in different ways (reflecting their different natural linewidths and different true cross sections) as the column number (pressure) is reduced. At the lowest column number at which measurements were made [78], the derived oscillator strength order and relative magnitudes are consistent with the relative intensities in the electron energy loss based measurement shown in figure 2.1(b) of the present work. However, the errors bars in figure 3 of ref. [78] are necessarily very large at the lowest pressures at which oscillator strength measurements were made, and as a result the absolute magnitudes of the oscillator strengths are still significantly in error (see section 8.2.2 below of the present work). It is clear that the errors are different for every transition because of the different natural linewidths. In addition, extrapolation of optical data to low pressure places the most emphasis on the least accurate data obtained at the lowest pressures. Therefore, as a result of finite bandwidth considerations, oscillator strength measurements obtained by Beer–Lambert law photoabsorption methods must, at best, be regarded with extreme caution since it is clear that very large errors can occur in the measured oscillator strengths even where measurements are made as a function of pressure. Conversely, the

efficacy of Bethe–Born converted electron energy loss spectra, obtained directly using dipole (e,e) spectroscopy at negligible momentum transfer, as a means of obtaining accurate optical oscillator strengths in both the discrete [27,37,38–40] and continuum [30] regions has now been well established.

The preceding perspectives concerning the accuracies of various types of absolute photoabsorption oscillator strength determination are important when considering the results of other studies using such information. For example, the extreme ultraviolet emission from nitrogen excited by electron impact has been studied by Zipf and McLaughlin [294] for the two excited valence states and several Rydberg states. Similar studies have also been made by Zipf and Gorman [295] and by James *et al.* [297] for the $b^1\Pi_u$ state, and by Ajello *et al.* [296] for the $c^1\Sigma_u^+$ and $b^1\Sigma_u^+$ Rydberg states. In these studies the emission cross sections and the predissociation branching ratios for these states were reported. The excitation cross sections, which were used to obtain the predissociation branching ratios from the measured emission cross sections, were derived from previously published optical oscillator strengths [13,78,304]. Zipf and McLaughlin [294] and Zipf and Gorman [295] obtained optical oscillator strength values from the relative electron scattering data of Geiger and Schroder [304], with correction for the scattering geometry of the spectrometer and also taking into account the absolute generalized oscillator strength data of Lassetre and Skerbele [13]. James *et al.* [297] converted the excitation cross sections reported by Zipf and Gorman [295] for the $b^1\Pi_u$ vibrational states at an impact energy of 200 eV to those which would be obtained at an impact energy of 100 eV and normalized the data using the absolute optical oscillator

strength value for the (4,0) transition reported by Lawrence *et al.* [78]. Ajello *et al.* [296] obtained optical oscillator strengths for the $c^1\Sigma_u^+$ and $b^1\Sigma_u^+$ states from their own experimental measurements using the relative flow technique and by applying the modified Born approximation formulation to the measured absolute emission cross sections.

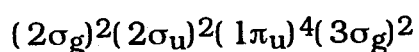
As indicated above, electron impact methods based on electron energy loss spectroscopy have also been applied to study the discrete electronic transitions of nitrogen [13,15,18,81,82,87,304,322–324]. Experimental conditions of low electron impact energy and variable scattering angle have been employed by several groups [13,15,18,322–324]. In these studies generalized oscillator strengths as a function of momentum transfer (angle) for various discrete transitions were determined and optical oscillator strengths were obtained by extrapolating the generalized oscillator strengths to zero momentum transfer for each transition [13,18,324]. While Geiger and Stickel [82] and Geiger and Schroder [304] obtained high-resolution dipole-dominated electron energy loss spectra of nitrogen in the valence discrete region by using very high incident impact energies (25–33 keV) and small scattering angles ($1-4 \times 10^{-4}$ radians), no absolute oscillator strengths were derived. In other work Wight *et al.* [87] reported absolute dipole oscillator strengths for the photoabsorption of nitrogen in the limited energy region 10–70 eV using low resolution dipole (e,e) spectroscopy with 8 keV impact energy and zero-degree mean scattering angle. However, the absolute scale was obtained by Wight *et al.* [87] by normalizing in the smooth continuum at 32 eV to the absolute photoabsorption data previously reported by Samson and Cairns [325]. In addition, the resolution of the spectrum reported by Wight *et al.* [87] was

limited to 0.5 eV FWHM and as a result absolute optical oscillator strengths for the individually resolved discrete vibronic transitions of molecular nitrogen could not be determined.

In summary, direct photoabsorption studies of the oscillator strengths for the discrete excitation of molecular nitrogen are clearly in error due to "line saturation" effects, while earlier high resolution electron impact studies have provided only relative intensities or in other cases involve uncertainties due to the necessary extrapolations to zero momentum transfer. Definitive absolute photoabsorption oscillator strength measurements in the discrete region of nitrogen at high resolution should however be possible by electron energy loss measurements obtained directly at the optical limit, with the absolute scale established independently *via* TRK sum-rule considerations [30]. Therefore, in the present work, the high resolution dipole (e,e) method, as recently used to measure absolute optical oscillator strengths for discrete transitions over the entire spectral range for the noble gas atoms [37-39] (see chapters 4-6) and molecules [27,40] (see chapter 7), is now applied to the valence shell discrete transitions of molecular nitrogen. The excellent agreement obtained between experimental and theoretical optical oscillator strengths for "benchmark" targets such as helium [37] (see chapter 4) and molecular hydrogen [40] (see chapter 7) has confirmed the high accuracy of the high resolution dipole (e,e) method. In order to independently establish the absolute oscillator strength scale for molecular nitrogen, comprehensive new low resolution dipole (e,e) measurements have also been made in the energy range 10-200 eV and these data have been placed on an absolute scale by valence shell TRK sum rule normalization.

8.2 Results and Discussion

The photoabsorption oscillator strengths and spectral assignments for molecular nitrogen are conveniently discussed with reference to the ground state molecular-orbital, independent particle, valence shell electronic configuration, which may be written as:



8.2.1 Low Resolution Absolute Photoabsorption Oscillator Strength Measurements for Molecular Nitrogen (11–200 eV)

A relative valence shell oscillator strength spectrum was obtained by Bethe–Born conversion of the electron energy loss spectrum measured using the low resolution (~1 eV FWHM) dipole (e,e) spectrometer in the energy region 11–200 eV. The data were least-squares fitted to the function AE^{-B} over the energy region 90–200 eV. The fit gave $B=2.283$ and on this basis the fraction of valence-shell oscillator strength above 200 eV was estimated to be 5.6%. The total area was then valence shell TRK sum-rule normalized to a value of 10.3, which includes the total number of valence electrons (10) plus a small estimated correction (0.3) for the Pauli-excluded transitions from the core orbitals to the already occupied ground state valence orbitals [52,53]. Figures 8.1(a) and (b) show the resulting absolute optical oscillator strength spectra of nitrogen in the energy regions 10–50 and 50–200 eV respectively, compared with previously reported experimental data [87,175,292,326–329]. Numerical values of the absolute photoabsorption oscillator strengths for nitrogen

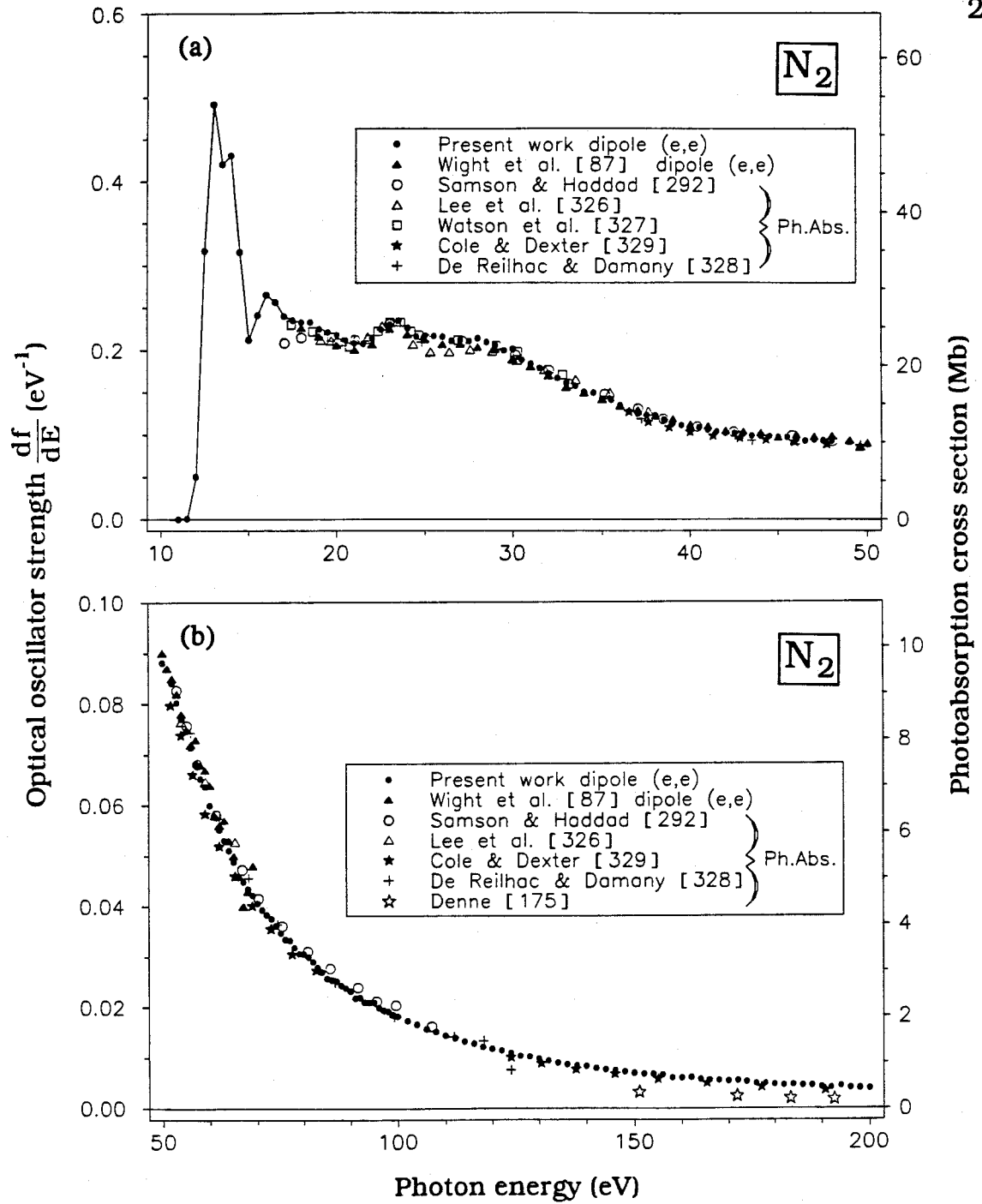


Figure 8.1: Absolute oscillator strengths for the photoabsorption of molecular nitrogen measured using the low resolution (FWHM=1 eV) dipole (e,e) spectrometer (a) comparison with previously reported experimental data [87,292,326–329] in the energy region 10–50 eV. (b) comparison with previously reported experimental data [87,175,292,326,328,329] in the energy region 50–200 eV.

obtained at low resolution in the present work from 11–200 eV are summarized in table 8.1. It is important to note that in the discrete region the low resolution data in table 8.1 represent an integral over the unresolved transitions. More detailed quantitative information on the discrete region is available from the high resolution spectra (see section 8.2.2 below).

Immediately it can be seen in figures 8.1(a) and 8.1(b) that the present results are in good agreement with the photoabsorption continuum data reported earlier by Samson and Haddad [292]. The data reported by Cole and Dexter [329] are slightly lower than the present work while those reported by Denne [175] in the energy region 150–195 eV are ~50% lower. The earlier electron impact based dipole (e,e) data reported by Wight *et al.* [87] are slightly lower than the present work in the energy region 18–35 eV but become higher in the energy region above 50 eV up to the limit of their measurements at 70 eV. However, it should also be pointed out that the relative data of Wight *et al.* [87] were normalized in the smooth continuum at 32 eV to the direct optical photoabsorption data reported much earlier by Samson and Cairns [325]. In contrast the present work is valence shell TRK sum-rule normalized and is thus independent of any other measurements. The presently obtained low resolution photoabsorption data has been used to establish an absolute scale for the high resolution measurements described in the following section.

Table 8.1

Absolute differential optical oscillator strengths for the photoabsorption of molecular nitrogen obtained using the low resolution (1 eV FWHM) dipole (e,e) spectrometer (11–200 eV)

Energy (eV)	Oscillator Strength (10^{-2}eV^{-1})	Energy (eV)	Oscillator Strength (10^{-2}eV^{-1})	Energy (eV)	Oscillator Strength (10^{-2}eV^{-1})
11.0	0.00	20.0	21.83	29.0	20.56
11.5	0.08	20.5	21.21	29.5	19.95
12.0	5.03	21.0	20.83	30.0	20.14
12.5	31.74	21.5	20.76	30.5	18.84
13.0	49.14	22.0	21.39	31.0	18.35
13.5	42.02	22.5	22.47	31.5	17.89
14.0	43.06	23.0	23.05	32.0	17.21
14.5	31.61	23.5	23.52	32.5	16.69
15.0	21.23	24.0	22.64	33.0	16.14
15.5	24.14	24.5	21.62	33.5	15.72
16.0	26.57	25.0	21.69	34.0	15.04
16.5	25.71	25.5	21.66	34.5	14.94
17.0	24.04	26.0	21.57	35.0	14.22
17.5	23.56	26.5	21.08	35.5	14.09
18.0	23.31	27.0	21.17	36.0	13.41
18.5	23.33	27.5	21.04	36.5	12.74
19.0	22.52	28.0	21.34	37.0	12.45
19.5	22.16	28.5	20.92	37.5	12.30

Table 8.1 (continued)

Energy (eV)	Oscillator Strength (10^{-2}eV^{-1})	Energy (eV)	Oscillator Strength (10^{-2}eV^{-1})	Energy (eV)	Oscillator Strength (10^{-2}eV^{-1})
38.0	12.27	49.0	9.08	70.0	4.06
38.5	11.76	50.0	8.81	71.0	3.94
39.0	11.26	51.0	8.68	72.0	3.83
39.5	11.09	52.0	8.41	73.0	3.75
40.0	10.78	53.0	8.03	74.0	3.62
40.5	10.85	54.0	7.71	75.0	3.47
41.0	10.55	55.0	7.47	76.0	3.35
41.5	10.37	56.0	7.14	77.0	3.33
42.0	10.15	57.0	6.82	78.0	3.18
42.5	10.16	58.0	6.53	79.0	3.06
43.0	10.02	59.0	6.37	80.0	3.06
43.5	9.85	60.0	6.00	81.0	3.00
44.0	9.81	61.0	5.78	82.0	2.90
44.5	9.79	62.0	5.52	83.0	2.79
45.0	9.69	63.0	5.31	84.0	2.70
45.5	9.68	64.0	5.11	85.0	2.58
46.0	9.51	65.0	4.89	86.0	2.55
46.5	9.27	66.0	4.60	87.0	2.52
47.0	9.37	67.0	4.49	88.0	2.44
47.5	9.31	68.0	4.34	89.0	2.39
48.0	9.22	69.0	4.22	90.0	2.32

Table 8.1 (continued)

Energy (eV)	Oscillator Strength (10 ⁻² eV ⁻¹)	Energy (eV)	Oscillator Strength (10 ⁻² eV ⁻¹)	Energy (eV)	Oscillator Strength (10 ⁻² eV ⁻¹)
91.0	2.18	124.0	1.09	166.0	0.562
92.0	2.20	126.0	1.04	168.0	0.562
93.0	2.11	128.0	1.03	170.0	0.542
94.0	2.10	130.0	0.986	172.0	0.549
95.0	2.10	132.0	0.948	174.0	0.526
96.0	2.00	134.0	0.908	176.0	0.494
97.0	1.94	136.0	0.879	178.0	0.496
98.0	1.92	138.0	0.848	180.0	0.476
99.0	1.85	140.0	0.835	182.0	0.465
100.0	1.82	142.0	0.801	184.0	0.471
102.0	1.74	144.0	0.773	186.0	0.454
104.0	1.67	146.0	0.755	188.0	0.460
106.0	1.57	148.0	0.726	190.0	0.431
108.0	1.52	150.0	0.702	192.0	0.412
110.0	1.45	152.0	0.682	194.0	0.445
112.0	1.40	154.0	0.685	196.0	0.411
114.0	1.33	156.0	0.671	198.0	0.401
116.0	1.28	158.0	0.613	200.0	0.392
118.0	1.22	160.0	0.608		
120.0	1.18	162.0	0.614		
122.0	1.15	164.0	0.581		

$$\sigma \text{ (Mb)} = 1.0975 \times 10^2 \frac{df}{dE} \text{ eV}^{-1}$$

8.2.2 High Resolution Absolute Photoabsorption Oscillator Strength Measurements for Molecular Nitrogen (12–22 eV)

Figure 8.2 shows the absolute optical oscillator strength spectrum for the photoabsorption of molecular nitrogen in the energy region 12–22 eV obtained using the high resolution dipole (e,e) spectrometer (0.048 eV FWHM). Also shown on figure 8.2 is the presently determined low resolution dipole (e,e) data, the earlier low resolution electron impact based data of Wight *et al.* [87] and the photoabsorption data of Samson and Haddad [292]. It can be seen in figure 8.2 that the present high resolution (HR) and the various low resolution (LR) data are in good agreement over the continuum region. Similarly in the discrete region the measurements are consistent when the large differences in energy resolution (0.048 eV vs 1 eV FWHM) are taken into account. The present HR data in the continuum 18–22 eV are also in good quantitative agreement with the photoabsorption data of Samson and Haddad [292].

Figures 8.3, 8.4 and 8.5 show expanded views of figure 8.2 in the energy regions 12.4–13.4, 13.2–15 and 15–19 eV respectively. The detailed qualitative spectroscopy of molecular nitrogen is well known from higher resolution optical and electron energy loss spectra and the indicated assignments and energy positions shown are as given in refs. [80,300,304,317]. The most prominent transitions below 15 eV correspond to the valence excitations to the $b^1\Pi_u$ and $b^1\Sigma_u^+$ states, and the lowest members of the three ($3\sigma_g \rightarrow 3p\sigma_u$) $c^1\Sigma_u^+$, ($3\sigma_g \rightarrow 3p\pi_u$) $c^1\Pi_u$ and ($1\pi_u \rightarrow 4\sigma_g$) $o^1\Pi_u$ Rydberg series. In the energy region 15–17.5 eV, the spectrum involves mainly transitions to higher members of the $c^1\Sigma_u^+$, $c^1\Pi_u$ and $o^1\Pi_u$ Rydberg series. The assignments and energy positions for

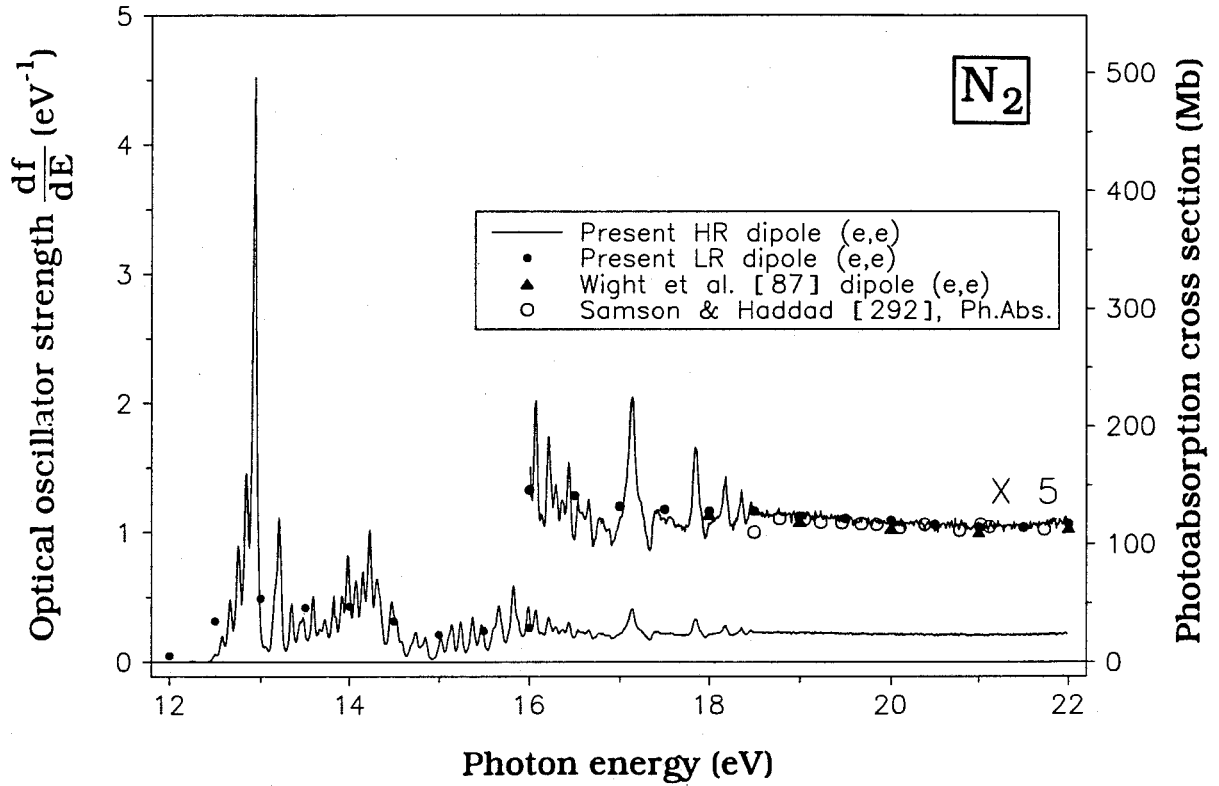


Figure 8.2: Absolute oscillator strengths for the photoabsorption of molecular nitrogen in the energy region 12–22 eV measured using the high resolution dipole (e,e) spectrometer (FWHM=0.048 eV).

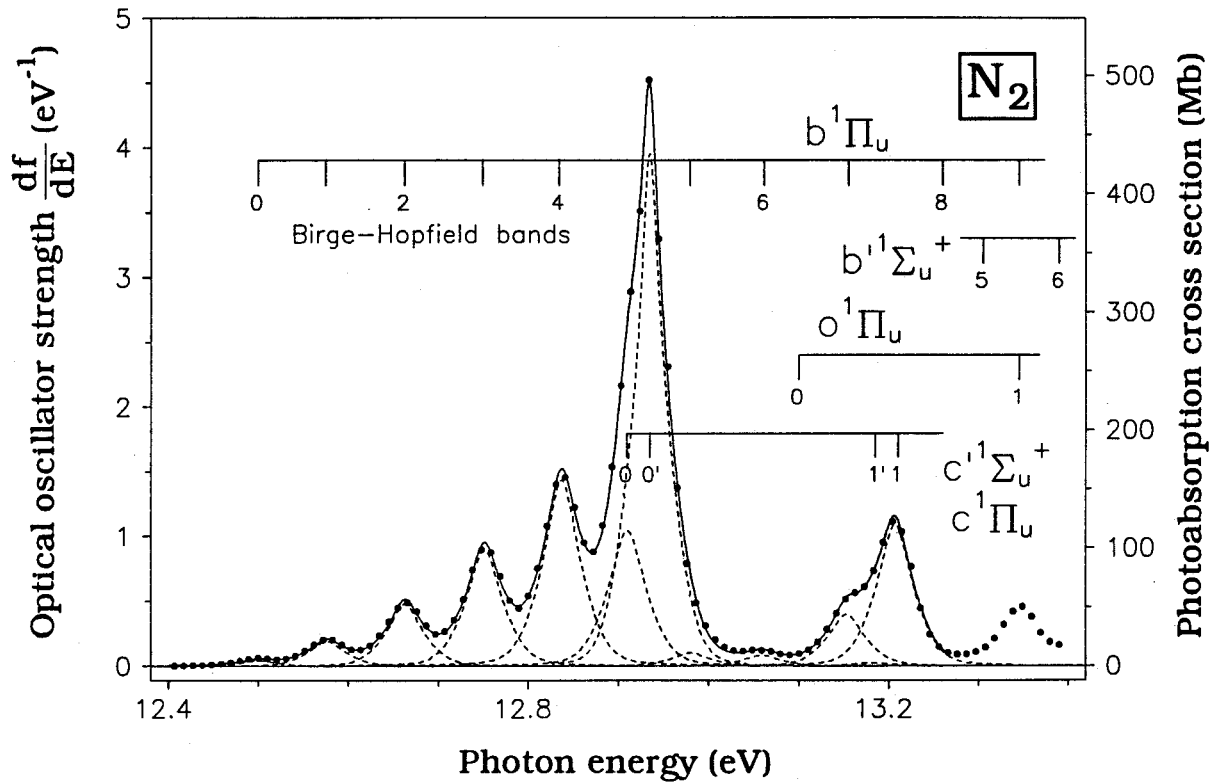


Figure 8.3: Expanded view of figure 8.2 for the photoabsorption of molecular nitrogen in the energy region 12.4–13.4 eV. The assignments are taken from references [300,304,317]. Deconvoluted peaks are shown as dashed lines and the solid line shows the total fit to the experimental data.

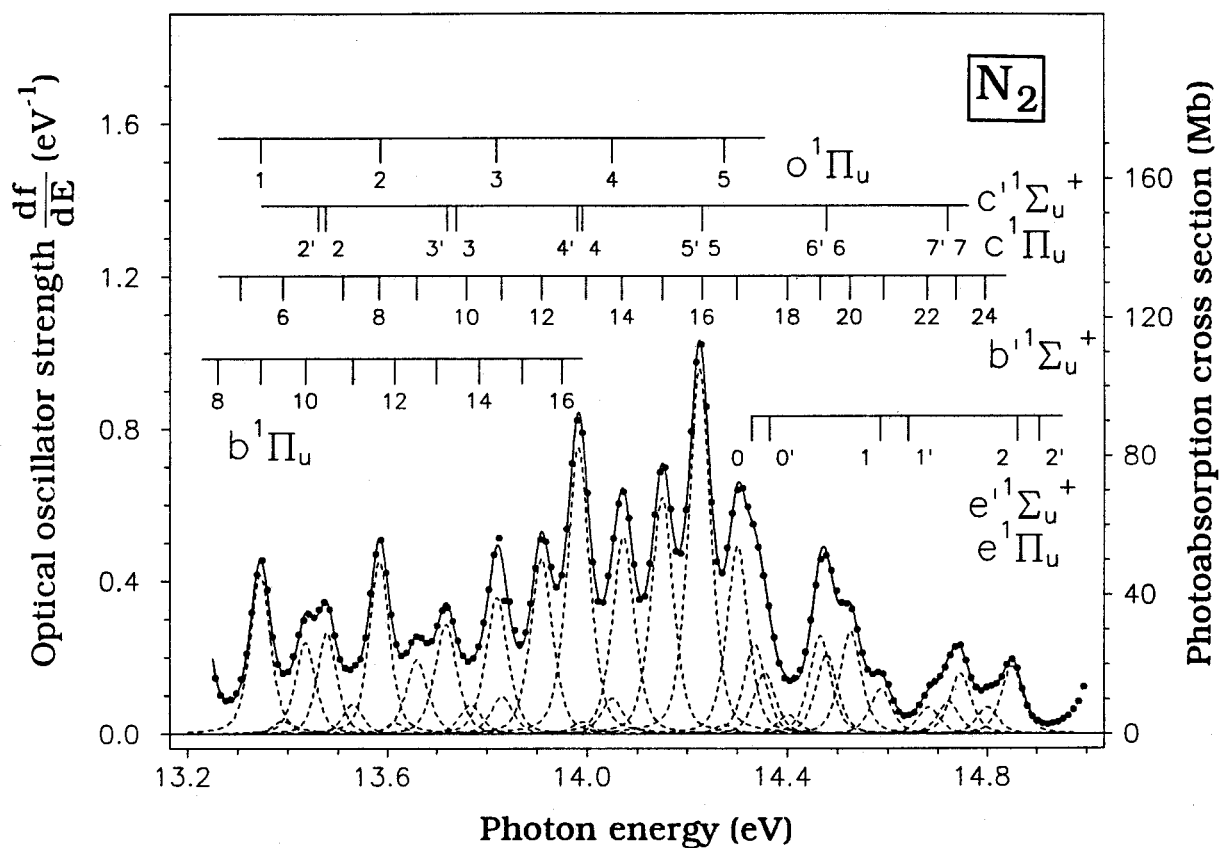


Figure 8.4: Expanded view of figure 8.2 for the photoabsorption of molecular nitrogen in the energy region 13.2–15.0 eV. The assignments are taken from references [300,304,317]. Deconvoluted peaks are shown as dashed lines and the solid line shows the total fit to the experimental data.

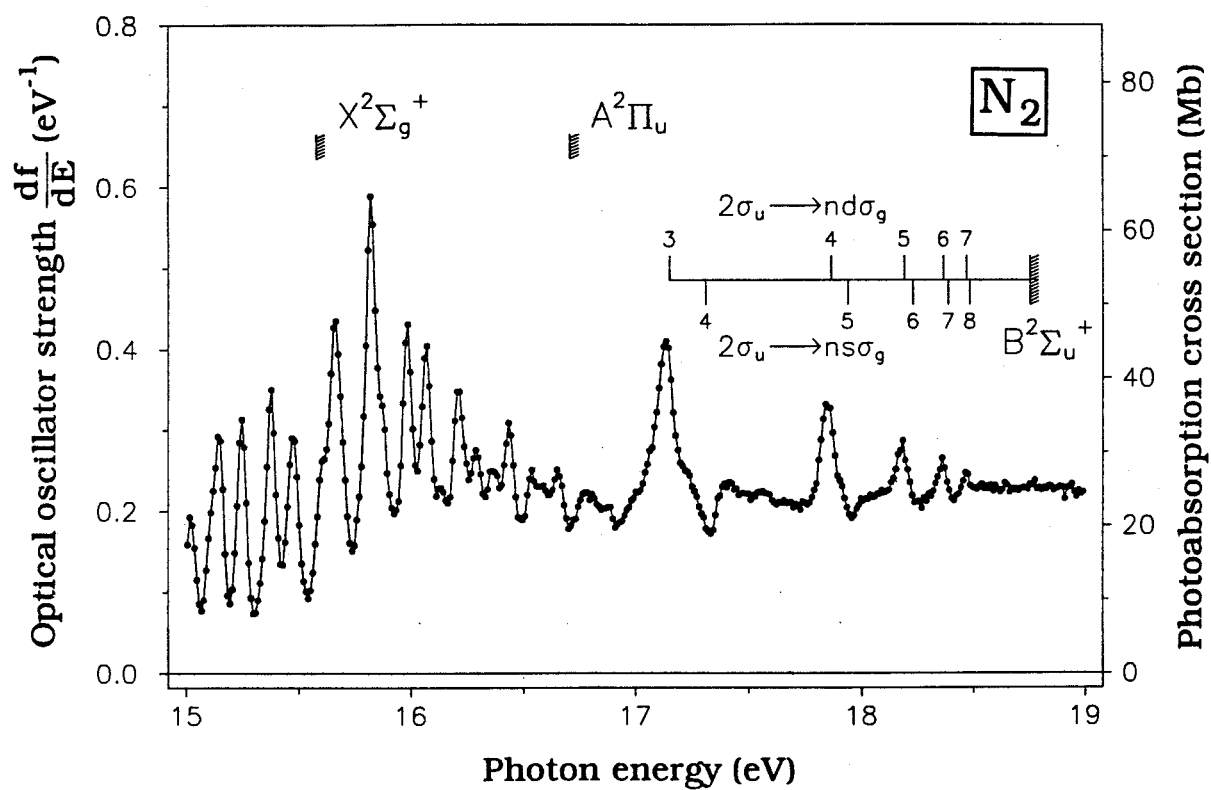


Figure 8.5: Expanded view of figure 8.2 for the photoabsorption of molecular nitrogen in the energy region 15–19 eV. The assignments are taken from references [80,300,317].

these transitions are not shown in figure 8.5 due to heavy overlapping in this region. The autoionization profiles in the energy region 17.1–18.5 eV are due to transitions from the $2\sigma_u \rightarrow n\sigma_g$ "window resonances", and the $2\sigma_u \rightarrow n d\sigma_g$ Rydberg series [80]. The "window resonances" are caused by destructive quantum mechanical interference with the underlying direct ionization continuum.

In the present work integration of the area under each spectral peak will give directly the absolute optical oscillator strength for the respective discrete vibronic transition. Since the energy positions of the peaks are very well known [80,300,304,317], a curve fitting program using Voigt-profiles has been used to provide an accurate deconvolution of the partially resolved peaks in the energy region 12.4–14.9 eV. Although they should be slightly asymmetric due to unresolved rotational structure (as observed for example in the very high resolution electron energy loss spectrum obtained by Geiger and Schroder [304]), the peaks are expected to be essentially symmetric at the resolution of the present work. Accordingly symmetric peak profiles have been used in the curve-fitting procedure. The dashed lines in figures 8.3 and 8.4 show the resulting deconvoluted peaks. Absolute optical oscillator strengths obtained from the deconvoluted peak areas are summarized in table 2. The assignments and energy positions shown in table 8.2 are taken from the paper of Geiger and Schroder [304]. The uncertainties of the area determinations (and thus the oscillator strengths) in the present work are estimated to be ~5–10% for the relatively strong and well separated peaks in the energy region 12.40–13.27 eV, and ~10–20% for the remaining peaks at higher energies.

Table 8.2

Absolute optical oscillator strengths for discrete transitions from the ground state of molecular nitrogen in the energy region 12.50–14.86 eV[#]

Energy (eV)	Final electronic state	Upper level vibrational number (v')	Integrated oscillator strength
12.500	$b^1\Pi_u$	0	0.00254
12.575	$b^1\Pi_u$	1	0.0113
12.663	$b^1\Pi_u$	2	0.0272
12.750	$b^1\Pi_u$	3	0.0526
12.835	$b^1\Pi_u$	4	0.0861
12.910	$c^1\Pi_u$	0	0.0635
12.935	$c^1\Sigma_u^+$	0	0.195
12.980	$b^1\Pi_u$	5	0.00613
13.062	$b^1\Pi_u$	6	0.00500
13.100	$o^1\Pi_u$	0	---
13.156	$b^1\Pi_u$	7	0.0237
13.185	$c^1\Sigma_u^+$	1	0.00147
13.210	$c^1\Pi_u$	1	0.0640
13.260	$b^1\Pi_u$	8	---
13.305	$b^1\Sigma_u^+$	5	---
13.345	$b^1\Pi_u$	9	} 0.0258
	$o^1\Pi_u$	1	
13.390	$b^1\Sigma_u^+$	6	0.00216
13.435	$b^1\Pi_u$	10	0.0147
13.475	$c^1\Pi_u$	2	0.0155
13.530	$b^1\Pi_u$	11	0.00484

Table 8.2 (continued)

Energy (eV)	Final electronic state	Upper level vibrational number (v')	Integrated oscillator strength
13.585	$o^1\Pi_u$	2	0.0277
13.615	$b^1\Pi_u$	12	0.00181
13.660	$b^1\Sigma_u^+$	9	0.0128
13.700	$b^1\Pi_u$	13	---
13.720	$c^1\Sigma_u^+$	3	0.0190
13.760	$b^1\Sigma_u^+$	10	} 0.00510
13.785	$b^1\Pi_u$	14	
13.820	$o^1\Pi_u$	3	0.0236
13.830	$b^1\Sigma_u^+$	11	0.00654
13.870	$b^1\Pi_u$	15	---
13.910	$b^1\Sigma_u^+$	12	0.0303
13.950	$b^1\Pi_u$	16	---
13.980	$c^1\Sigma_u^+$	4	0.0496
13.990	$c^1\Pi_u$	4	0.00210
13.998	$b^1\Sigma_u^+$	13	---
14.050	$o^1\Pi_u$	4	0.00620
14.070	$b^1\Sigma_u^+$	14	0.0341
14.150	$b^1\Sigma_u^+$	15	0.0409
14.230	$b^1\Sigma_u^+$	16	} 0.0632
	$c^1\Pi_u$	5	
	$c^1\Sigma_u^+$	5	
14.275	$o^1\Pi_u$	5	0.00155

Table 8.2 (continued)

Energy (eV)	Final electronic state	Upper level vibrational number (v')	Integrated oscillator strength
14.300	$b'^1\Sigma_u^+$	17	0.0318
14.330	$e^1\Pi_u$	0	0.0153
14.350	$e'^1\Sigma_u^+$	0	0.0104
14.400	$b'^1\Sigma_u^+$	18	0.00326
14.465	$b'^1\Sigma_u^+$	19	0.0166
14.478	$c'^1\Sigma_u^+$	6	0.0135
14.525	$b'^1\Sigma_u^+$	20	0.0173
14.585	$e^1\Pi_u$	1	0.00761
14.680	$b'^1\Sigma_u^+$	22	0.00455
14.720	$c^1\Pi_u$	7	0.00547
	$c'^1\Sigma_u^+$	7	
14.737	$b'^1\Sigma_u^+$	23	0.0102
14.795	$b'^1\Sigma_u^+$	24	0.00455
14.839	$n=5^1\Pi_u$	0	0.0113
14.860	$e^1\Pi_u$	2	---

The energy positions and assignments were obtained from ref. [304].

Tables 8.3–8.7 summarize the absolute, vibrationally resolved oscillator strengths for the electronic transitions from the ground state to each of the $b^1\Pi_u$, $b^1\Sigma_u^+$, $c^1\Sigma_u^+$, $c^1\Pi_u$ and $o^1\Pi_u$ states, along with previously published data [78,79,294–297]. For the overlapping transitions such as $v'=9$ of $b^1\Pi_u$ and $v'=1$ of $o^1\Pi_u$, as shown in table 8.2, the oscillator strength value for each individual transition was estimated from the ratio of the relative band strengths for these states as calculated by Stahel *et al.* [306]. Similar procedures were employed for the other unresolved states indicated in table 8.2. It can be seen in tables 8.3–8.7 that great variations exist in the absolute vibronic oscillator strengths reported by various groups using different experimental techniques and methods of normalization [78,79,294–297].

The photoabsorption data of Lawrence *et al.* [78] shown in tables 8.3, 8.5 and 8.6 are more than 30% lower than the present work even though the data were obtained by extrapolating the measured oscillator strength values to low pressure ($N < 10^{13}$ cm⁻²) in an attempt to account for the "line saturation" effects. However, as has been pointed out in refs. [11,37] and discussed in the introduction of this chapter, this kind of extrapolation procedure may lead to large errors in the resulting oscillator strength values since it relies heavily on the least accurate data measured at the lowest pressure. Carter [79] has reported similar measurements for nitrogen as a function of pressure but only extrapolated down to a column number N of 10^{14} cm⁻². Despite the extrapolation the absolute oscillator strength data reported by Carter [79] still show serious "line saturation" effects for many transitions, and the errors are especially large in the cases of $v'=4$ of the $b^1\Pi_u$ state, $v'=16$ of the $b^1\Sigma_u^+$ state, $v'=0$ of the $c^1\Sigma_u^+$ state and $v'=0$ of the $c^1\Pi_u$ state (see tables 8.3–8.6).

Absolute optical oscillator strengths for transitions to the vibronic bands of the valence $b^1\Pi_u$ state from the ground state of molecular nitrogen

Energy (eV)	v'	Present work	James <i>et al.</i> [297]†	Zipf and Mclaughlin [294]@	Carter [79]#	Lawrence <i>et al.</i> [78]
12.500	0	0.00254	0.0014	0.00239		
12.575	1	0.0113	0.0081	0.0139		
12.663	2	0.0272	0.0182	0.0311	0.035	
12.750	3	0.0526	0.0343	0.0579	0.058	0.02
12.835	4	0.0861	0.0550	0.0922	0.047	0.055
12.980	5	0.00613	0.0029	0.00473		
13.062	6	0.00500	0.0027	0.00437		
13.156	7	0.0237	0.0153	0.0248	0.019	
13.260	8	---	0.0003	0.000506		
13.345	9	0.00466*	0.0031	0.0050*		
13.435	10	0.0147	0.0093	0.0146	0.013	
13.530	11	0.00484	0.0032	0.00439	0.0046	
13.615	12	0.00181	0.0007	0.00126	0.0042	
13.700	13	---			0.007	
13.785	14	0.00290	0.0008	0.00131		
13.870	15	---	0.0005	0.000887		
13.950	16	---	0.0004	0.000752		

† Data were normalized on Lawrence *et al.* [78] at $v'=4$.

@ The same set of values was quoted in the article of Zipf and Gorman [295].

Values were obtained at a column number N of 10^{14} cm^{-2} .

* This transition cannot be separated from $v'=1$ of the $o^1\Pi_u$ state. The value was obtained from the ratio of the relative band strengths of these two states as calculated by Stahel *et al.* [306].

Absolute optical oscillator strengths for transitions to the vibronic bands of the valence $b^1\Sigma_u^+$ state from the ground state of molecular nitrogen

Energy (eV)	v'	Present work	Ajello <i>et al.</i> [296]	Zipf and MacLaughlin [294]	Carter [79]#
	0				
	1				
	2				
	3				
	4				
13.305	5		0.00135	0.00123	
13.390	6	0.00216	0.002649	0.00260	0.0075
	7		0.003409		
	8		0.022107		
13.660	9	0.0128	0.009529	0.0102	0.0048
13.760	10	0.00220	0.001643	0.00173	
13.830	11	0.00654	0.003504	0.00367	
13.910	12	0.0303	0.030297	0.0316	0.019
13.998	13		0.004443	0.00455	
14.070	14	0.0341	0.041825	0.0424	
14.150	15	0.0409	0.054902	0.0493	0.034
14.230	16	0.0626*	0.067792	0.0667*	0.025
14.300	17	0.0318	0.037148	0.0368	0.025
14.400	18	0.00326	0.003366	0.00329	
14.465	19	0.0166	0.021500	0.0208	
14.525	20	0.0173	0.018373	0.0177	0.016
	21		0		0.0076
14.680	22	0.00455	0.005532	0.00522	0.0052
14.737	23	0.00897	0.009411	0.00880	
14.795	24	0.00363	0.003823	0.00356	0.0044

Values were obtained at a column number N of 10^{14} cm^{-2} .

* This transition cannot be separated from $v'=5$ of the $c^1\Sigma_u^+$ state. The value was obtained from the ratio of the relative band strengths of these two states as calculated by Stahel *et al.* [306].

Table 8.5
Absolute optical oscillator strengths for transitions to the vibronic bands of the lowest member of the Rydberg $c'1\Sigma_u^+$ state from the ground state of molecular nitrogen

Energy (eV)	v'	Present work	Ajello <i>et al.</i> [296]	Zipf and McLaughlin [294]	Carter [79]#	Lawrence <i>et al.</i> [78]
12.935	0	0.195	0.1567	0.217	0.065	0.14
13.185	1	0.00147	0.0038	0.00199		
	2		0.0027		0.011	
13.720	3	0.0190	0.0136	0.0207	0.029	
13.980	4	0.0496	0.0285	0.0592		
14.230	5	0.0006*	0	0.0007*	0.0039	
14.478	6	0.0135	0.0179	0.0176		

Values were obtained at a column number N of 10^{14} cm^{-2} .

* This transition cannot be separated from $v'=16$ of the $b'1\Sigma_u^+$ state. The value was obtained from the ratio of the relative band strengths of these two states as calculated by Stahel *et al.* [306].

Table 8.6
Absolute optical oscillator strengths for transitions to the vibronic bands of the lowest member of the Rydberg $c^1\Pi_u$ state from the ground state of molecular nitrogen

Energy (eV)	v'	Present work	Zipf and McLaughlin [294]	Carter [79]#	Lawrence <i>et al.</i> [78]
12.910	0	0.0635	0.0656	0.037	0.040
13.210	1	0.0640	0.0682		
13.475	2	0.0155	0.0172	0.018	
13.990	4	0.00210			
14.230	5		0.00530		

Values were obtained at a column number N of 10^{14} cm^{-2} .

Table 8.7
Absolute optical oscillator strengths for transitions to the vibronic bands of the lowest member of the Rydberg $o^1\Pi_u$ state from the ground state of molecular nitrogen

Energy (eV)	v'	Present work	Zipf and McLaughlin [294]	Carter [79]#
13.100	0		0.00049	
13.345	1	0.0211*	0.0226*	
13.585	2	0.0277	0.0278	0.021
13.820	3	0.0236	0.0329	0.030
14.050	4	0.00620	0.00506	
14.275	5	0.00155	0.00321	

Values were obtained at a column number N for 10^{14} cm^{-2} .

* This transition cannot be separated from $v'=9$ of the $b^1\Pi_u$ state. The value was obtained from the ratio of the relative band strengths of these two states as calculated by Stahel *et al.* [306].

It can also be seen in tables 8.3–8.7 that although the absolute vibronic oscillator strengths reported by Zipf and McLaughlin [294], Ajello *et al.* [296], James *et al.* [297] and the present results show variations between each other, the relative oscillator strength values for the vibronic levels of a given electronic transition are reasonably consistent. These differences between the data sets are therefore likely caused by the different ways in which the data have been made absolute. For the $b^1\Pi_u$ vibronic bands, the data of James *et al.* [297], which were normalized at $v'=4$ to the value reported by Lawrence *et al.* [78], are lower than the presently reported values. This observation and the differences with the present work are consistent with the fact that the data of Lawrence *et al.* [78] still show "line saturation" effects at the lowest pressure used for measurement (see above discussion). The absolute oscillator strength data reported by Zipf and McLaughlin [294] are in general slightly higher than the present results. However, it has to be pointed out that Zipf and McLaughlin [294] did not make any direct oscillator strength measurement. Their oscillator strength data [294], which were used to calculate the predissociation branching ratios by combining with their measured emission cross sections, were in fact derived from the relative electron impact data of Geiger and Schroder [304] by normalizing on the absolute generalized oscillator strength data of Lassette and Skerbele [13]. The data reported by Lassette and Skerbele [13] were in turn obtained from the earlier limiting oscillator strengths work of Silverman and Lassette [18], which had to be renormalized [13] by multiplying a factor (0.754) in order to correct for an error in the pressure measurements. Ajello *et al.* [296] determined

absolute oscillator strength data from their own measurements, but their results have a stated uncertainty of 22%.

By summing up the appropriate vibronic oscillator strengths shown in tables 8.3–8.7, the total absolute oscillator strengths for the $b^1\Pi_u$ and $b^1\Sigma_u^+$ excited valence states, and the lowest members of $c^1\Pi_u$, $c^1\Sigma_u^+$ and $o^1\Pi_u$ Rydberg states can be obtained. The results are summarized in table 8.8 where previously available experimental [294,296,297,324] and theoretical data [299–303,306] are also shown for comparison. It can be seen that there are large variations between the reported values. Except in the case of the $o^1\Pi_u$ state, the theoretical data of Bielschowsky *et al.* [303], calculated using the configuration interaction method, show better agreement with the present results than those calculated using the Hartree–Fock method. The calculations reported by Stahel *et al.* [306] only show good agreement with the present values for the $c^1\Pi_u$ state, while the calculated values for the other states are all lower. The total oscillator strengths for the five excited states reported by Zipf and McLaughlin [294] are somewhat higher than the presently reported data, which is consistent with the vibrationally resolved results in tables 8.3–8.7. Similarly, the total oscillator strength value for the $b^1\Pi_u$ state reported by James *et al.* [297] is ~36% lower than the present value. However, this is consistent with the fact that the normalization [297] was obtained using the vibronic oscillator strength for $v'=4$ of the $b^1\Pi_u$ state measured by Lawrence *et al.* [78], which is lower than the present work by the same amount, as shown in table 8.3.

The spectrum above 14.92 eV involves many highly overlapped transitions. Therefore absolute integrated oscillator strengths over small energy intervals in the energy region 14.92–16.91 eV have been

Table 8.8

Total absolute optical oscillator strengths for transitions to the $b^1\Pi_u$ and $b^1\Sigma_u^+$ valence states, and the lowest members of the $c^1\Pi_u$, $c^1\Sigma_u^+$ and $o^1\Pi_u$ Rydberg states from the ground state of molecular nitrogen

	$b^1\Pi_u$	$b^1\Sigma_u^+$	$c^1\Pi_u$	$c^1\Sigma_u^+$	$o^1\Pi_u$
Experiment:					
Present work	0.243	0.278	0.145	0.279	0.080
James <i>et al.</i> [297]	0.156				
Ajello <i>et al.</i> [296]		0.321		0.223	
Zipf and McLaughlin [294]	0.283	0.310	0.156	0.317	0.0921
Chutjian <i>et al.</i> [324]		0.10	0.080	0.12	0.026
Theory:					
Bielschowsky <i>et al.</i> [303]					
(a) Hartree-Fock	0.68	0.62	0.07	0.06	0.11
(b) CI	0.41	0.31	0.09	0.26	0.15
Stahel <i>et al.</i> [306]	0.124	0.209	0.141	0.139	0.061
Kosman and Wallace [300]			0.0641	0.0493	0.136
Hazi [302]		0.47		0.11	
Rescigno <i>et al.</i> [299]			0.0681	0.0591	0.149
Rose <i>et al.</i> [301]	0.32	0.49		0.11	

Table 8.9

Integrated absolute optical oscillator strengths in selected regions over the energy range 14.92–16.91 eV for excitation of molecular nitrogen

Energy range (eV)	Integrated oscillator strength
14.92–15.07	0.0139
15.07–15.19	0.0228
15.19–15.30	0.0196
15.30–15.43	0.0245
15.43–15.54	0.0212
15.54–15.74	0.0510
15.74–15.93	0.0606
15.93–16.03	0.0300
16.03–16.11	0.0270
16.11–16.17	0.0115
16.17–16.26	0.0260
16.26–16.33	0.0184
16.33–16.40	0.0156
16.40–16.49	0.0236
16.49–16.70	0.0476
16.70–16.91	0.0426

obtained, and these are summarised in table 8.9. Comparison with the previously reported photoabsorption data in this energy range is difficult because of different instrumental energy resolutions and also because of the presence of "line saturation" effects in the photoabsorption data. Finally, it can be noted that the oscillator strength distribution of molecular nitrogen was reviewed earlier by Berkowitz [143], using the experimental data available before 1980. Berkowitz obtained a value of 1.153 for the integrated oscillator strength below 15.56 eV using the data of Lassetre and Skerbele [13] and a value of 0.3299 in the 15.56–16.76 eV energy region based on the data of Carter [79]. In the present work these integrated values are determined to be 1.173 and 0.319, respectively.

8.3 Conclusions

In the present work comprehensive oscillator strength measurements have been obtained throughout the UV and soft x-ray energy regions for the photoabsorption of molecular nitrogen. Absolute optical oscillator strengths have been measured in the energy region 11–200 eV using low resolution dipole (e,e) spectroscopy and TRK sum-rule normalization. The present continuum results are in good agreement with the photoabsorption data reported by Samson and Haddad [292]. Absolute optical oscillator strengths in the 12–22 eV region of discrete excitation have also been measured using the high resolution dipole (e,e) method recently developed in this laboratory. The absolute scale was obtained by normalizing in the smooth continuum region at 20 eV to the absolute photoabsorption value determined using the low resolution

dipole (e,e) spectrometer. The transition peaks below 14.9 eV have been deconvoluted to obtain the absolute photoabsorption oscillator strength values for individual vibronic transitions. The presently determined absolute optical oscillator strengths for excitation to the $b^1\Pi_u$ and $b^1\Sigma_u^+$ valence states, and the $c^1\Pi_u$, $c^1\Sigma_u^+$ and $o^1\Pi_u$ Rydberg states have been compared with previously reported experimental and theoretical data. Large differences between the various reported data sets are observed. However, it is found that the relative oscillator strength values for the vibronic bands determined from the present work and some of the previously reported [294,296,297] data are reasonably consistent. This suggests that the differences in these cases are most likely due to the different normalization procedures used to establish the absolute scales. In the present work the absolute optical oscillator strength scale has been established by independent procedures. The accuracy of the presently determined absolute optical oscillator strengths for the photoabsorption of molecular nitrogen in the discrete region can be justified by a consideration of the results for the noble gases [37–39] (chapters 4–6) and molecular hydrogen [40] (chapter 7) which have been recently obtained using the same instrumentation and techniques. The present work also clearly demonstrates the existence of serious errors due to "line saturation" (bandwidth) effects in absolute oscillator strength (cross section) determinations for discrete transitions in molecular nitrogen made using Beer–Lambert law photoabsorption techniques, even where the measurements have been made as a function of pressure. Such considerations will be of concern in absolute oscillator strength determinations for all atoms and molecules using Beer–Lambert law photoabsorption methods.

Chapter 9

Absolute Optical Oscillator Strengths for the Photoabsorption of Molecular Oxygen (5–30 eV) at High Resolution

9.1 Introduction

Since oxygen is the second most abundant species within the earth's atmosphere, an accurate knowledge of absolute oscillator strengths (cross sections) for the photoabsorption of molecular oxygen in the valence discrete region is of great importance in aeronomy and in other areas such as nuclear physics, radiation physics and astrophysics. The dissociation and predissociation of molecular oxygen by the absorption of solar radiation can also be used to determine the oxygen density profile at high altitudes and such processes play an important role in atmospheric phenomena such as aurora and dayglow. Molecular oxygen is also of particular theoretical interest and challenge since it is an open shell system.

The photoabsorption spectrum of oxygen has been studied extensively. Critical reviews and compilations of the spectroscopic data of oxygen can be found in several papers [46,330,331]. Although Beer-Lambert law photoabsorption methods have often been used to obtain quantitative results for discrete transitions, it has been pointed out [37,46] (see chapter 2) that absolute oscillator strengths (cross sections) measured by direct absorption of photons may be subject to considerable error because of "line saturation" effects due to the finite resolution (bandwidth) of the optical spectrometer. Such effects can be severe for

discrete transitions with very narrow natural linewidth and high cross section. For example, Yoshino *et al.* [55] have noted that the Schumann–Runge (12,0) band of $^{18}\text{O}_2$ is too sharp for its absolute cross section to be measured by conventional Beer–Lambert law photoabsorption techniques.

The Schumann–Runge band system of molecular oxygen, which involves transitions from the ground $X^3\Sigma_g^-$ to the $B^3\Sigma_u^-$ state, has been studied extensively by many workers. On the low energy side the system consists of sharp discrete transitions with very low oscillator strength, which have been measured by Lewis *et al.* [332] using the curve of growth method to allow for bandwidth effects. At higher energy in the 7–9.8 eV region the absorption spectrum of oxygen is dominated by the broad and generally featureless Schumann–Runge continuum, for which many Beer–Lambert law photoabsorption measurements of the absolute cross section have been made [333–342]. Ab-initio theoretical calculations have been reported by Buenker and Peyerimhoff [343] and by Allison *et al.* [344] for the oscillator strengths of the Schumann–Runge continuum region, taking into account the mixing between the valence $B^3\Sigma_u^-$ and the Rydberg $E^3\Sigma_u^-$ (or $B'^3\Sigma_u^-$ in other notation) states. Allison *et al.* [344] also took into account the contributions from the $1^3\Pi_u$ state and reported cross sections and structural features that were consistent with the existing experimental results. Wang *et al.* [342] performed an experimental absolute photoabsorption measurement of oxygen in the Schumann–Runge continuum region, and by fitting their theoretical calculations to the observed data, they reported potential curves and transitions moments for the mixed Rydberg–valence $B^3\Sigma_u^-$ and mixed valence–Rydberg $E^3\Sigma_u^-$ states.

On the high energy side of the Schumann–Runge continuum, there are several diffuse bands. The three prominent peaks at 9.96 eV (longest), 10.28 eV (second) and 10.57 eV (third) have been assigned by Yoshimine *et al.* [345] and Buenker *et al.* [346] as transitions to the three lowest vibrational levels of the mixed valence–Rydberg $E^3\Sigma_u^-$ state. Yoshimine *et al.* [345], Buenker *et al.* [346] and Li *et al.* [347] have computed the absolute oscillator strengths for these three bands. Beer–Lambert law–type photoabsorption measurements have also been performed for these diffuse bands [334,336,340], including a recent study by Lewis *et al.* [348,349], who made measurements on isotopic molecular oxygen ($^{18}\text{O}_2$) and for the first time analyzed the data using Beutler–Fano type resonance profiles.

Electron energy loss spectroscopy (EELS) has also been used to study the electronic excitation spectrum of molecular oxygen [13,16,17,92,350,351] in the valence discrete region. Since electron impact excitation is non–resonant as described in chapter 2, EELS based methods of determining optical oscillator strengths have the enormous advantage that they are not subject to the limitations of "line–saturation" (i.e. bandwidth) effects which cause difficulties in Beer–Lambert law photoabsorption measurements [37,46]. Using measurements of inelastically scattered electrons obtained at a range of scattering angles, absolute optical oscillator strengths for oxygen in the discrete and continuum regions were derived by Lassetre and co–workers [13,16,17] from extrapolation of the measured generalized oscillator strengths to zero momentum transfer. With the use of extremely high impact energy (25 keV) and small scattering angle, Geiger and Schroder [350] reported a very high resolution electron energy loss spectrum of oxygen in the

energy loss region 6.8–21 eV, but only relative intensities (not absolute oscillator strengths) were obtained. Huebner *et al.* [351] have reported data in the energy region 6–14 eV which were derived from high resolution electron energy loss measurements obtained at an impact energy of only 100 eV and at a small scattering angle (0.02 rad.). The measured oscillator strengths are questionable in this case [351] since the experimental conditions correspond to a rather large momentum transfer ($\mathbf{K}^2=0.01$ and 0.04 a.u. at 6 eV and 14 eV respectively). The absolute scale was established by Huebner *et al.* [351] by normalizing the spectrum to an average optical value [46] at a single point in the Schumann–Runge continuum region where the photoabsorption measurements were mutually in best agreement. An independent TRK sum rule normalization method was used by Brion *et al.* [92] to obtain absolute oscillator strengths for the photoabsorption of oxygen in the energy region 5–300 eV from Bethe–Born converted electron energy loss spectra. These latter results [92] were determined directly at negligible momentum transfer using a low resolution ($\Delta E=1$ eV FWHM) dipole (e,e) spectrometer with an impact energy of 8 keV and a mean scattering angle of zero degrees.

In the presently reported work, the recently developed [36,37] high resolution dipole (e,e) method which has already been applied successfully to measurements for the noble gases [36–39] (see chapters 4–6) and several small molecules [27,40,41] (see chapters 7 and 8), has been used to measure directly, at negligible momentum transfer, the absolute oscillator strengths for oxygen in the energy region 6–30 eV at a resolution of 0.048 eV FWHM. The absolute scale has been obtained by normalizing in the smooth continuum at 26 eV to the previously reported

absolute oscillator strength value determined by Brion *et al.* [92] using a low resolution dipole (e,e) spectrometer.

9.2 Results and Discussion

The photoabsorption oscillator strengths and spectral assignments of molecular oxygen are conveniently discussed with reference to the ground state molecular-orbital, independent particle, valence shell electronic configuration, which may be written as:

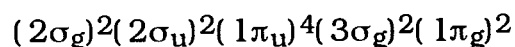


Figure 9.1 shows the presently measured absolute differential oscillator strength spectrum of molecular oxygen measured in the energy region 5–30 eV by high resolution dipole (e,e) spectroscopy at a resolution of 0.048 eV FWHM. Several vibrational progressions are clearly visible. The two other sets of data shown in figure 9.1 are the low resolution (1 eV FWHM) dipole (e,e) data (open triangles) reported earlier at 1 eV intervals by Brion *et al.* [92] and the photoabsorption data (open circles) measured by Samson and Haddad [292] using a double ion chamber method. The double ion chamber results [292] are not compared with the present work in the region of the sharp autoionizing structure (12–18 eV) because of significant differences in energy resolution and also because the optical measurements may be subject to "line saturation" effects. Therefore the data of reference [292] are only shown in figure 9.1 in the generally smoother spectral region above 18 eV. It can be seen from figure 9.1 that the present results are in very good quantitative

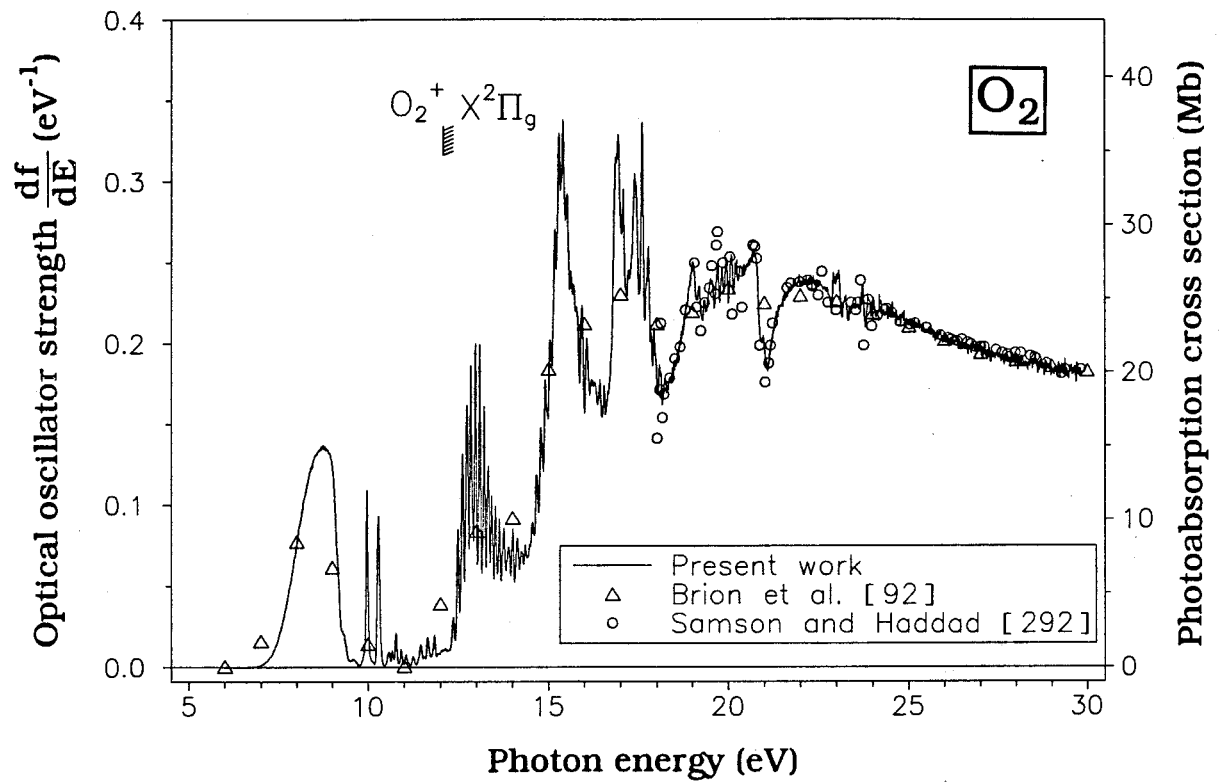


Figure 9.1: Absolute oscillator strengths for the photoabsorption of molecular oxygen in the energy region 5–30 eV measured using the high resolution dipole (e,e) spectrometer (FWHM=0.048 eV).

agreement with the earlier data of Brion *et al.* [92] and also those of Samson and Haddad [292] in the smooth continuum region (where the cross section will be effectively independent of resolution). At lower energies the presently obtained high resolution spectrum is seen to be consistent with the data of Brion *et al.* [92] given the differences in resolution. The total integrated oscillator strengths below 18 eV for both the high and low resolution spectra are in very good agreement with each other, giving values of 1.13 and 1.12 respectively. In the present work, integration of the measured high resolution differential oscillator strength spectrum over a given energy region will give directly the absolute oscillator strength for that region. The uncertainties in the presently reported absolute oscillator strengths are estimated to be $\pm 5\%$.

Figure 9.2 shows an expanded view of figure 9.1 in the energy region 6.5–10 eV showing the absolute oscillator strengths for the Schumann–Runge continuum. The weak Schumann–Runge bands below 7 eV which are several orders of magnitude smaller in oscillator strength than the continuum could not be observed in the present work. In figures 9.2 (a) and (b) the present results are compared with previously published experimental [334–336,338–342,351] and theoretical [342,344] results respectively. Immediately it can be seen from figure 9.2 (a) that the present results are in excellent agreement with most of the other experimental data. The data of Ditchburn and Heddle [335] are much higher than all the other experimental data while those of Goldstein and Mastrup [339] are somewhat lower in the energy region around the continuum maximum. For the experimental work shown in figure 9.2 (a) only the present high resolution dipole (e,e) measurements and the data of Huebner *et al.* [351] are derived from electron energy loss

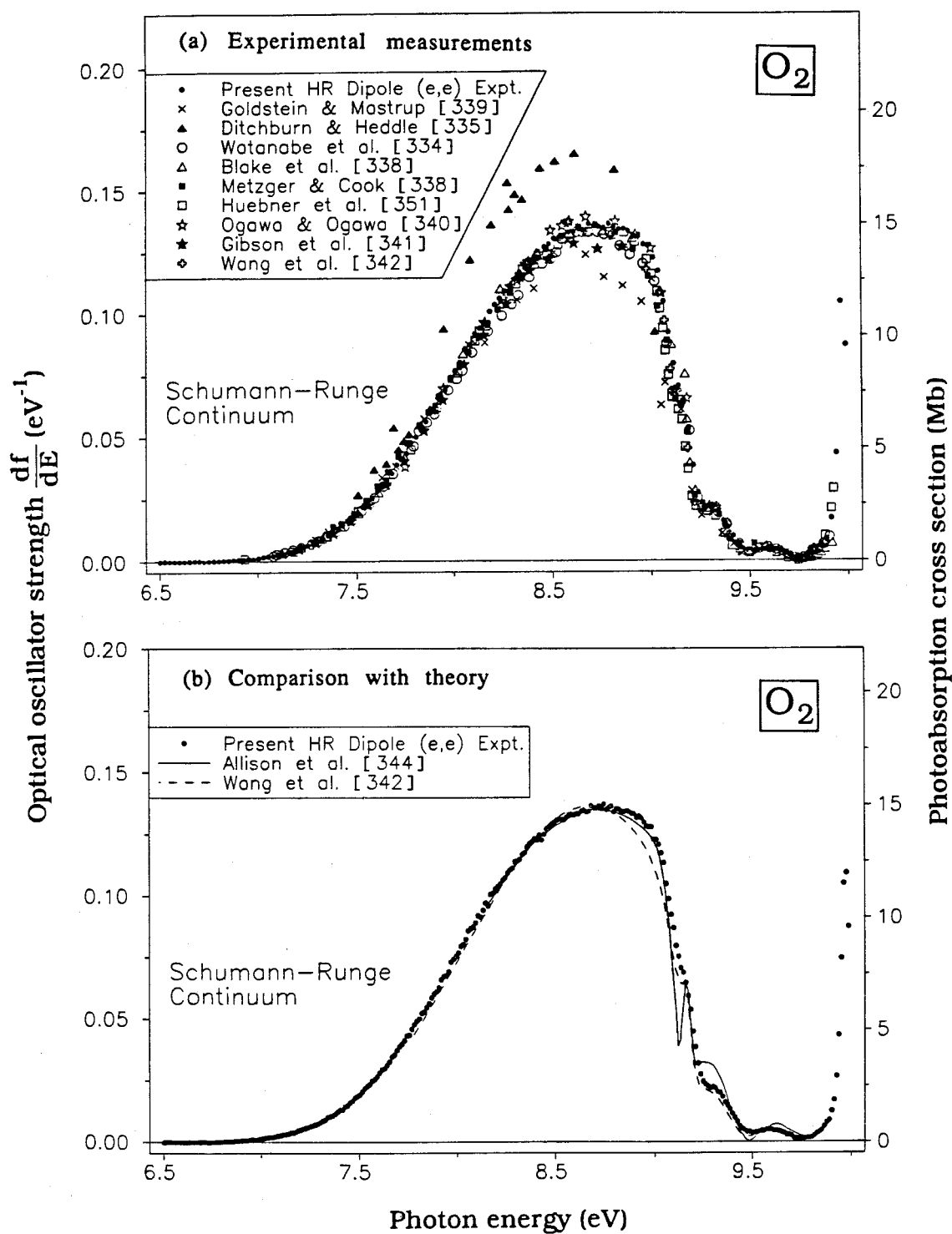


Figure 9.2: Absolute oscillator strengths for the photoabsorption of molecular oxygen. Expanded view of figure 9.1 in the energy region 6.5–10 eV, showing the Schumann–Runge continuum region. (a) comparison with previously published experimental data [334–336,338–342,351] (b) comparison with theory [342,344]

spectra. The remainder are Beer-Lambert law photoabsorption measurements [334-336,338-342] which in this particular energy region should not be subject to "line-saturation" effects due to the broad nature of the Schumann-Runge continuum in oxygen. Note that the data of Huebner *et al.* [351] were normalized at the continuum maximum (8.61 eV) to the average of the optical data [46] which were available at that time and therefore reasonable agreement with the photoabsorption data is not surprising. In contrast, the present high resolution dipole (e,e) spectrum was made absolute using the TRK sum-rule normalized low resolution dipole (e,e) work of Brion *et al.* [92] in the smooth continuum region at 26 eV, which is ~17 eV above the Schumann-Runge continuum maximum. The Bethe-Born conversion process (see experimental section 3.3) results in a very large change in relative intensity of the two continua between the original electron energy loss data and the relative optical oscillator strength spectrum. Therefore any inaccuracy in the Bethe-Born conversion factor for the spectrometer would produce spurious oscillator strengths. The validity and accuracy of the Bethe-Born conversion factor for the high resolution dipole (e,e) spectrometer used in the present work has previously been confirmed down to ~11 eV by comparison of measurements and highly accurate ab-initio calculations for helium [37] and molecular hydrogen [40]. The results for the Schumann-Runge continuum of oxygen now provide a further stringent test of the accuracy with which the Bethe-Born conversion factor for the high resolution dipole (e,e) spectrometer has been determined and in particular in the region down to 7 eV. This is important to establish since the Bethe-Born conversion factor was obtained from a comparison of high and low resolution dipole (e,e) measurements above 22 eV in the

ionization continua of helium [37] and neon [38] (see chapter 3). The Bethe–Born factor below 22 eV was then obtained by curve fitting the measured quantity above 22 eV and extrapolating to lower energies. The excellent agreement of the present work with many previously published photoabsorption measurements of the absolute oscillator strengths in the Schumann–Runge continuum region of oxygen is a very strong indication that the Bethe–Born conversion factor is well characterized for the high resolution dipole (e,e) instrument, even in the low energy loss (photon energy) range.

By extrapolating measured relative generalized oscillator strengths to zero momentum transfer, Lassetre *et al.* [13] obtained an integrated oscillator strength of 0.179 for the Schumann–Runge continuum region, over the range 6.56–9.46 eV, following correction of their previously published data [16,17]. By integrating the same energy region, the present work gives a slightly lower oscillator strength of 0.169. In the other electron impact based work using low impact energy, Huebner *et al.* [351] reported an integrated oscillator strength of 0.161 for the Schumann–Runge continuum.

In figure 9.2(b), the present measurements are compared with the theoretical work reported by Allison *et al.* [344] and Wang *et al.* [342]. Both sets of calculated data show reasonable agreement with the present work. However, it must be pointed out that Allison *et al.* [344] employed a semiempirical method in which the calculated potential curve and the transition moment were adjusted in order to reproduce oscillator strength values and structural features consistent with the experimental results [340]. The theoretical results of Wang *et al.* [342], on the other hand, were obtained by fitting to their own measurements of the

Schumann–Runge continuum region. They then reported potential curves and transition moments for the $B^3\Sigma_u^-$ and $E^3\Sigma_u^-$ mixed–Rydberg–valence states, and also the $1^3\Pi_u$ valence state, which were obtained from the fitting procedures. Thus, although the existing theoretical absolute oscillator strength values for the Schumann–Runge continuum region appear to show good agreement with the present work, it should be remembered that both of these theoretical results depend for their success on experimental values.

Figures 9.3(a) and (b) show expanded views of figure 9.1 in the energy regions 9.5–15 eV and 14–25 eV respectively. The ionization potentials for the states shown were obtained from the photoelectron work of Edqvist *et al.* [353]. The first ionization potential due to the ejection of an electron from the $1\pi_g$ orbital occurs at 12.071 eV. In figure 9.3(a) several diffuse bands are observed in the energy region from 9.7 eV to just below the first ionization potential. Due to the diffuse nature of the peaks compared with the relatively narrow bandwidth that can be obtained in optical experiments in this energy region, absolute oscillator strengths (photoabsorption cross sections) for these diffuse bands that have been measured using the Beer–Lambert photoabsorption method are expected to be reasonably accurate [334,336,340,348,349]. The three prominent peaks at 9.96, 10.28 and 10.57 eV, corresponding to the longest, second and third bands respectively, have been assigned [345,346] as transitions to the vibrational levels $v'=0, 1$ and 2 of the mixed valence–Rydberg $E^3\Sigma_u^-$ state. The absolute oscillator strengths for the diffuse bands in the energy region 9.7–12.07 eV were determined in the present work and the results are summarized in table 9.1 along with previously available experimental [340,349,351] and theoretical [345–

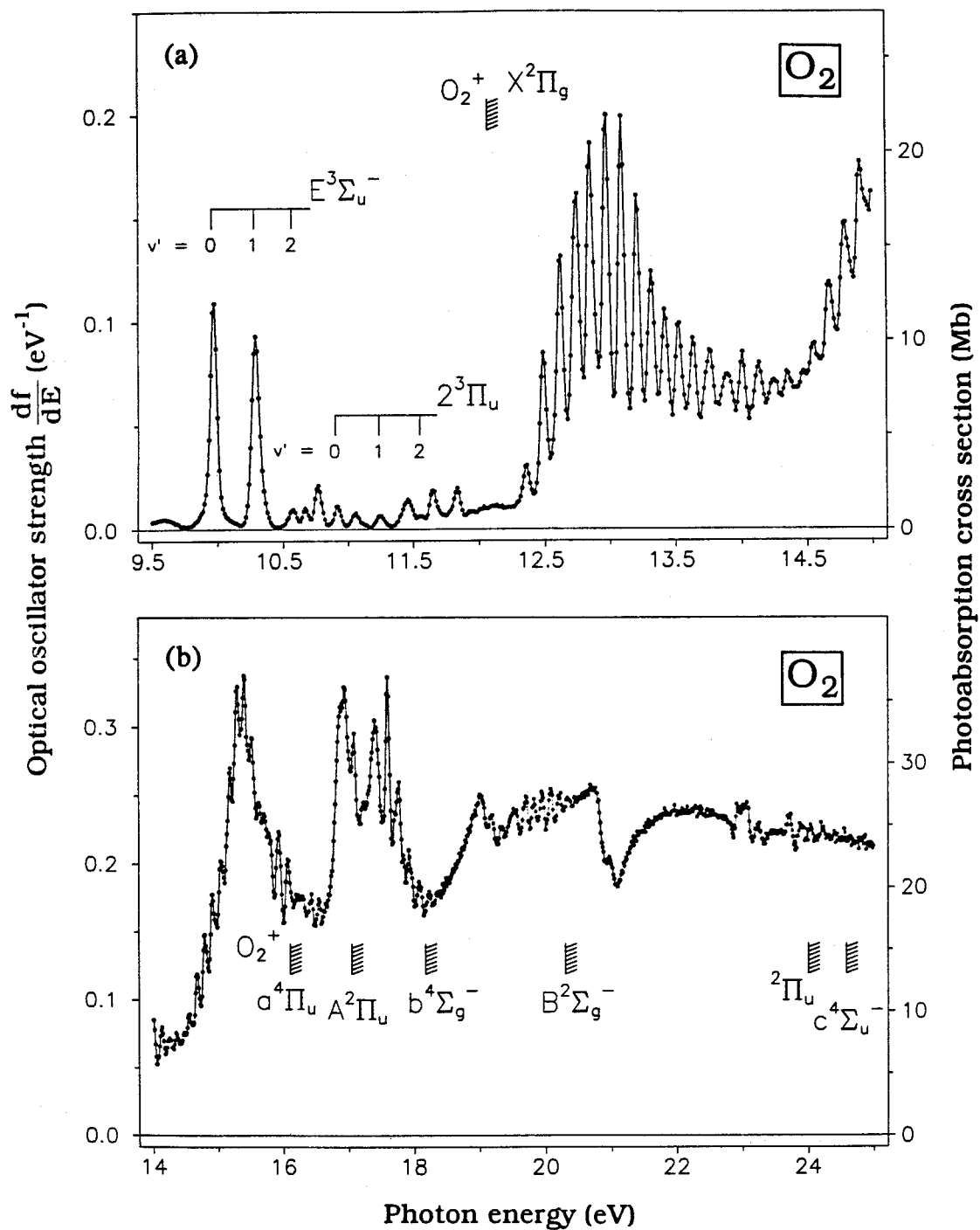


Figure 9.3: Absolute oscillator strengths for the photoabsorption of molecular oxygen. The ionization potentials have been obtained from ref. [353]. (a) in the energy region 9.5–15 eV. The assignments of the vibrational levels $v'=0, 1$ and 2 of the $E^3\Sigma_u^-$ and $2^3\Pi_u$ states are taken from the theoretical work of Buenker *et al.* [346]. (b) in the energy region 14–25 eV.

Table 9.1
Absolute optical oscillator strengths for the photoabsorption of molecular oxygen in the energy region
9.75–11.89 eV

Assignment*	Energy range (eV)	Absolute optical oscillator strengths						
		Experimental measurements			Theoretical calculations			
		Electron impact based methods		Beer-Lambert law				
		Present work	Huebner <i>et al.</i> [351]	Lewis <i>et al.</i> [349]	Ogawa and Ogawa [340]	Buenker <i>et al.</i> [346]	Yoshimine <i>et al.</i> [345]	Li <i>et al.</i> [347]
$E^3\Sigma_u^-$ $v'=0$	9.75 — 10.17	0.00844	0.001024		0.00833	0.0136	0.0103	0.01742
	10.17 — 10.44	0.00759	0.00804	0.00705#	0.00706	0.0157	0.0124	0.00562
	10.44 — 10.62	0.000827	0.00147	0.00078	0.000770	0.007	0.00412	0.00061
?	10.62 — 10.71	0.000652	0.000650		0.000660			
	10.71 — 10.84	0.00146	0.00242		0.00140			
$2^3\Pi_u$ $v'=0$	10.84 — 10.98	0.000814	0.000900		0.000820	0.0009		
	10.98 — 11.17	0.000733	0.00159		0.000752			
?	11.17 — 11.33	0.000606	0.00110		0.000497	0.0007		
	11.33 — 11.52	0.00147	0.00210					
$2^3\Pi_u$ $v'=1$	11.52 — 11.59	0.000419	0.000502					
	11.59 — 11.74	0.00169	0.00205					
?	11.74 — 11.89	0.00174	0.00163					
	11.89 — 12.07	0.00169	0.00283					

* The assignments were taken from ref. [346].

This value was obtained from the average of the integrated oscillator strengths for $O^{16}O^{18}$ and $^{18}O_2$ in the energy region 10.19–10.35 eV.

347] data. Column two in table 9.1 gives the energy regions over which integration was performed in order to obtain the absolute oscillator strength for each diffuse peak. The absolute oscillator strength values reported by Ogawa and Ogawa [340] were obtained by integrating their Beer-Lambert law photoabsorption data over the same energy regions. It can be seen from table 9.1 that the present results are consistent with the photoabsorption work of Ogawa and Ogawa [340], as expected (see above). The recent Beer-Lambert law photoabsorption work of Lewis *et al.* [349] for the second and third bands is also in good agreement with the present work and with that of Ogawa and Ogawa [340]. For the lowest ($E^3\Sigma_u^-(v=0)$) band, the data reported by Lewis *et al.* [348] are only for the energy region 9.95–9.98 eV compared with 9.75–10.17 eV for both the present work and that of Ogawa and Ogawa [340]. Hence the data of Lewis *et al.* [348] cannot be compared directly with the present work in this region. However, as demonstrated in the work of Lewis *et al.* [348], their absolute cross sections in the limited energy region 9.95–9.98 eV are in excellent agreement with the measurements of Ogawa and Ogawa [340] and thus also with the present work. The electron impact based oscillator strength data reported by Huebner *et al.* [351] are in general higher than the present results and the data of Ogawa and Ogawa [340]. It should be noted that the accuracy of the Bethe-Born factor used by Huebner *et al.* [351] was not known over a wide energy range. In addition they employed an impact energy of only 100 eV to measure the energy loss spectrum and this is too low an impact energy to obtain a dipole-only spectrum (i.e. the momentum transfer \mathbf{K} is too large). Several vibronic bands in the $X^3\Sigma_g^- \rightarrow \alpha^1\Sigma_u^+$ and $X^3\Sigma_g^- \rightarrow \beta^3\Sigma_u^+$ systems in the energy region 9.8–10.6 eV, which are dipole-forbidden transitions, were

observed even in direct photoabsorption measurements [331,349]. The intensities of these dipole-forbidden peaks would be expected to be significantly higher in the electron energy loss spectrum of Huebner *et al.* [351], which would cause higher oscillator strength values for those energy regions involving dipole-forbidden peaks. The present work, using an impact energy of 3000 eV and zero degree scattering angle, does not suffer from this problem.

Ab-initio configuration interaction theoretical methods have been used by three groups [345–347] to calculate the absolute oscillator strengths for the vibrational levels $v'=0, 1$ and 2 of the mixed-valence Rydberg $E^3\Sigma_u^-$ state. The theoretical calculations reported by Yoshimine *et al.* [345] and Buenker *et al.* [346], which assigned the longest, second and third bands as the vibrational levels $v'=0, 1$ and 2 of the mixed valence–Rydberg $E^3\Sigma_u^-$ state from the calculated energy levels, give oscillator strength values for these three bands which are much higher than the present and other experimental values. The recent work of Li *et al.* [347] shows better agreement with the present results for the $v'=1$ and 2 bands while the value reported by Li *et al.* [347] for $v'=0$ is even higher than that reported by Yoshimine *et al.* [345] and Buenker *et al.* [346]. Buenker *et al.* [346] also assigned three other peaks at energies of 10.90, 11.24 and 11.55 eV as the vibronic bands $v'=0, 1$ and 2 of the mixed valence–Rydberg $2^3\Pi_u$ state. The calculated [346] oscillator strengths for these three peaks are only slightly higher than the present results as seen in table 9.1. The electron impact data reported by Lassetre *et al.* [13] give an oscillator strength of 0.020 for the energy region 9.46–10.7 eV while the present estimate for the same energy range is 0.0185. The total oscillator strength sum up to the first

ionization potential (12.07 eV) was determined to be 0.198 in the present work, which is exactly the same value as was reported by Huebner *et al.* [351]. However, it should be remembered that the oscillator strength sum below 9.46 eV reported by Huebner *et al.* [351] is slightly lower than that in the present work, while in the energy region 9.46–12.07 eV their reported value is slightly higher.

In the energy region 12–17 eV most of the bands in the photoabsorption spectrum of oxygen have not been classified, while from 17–25 eV there are many Rydberg series converging on the various ionization limits shown on figure 9.3(b). The energy positions and the assignments of these Rydberg states can be found in the critical compilation published by Krupenie [331]. Table 9.2 shows the present integrated oscillator strength values over selected energy intervals in the energy region 12.07–18.29 eV. The electron impact study by Huebner *et al.* [351] (which like the present work is free of "line-saturation" effects) also reported integrated absolute oscillator strength values in the energy region 12.10–14.04 eV. These values [351], also shown in table 9.2, are in general somewhat higher than the present results. The absolute oscillator strength sum in the energy region 12.10–14.04 eV was estimated to be 0.181 by Huebner *et al.* [351], while the present result for the same energy region is 0.151. The value reported by Huebner *et al.* [351] is ~20% higher than the present result which is consistent with the generally higher values reported by Huebner *et al.* [351] from 9.75–11.89 eV as seen in table 9.1. In the review paper of Hudson [46], it was pointed out that much of the Beer-Lambert photoabsorption cross section data for oxygen [354–356] in the energy region 12.10–20.66 eV is subject to bandwidth errors (or "line-saturation" effects) and also

Table 9.2

Integrated absolute optical oscillator strengths for the photoabsorption of molecular oxygen over intervals in the energy region 12.07–18.29 eV

Energy range (eV)	Integrated absolute optical oscillator strengths	
	Present work	Huebner <i>et al.</i> [351]
12.070 — 12.240	0.00176	0.00182
12.240 — 12.412	0.00325	0.00379
12.412 — 12.538	0.00611	0.00725
12.538 — 12.673	0.0106	0.01176
12.673 — 12.794	0.0134	0.01483
12.794 — 12.915	0.0149	0.01724
12.915 — 13.026	0.0147	0.01641
13.026 — 13.152	0.0147	0.01567
13.152 — 13.263	0.0117	0.01390
13.263 — 13.369	0.00999	0.01186
13.369 — 13.476	0.00861	0.00987
13.476 — 13.577	0.00793	0.01033
13.577 — 13.684	0.00775	0.00952
13.684 — 13.814	0.00925	0.01166
13.814 — 13.954	0.00941	0.01424
13.954 — 14.056	0.00701	0.01027
14.056 — 14.181	0.00852	
14.181 — 14.302	0.00812	

Table 9.2 (continued)

Energy range (eV)	Integrated absolute optical oscillator strengths	
	Present work	Huebner <i>et al.</i> [351]
14.302 — 14.408	0.00736	
14.408 — 14.488	0.00573	
14.488 — 14.603	0.00948	
14.603 — 14.728	0.0127	
14.728 — 14.853	0.0160	
14.853 — 14.978	0.0195	
14.978 — 15.092	0.0214	
15.092 — 15.217	0.0294	
15.217 — 15.332	0.0340	
15.332 — 15.472	0.0427	
15.472 — 15.587	0.0310	
15.587 — 15.862	0.0614	
15.862 — 16.006	0.0282	
16.006 — 16.151	0.0266	
16.151 — 16.351	0.0345	
16.351 — 16.481	0.0216	
16.481 — 16.581	0.0164	
16.581 — 17.171	0.147	
17.171 — 17.514	0.0897	
17.514 — 17.875	0.0882	
17.875 — 18.287	0.0740	

systematic errors. Based on the photoabsorption data reported by Matsunaga and Watanabe [356], the absolute integrated oscillator strength in the energy region 12.07–16.53 eV was estimated to be 0.724 by Berkowitz [143]. However, we find that a reanalysis of the data of Matsunaga and Watanabe [356] gives an integrated absolute oscillator strength value of 0.587. This value we have obtained by digitizing figures 1 and 2 of ref. [356]. Alternatively we have obtained a value of 0.685 from the reported [356] numerical oscillator strength values in table 1 of ref. [356]. The difference occurs since the tabulated numerical values reported in the paper of Matsunaga and Watanabe [356] only include one third of their actual experimental data. Thus, insufficient data are given to obtain an accurate integration of the spectral area. Therefore, it would seem that Berkowitz [143] made use of the limited tabulated numerical values reported by Matsunaga and Watanabe [356] in order to obtain the integrated oscillator strength in the energy region 12.07–16.53 eV. The present dipole (e,e) work for the same region gives an integrated oscillator strength of 0.578, which agrees well with the presently revised value of 0.587 obtained by digitizing the data in figures 1 and 2 reported by Matsunaga and Watanabe [356]. Digitizing the figures of other photoabsorption work reported by Huffman *et al.* [354] for the energy region 12.07–16.53 eV, an integrated oscillator strength of 0.685 was obtained, which is ~20% higher than the value determined in the present work. This is again consistent with the work of Matsunaga and Watanabe [356], in which they state that the data of Huffman *et al.* [354] were 20–30% higher than their measured values in this energy region.

9.3 Conclusions

Absolute optical oscillator strengths for molecular oxygen have been measured by high resolution dipole (e,e) spectroscopy in the energy region 5–30 eV, which are free of "line-saturation" (bandwidth) effects. Absolute optical oscillator strengths for the broad Schumann–Runge continuum region of oxygen determined in the present work are in excellent agreement with most previously reported experimental results. This gives considerable confidence in the accuracy of the previously determined Bethe–Born conversion factor for the high resolution dipole (e,e) spectrometer used in the present work, when extrapolated down to 7 eV. This in turn lends support to the accuracy of the absolute oscillator strengths previously reported for argon, krypton and xenon [39] (see chapter 6), hydrogen [40] (see chapter 7) and nitrogen [41] (see chapter 8) from this laboratory. The electron impact data reported by Huebner *et al.* [351] for oxygen are in general higher than the present work for the electronic transitions higher in energy than the Schumann–Runge continuum. This may be due to appreciable contributions from dipole forbidden transitions due to the low impact energy of 100 eV, or alternatively to inaccuracies in the Bethe–Born conversion factor employed by Huebner *et al.* [351].

For the diffuse discrete bands in the oxygen spectrum in the 9.7–12.071 eV energy region, the presently determined absolute oscillator strengths are in good agreement with the photoabsorption measurements of Ogawa and Ogawa [340]. The present work is also in good agreement with the integrated oscillator strength value reported by Matsunaga and Watanabe [356] in the energy region 12.07–16.53 eV. "Line-saturation"

effects which have caused severe difficulties in some of the direct Beer-Lambert law photoabsorption measurements in the valence discrete excitation regions of the electronic spectra of hydrogen [40] (see chapter 7) and nitrogen [41] (see chapter 8) are not found for the transitions studied in the present work in molecular oxygen. This is probably due to the generally broader nature of the transition peaks in the oxygen spectrum, in contrast to the situation for hydrogen and nitrogen (see chapters 7 and 8). Such broadening is to be expected in oxygen above 12.07 eV (the first ionization potential) due to the short lifetimes of the rapidly autoionizing excited states associated with the higher ionization limits.

Chapter 10

Absolute Optical Oscillator Strengths for the Discrete and Continuum Photoabsorption of Carbon Monoxide (7–200 eV) and Transition Moments for the $X^1\Sigma^+ \rightarrow A^1\Pi$ System

10.1 Introduction

Carbon monoxide is of great importance in astrophysics since it is the second most abundant interstellar molecule after hydrogen. It has been detected in interstellar clouds and also in comets and planetary atmospheres. Quantitative spectroscopic data such as the absolute oscillator strengths (cross sections) for the photoabsorption and photodissociation of carbon monoxide provide valuable information for the understanding of the formation and properties of interstellar matter [357,358]. Since molecular hydrogen cannot be observed directly in dense opaque regions such as in our galaxy, carbon monoxide has been utilized as a tracer of molecular hydrogen [357,358]. Absolute optical oscillator strengths for the photoabsorption of carbon monoxide in the valence discrete region can also be used to determine molecular abundances in planetary and stellar atmospheres [232]. In electron impact experiments, the excitation cross section at sufficiently high impact energy is related to the optical oscillator strength. Therefore, the latter quantities can be used to normalize relative experimental electron impact excitation cross sections [359]. Moreover, the absolute electron impact excitation cross sections can be used in combination with the emission cross sections to determine the predissociation yields for

carbon monoxide, which are useful quantities in constructing photochemical models of molecular clouds [360]. However, the existing absolute optical oscillator strength (cross section) data for the photoabsorption of carbon monoxide in the valence discrete region show large differences in the magnitudes of the absolute oscillator strengths between the various experimental and theoretical values. In contrast, there is generally better agreement between the various available measurements in the higher energy smooth continuum regions [30].

Absolute optical oscillator strengths for the valence shell discrete transitions of carbon monoxide have been calculated by several groups. Absolute optical oscillator strengths for the discrete transitions from the $X^1\Sigma^+$ ground state to the $A^1\Pi$, $C^1\Sigma^+$ and $B^1\Sigma^+$ excited states have been calculated by Rose *et al.* [301] and Coughran *et al.* [361], using an equation-of-motion (or random-phase approximation) method, by Wood [362], using a configuration interaction (CI) method and by Nielsen *et al.* [363] using the second order polarization propagator approach (SOPPA). In other work, Lynch *et al.* [364] have calculated the dipole moments and oscillator strengths for the low-lying valence states of carbon monoxide by applying the multiconfigurational random phase approximation (MCRPA). Padial *et al.* [365], have constructed pseudospectra of discrete transition frequencies and calculated the oscillator strengths for the discrete and continuum excitations from the occupied molecular orbitals by employing the Stieltjes-Tchebycheff (S-T) technique and separated-channel, static-exchange calculations. Ab initio CI calculations have been performed by Cooper and Langhoff [366], Kirby and Cooper [367] and Chantranupong *et al.* [368]. In particular, calculations of the absolute optical oscillator strengths for the transitions to the individual vibronic

levels of the $A^1\Pi$, $C^1\Sigma^+$ and $B^1\Sigma^+$ excited states have been reported by Kirby and Cooper [367] and Chantranupong *et al.* [368] while Cooper and Langhoff [366] have calculated the theoretical radiative lifetimes for those same vibronic states.

A large number of experimental photoabsorption studies of carbon monoxide have been made and critical reviews and compilations of the available spectroscopic data can be found in refs. [30,46,369–371]. Photoabsorption methods [372–392] have been commonly employed and quantitative measurements based on the Beer–Lambert law [376,379,380,385–388,391,392] have provided much of the existing absolute optical oscillator strength data. However, as pointed out earlier by Hudson [46] and discussed in further detail recently by Chan *et al.* [37,41] (see chapter 2) the Beer–Lambert law is only strictly valid in the hypothetical situation of infinite experimental energy resolution (i.e. zero bandwidth). Thus in practice Beer–Lambert law photoabsorption data for discrete transitions will be subject to so-called "line-saturation" effects (i.e. bandwidth–linewidth interactions) which lead to errors in the derived oscillator strengths. These arise from the logarithmic transform involved in Beer–Lambert law photoabsorption methods and the resonant nature of photon induced excitation. Since the peaks in the vibronic spectra for production of the $A^1\Pi$, $B^1\Sigma^+$ and $C^1\Sigma^+$ excited states of carbon monoxide have extremely narrow natural linewidths, the absolute oscillator strengths measured for these bands using Beer–Lambert law photoabsorption techniques may be expected to exhibit severe "line-saturation" effects. For instance, the oscillator strengths for the vibrational bands of the $A^1\Pi$ excited state measured by Lee and Guest [387] using the Beer–Lambert law are found to be an order of magnitude

higher than those reported by Myer and Samson [385] which were measured at a lower resolution. While Lee and Guest [387] correctly stated that the cross sections at the peak maxima would be affected by the monochromator bandwidth, their claim that the integrated cross section over the molecular band (i.e. the integrated oscillator strength) would be independent of the bandwidth is incorrect. This is convincingly demonstrated in refs. [37,391], where it is shown that it is not only the peak maximum that is affected by the incident bandwidth, but also more importantly the integrated cross section for the transition, which will be smaller than the true value. These spurious effects are further illustrated by the fact that the photoabsorption oscillator strength value reported by Lee and Guest [387] for production of the $v'=0$ level of the $A^1\Pi$ state is found to be only ~50% of the value obtained by Lassetre and Skerbele [69] using an electron impact based method. In other more recent photoabsorption work, Eidelsberg *et al.* [392] and Letzelter *et al.* [388] have reported discrete oscillator strengths for carbon monoxide excitation in the VUV energy regions 8.00–9.92 eV and 10.78–14.01 eV respectively. In order to minimize the "line saturation" effects involved in using Beer–Lambert law photoabsorption, the integrated absorption was measured in these studies [388,392] as a function of pressure and the integrated cross section was determined at pressures low enough such that the integrated absorption varied linearly with pressure. These procedures used by Eidelsberg *et al.* [392] and Letzelter *et al.* [388] are similar to those involved in measuring the integrated cross section at several different pressures and extrapolating to low pressure in an attempt to obtain the true integrated cross section. However, these kinds of procedures put the most weight on the least accurate data

determined at the lowest sample pressures [37,46] and as a result the integrated cross sections measured by Eidelsberg *et al.* [392] and by Letzelter *et al.* [388] are most likely still subject to errors as was found in the case of nitrogen [37,41] (see chapter 8). Oscillator strengths for the vibrational levels of the $A^1\Pi$ band have also been reported by Rich [393] using absorption measurements based on the shock tube technique and curves of growth analyses.

Lifetime measurements [202,251,394–408] have been extensively employed for studying the valence shell discrete transitions of carbon monoxide. However, large discrepancies exist between the various reported experimental values. The lifetimes for the vibronic levels of the $A^1\Pi$ state have been measured by several groups [251,398–400,406,407]. It has been found [407] that the decay rates for some of the vibronic levels of the $A^1\Pi$ state are affected by perturbations from the nearby $a^3\Sigma^+$, $e^3\Sigma^-$, $d^3\Delta$, $I^1\Sigma^-$ and $D^1\Delta$ states. These kinds of perturbations cause the measured lifetimes to differ by up to 20% from the true values. Field *et al.* [407] have derived deperturbed lifetimes for the vibronic levels of the $A^1\Pi$ state and reported a linear dipole moment function from their data. This function was used by Kirby and Cooper [367] to calculate the absolute oscillator strengths for photoabsorption from the ground state to the vibronic bands of the $A^1\Pi$ state. Furthermore, in order to convert the lifetimes of the vibronic levels of the $B^1\Sigma^+$ and $C^1\Sigma^+$ bands to oscillator strengths, it is necessary to know the branching ratios for the two systems (B–X, B–A) and (C–X, C–A).

Electron impact methods based on electron energy loss spectroscopy have also been applied to study the oscillator strengths for the valence shell discrete [69,107,409] and continuum [87] transitions of

carbon monoxide. As pointed out in chapter 2, electron impact excitation is non-resonant even for discrete transitions, and because no logarithmic transform is needed to obtain the cross section (in contrast to Beer-Lambert photoabsorption) no "line saturation" (i.e bandwidth) errors can occur. Lassetre and Skerbele [69] have measured generalized oscillator strengths (GOS) for selected discrete transitions of carbon monoxide as a function of momentum transfer using electron energy loss spectroscopy and varying the scattering angle. Absolute optical oscillator strengths for the four discrete electronic transitions of carbon monoxide were reported [69] by extrapolating a series of GOS measurements for each transition to zero momentum transfer and normalizing their relative data on the absolute elastic electron cross sections measured by Bromberg [410]. Wight *et al.* [87], using a 8 keV energy incident electron beam and zero-degree mean scattering angle in a low resolution dipole (e,e) experiment, have determined the photoabsorption oscillator strengths of carbon monoxide in the energy region 7–70 eV. However, the data reported by Wight *et al.* [87] were made absolute by normalization to previously published absolute photoionization data reported by Samson and Cairns [325] in the smooth continuum region at 30 eV. Furthermore, since the resolution of the spectrum recorded by Wight *et al.* [87] was only 0.5 eV FWHM, oscillator strengths for the individual vibronic transitions could not be determined in the discrete region of the spectrum. In addition, it appears, from recent investigations using the same apparatus, that Wight *et al.* [87] did not make adequate corrections for background gases and non-spectral electrons in their measurements.

In the present work, the high resolution dipole (e,e) method as recently used to measure absolute photoabsorption oscillator strengths for the discrete transitions of the noble gas atoms [37–39] (see chapters 4–6) and several small molecules [27,40–42,411] (see chapters 7–9), is now applied to quantitatively study of the valence shell discrete transitions of carbon monoxide. In addition, new wide ranging (7–200 eV) measurements of the photoabsorption absolute oscillator strengths for carbon monoxide have been made using low resolution dipole (e,e) spectroscopy. The absolute scale of the present measurements is established independently of any other measurements by using TRK sum-rule considerations [30]. The accuracy of the high resolution and low resolution dipole (e,e) methods has been confirmed by studies comparing measurements with "benchmark" theoretical calculations for helium [37] (see chapter 4) and molecular hydrogen [40] (see chapter 7). In addition, results for molecular oxygen [42] (see chapter 9) and nitrogen [41] (see chapter 8) have supported the accuracy of the energy dependent Bethe–Born conversion factor for the high resolution dipole (e,e) spectrometer when extrapolated down to lower equivalent photon energies than were used for its original determination using measurements for helium [37] and neon [38].

10.2 Results and Discussion

The electronic transitions and photoabsorption oscillator strengths of carbon monoxide are conveniently discussed with reference to its ground state molecular–orbital valence shell independent particle configuration which may be written as

$$(3\sigma)^2(4\sigma)^2(1\pi)^4(5\sigma)^2$$

10.2.1 Low Resolution Absolute Photoabsorption Oscillator Strength Measurements for Carbon Monoxide (7–200 eV)

A relative oscillator strength spectrum was obtained by Bethe–Born conversion of the electron energy loss spectrum measured with the low resolution (~ 1 eV FWHM) dipole (e,e) spectrometer in the energy region 7–200 eV. The data were least-squares fitted to the function AE^{-B} over the energy region 90–200 eV. The fit gave $B=2.243$ and on this basis the fraction of the valence-shell oscillator strength above 200 eV was estimated to be 6.7%. The total area was then TRK sum-rule normalized to a value of 10.3, which includes the total number of valence electrons (10) plus a small estimated correction (0.3) for the Pauli-excluded transitions from the K shells to the already occupied valence shell orbitals [52,53]. Figures 10.1(a) and 10.1(b) show the resulting absolute optical oscillator strengths for carbon monoxide obtained in the present work at low resolution in the energy regions 5–50 and 50–200 eV respectively. Previously reported experimental data [87,292,325,328,329,412] are also shown for comparison. Numerical values of the presently determined absolute photoabsorption oscillator strengths for carbon monoxide obtained in the present work from 7–200 eV are summarized in table 10.1.

It can be seen in figures 10.1(a) and 10.1(b) that the present results are in extremely good agreement with the photoabsorption data reported by Samson and Haddad [292]. The data reported by Lee *et al.*

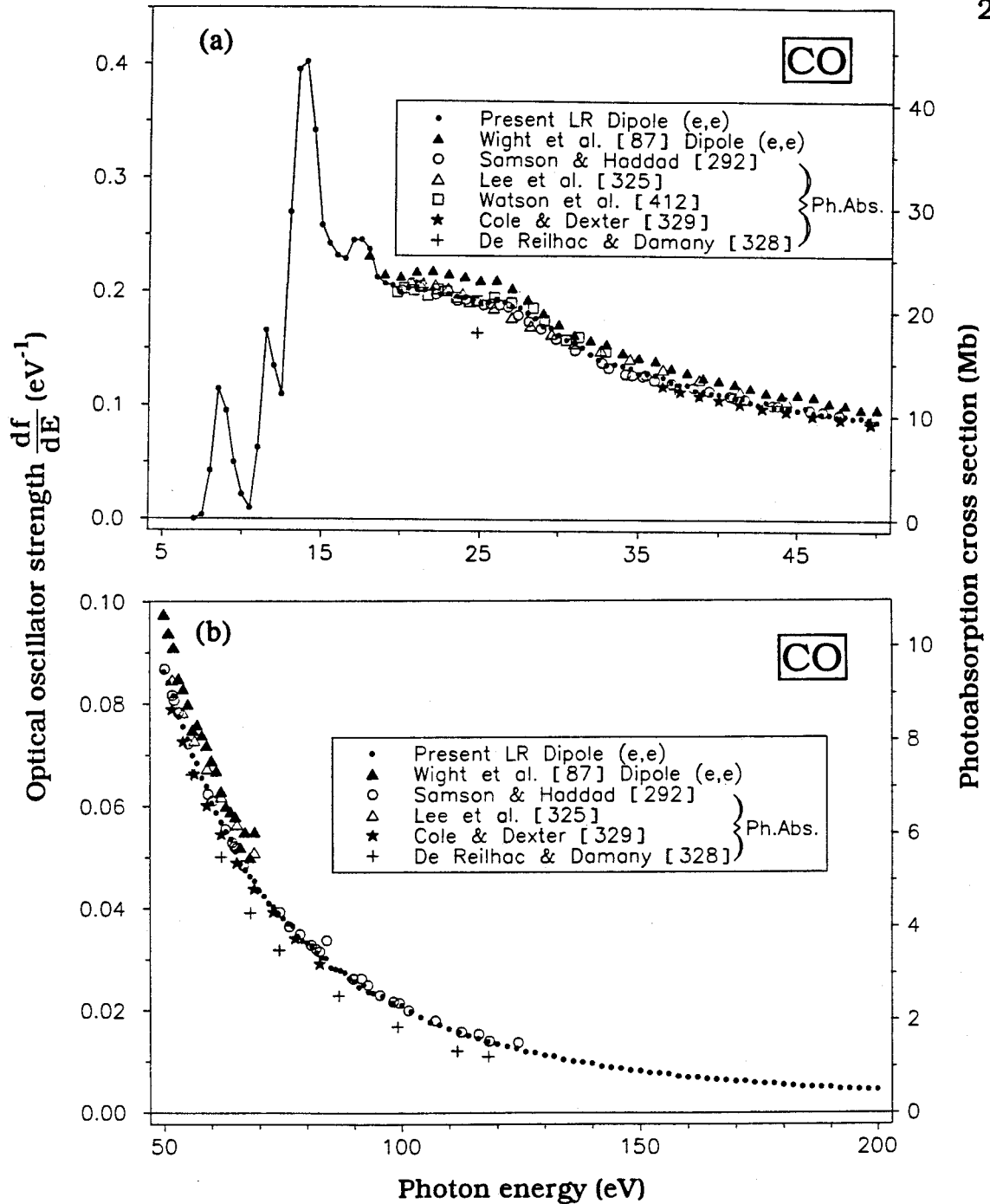


Figure 10.1: Absolute oscillator strengths for the photoabsorption of carbon monoxide measured using the low resolution (FWHM=1 eV) dipole (e,e) spectrometer (a) comparison with previously reported experimental data [87,292,325,328,329,412] in the energy region 5–50 eV. (b) comparison with previously reported experimental data [87,292,325,328,329] in the energy region 50–200 eV.

Table 10.1

Absolute differential optical oscillator strengths for the photoabsorption of carbon monoxide obtained using the low resolution (1 eV FWHM) dipole (e,e) spectrometer (7–200 eV)

Energy (eV)	Oscillator Strength (10^{-2}eV^{-1})	Energy (eV)	Oscillator Strength (10^{-2}eV^{-1})	Energy (eV)	Oscillator Strength (10^{-2}eV^{-1})
7.0	0.00	16.0	23.15	25.0	19.03
7.5	0.35	16.5	22.87	25.5	19.07
8.0	4.24	17.0	24.47	26.0	19.36
8.5	11.40	17.5	24.53	26.5	19.10
9.0	9.48	18.0	23.72	27.0	18.72
9.5	4.98	18.5	21.25	27.5	18.60
10.0	2.14	19.0	20.72	28.0	18.12
10.5	0.97	19.5	20.55	28.5	17.67
11.0	6.25	20.0	19.97	29.0	16.97
11.5	16.57	20.5	20.30	29.5	16.80
12.0	13.43	21.0	20.18	30.0	16.20
12.5	10.95	21.5	20.15	30.5	15.76
13.0	26.97	22.0	20.22	31.0	15.48
13.5	39.50	22.5	19.75	31.5	15.09
14.0	40.19	23.0	19.80	32.0	14.50
14.5	34.16	23.5	19.59	32.5	14.03
15.0	25.82	24.0	19.48	33.0	13.55
15.5	24.20	24.5	19.23	33.5	13.61

Table 10.1 (continued)

Energy (eV)	Oscillator Strength (10^{-2}eV^{-1})	Energy (eV)	Oscillator Strength (10^{-2}eV^{-1})	Energy (eV)	Oscillator Strength (10^{-2}eV^{-1})
34.0	13.45	45.0	9.62	62.0	5.69
34.5	13.28	45.5	9.82	63.0	5.51
35.0	12.80	46.0	9.39	64.0	5.36
35.5	12.80	46.5	9.31	65.0	5.12
36.0	12.66	47.0	9.24	66.0	4.87
36.5	12.47	47.5	9.01	67.0	4.76
37.0	12.03	48.0	9.13	68.0	4.63
37.5	11.84	48.5	8.94	69.0	4.54
38.0	11.81	49.0	9.01	70.0	4.35
38.5	11.33	49.5	8.84	71.0	4.25
39.0	11.26	50.0	8.63	72.0	4.10
39.5	11.05	51.0	8.42	73.0	4.03
40.0	11.01	52.0	8.17	74.0	3.90
40.5	10.91	53.0	7.75	75.0	3.81
41.0	10.69	54.0	7.56	76.0	3.71
41.5	10.64	55.0	7.32	77.0	3.66
42.0	10.31	56.0	7.00	78.0	3.46
42.5	10.11	57.0	6.85	79.0	3.37
43.0	10.33	58.0	6.56	80.0	3.34
43.5	9.88	59.0	6.40	81.0	3.27
44.0	9.83	60.0	6.07	82.0	3.13
44.5	9.88	61.0	5.88	83.0	3.05

Table 10.1 (continued)

Energy (eV)	Oscillator Strength (10 ⁻² eV ⁻¹)	Energy (eV)	Oscillator Strength (10 ⁻² eV ⁻¹)	Energy (eV)	Oscillator Strength (10 ⁻² eV ⁻¹)
84.0	3.03	118.0	1.40	162.0	0.697
85.0	2.85	120.0	1.35	164.0	0.667
86.0	2.82	122.0	1.30	166.0	0.658
87.0	2.79	124.0	1.26	168.0	0.642
88.0	2.75	126.0	1.20	170.0	0.617
89.0	2.63	128.0	1.18	172.0	0.625
90.0	2.58	130.0	1.12	174.0	0.588
91.0	2.46	132.0	1.10	176.0	0.582
92.0	2.51	134.0	1.05	178.0	0.576
93.0	2.37	136.0	1.01	180.0	0.546
94.0	2.35	138.0	0.991	182.0	0.535
96.0	2.28	140.0	0.969	184.0	0.515
98.0	2.15	142.0	0.909	186.0	0.509
100.0	2.10	144.0	0.887	188.0	0.507
102.0	1.98	146.0	0.868	190.0	0.502
104.0	1.88	148.0	0.834	192.0	0.471
106.0	1.77	150.0	0.820	194.0	0.473
108.0	1.72	152.0	0.787	196.0	0.467
110.0	1.65	154.0	0.781	198.0	0.451
112.0	1.58	156.0	0.768	200.0	0.461
114.0	1.51	158.0	0.716		
116.0	1.46	160.0	0.702		

$$\sigma \text{ (Mb)} = 1.0975 \times 10^2 \frac{df}{dE} \text{ eV}^{-1}$$

[325] are higher than the present data at energies above 30 eV while the data reported by De Reilhac [328] are ~15% lower than the present results at 25 eV and also at energies above 60 eV. The data reported by Cole and Dexter [329] are in general slightly lower than the present work. The earlier electron impact based dipole (e,e) data reported by Wight *et al.* [87] are ~10% higher than the present work. It should be pointed out that the data of Wight *et al.* [87] were normalized in the smooth continuum at 30 eV on the earlier optical data of Samson and Cairns [325] and in addition it appears that adequate background subtraction procedures were not employed. The present work is TRK sum-rule normalized and thus independent of any other measurements. The present low resolution data has been used to establish the absolute scale for the high resolution data as described in the following section.

10.2.2 High Resolution Absolute Photoabsorption Oscillator Strength Measurements for Carbon Monoxide (12–22 eV)

Figure 10.2 shows the absolute optical oscillator strength spectrum for the photoabsorption of carbon monoxide in the energy region 7–21 eV obtained from the high resolution (0.048 eV FWHM) dipole (e,e) spectrometer. The presently determined low resolution dipole (e,e) data and the photoabsorption data of Samson and Haddad [292] are also shown for comparison. It can be seen in figure 10.2 that the present high resolution (HR) and low resolution (LR) data are in excellent agreement over the continuum energy region. Similarly, in the discrete region the HR and LR measurements are consistent when the large differences in energy resolution (0.048 eV vs 1 eV FWHM) are taken into account. The

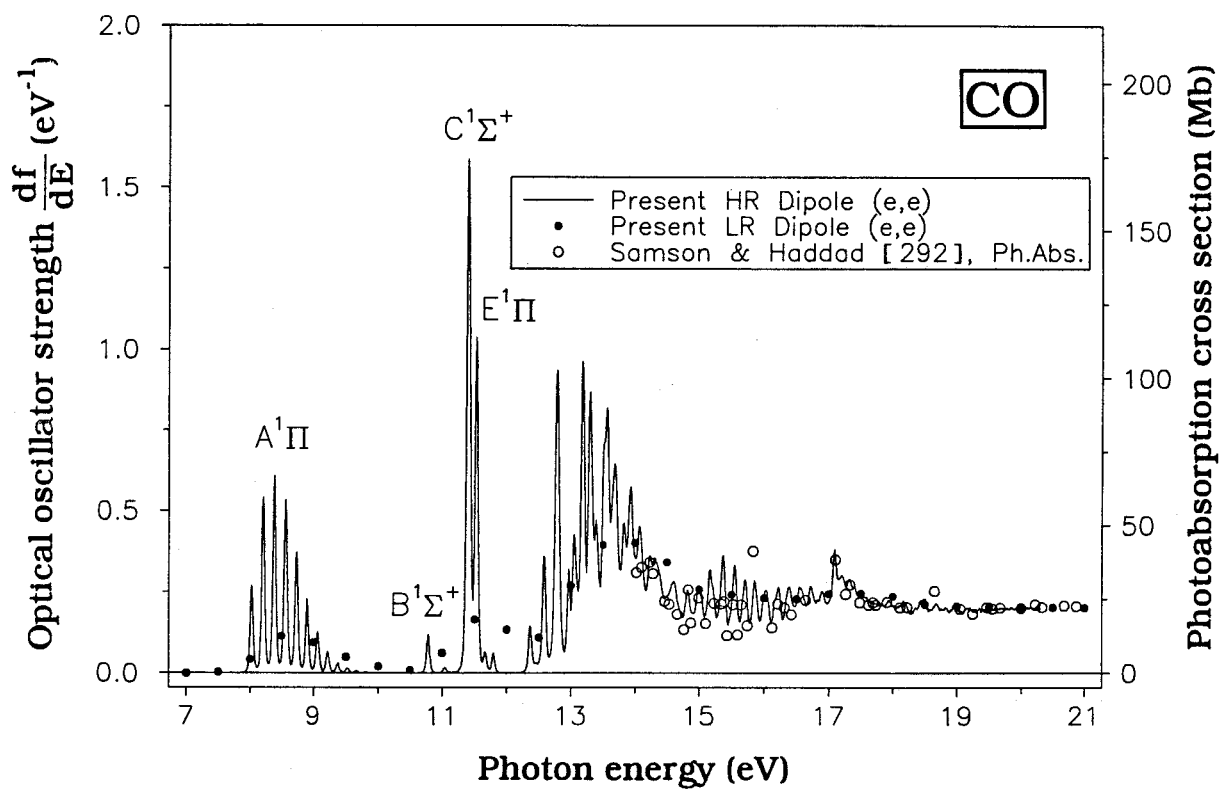


Figure 10.2: Absolute oscillator strengths for the photoabsorption of carbon monoxide in the energy region 7-21 eV measured using the high resolution dipole (e,e) spectrometer (FWHM=0.048 eV).

present HR data in the continuum 17–21 eV are also in good quantitative agreement with the photoabsorption data of Samson and Haddad [292].

Figure 10.3 shows the absolute optical oscillator strength spectrum for the vibronic bands of the $A^1\Pi$ state of carbon monoxide in the energy region 7.5–10.5 eV. The energy positions have been taken from the detailed spectroscopic studies reported in refs. [369,370,378]. A curve-fitting program using Voigt profiles has been employed to deconvolute the spectrum and the resulting deconvoluted peaks are shown as the dashed lines in figure 10.3, while the total fit is shown as a solid line. In the present work, integration of each peak area gives directly the absolute optical oscillator strength for the corresponding vibronic transition. Absolute vibronic optical oscillator strengths for $v'=0-12$ of the $A^1\Pi$ state were thus obtained and the results are summarized in table 10.2. Previously reported experimental [69,251,387,392,393,407] and theoretical [367,368] values are also shown for comparison. The uncertainties of the present results are estimated to be ~5% for resolved peaks and ~10% for unresolved peaks due to additional errors in the deconvolution process. Lee and Guest [387] obtained spectra for all the vibronic bands of the $A^1\Pi$ state using Beer–Lambert law photoabsorption methods. However, only the numerical oscillator strength value for the $v'=0$ vibronic band was reported and that value is ~40% lower than the present result. The photoabsorption data reported by Lee and Guest [386] are still subject to "line saturation" effects even though the authors state that their results were independent of the monochromator bandwidth (see discussion in the introduction of the present chapter, and chapter 2 for a more detailed discussion of "line saturation" effects). Eidelsberg *et al.* [392] recently attempted to avoid "line saturation"

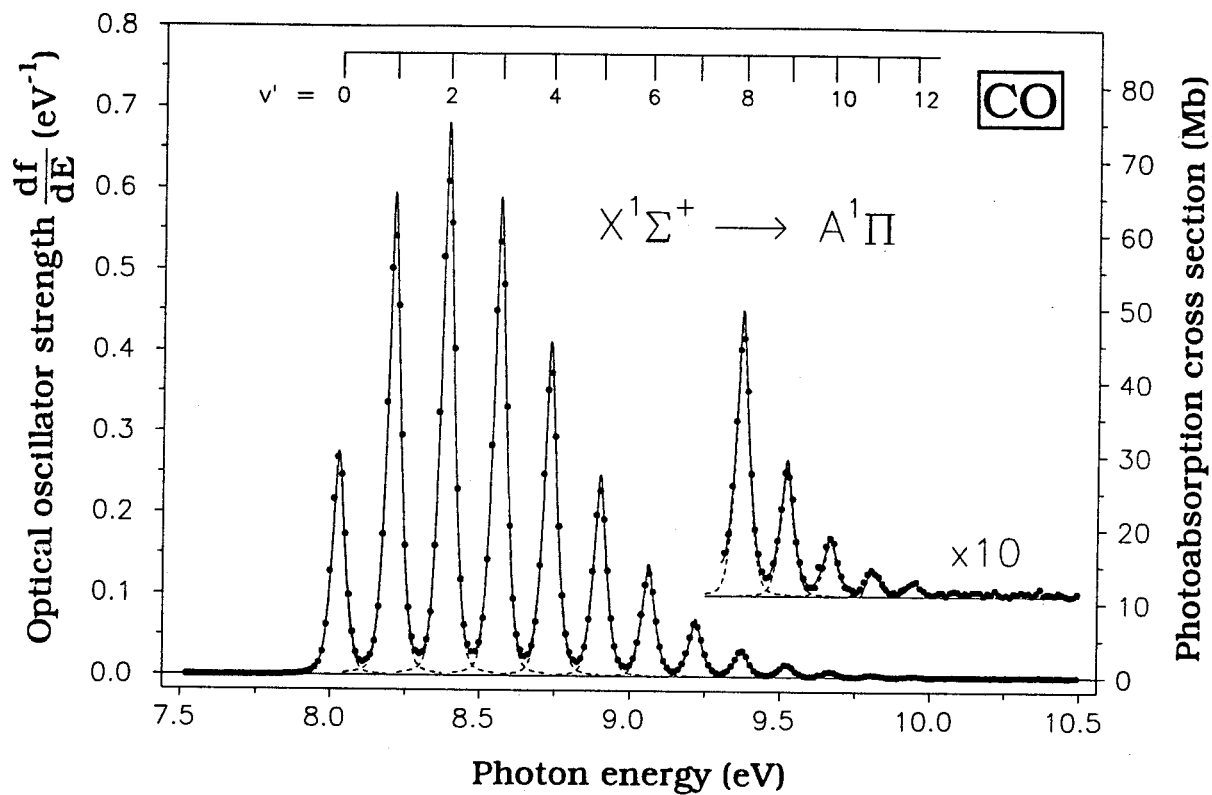


Figure 10.3: Absolute oscillator strengths for the photoabsorption of carbon monoxide in the energy region 7.5–10.5 eV at 0.048 eV FWHM. The energy positions are taken from references [369,370,378]. Deconvoluted peaks are shown as dashed lines and the solid line represents the total fit to the experimental data.

Table 10.2

Absolute optical oscillator strengths for the vibronic bands of the $X^1\Sigma^+ \rightarrow A^1\Pi$ transition of carbon monoxide

v	Experimental results						Theory		
	Electron impact based work		Photoabsorption (Beer-Lambert law)	Curves of growth	Lifetime measurements		(I)	(II)	
	Present HR dipole (e,e)	Lassette & Skerbele [69]	Eideisberg et al. [392]	Lee & Guest [387]	Rich [393]	Field et al. [407]*	Hesser [251]	Chantranupang et al. [368]	Kirby & Cooper [367]
0	0.0162	0.0200	0.0165	0.0096		0.0156	0.0111	0.0148	0.0155
1	0.0351	0.0380	0.0337		0.027	0.0343	0.0226	0.0356	0.0324
2	0.0402	0.0429	0.0424		0.033	0.0412	0.0162	0.0473	0.0373
3	0.0347	0.0360	0.0377			0.0361	0.0146	0.0462	0.0316
4	0.0242	0.0251	0.0258			0.0358	0.0074	0.0371	0.0220
5	0.0145	0.0155	0.0163			0.0161	0.0024	0.0262	0.0134
6	0.00805	0.00848	0.0104			0.0091		0.0168	0.0075
7	0.00414	0.00437	0.0059			0.0048		0.0010	0.0039
8	0.00202	0.00217	0.0029			0.0024			0.0019
9	0.00095	0.00108	0.0014			0.0011			0.0009
10	0.00041	0.00050	0.00065			0.0005			0.0004
11	0.00018	0.00025	0.00028						
12	0.00009	0.00010	0.00013						

* as derived by Kirby and Cooper [367] using the linear dipole moment reported by Field et al. [407].

effects by determining the integrated cross sections at pressures low enough that the integrated absorption varied linearly with pressure. The photoabsorption data reported by Eidelsberg *et al.* [392] are in much better agreement with the present work than other optical work [385,387]. The photoabsorption values reported by Rich [393] for the $v'=1$ and 2 levels of the $A^1\Pi$ state using a shock-tube experiment with a curves-of-growth analysis are ~25% lower than the present work. Two sets of vibronic oscillator strength values for the $A^1\Pi$ state obtained from lifetime measurements [251,407] have been reported. Hesser [251] converted lifetime data to optical oscillator strengths by using the measured vibrational band emission intensities. However, the so-obtained oscillator strength values are much smaller than the presently reported results. In other lifetime work, Field *et al.* [407] discussed the discrepancies between different lifetime measurements and determined the deperturbed lifetimes for the vibronic bands of the $A^1\Pi$ state. They also derived a linear dipole moment function from the deperturbed lifetimes. Kirby and Cooper [367] then used the linear dipole moment reported by Field *et al.* [407] to derive oscillator strengths for the $A^1\Pi$ state vibronic bands which are found to be in good agreement with the present work. The only previously reported electron impact based oscillator strength data for the $A^1\Pi$ bands of carbon monoxide are from Lassette and Skerbele [69], who measured generalized oscillator strengths as a function of momentum transfer and obtained optical oscillator strengths by extrapolating to zero momentum transfer. The absolute scale for these measurements [69] was obtained by normalizing on independent measurements of the absolute elastic scattering cross section [410]. The data reported by Lassette and Skerbele [69] are in

general ~5–10% higher than the present values and the differences can be largely attributed to the normalization procedures [69]. In theoretical work, two sets of oscillator strength calculations for the vibronic bands of the $A^1\Pi$ state have been recently published. The theoretical values reported by Kirby and Cooper [367] are ~5–10% lower than the present experimental values, while the theoretical results reported by Chantranupong *et al.* [368] show much greater discrepancies with the present work, in terms of both the absolute magnitudes of the oscillator strengths and also in the shape of the vibrational envelope of the band.

The absolute total oscillator strength for the $A^1\Pi$ state is obtained by summing the oscillator strengths for all the vibronic bands. Table 10.3 summarizes the present result, where it is compared with previously reported experimental [69,392,407] and theoretical [301,361–365,367,368] values. It can be seen that all the experimental [69,392,407] values, including that obtained in the present work, are in quite good agreement with each other, with values in the range 0.180 to 0.195. In contrast, the theoretical values [301,361–365,367,368] vary from 0.11 to 0.342. The theoretical value reported by Lynch *et al.* [364] is consistent with the present work while that of Kirby and Cooper is ~9% lower.

Figure 10.4 shows the presently measured absolute optical oscillator strength spectrum for photoabsorption to the vibrational levels of the $B^1\Sigma^+$, $C^1\Sigma^+$ and $E^1\Pi$ excited states of carbon monoxide in the energy region 10.5–12 eV. The assignments and energy positions have been taken from refs. [369,370,378]. The deconvoluted peaks resulting from a curve fit to the experimental data are shown as the dashed lines in figure 10.4, while the total fit is shown as the solid line. Table 10.4

Table 10.3

Absolute total optical oscillator strength for the $X^1\Sigma^+ \rightarrow A^1\Pi$ transition of carbon monoxide

	Absolute optical oscillator strength for the $A^1\Pi$ state
Theory:	
Chantranupong <i>et al.</i> [368]	0.2250
Kirby and Cooper [367]	0.1636
Lynch <i>et al.</i> [364]	0.18
Nielsen <i>et al.</i> [363]	0.1208
Padial <i>et al.</i> [365]	0.342
Wood [362]	0.24
Coughran <i>et al.</i> [361]	0.14
Rose <i>et al.</i> [301]	0.11
Experiment:	
Present work	0.1807
Eidelsberg <i>et al.</i> [392]	0.1941
Field <i>et al.</i> [407]	0.187
Lassette and Skerbele [69]	0.1945

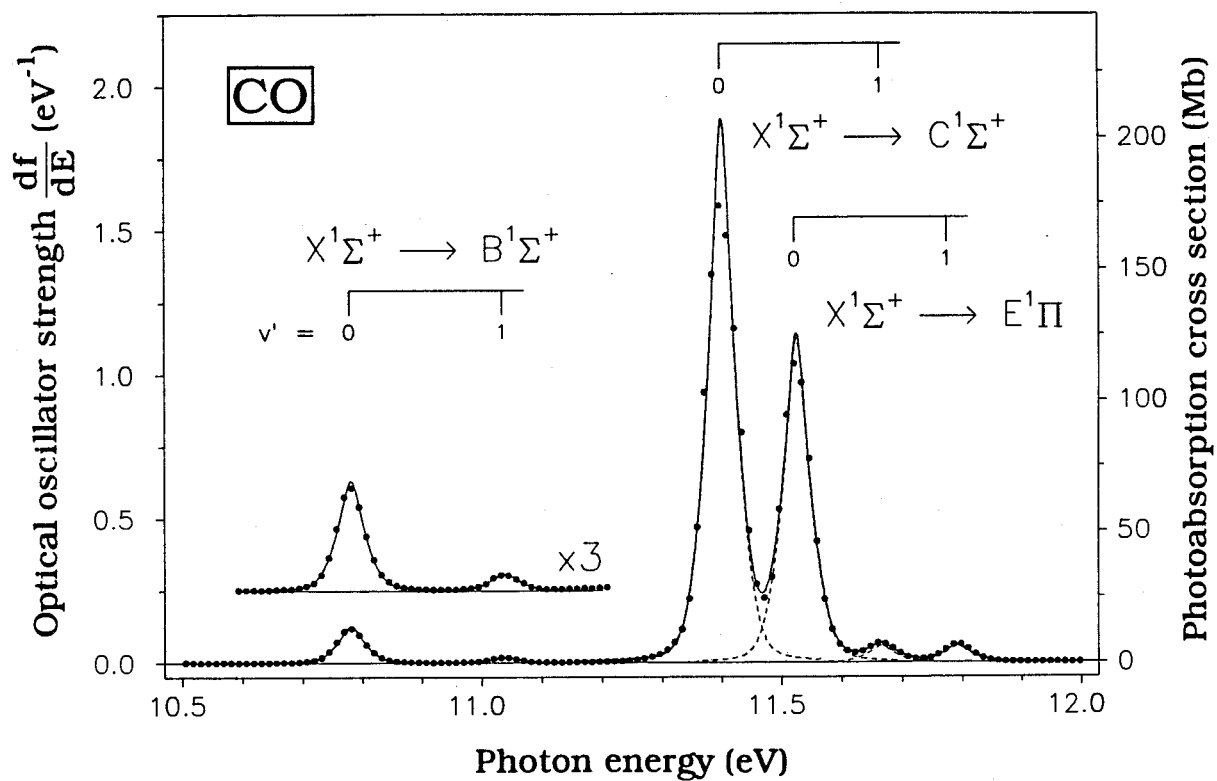


Figure 10.4: Absolute oscillator strengths for the photoabsorption of carbon monoxide in the energy region 10.5–12 eV at 0.048 eV FWHM. The assignments and energy positions are taken from references [369,370,378]. Deconvoluted peaks are shown as dashed lines and the solid line represents the total fit to the experimental data.

Table 10.4
Absolute optical oscillator strengths for the vibronic bands of the transitions from the $X^1\Sigma^+$ ground state to the $B^1\Sigma^+$, $C^1\Sigma^+$ and $E^1\Pi$ excited electronic states of carbon monoxide

	Absolute optical oscillator strength					
	$B^1\Sigma^+$		$C^1\Sigma^+$		$E^1\Pi$	
	$v'=0$	$v'=1$	$v'=0$	$v'=1$	$v'=0$	$v'=1$
Theory:						
Chantranupong <i>et al.</i> [368]	0.00508	0.00052	0.0647	0.0049	0.0274	0.00329
Kirby and Cooper [3674]	0.0021	0.0003	0.1181	0.0018	0.049	0.0050
Nielsen <i>et al.</i> [363]	0.00285		0.1327			
Padial <i>et al.</i> [365]	0.00448		0.0495			0.0110
Wood [362]	0.060		0.084			
Coughran <i>et al.</i> [361]	0.00300		0.0400			
Rose <i>et al.</i> [301]	0.00480		0.1200			
Experiment:						
Present work	0.00803	0.00132	0.1177	0.00356	0.0706	0.00353
Letzelter <i>et al.</i> [388]	0.0045	0.0007	0.0619	0.0028	0.0365	0.0025
Lee and Guest [387]	0.0024		0.0127		0.0181	
Lassette and Skebele [69]	0.0153		0.163		0.094	

summarizes the presently measured absolute optical oscillator strengths for the vibronic bands of the $B^1\Sigma^+$, $C^1\Sigma^+$ and $E^1\Pi$ excited states. where they are compared with previously reported experimental [69,387,388] and theoretical [301,361–363,365,367,368] values. Experimentally, there are many reported lifetime measurements [202,251,394–397,401–406,408] for the $B^1\Sigma^+$ and $C^1\Sigma^+$ states. Large variations have been found among the reported lifetime values. Moreover, in order to convert the lifetime data to absolute oscillator strengths, the branching ratios for the two systems (B–X, B–A) and (C–X, C–A) must be known. Carlson *et al.* [406], using the branching ratios measured by Aarts and De Heer [359], and Krishnakumar and Srivastava [408], using the branching ratios measured by Dotchin and Chupp [402], have converted their lifetime data to absolute oscillator strength values. However, the branching ratios reported by the two groups [359,402] differ significantly for the (B–X, B–A) system and are slightly different for the (C–X, C–A) system. Thus, different oscillator strength values will be obtained from the same set of lifetime data when using the different branching ratios. For example, from the lifetime data reported by Hesser [69], absolute oscillator strength values of 0.0054 and 0.119 were obtained respectively for the $v'=0$ band of the $B^1\Sigma^+$ and $C^1\Sigma^+$ states when using the branching ratios reported by Dotchin and Chupp [402] while values of 0.0079 and 0.1350 were obtained when using the branching ratios reported by Aarts and De Heer [359]. For this reason, the data obtained from the lifetime measurements are not shown in table 10.4. A summary of the lifetime measurements and also the converted oscillator strengths using various branching ratios can be found in refs. [406,408]. It can be seen from table 10.4 that, unlike the situation for the $A^1\Pi$ state, large variations

exist among the reported experimental oscillator strength values for the $B^1\Sigma^+$, $C^1\Sigma^+$ and $E^1\Pi$ states [69,387,388]. The photoabsorption data measured by Lee and Guest [387] are much lower (< 30%) than the present values, presumably due to serious "line saturation" effects as discussed above. The photoabsorption data of Letzelter *et al.* [388] are also ~25–50% lower than the present work. This difference is somewhat surprising since the experimental procedures employed by Letzelter *et al.* [388] are the same as those used by Eidelsberg *et al.* [392] for their measurements on the vibronic bands of the $A^1\Pi$ state which are found to be in good agreement with the present work (see table 10.2). In other experimental work, the electron impact based data of Lassette and Skerbele [69] are found to be much higher than the present results.

Turning to theory, absolute vibronic oscillator strengths for the $B^1\Sigma^+$, $C^1\Sigma^+$ and $E^1\Pi$ states have been calculated by several groups [301,361–363,365]. Since the vibrational oscillator strengths for $v'=2$ and the higher bands of these states have been calculated to be much smaller (< 1%) than the values for the $v'=0$ and 1 bands [367], the data reported in refs. [301,361–363,365] should be almost equal to the sum of the oscillator strengths for the $v'=0$ and 1 bands determined in the present experimental work. These values are shown in table 10.4. It can be seen that large differences exist between the various theoretical results [301,361–363,365,367,368], and that no single set of theoretical data is consistent with the present work. Only the oscillator strength for the $v'=0$ level of the $C^1\Sigma^+$ state reported by Kirby and Cooper [367], and the oscillator strength sum for the $C^1\Sigma^+$ state reported by Rose *et al.* [301], are in agreement with the present work.

The absolute optical oscillator strength spectrum determined in the present work for the higher energy excited states in the energy region 12–20 eV is shown in figure 10.5. The energy positions of the ionization thresholds have been taken from refs. [369,413]. Detailed assignments of this energy region can be found in refs. [358,386]. Integrated oscillator strengths determined from the present work over small energy ranges are summarised in table 10.5. The photoabsorption data reported by Stark *et al.* [391] and Letzelter *et al.* [388] were obtained at a much higher resolution than the present work. Therefore, the oscillator strengths for several transitions in references [388] and [391], corresponding to the energy ranges shown in table 10.5, have been summed and are compared with the present results. Also shown in table 10.5, the photoabsorption data of Stark *et al.* [391] were obtained *via* direct Beer–Lambert law photoabsorption measurements, using a resolution 20 times higher than in the work of Letzelter *et al.* [388], and an attempt was made to monitor the "line–saturation" effects by comparing the photoabsorption values measured at a variety of pressures. Even under such experimental conditions, "line–saturation" effects were reported for some very sharp features [391]. As shown in table 10.5, the two sets of photoabsorption data [388,391] are found to be somewhat lower than the present work even though precautions were taken to try to minimize "line–saturation" effects. The oscillator strength distribution of carbon monoxide has been reviewed by Berkowitz [143] using the experimental data available before 1980. Berkowitz obtained an oscillator strength value of 0.7921 for the energy region between 12 and 14 eV, using the photoabsorption data of Huffman *et al.* [380], while a value of 0.8165 was obtained using the photoabsorption data of Cook *et al.* [382].

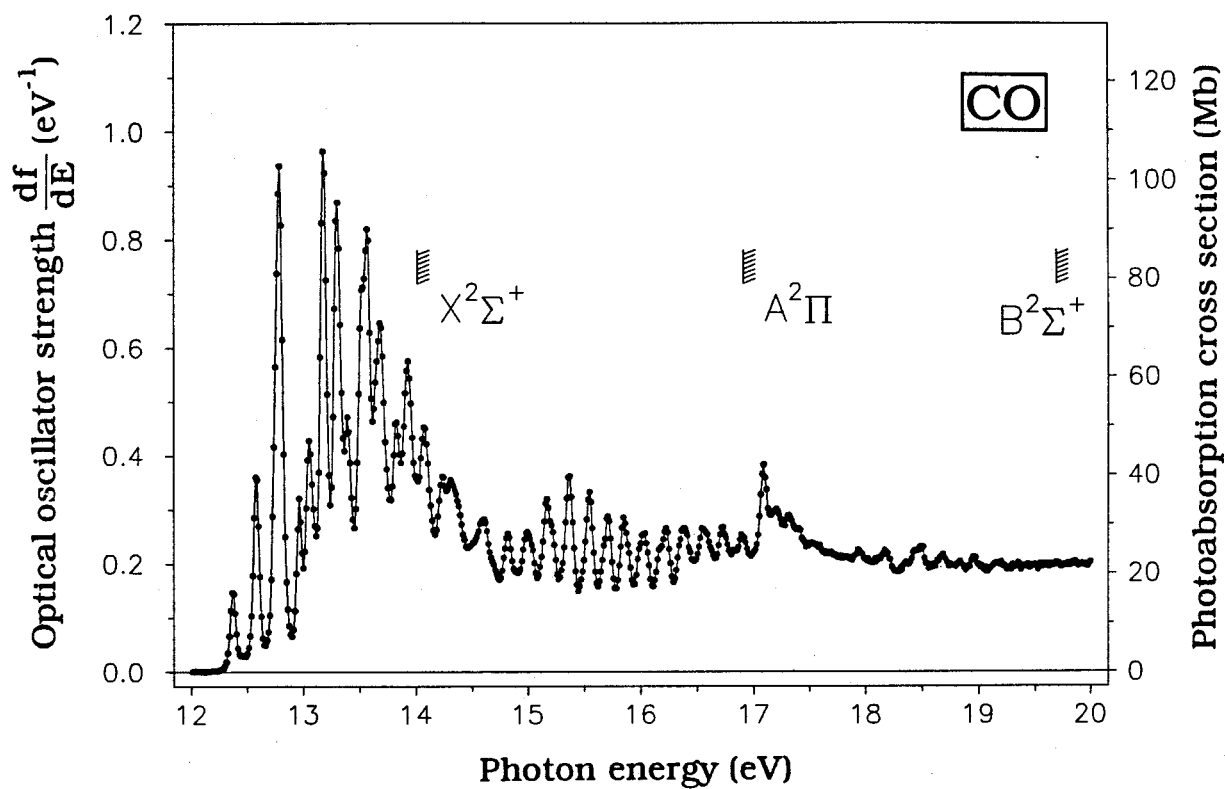


Figure 10.5: Absolute oscillator strengths for the photoabsorption of carbon monoxide in the energy region 12–20 eV at 0.048 eV FWHM. The assignments and energy positions of the ionization thresholds are taken from references [369,413].

Table 10.5

Integrated absolute optical oscillator strengths for the photoabsorption of carbon monoxide over energy intervals in the region 12.13–16.98 eV

Energy range (eV)	Integrated absolute optical oscillator strength		
	Present work	Stark <i>et al.</i> [391]	Letzelter <i>et al.</i> [388]
12.130 — 12.463	0.0113		0.00802
12.463 — 12.655	0.0270	0.0208	0.0163
12.655 — 12.896	0.0857	0.0438	0.0579
12.896 — 13.001	0.0202	0.0148	0.0138
13.001 — 13.115	0.0365	0.0301	0.0324
13.115 — 13.237	0.0721	0.0538	0.0472
12.237 — 13.364	0.0748	0.0594	0.0569
13.364 — 13.452	0.0337	0.0251	0.0278
13.452 — 13.614	0.0982		0.0719
13.614 — 13.780	0.0820		0.0706
13.780 — 13.867	0.0358		0.0327
13.867 — 14.016	0.0678		
14.016 — 14.169	0.0558		
14.169 — 14.458	0.0900		
14.458 — 14.743	0.0665		
14.743 — 14.902	0.0334		

Table 10.5 (continued)

Energy range (eV)	Integrated absolute optical oscillator strength		
	Present work	Stark <i>et al.</i> [391]	Letzelter <i>et al.</i> [388]
14.902 — 15.085	0.0402		
15.085 — 15.296	0.0449		
15.269 — 15.443	0.0430		
15.443 — 15.621	0.0406		
15.621 — 15.780	0.0347		
15.780 — 15.939	0.0346		
15.939 — 16.107	0.0356		
16.107 — 16.286	0.0386		
16.286 — 16.470	0.0417		
16.470 — 16.658	0.0443		
16.658 — 16.822	0.0343		
16.822 — 16.978	0.0366		

The present estimate for the same energy region is 0.640. The photoabsorption data reported by Huffman *et al.* [380] and Cook *et al.* [382] are ~25% higher than the present result, which is presumably due to errors in the pressure and/or light intensity measurements in these direct optical studies. On the other hand, it has been mentioned above (see table 10.5) that the recently reported high resolution photoabsorption data of Stark *et al.* [391] and Letzelter *et al.* [388] are somewhat lower than the present work in the energy region ~12.1–13.9 eV. Hence, the data of Stark *et al.* [391] and Letzelter *et al.* [388] would be much smaller than the data of Huffman *et al.* [380] and Cook *et al.* [382] over the same energy region. These large differences in oscillator strengths between different photoabsorption determinations reveal some further difficulties involved in absolute intensity measurements when using the Beer–Lambert law, in addition to the "line saturation" effects.

10.2.3 The Variation of Transition Moment with Internuclear Distance for the Vibronic Bands of the $X^1\Sigma^+ \rightarrow A^1\Pi$ Electronic Transition

The vibronic band oscillator strength ($f_{v'v''}$) for excitation to the $A^1\Pi$ state is related to the electronic transition moment $|R_e(r_{v'v''})|$ through equation 7.5 [40,367,368]. In the present work, the absolute optical oscillator strengths ($f_{v'0}$) for the vibronic bands for excitation to the $A^1\Pi$ state have been measured directly (see table 10.2). The Franck–Condon factors $q_{v'0}$ and the centroids $r_{v'0}$ can be taken from ref. [392], in which the values were calculated from the deperturbed RKR $A^1\Pi$ potential determined by Field [414] and revised molecular parameters for the

ground $X^1\Sigma^+$ state [415]. The energies ($E_{v'}-E_{v''}$) have been taken from refs. [369,370,378]. G is the statistical weighting factor which is equal to 2 for a $\Sigma\rightarrow\Pi$ transition. The electronic transition moment $|R_e(r_{v'v''})|$ can then be derived from equation 7.5 for each vibronic band. The resulting values of $|R_e(r_{v'v''})|$ are plotted as a function of $r_{v'0}$ in figure 10.6, which shows the variation of electronic transition moment with internuclear distance in carbon monoxide for the vibronic bands of the $A^1\Pi$ state. Previously reported experimental [392,407,416] and theoretical [367,368] values are also shown for comparison. From the measured deperturbed lifetime data, Field *et al.* [407] have derived a linear dipole moment function of the form

$$|R_e(r_{v'0})| = 7.48 (1 - 0.683 r_{v'0}) \quad (10.1)$$

In other work involving laser induced fluorescence measurements to sample the electronic dipole moment at large internuclear distance (1.35–1.80 Å), combined with the data reported by Field *et al.* [407] at lower internuclear distance, De Leon [416] has derived an electronic dipole moment function of the form

$$|R_e(r_{v'0})| = 1.5741 (1 - 1.17722 r_{v'0} + 0.35013 r_{v'0}^2) \quad (10.2)$$

As shown in figure 10.6, the dipole moment functions reported by Field *et al.* [407] (solid line) and De Leon [416] (dashed line) are in good agreement with the present work only for internuclear distances ($r_{v'0}$) above 1.1 Å, and their values become much higher than the present experimental results at low $r_{v'0}$. The photoabsorption work of Eidelsberg

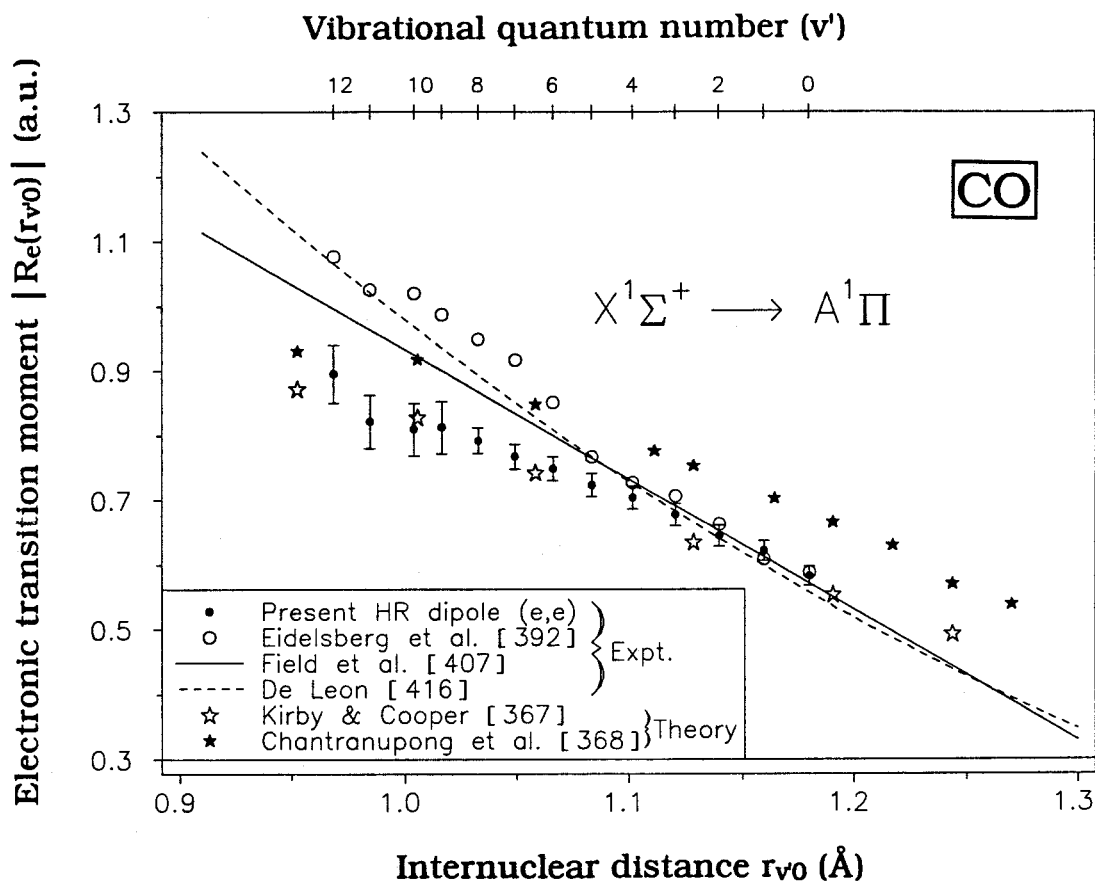


Figure 10.6: The electronic transition moment $|R_e(r_{v0})|$ in atomic units (a.u.) as a function of the internuclear distance r_{v0} in Ångstroms (Å) for the vibronic bands of the $X^1\Sigma^+ \rightarrow A^1\Pi$ transition.

et al. [392] shows results similar to the predictions by Field *et al.* [407] and by De Leon [416]. On the other hand, the theoretical work of Kirby and Cooper [367] is in very good agreement with the present work over the entire range of study, while the values calculated by Chantranupong *et al.* [368] are much higher than the present results.

10.3 Conclusions

Absolute optical oscillator strengths for the photoabsorption of carbon monoxide have been measured in the energy region from 7–200 eV. The data were TRK sum-rule normalized and thus are independent of any other measurements. Absolute optical oscillator strengths for the vibronic bands of the $A^1\Pi$, $C^1\Sigma^+$, $B^1\Sigma^+$ and $E^1\Pi$ states have been reported. Good agreement is found (see table 10.2) between the present and some of the previously published experimental [69,392,407] and theoretical [367] results for the vibronic bands of the $A^1\Pi$ state. In contrast (see table 10.4) considerable differences are seen for the vibronic band oscillator strengths for the $C^1\Sigma^+$, $B^1\Sigma^+$ and $E^1\Pi$ states. It is noteworthy that severe "line saturation" effects due to incident photon bandwidth are observed in some of the photoabsorption measurements (e.g. refs. [385,387,391]) for the discrete transitions in carbon monoxide. The procedures employed by Letzelter *et al.* [388] and by Eidelsberg *et al.* [392] can lower the errors due to "line saturation" effects in direct Beer-Lambert law photoabsorption experiments, however, these kinds of procedures place the most weight on the least accurate data obtained at low pressure, which may be the reason for the discrepancies between the present work and the data reported by Letzelter *et al.* [388], even though

the data reported by Eidelsberg *et al.* [392] are consistent with the present work. For the lifetime measurements, accurate branching ratios are necessary in order to obtain reliable absolute optical oscillator strengths. In contrast, the present dipole (e,e) method provides a direct means for measuring the absolute optical oscillator strengths for the discrete transitions of carbon monoxide, free of "line saturation" effects. The variation of the electronic transition moment with the C–O internuclear distance for the $A^1\Pi$ state derived from the present measurements was found to be in good agreement with the theoretical results of Kirby and Cooper [367].

Chapter 11

Absolute Optical Oscillator Strengths for the Photoabsorption of Nitric Oxide (5–30 eV)

11.1 Introduction

Absolute optical oscillator strengths for photoabsorption by nitric oxide (NO) in the valence discrete region are of interest in areas such as atmospheric sciences [417,418] and the development of lasers [419]. Nitric oxide is found in air at high temperatures and also occurs in the upper atmosphere. In addition, nitric oxide is a major atmospheric pollutant since it is a product of internal combustion engines and combustion power plants. An accurate knowledge of the nitric oxide concentration is essential for the understanding of atmospheric chemistry [417]. Oscillator strengths for the γ ($A^2\Sigma^+-X^2\Pi$) absorption bands of nitric oxide have been used to estimate column densities in the mesosphere [418]. The γ bands have also been considered as the basis of an optically pumped laser involving bound electronic states with inherently narrow linewidths [419].

Below 8 eV, the valence-shell excitation spectrum of nitric oxide consists mainly of discrete transitions belonging to the γ ($A^2\Sigma^+-X^2\Pi$), β ($B^2\Pi-X^2\Pi$), δ ($C^2\Pi-X^2\Pi$) and ϵ ($D^2\Sigma^+-X^2\Pi$) systems. Ory [420] has calculated Franck-Condon factors for the δ and ϵ systems using Morse oscillator wavefunctions. In the same study [420], the total electronic oscillator strengths for the γ , β , δ and ϵ systems have been derived by assuming a constant electronic transition moment and using published

experimental data for the oscillator strengths of a number of individual vibronic levels. Cooper [421] has calculated the electronic transition moments for the β and δ systems of nitric oxide using ab initio configuration interaction methods. In other work, multireference configuration interaction (MRCI) methods have been used by de Vivie and Peyerimhoff [422] and Langhoff *et al.* [423,424] to calculate the lifetimes, Einstein coefficients (A) and transition moment functions for excited states of nitric oxide. Rydberg–valence state interactions occur between excited bound levels of nitric oxide, and perturbations between the vibronic excited levels of 2Π symmetry have been studied by Gallusser and Dressler [425]. The absolute scale of the calculated (perturbed) oscillator strengths reported by Gallusser and Dressler [425] was adjusted by referencing to previously reported experimental values [426]. In addition, the unperturbed oscillator strengths were also calculated [425].

In experimental work, the energy levels of nitric oxide have been studied extensively using photoabsorption methods [427–436], but relatively few studies have been made of the associated oscillator strengths. Critical reviews and compilations of the spectroscopic data up to 1976 can be found in refs. [46,330,437,438]. Beer–Lambert law photoabsorption measurements [46,326,330,439–445] have provided much of the existing absolute optical oscillator strength data for nitric oxide. However, as has been pointed out earlier [37,46] (see chapter 2) Beer–Lambert law photoabsorption data for discrete transitions are subject to so-called "line-saturation" (bandwidth) effects which result in the measured oscillator strengths being too small. These spurious effects are more severe for transition with narrow linewidth and high cross section as illustrated in recent studies of the electronic spectra of

nitrogen [41] (see chapter 8) and carbon monoxide [43] (see chapter 10). Similar "line saturation" effects can be seen in the photoabsorption measurements of nitric oxide in the energy region 5.39–11.27 eV reported by Marmo [439]. In the latter work [439], a decrease in the observed photoabsorption cross sections was found for some of the discrete transitions of nitric oxide at high sample pressure, while this behavior was not observed in the continuum. Improved determinations of the absolute oscillator strengths for the valence discrete transitions of nitric oxide using the Beer–Lambert law were subsequently reported by Weber and Penner [440], Bethke [426] and Hasson and Nicholls [441]. In order to minimize the "line saturation" effects in these studies [426,440,441], the nitric oxide sample was mixed with a very high pressure of noble gas so that the linewidths for the discrete transitions of nitric oxide were collisionally broadened and therefore much smaller than the bandwidth of the spectrometer [426,440,441]. Other measurements of the absolute photoabsorption oscillator strengths for the discrete transitions of nitric oxide have been reported by Mandelman and Carrington [446] using the resonance–line absorption method, by Callear and Pilling [447] using the curves–of–growth method, and by Pery–Thorne and Banfield [448] and Farmer *et al.* [449,450] using the "Hook" method (which measures the rate of change of the refractive index near an absorption region). Shock tube emission and absorption measurements were also carried out by Keck *et al.* [451] and Daiber and Williams [452], respectively, to estimate electronic oscillator strengths for some discrete transitions of nitric oxide. In other work, Mandelman *et al.* [453] have reported the oscillator strength for the δ (0,0) band by measuring the absolute intensity of the recombination emission.

Lifetime measurements [251,394,417,454–467] have been extensively employed for studying various discrete transitions of nitric oxide but differences exist in the measured values. Moreover, in order to convert the lifetime values to oscillator strengths, the branching ratios must be known. The branching ratios can be obtained from relative emission intensities and such measurements have been carried out by several groups [251,461,466–474]. However, the reported branching ratios also show large differences. For example, the branching ratio for the γ (0,0) band was measured by Callear *et al.* [469] and Hesser [251] as 0.143 and 0.24 respectively.

Electron impact methods based on electron energy loss spectroscopy have also been used to study the discrete and continuum regions of the excitation spectrum of nitric oxide. In early work, Lassetre *et al.* [475] measured the electron energy loss spectrum of nitric oxide in the energy region 5–9.5 eV at 50 eV impact energy and zero-degree scattering angle, but no absolute oscillator strengths for the discrete transitions were reported. Later, quantitative low resolution dipole (e,e) work by Iida *et al.* [93] reported absolute oscillator strengths for the photoabsorption of nitric oxide in the energy region 6–190 eV. In this study [93], the absolute scale was established using TRK sum-rule normalization. However, since the resolution of the spectrum recorded by Iida *et al.* [93] was limited to 1 eV FWHM, the oscillator strengths for individual discrete transitions could not be determined. The absolute oscillator strength data reported by Iida *et al.* [93] in the continuum have been compared with direct optical studies [326,445] in the data compilation of Gallagher *et al.* [30].

In the present work, the high resolution dipole (e,e) method, which has recently been used to measure absolute oscillator strengths for the discrete transitions of noble gas atoms [37–39] (see chapters 4–6) and several small molecules [27,40–43,411] (see chapters 7–10), is now applied to study the valence shell discrete transitions of nitric oxide. The absolute photoabsorption oscillator strengths obtained using the dipole (e,e) method are not subject to "line saturation" effects since electron impact excitation is non-resonant and because no logarithmic transform is required in order to convert the measured experimental quantities to oscillator strengths, in contrast to Beer–Lambert law photoabsorption. The absolute scale of the present high resolution dipole (e,e) measurements is established by normalizing in the smooth photoabsorption continuum at 25 eV to the photoabsorption oscillator strength reported by Iida *et al.* [93]. The high reliability of the high resolution dipole (e,e) method has been confirmed by a comparison of the results of the measurements for helium [37] (see chapter 4) and molecular hydrogen [40] (see chapter 7) with highly accurate ab-initio calculations. In addition, the results for molecular oxygen [42] (see chapter 9) are particularly relevant to the present work, since they have established the accuracy of the Bethe–Born factor of the high resolution dipole (e,e) spectrometer when extrapolated down to equivalent photon energies as low as 6 eV.

11.2 Results and Discussion

The oscillator strength spectra of nitric oxide are conveniently discussed by reference to its ground state molecular-orbital valence shell independent particle configuration which may be written as

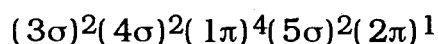


Figure 11.1 (solid line) shows the absolute optical oscillator strength spectrum of nitric oxide in the energy region 5–30 eV obtained in the present work using the high resolution (0.048 eV FWHM) dipole (e,e) spectrometer. The low resolution dipole (e,e) photoabsorption data previously determined by Iida *et al.* [93], and the photoabsorption data of Lee *et al.* [326] and of Gardner *et al.* [445] are also shown for comparison. It can be seen in figure 11.1 that the present high resolution (HR) results and the low resolution (LR) data reported by Iida *et al.* [93] are in excellent agreement over the continuum region. Similarly in the discrete region the high and low resolution dipole (e,e) measurements are highly consistent when the large differences in energy resolution (0.048 eV vs 1 eV FWHM) are taken into account. The presently obtained HR data in the continuum 21–30 eV are also in good quantitative agreement with the photoabsorption data of Gardner *et al.* [445], while the data of Lee *et al.* [326] are 10–15% lower than the present work.

Figures 11.2–11.4 are expanded views of figure 11.1 in the energy regions 5–8.2, 8–13 and 13–22 eV respectively. The assignments and energy positions of the excited states and ionization thresholds have been taken from the detailed spectroscopic studies reported in refs.

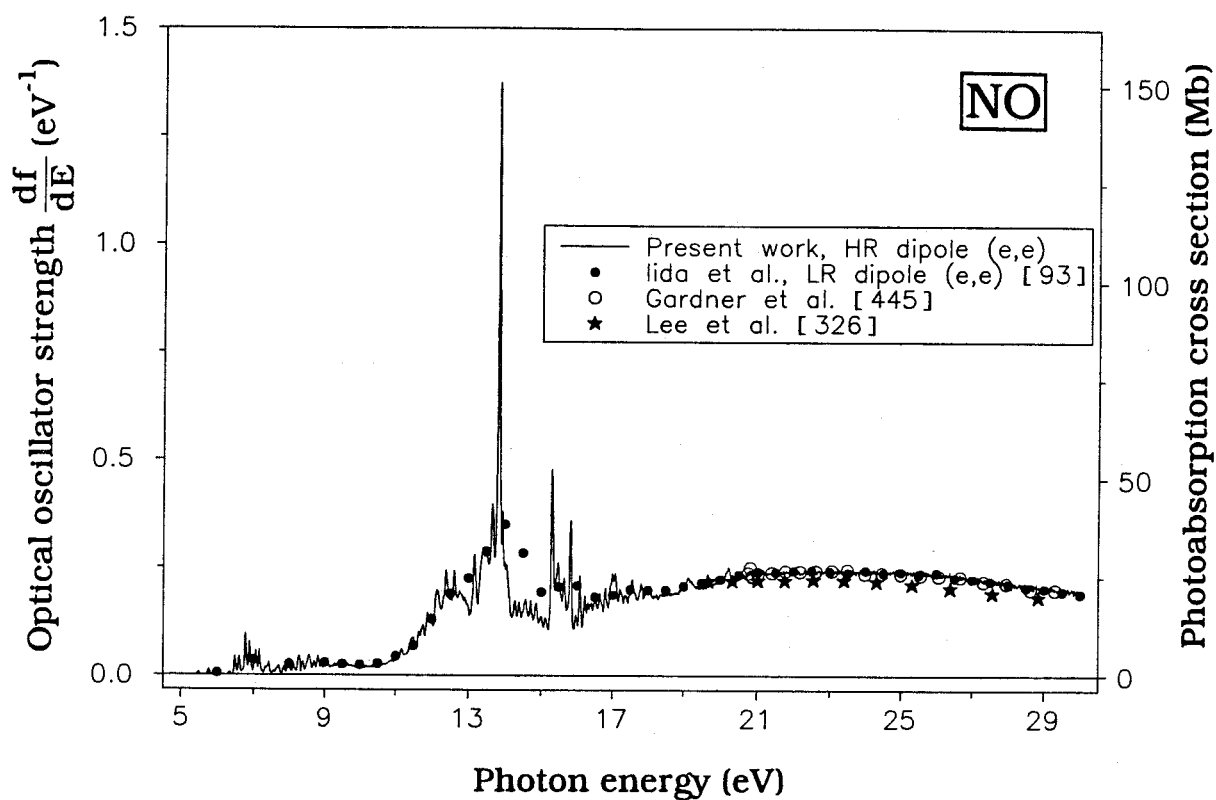


Figure 11.1: Absolute oscillator strengths for the photoabsorption of nitric oxide in the energy region 5–30 eV measured using the high resolution dipole (e,e) spectrometer (FWHM=0.048 eV).

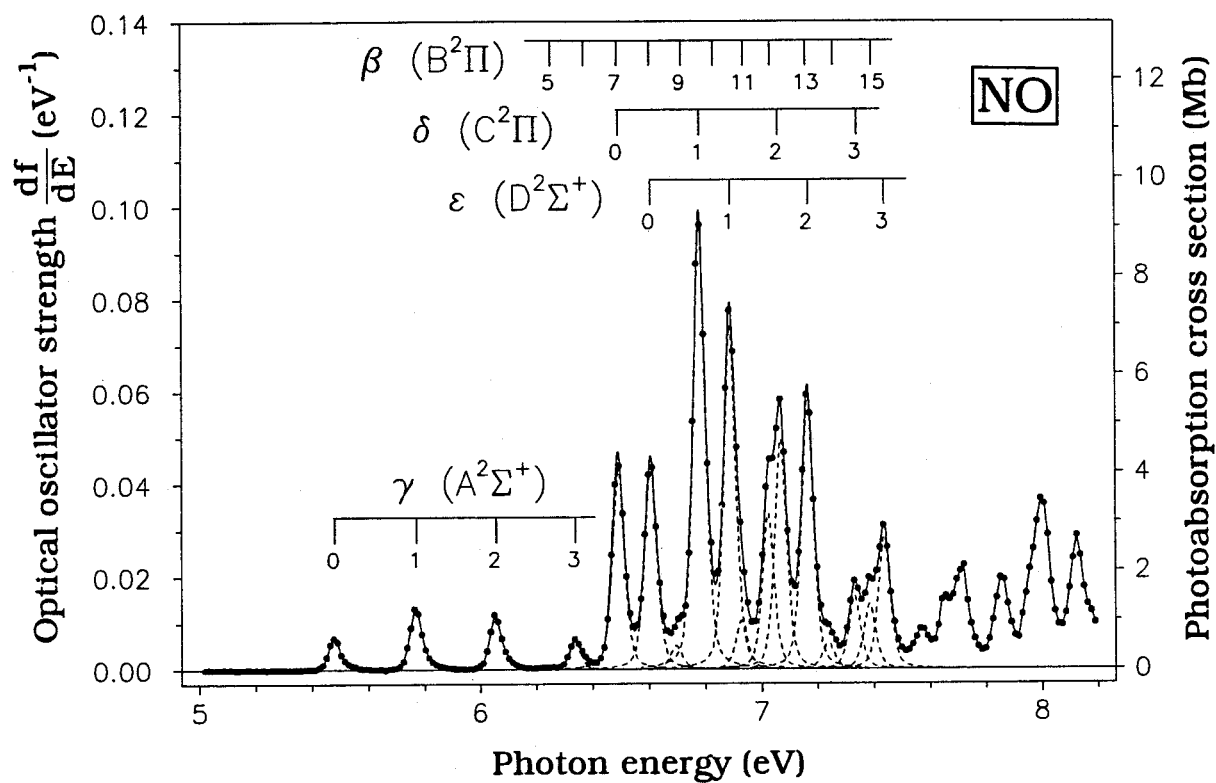


Figure 11.2: Expanded view of figure 11.1 in the energy region 5–8.2 eV. The assignments are taken from references [425,437]. Deconvoluted peaks are shown as dashed lines and the solid line represents the total fit to the experimental data.

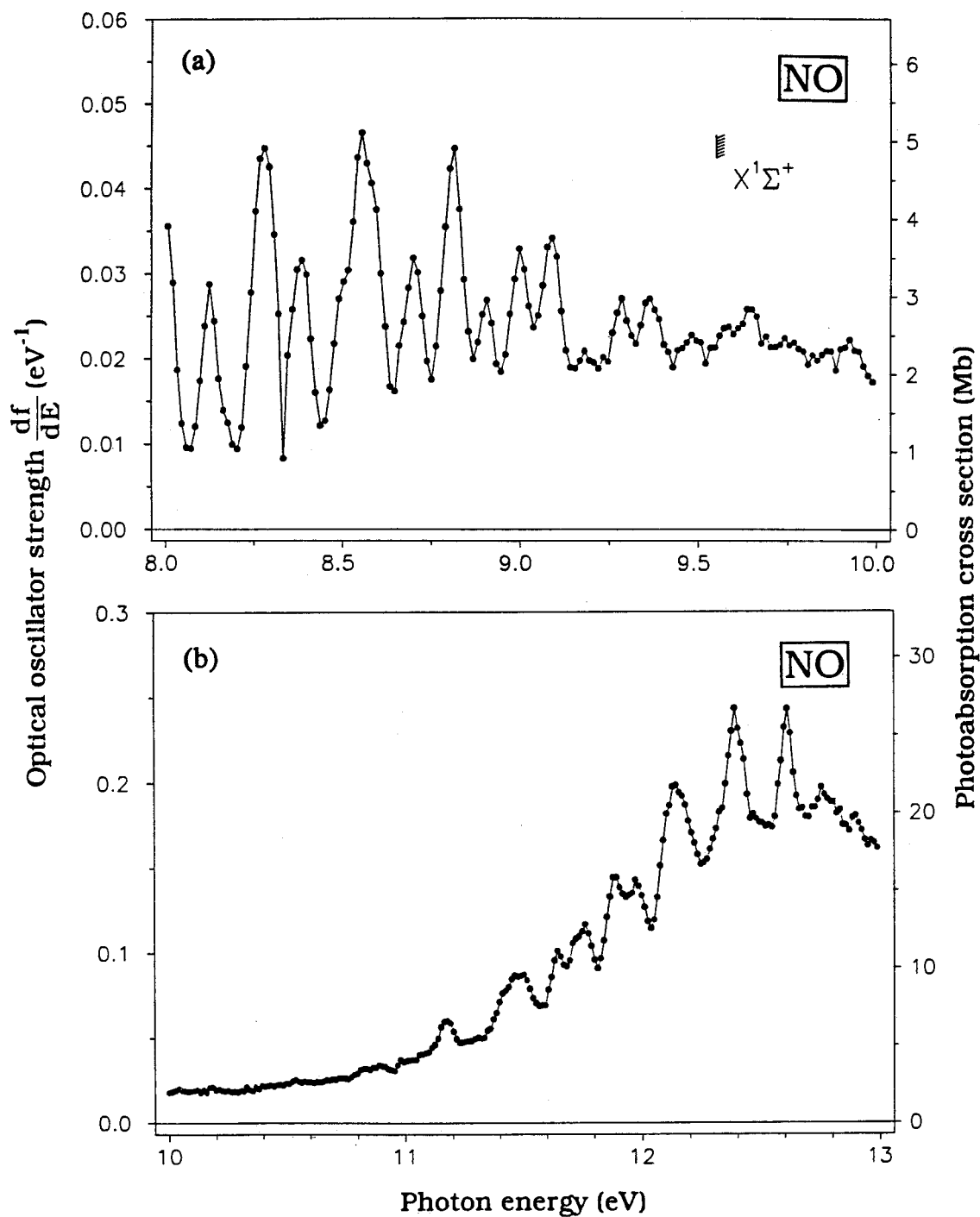


Figure 11.3: Expanded view of figure 11.1. The ionization limit for the $X^1\Sigma^+$ edge is taken from reference [476]. (a) in the energy region 8–10 eV. (b) in the energy region 10–13 eV.

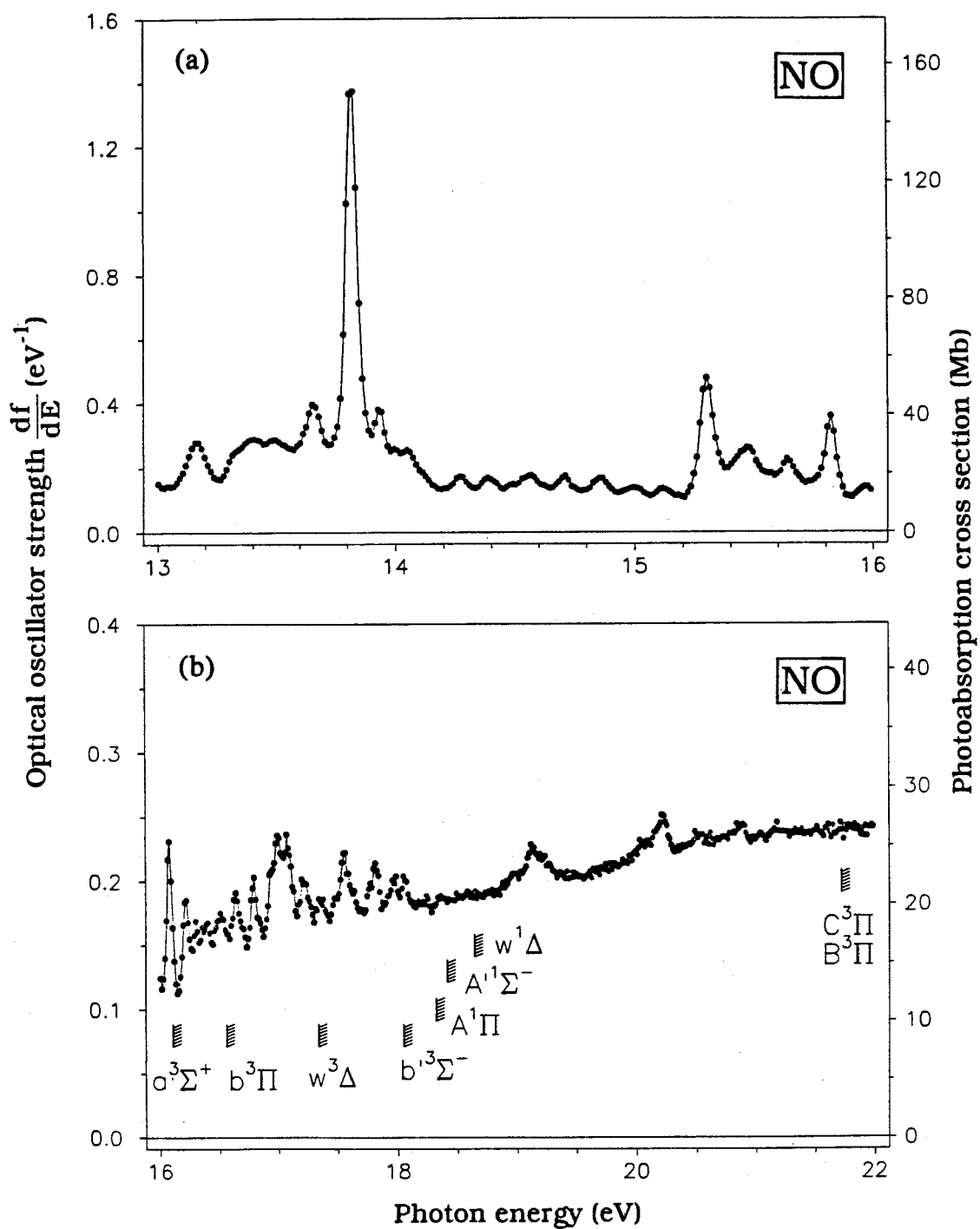


Figure 11.4: Expanded view of figure 11.1. The ionization limits are taken from reference [476]. (a) in the energy region 13–16 eV. (b) in the energy region 16–22 eV.

[425,437,476]. Figure 11.2 shows the discrete transitions below 8 eV. A curve-fitting program was used to deconvolute the spectrum between 6.25–7.5 eV and the resulting deconvoluted peaks are shown as dashed lines in figure 11.2. The total fit to the data is shown as the solid line. In the present work, integration of the peak area gives directly the absolute optical oscillator strength for the corresponding vibronic transition. Absolute vibronic optical oscillator strengths for the discrete transitions in the energy region 5.48–7.44 eV determined in the present work are summarized in table 11.1. The oscillator strength for the β (5,0) band was obtained by subtracting the leading edge of the tail of the curve fitted to the γ (3,0) band from the present experimental data in the energy region 6.194–6.280 eV. The uncertainties in the present results are estimated to be ~5–10% for the strong, partially resolved peaks and ~10–20% for the remaining peaks due to the additional errors in the deconvolution processes.

Tables 11.2–11.5 summarize the presently determined absolute vibrationally resolved oscillator strengths for the electronic transitions to the γ , β , δ and ϵ states. Previously reported experimental and theoretical data are also shown for comparison. For the overlapping β (7,0) and δ (0,0) bands (see table 11.1), the oscillator strength for each of the individual transitions (shown in tables 11.3 and 11.4 respectively) was estimated using the ratio of the oscillator strengths for these bands calculated by Gallusser and Dressler [425] in conjunction with a total oscillator strength for the bands determined from the presently reported spectrum. The oscillator strength contributions of the other overlapping bands such as the γ (4,0), γ (5,0), γ (6,0), β (8,0), β (10,0) and β (13,0) are assumed to be negligible compared with the dominant δ and ϵ peaks,

Table 11.1

Absolute optical oscillator strengths for discrete transitions from the ground state of nitric oxide in the energy region 5.48–7.44 eV[#]

Energy (eV)	Final state (v',v'')	Oscillator strength
5.481	γ (0,0)	0.000420
5.771	γ (1,0)	0.000824
6.057	γ (2,0)	0.000730
6.256	β (5,0)	0.000029
6.340	γ (3,0)	0.000356
6.374	β (6,0)	0.000037
6.494	β (7,0) + δ (0,0)	0.00267
6.608	γ (4,0) + β (8,0) + ϵ (0,0)	0.00275
6.718	β (9,0)	0.000314
6.782	β (10,0) + δ (1,0)	0.00601
6.891	γ (5,0) + ϵ (1,0)	0.00461
6.939	β (11,0)	0.000648
7.035	β (12,0)	0.00209
7.063	δ (2,0)	0.00308
7.168	γ (6,0) + β (13,0) + ϵ (2,0)	0.00367
7.259	β (14,0)	0.000354
7.342	δ (3,0)	0.000976
7.396	β (15,0)	0.000870
7.438	ϵ (3,0)	0.00179

[#] The assignments and energy positions have been taken from refs. [425,426,437].

Table 11.2
Absolute optical oscillator strengths for the vibronic bands of the γ ($X^2\Pi \rightarrow A^2\Sigma^+$) transition in nitric oxide

	Absolute oscillator strengths for the γ ($v',0$) band			
	$v'=0$	$v'=1$	$v'=2$	$v'=3$
Theory:				
Langhoff <i>et al.</i> [423]	0.000377	0.000731	0.000620	
de Vivie and Peyerimhoff [422]	0.00104	0.00247		
Experiment:				
Present work (HR dipole (e,e))	0.000420	0.000824	0.000730	0.000356
Piper and Cowles [473] (Branching ratios)	0.00039	0.00082	0.00081	
McGee <i>et al.</i> [470] (Branching ratios)	0.000323			
Mohlmann <i>et al.</i> [459] (Branching ratios and lifetimes)	0.000404	0.000829	0.000750	
Brzowski <i>et al.</i> [457] (Branching ratios and lifetimes)	0.000345			

Table 11.2 (continued)

	Absolute oscillator strengths for the γ ($v',0$) band			
	$v'=0$	$v'=1$	$v'=2$	$v'=3$
Experiment:				
Farmer <i>et al.</i> [449] ("Hook" method)	0.00040	0.000809	0.000700	0.000240
Pery-Thorne and Banfield [448] ("Hook" method)	0.000364			
Hesser [251] (Branching ratios and lifetimes)	0.00025	0.00030	0.00171	
Bethke [426] (Photoabsorption)	0.000399	0.000788	0.000673	0.000360
Weber and Penner [440] (Photoabsorption)	0.00041	0.00088	0.00067	

Table 11.3

Absolute optical oscillator strengths for the vibronic bands of the β ($X^2\Pi \rightarrow B^2\Pi$) transition in nitric oxide

v'	Absolute oscillator strengths for the β ($v',0$) band		
	Experimental		Theoretical
	Present work (HR Dipole (e,e))	Bethke [426] (Photoabsorption)	Gallusser and Dressler [425]
0			0
1			0
2		0.00000155	0
3		0.00000461	0
4		0.0000138	0.00001
5	0.000029	0.0000264	0.00002
6	0.000037	0.0000462	0.00004
7	0.000375	0.000350	0.00036
8			0.00012
9	0.000314	0.000358	0.00034
10			0.00003
11	0.000648	0.000362	0.00035
12	0.00209	0.00231	0.00245
13			0.00001
14	0.000354	0.000201	0.00015
15	0.000870		0.00071

Table 11.4
Absolute optical oscillator strengths for the vibronic bands of the δ ($X^2\Pi \rightarrow C^2\Pi$) transition in nitric oxide

	Absolute oscillator strengths for the δ ($v',0$) band			
	$v'=0$	$v'=1$	$v'=2$	$v'=3$
Theory:				
de Vivie and Peyerimhoff [422]	0.00249			
Gallusser and Dressler [425]	0.00220	0.00610	0.00259	0.00098
Experiment:				
Present work	0.00229	0.00601	0.00308	0.000976
(HR dipole (e.e))				
Brzowski <i>et al.</i> [457]	0.00204			
(Lifetimes)*				
Mandelmann and Carrington [446]	0.0022			
(Resonance-line absorption)				
Mandelman <i>et al.</i> [453]	0.00213			
(Radiative recombination of N+O)				
Callear and Pilling [447]	0.00560			
(Curve-of growth)				
Bethke [426]	0.00214	0.00578	0.00274	
(Photoabsorption)				

* The value was obtained by assuming a constant electronic transition moment for the δ bands.

Table 11.5
Absolute optical oscillator strengths for the vibronic bands of the ϵ ($X^2\Pi \rightarrow D^2\Sigma^+$) transition
in nitric oxide

	Absolute oscillator strengths for the ϵ ($v', 0$) band		
	$v'=0$	$v'=1$	$v'=2$
Theory: de Vivie and Peyerimhoff [422]	0.00196	0.00245	
Experiment: Present work (HR dipole (e,e)) Hesser [251] (Branching ratios and lifetimes) Bethke [426] (Photoabsorption)	0.00263	0.00461	0.00179
			0.00367
			0.00460
	0.00242	0.00460	0.00332

since the γ bands have small oscillator strength values even for the lower vibrational members. In this regard it should also be noted that the calculations performed by Gallusser and Dressler [425] have also reported very small oscillator strength values for the β (8,0), β (10,0) and β (13,0) bands. Similar assumptions concerning contributions from the overlapping bands have also been made to the photoabsorption data reported by Bethke [426].

It can be seen from table 11.2 that the various experimental values for the γ bands are generally in reasonable agreement with each other except for those reported by Hesser [251]. Hesser [251], Brzozowski *et al.* [457] and Mohlmann *et al.* [459] have measured both branching ratios and lifetimes while Piper and Cowles [473] and McGee *et al.* [471] have only measured the branching ratios, and the oscillator strength values reported by these authors [471,473] were obtained by using previously published experimental lifetimes. The data reported by Mohlmann *et al.* [459] for the γ bands are in excellent agreement with the present work, while the data reported by Piper and Cowles [473] for $v'=0$ and 1 are also consistent with the present work, but their value for $v'=2$ is slightly higher. In contrast, the values reported by Brzozowski *et al.* [457] and McGee *et al.* [471] for $v'=0$ are ~20% lower than the present result. The "Hook" method was employed by two groups [448,449]. The value for $v'=0$ reported by Pery-Thorne and Banfield [448] is slightly lower than the present value. In the other work [449], the values reported by Farmer *et al.* [449] show good agreement with the present work for $v'=0-2$ while the value for $v'=3$ is ~33% lower. The Beer-Lambert law photoabsorption measurements reported by Weber and Penner [440] and Bethke [426], which were obtained by collisionally broadening the natural

linewidths of the discrete transitions of nitric oxide with noble gases, show very good agreement with the present work. However, the data [426,440] will still be subject to "line saturation" effects (which however may be smaller than other experimental uncertainties in the present cases) since it has been pointed out in ref. [37] (see chapter 2) that "line saturation" effects will always occur since perfect resolution (i.e. zero bandwidth) cannot be obtained. Turning to theory, MRCI methods have been used by de Vivie and Peyerimhoff [422] and by Langhoff *et al.* [423]. The values calculated by Langhoff *et al.* [423] for the γ bands are ~10–15% lower than the present work while those reported by de Vivie and Peyerimhoff [422] are much higher than the present results.

Table 11.3 shows the present and previously published [425,426] oscillator strength results for the β bands of nitric oxide and demonstrates the irregularities in the oscillator strength distributions caused by configuration interactions between the valence and the Rydberg states of 2Π symmetry. Note that the oscillator strengths calculated by Gallusser and Dressler [425] were obtained by adjusting the electronic transition moments of the β and δ bands by reference to the photoabsorption data reported by Bethke [426]. Hence, the calculated values of Gallusser and Dressler [425] are consistent with the data reported by Bethke [426]. The present results are in reasonable agreement with the data of Bethke [426] except for the $v'=11$ and 14 bands for which the present values are somewhat higher. The larger discrepancies in the cases of these two bands may arise from deconvolution errors.

The present and previously published [422,423,426,446,447,453,457] results for the δ bands are shown in

table 11.4. It can be seen that the reported experimental and theoretical data are in very good agreement with each other with the exception that the value for $\nu'=0$ reported by Callear and Pilling [447], using the curve-of-growth method, is much higher than the other results. For the ϵ bands as shown in table 11.5, the present results are again in good agreement with the data of Bethke [426]. On the other hand, the lifetime data of Hesser [251] and also the theoretical values of de Vivie and Peyerimhoff [422] are considerably lower than than the present results.

Absolute integrated oscillator strengths over selected ranges in the energy region 7.52–9.43 eV are summarized in table 11.6. Marmo [439] has also reported photoabsorption data in this energy region, but the data are not shown in table 11.6 since they are subject to the "line saturation" effects as discussed above. In contrast the present work provides a quantitative determination of oscillator strength below the first ionization threshold.

Berkowitz [143] has performed a sum-rule analysis on all experimental oscillator strength data for nitric oxide available before 1980 and obtained an integrated oscillator strength value of 14.17 from the lower limit of the data at 8.86 to infinity. As stated by Berkowitz [143], this analysis therefore implies that the integrated oscillator strength below 8.86 eV is 0.83 by difference (i.e. 15.00 minus 14.17). In contrast, the presently measured integrated oscillator strength sum up to 8.86 eV gives a very different value of 0.0603. The present result therefore strongly suggests that the published data used by Berkowitz [143] misses appreciable oscillator strength at higher energies. In the energy region 10–22 eV, the absorption spectrum of nitric oxide (figures 11.3 and 11.4) consists of several unclassified bands and also numerous

Table 11.6**Integrated absolute optical oscillator strengths over the energy region 7.52–9.43 eV in the photoabsorption of nitric oxide**

Energy range (eV)	Integrated oscillator strength
7.517 — 7.606	0.000615
7.606 — 7.789	0.00235
7.789 — 7.907	0.00139
7.907 — 8.065	0.00335
8.065 — 8.199	0.00225
8.199 — 8.333	0.00389
8.333 — 8.442	0.00250
8.442 — 8.641	0.00598
8.641 — 8.747	0.00259
8.747 — 8.868	0.00375
8.868 — 8.941	0.00168
8.941 — 9.039	0.00255
9.039 — 9.148	0.00297
9.148 — 9.221	0.00144
9.221 — 9.323	0.00232
9.323 — 9.428	0.00251

transitions to the many Rydberg series converging to the triplet and singlet ionization limits corresponding to the ejection of a 5σ , 1π or 4σ electron. Details concerning the assignments and energy positions of these Rydberg series can be found in refs. [430,432,433]. Above the first ionization potential the discrete peaks are broadened by autoionization and therefore Beer-Lambert law photoabsorption studies in this region would be expected to be less affected by "line saturation" effects. This is supported by a comparison of the present spectrum (figures 11.3 and 11.4) and the photoabsorption data reported by Watanabe *et al.* [443]. Using the data of Watanabe *et al.* [443], Berkowitz [143] reported an oscillator strength sum of 1.413 in the energy region 8.86–18.44 eV which is in good agreement with the present result of 1.435.

11.3 Conclusions

Absolute optical oscillator strengths for the photoabsorption of nitric oxide in the valence discrete region 5–30 eV have been measured. Previously reported low resolution sum-rule normalized dipole (e,e) data [93] have been used to establish the absolute scale for the present high resolution measurements. The presently determined absolute scale is thus completely independent of any direct optical data and the oscillator strengths are free of "line saturation" effects. Absolute optical oscillator strengths for the vibrational bands of the γ , β , δ and ϵ states are reported. The results are in generally good agreement with absolute photoabsorption data. This good agreement in the case of nitric oxide arises because in general the oscillator strengths for discrete transitions below the first ionization potential are not large. Furthermore, the

pressure broadening techniques used in the Beer-Lambert photoabsorption studies reported by Bethke [426] enable the "line saturation" effects to be considerably reduced.

Chapter 12

Concluding Remarks

A new high resolution dipole (e,e) method has been developed for the measurements of absolute optical oscillator strengths for discrete and continuum transitions throughout the valence shell electronic spectra of gaseous atoms and molecules. The present work has presented absolute optical oscillator strengths for the discrete and continuum excitations of five noble gases (He, Ne, Ar, Kr and Xe) and five diatomic gases (H₂, N₂, O₂, CO and NO). The new measurements have considerably extended the range of measured absolute oscillator strength data for the above gases. The present results for the discrete excitation transitions ($1^1S \rightarrow n^1P$, $n=2-7$) of helium and for the Lyman and Werner bands of hydrogen are in excellent agreement with high-level ab-initio quantum-mechanical calculations. These findings confirm the viability of the high resolution dipole (e,e) method and in particular the accuracy of the Bethe-Born conversion factor determined for the high resolution dipole (e,e) spectrometer. The good agreement of the present measurements in the Schumann-Runge continuum region of oxygen with most previously reported experimental results further support the accuracy of the high resolution Bethe-Born conversion factor when extrapolated down to lower energy (7 eV). The results also confirm the validity of the Bethe-Born approximation for high energy electron scattering and the suitability of the high resolution dipole (e,e) method using TRK sum rule normalization for general application to the measurement of optical

oscillator strengths for discrete electronic excitations in atoms and molecules at high resolution.

The present work has also provided a detailed analysis of the "line saturation" (bandwidth) effects that can occur in quantitative photoabsorption cross section measurements for discrete transitions when using Beer–Lambert law methods. In contrast, the presently developed dipole (e,e) method provides a ready means of oscillator strength measurement for atoms and molecules across the entire valence shell region at high resolution and does not suffer from the problems of "line saturation" effects that can complicate Beer–Lambert law photoabsorption studies. Because of such "line saturation" effects, no direct Beer–Lambert law photoabsorption measurements have been reported in the literature for the valence discrete transitions of the noble gases and molecular hydrogen due to their very narrow natural linewidths and high cross section. The present work has provided the first comprehensive oscillator strength measurements for atomic helium and molecular hydrogen. These new measurements are in excellent agreement with high–level ab–initio quantum–mechanical calculations. Severe "line saturation" effects have been confirmed in previously reported Beer–Lambert law photoabsorption spectra for various valence discrete transitions of molecular nitrogen, carbon monoxide and nitric oxide.

References

- [1] Proceedings of Workshop on Electronic and Ionic Collision Cross Sections Needed in the Modeling of Radiation Interactions with Matter, 1983 (Argonne National Laboratory, Argonne 1984), Report No. ANL-84-28.
- [2] L. C. Green, P. P. Rush and C. D. Chandler, *Astrophys. J. Suppl. Ser.* **3**, 37 (1957).
- [3] A. Dalgarno and A. L. Stewart, *Proc. Phys. Soc. (London)* **76**, 49 (1960).
- [4] B. Schiff and C. L. Pekeris, *Phys. Rev. A* **134**, 638 (1964).
- [5] L. C. Green, N. C. Johnson and E. K. Kolchin, *Astrophys. J.* **144**, 369 (1967).
- [6] A. Dalgarno and E. M. Parkinson, *Proc. Roy. Soc. (London)* **A 301**, 253 (1967).
- [7] A. W. Weiss, *J. Res. Natl. Bur. Std.* **71A**, 163 (1967).
- [8] B. Schiff, C. L. Pekeris and Y. Accad, *Phys. Rev. A* **4**, 885 (1971).
- [9] J. A. Fernley, K. T. Taylor and M. J. Seaton, *J. Phys. B* **20**, 6457 (1987).
- [10] H. Bethe, *Ann. Phys. (Leipzig)* **5**, 325 (1930).
- [11] M. Inokuti, *Rev. Mod. Phys.* **43**, 297 (1971).
- [12] Y. K. Kim, *Phys. Rev. A* **6**, 666 (1972).
- [13] E. N. Lassetre and S. Skerbele, "Methods of Experimental Physics", edited by D. Williams (Academic Press, New York), vol. **3**, Part B, p.868 (1974).
- [14] C. E. Brion and A. Hamnett, *Advan. Chem. Phys.* **45**, 1 (1981).
- [15] E. N. Lassetre and M. E. Krasnow, *J. Chem. Phys.* **40**, 1248 (1964).
- [16] E. N. Lassetre, S. M. Silverman and M. E. Krasnow, *J. Chem. Phys.* **40**, 1261 (1964).
- [17] S. M. Silverman and E. N. Lassetre, *J. Chem. Phys.* **40**, 2922 (1964).

- [18] S. M. Silverman and E. N. Lassette, *J. Chem. Phys.* **42**, 3420 (1965).
- [19] J. Geiger, *Z. Phys.* **175**, 530 (1963).
- [20] J. Geiger, *Z. Phys.* **177**, 138 (1964).
- [21] M. J. Van der Wiel, *Physica* **49**, 411 (1970).
- [22] M. J. Van der Wiel and G. Wiebes, *Physica* **53**, 225 (1971).
- [23] M. J. Van der Wiel and G. Wiebes, *Physica* **54**, 411 (1971).
- [24] G. Cooper, T. Ibuki, Y. Iida and C. E. Brion, *Chem. Phys.* **125**, 307 (1988).
- [25] W. Zhang, G. Cooper, T. Ibuki and C. E. Brion, *Chem. Phys.* **137**, 391 (1989).
- [26] E. B. Zarate, G. Cooper and C. E. Brion, *Chem. Phys.* **148**, 277 (1990).
- [27] X. Guo, G. Cooper, W. F. Chan, G. R. Burton and C. E. Brion, *Chem. Phys.* **161**, 453 (1992).
- [28] E. B. Zarate, G. Cooper and C. E. Brion, *Chem. Phys.* **148**, 289 (1990).
- [29] X. Guo, G. Cooper, W. F. Chan, G. R. Burton and C. E. Brion, *Chem. Phys.* **161**, 471 (1992).
- [30] J. W. Gallagher, C. E. Brion, J. A. R. Samson and P. W. Langhoff, *J. Phys. Chem. Ref. data* **17**, 9 (1988).
- [31] S. Daviel, C. E. Brion and A. P. Hitchcock, *Rev. Sci. Instrum.* **55**, 182 (1984).
- [32] K. H. Sze, C. E. Brion, M. Tronc, S. Bodeur and A. P. Hitchcock, *Chem. Phys.* **121**, 279 (1988).
- [33] K. H. Sze, C. E. Brion, A. Katrib and B. El-Issa, *Chem. Phys.* **137**, 369 (1989).
- [34] G. Cooper, K. H. Sze and C. E. Brion, *J. Am. Chem. Soc.* **111**, 5051 (1989).
- [35] W. Zhang, K. H. Sze, C. E. Brion, X. M. Tong and T. M. Li, *Chem. Phys.* **140**, 265 (1990).

- [36] W. F. Chan, G. Cooper, K. H. Sze and C. E. Brion, *J. Phys. B* **23**, L523 (1990).
- [37] W. F. Chan, G. Cooper and C. E. Brion, *Phys. Rev. A* **44**, 186 (1991).
- [38] W. F. Chan, G. Cooper, X. Guo and C. E. Brion, *Phys. Rev. A* **45**, 1420 (1992).
- [39] W. F. Chan, G. Cooper, X. Guo, G. R. Burton and C. E. Brion, *Phys. Rev. A* **46**, 149 (1992).
- [40] W. F. Chan, G. Cooper and C. E. Brion, submitted to *Chem. Phys.*.
- [41] W. F. Chan, G. Cooper, R. N. S. Sodhi and C. E. Brion, submitted to *Chem. Phys.*.
- [42] W. F. Chan, G. Cooper and C. E. Brion, submitted to *Chem. Phys.*.
- [43] W. F. Chan, G. Cooper and C. E. Brion, submitted to *Chem. Phys.*.
- [44] W. F. Chan, G. Cooper and C. E. Brion, submitted to *Chem. Phys.*.
- [45] J. A. R. Samson, "Advances in Atomic and Molecular Physics", (Academic, New York), vol. 2, p.177 (1966).
- [46] R. D. Hudson, *Rev. Geophys. Space Phys.* **6**, 305 (1971).
- [47] G. V. Marr and J. B. West, *At. Data Nucl. Data Tables*, **18**, 497 (1976).
- [48] J. B. West and J. Morton, *At. Data. Nucl. Data Tables* **22**, 103 (1978).
- [49] P. W. Milonni and J. H. Eberly, "Lasers", (John Wiley & Sons, New York), p.88-89 (1988).
- [50] U. Fano and J. W. Cooper, *Rev. Mod. Phys.* **40**, 441 (1968).
- [51] H. A. Bethe and E. E. Salpeter, "Quantum Mechanics of One and Two-Electron Atoms", (Springer-Verlag, Nerlin), p.256 (1957).
- [52] J. A. Wheeler and J. A. Bearden, *Phys. Rev.* **46**, 755 (1934).
- [53] J. L. Dehmer, M. Inokuti and R. P. Saxon, *Phys. Rev. A* **12**, 102 (1975).
- [54] W. L. Wiese, M. W. Smith and B. M. Glenon, "Atomic Transition Probabilities: Hydrogen through Neon", *Natl. Stand. Ref. Data Ser., Natl. Bur. Stand., NSRDS-NBS 4, Vol. I* (1966); W. L. Wiese, M. W. Smith and B. M. Miles, "Atomic Transition Probabilities: Sodium through Calcium", *NSRDS-NBS 22, Vol. II* (1969); G. A. Martin, J.

- R. Fuhr and W. L. Wiese, "Atomic Transition Probabilities: Scandium through Manganese", *J. Phys. and Chem. Ref. Data* **17**, Supple. 3 (1988); J. R. Fuhr, G. A. Martin and W. L. Wiese, Atomic Transition Probabilities: Iron through Nickel, *J. Phys. and Chem. Ref. Data* **17**, Supple. 4 (1988).
- [55] K. Yoshino, D. E. Freeman, J. R. Esmond, R. S. Friedman and W. H. Pakinson, *Planet. Space Sci.* **36**, 1201 (1988).
- [56] E. S. Fry and W. L. Williams, *Phys. Rev.* **183**, 81 (1969).
- [57] J. M. Burger and A. Lurio, *Phys. Rev. A* **3**, 64 (1971).
- [58] I. Martinso and W. S. Bickel, *Phys. Lett.* **30A**, 524 (1969).
- [59] R. Lincke and H. R. Griem, *Phys. Rev.* **143**, 66 (1966).
- [60] F. A. Korolyov and V. I. Odintsov, *Opt. Spectry.* **18**, 547 (1965).
- [61] H. G. Kuhn and J. M. Vaughan, *Proc. Roy. Soc. (London)* **A 277**, 297 (1964).
- [62] J. P. De Jongh and J. Van Eck, *Physica* **51**, 104 (1971).
- [63] W. B. Westerveld and J. Van Eck, *J. Quant. Spectrosc. Radiat. Transfer* **17**, 131 (1977).
- [64] S. Tsurubuchi, K. Watanabe and T. Arikawa, *J. Phys. B* **22**, 2969 (1989).
- [65] Y. M. Aleksandrov, P. F. Gruzdev, M. G. Kozlov, A. V. Loginov, R. V. Fedorchuk and M. N. Yakimenko, *Opt. Spectrosc.* **54**, 4 (1983).
- [66] W. R. Ferrell, M. G. Payne and W. R. Garrett, *Phys. Rev. A* **35**, 5020 (1987).
- [67] E. N. Lassetre, A. Skerbele and M. A. Dillon, *J. Chem. Phys.* **50**, 1829 (1969).
- [68] E. N. Lassetre, A. Skerbele and M. A. Dillon, *J. Chem. Phys.* **52**, 2797 (1970).
- [69] E. N. Lassetre and A. Skerbele, *J. Chem. Phys.* **54**, 1597 (1971).
- [70] A. Skerbele and E. N. Lassetre, *J. Chem. Phys.* **55**, 424 (1971).
- [71] I. V. Hertel and K. J. Ross, *J. Phys. B* **2**, 285 (1969).
- [72] S. Brodersen, *J. Opt. Soc. Am.* **44**, 22 (1954).
- [73] G. F. Lothian, *Analyst* **88**, 678 (1963).

- [74] R. D. Hudson and V. L. Carter, *J. Opt. Soc. Am.* **58**, 227 (1968).
- [75] J. W. C. Johns, W. A. Kreiner and J. Susskind, *J. Mol. Spectrosc.* **60**, 400 (1976).
- [76] G. R. Cook and P. H. Metzger, *J. Chem. Phys.* **41**, 321 (1964).
- [77] R. E. Huffman, Y. Tanaka and J. C. Larrabee, *J. Chem. Phys.* **39**, 910 (1963).
- [78] G. M. Lawrence, D. L. Mickey and K. Dressler, *J. Chem. Phys.* **48**, 1989 (1968).
- [79] V. L. Carter, *J. Chem. Phys.* **56**, 4195 (1972).
- [80] P. Gürtler, V. Saile and E. E. Koch, *Chem. Phys. Lett.* **48**, 245 (1977).
- [81] E. N. Lassetre, F. M. Glaser, V. D. Meyer and A. Skerbele, *J. Chem. Phys.* **42**, 3429 (1965).
- [82] J. Geiger and W. Stickel, *J. Chem. Phys.* **43**, 4535 (1965).
- [83] A. Hamnett, W. Stoll, G. R. Branton, C. E. Brion and M. J. Van der Wiel, *J. Phys. B* **9**, 945 (1976).
- [84] M. J. Van der Wiel and C. E. Brion, *J. Electron Spectrosc. Relat. Phenom.* **1**, 443 (1972/73).
- [85] C. Backx, R. R. Tol, G. R. Wight and M. J. Van der Wiel, *J. Phys. B* **8**, 2050 (1975).
- [86] C. Backx, G. R. Wight and M. J. Van der Wiel, *J. Phys. B* **9**, 315 (1976).
- [87] G. R. Wight, M. J. Van der Wiel and C. E. Brion, *J. Phys. B* **9**, 675 (1976).
- [88] C. E. Brion, *Comments At. Mol. Phys.* **16**, 249 (1985).
- [89] F. Carnovale, A. P. Hitchcock, J. P. D. Cook and C. E. Brion, *Chem. Phys.* **66**, 249 (1982).
- [90] F. Carnovale and C. E. Brion, *Chem. Phys.* **74**, 253 (1983).
- [91] C. E. Kuyatt and J. A. Simpson, *Rev. Sci. Instrum.* **38**, 103 (1967).
- [92] C. E. Brion, K. H. Tan, M. J. Van der Wiel and Ph. E. Van der Leeuw, *J. Elect. Spectrosc. Relat. Phenom.* **17**, 101 (1979).

- [93] Y. Iida, F. Carnovale, S. Daviel and C. E. Brion, *Chem. Phys.* **105**, 211 (1986).
- [94] R. P. Madden and K. Codling, *Astrophys. J.* **141**, 364 (1965).
- [95] H. D. Morgan and D. L. Ederer, *Phys. Rev. A* **29**, 1901 (1984).
- [96] D. W. Lindle, T. A. Ferrett, P. A. Heimann and D. A. Shirley, *Phys. Rev. A* **36**, 2112 (1987).
- [97] H. Kossmann, B. Krassig and V. Schmidt, *J. Phys. B* **21**, 1489 (1988).
- [98] D. H. Oza, *Phys. Rev. A* **33**, 824 (1986).
- [99] R. Gersbacher and T. T. Broad, *J. Phys. B* **23**, 365 (1990).
- [100] C. F. Fischer and M. Idrees, *J. Phys. B* **23**, 679 (1990).
- [101] J. F. Lowry, D. H. Tomboulion and D. L. Ederer, *Phys. Rev. A* **137**, 1054 (1965).
- [102] W. S. Watson, *J. Phys. B* **5**, 2292 (1972).
- [103] J. B. West and G. V. Marr, *Proc. Roy. Soc. (London) A* **349**, 397 (1976).
- [104] J. W. Cooper, *Phys. Rev.* **128**, 681 (1962).
- [105] K. L. Bell and A. E. Kingston, *Proc. Phys. Soc. (London)* **90**, 31 (1967).
- [106] W. F. Chan, G. Cooper and C. E. Brion, unpublished work.
- [107] S. M. Silverman and E. N. Lassetre, *J. Chem. Phys.* **40**, 1265 (1964).
- [108] U. Fano, *Phys. Rev.* **124**, 1866 (1961).
- [109] L. H. Auer and D. Mihalas, *Astrophys. J.* **184**, 151 (1973).
- [110] R. C. Elton, "X-Ray Lasers", Academic Press, (1990).
- [111] P. F. Gruzdev, *Opt. Spectrosc.* **22**, 170 (1967).
- [112] E. J. McGuire, *Phys. Rev.* **175**, 20 (1968).
- [113] D. J. Kennedy and S. T. Manson, *Phys. Rev. A* **5**, 227 (1972).
- [114] T. M. Luke, *J. Phys. B* **6**, 30 (1973).

- [115] P. G. Burke and K. T. Taylor, *J. Phys. B* **8**, 2620 (1975).
- [116] M. Ya. Amus'ya, N. A. Cherepkov and L. V. Chernsheva, *Sov. Phys. JETP* **33**, 90 (1971).
- [117] W. R. Johnson and K. T. Cheng, *Phys. Rev. A* **20**, 978 (1979).
- [118] F. A. Parpia, W. R. Johnson and V. Radojevic, *Phys. Rev. A* **29**, 3173 (1984).
- [119] P. Lee and G. L. Weissler, *Proc. Roy. Soc. (London)* **220A**, 71 (1953).
- [120] D. L. Ederer and D. H. Tombouliau, *Phys. Rev.* **133A**, 1525 (1964).
- [121] J. A. R. Samson, *J. Opt. Soc. Am.* **55**, 935 (1965).
- [122] J. A. R. Samson, "Handbuch der Physik", *Encyclopaedia of Physics*, Volume XXXI: Corpuscles and Radiation in Matter I, Springer-Verlag Berlin Heidelberg New York, p.147 (1982).
- [123] C. E. Kuyatt and J. A. Simpson, "Proceedings of the third International Conference on the Physics of Electronic and Atomic Collisions, London, 1963", edited by M. R. C. McDowell (North-Holland, Amsterdam) p.191 (1964).
- [124] R. P. Saxon, *Phys. Rev. A* **8**, 839 (1973).
- [125] F. Wuilleumier and M. O. Krause, *Phys. Rev. A* **10**, 242 (1974).
- [126] M. H. Hecht and I. Lindau, *J. Elect. Spectrosc. Rel. Phenom.* **35**, 211 (1985).
- [127] D. M. P. Holland, M. A. MacDonald and M. A. Hayes, *Chem. Phys.* **142**, 291 (1990).
- [128] N. Saito, I. Suzuki, H. Onuki and M. Nishi, *Rev. Sci. Instrum.* **60**, 2190 (1989).
- [129] F. A. Korolev, V. I. Odintsov and E. V. Fursova, *Opt. Spectrosc.* **16**, 304 (1964).
- [130] G. M. Lawrence and H. S. Liszt, *Phys. Rev.* **178**, 178 (1969).
- [131] J. Z. Klose, *Phys. Rev.* **188**, 45 (1969).
- [132] E. J. Knystautas and R. Drouin, *Astron. Astrophys.* **37**, 145 (1974).
- [133] D. J. G. Irwin, A. E. Livingston and J. A. Kernahan, *Can. J. Phys.* **51**, 1948 (1973).

- [134] N. D. Bhaskar and A. Lurio, Phys. Rev. A **13**, 1484 (1976).
- [135] S. Kazantsev and M. Chaika, Opt. Spectrosc. **3**, 273 (1971).
- [136] B. Decomps and M. Dumont, IEEE J. Quantum Elect. **QE-4**, 916 (1968).
- [137] M. Ducloy, Ann. de. Phys. **Ser14 t8**, 403 (1973-74).
- [138] E. L. Lewis, Proc. Phys. Soc. (London) **92**, 817 (1967).
- [139] W. B. Westerveld, Th. F. A. Mulder and J. Van Eck, J. Quant. Spectrosc. Radiat. Transfer **21**, 533 (1979).
- [140] S. Tsurubuchi, K. Watanabe and T. Arikawa, J. Phys. Soc. Japan **59**, 497 (1990).
- [141] J. Geiger, Phys. Lett. **33A**, 351 (1970).
- [142] S. Natali, C. E. Kuyatt and S. R. Mielczarek, unpublished observations (1973) as quoted in references [139] and [143].
- [143] J. Berkowitz, "Photoabsorption, Photoionization and Photoelectron Spectroscopy", (Academic Press, New York), p.80, p.99, p.103, p.109, p.111 (1979).
- [144] P. S. Kelly, J. Quant. Spectrosc. Radiat. Transfer **4**, 117 (1964).
- [145] M. Ya. Amus'ya, "Atomic Photoeffect", Plenum Press, New York and London, p.170 (1990).
- [146] A. Gold and R. S. Knox, Phys. Rev. **113**, 834 (1959).
- [147] M. Aymar, S. Feneuille and M. Klapisch, Nucl. Instrum. Methods **90**, 137 (1970).
- [148] P. F. Gruzdev and A. V. Loginov, Opt. Spectrosc. **35**, 1 (1973).
- [149] R. Albat and N. Gruen, J. Phys. B **7**, L9 (1974).
- [150] R. F. Stewart, Mol. Phys. **29**, 1577 (1975).
- [151] R. F. Stewart, Mol. Phys. **30**, 745 (1975).
- [152] B. L. Henke, P. Lee, T. J. Tanaka, R. L. Shimabukuro and B. K. Fujikawa, 'Low-Energy X-Ray Interaction Coefficients: Photoabsorption, Scattering, and Reflection', Atomic Data & Nuclear Data Tables, **27**, 1 (1982).
- [153] W. Lotz, J. Opt. Soc. Am. **60**, 206 (1970).

- [154] K. Codling, R. P. Madden and D. L. Ederer, *Phys. Rev.* **155**, 26 (1967).
- [155] C. E. Moore, "Atomic Energy Levels", *Natl. Bur. Stand. (U.S.) Circ. No. 467* (U.S. GPO, Washington, DC), **Vol. 1** (1949); **Vol. 2** (1952); **Vol. 3** (1958).
- [156] A. V. Loginov and P. F. Gruzdev, *Opt. Spectrosc.* **37**, 467 (1974).
- [157] P. F. Gruzdev and A. V. Loginov, *Opt. Spectrosc.* **39**, 464 (1975).
- [158] J. Z. Klose, *J. Quant. Spectrosc. Radiat. Transfer* **9**, 881 (1969).
- [159] A. A. Wills, A. A. Cafolla, A. Svensson and J. Comer, *J. Phys. B* **23**, 2013 (1990).
- [160] C. E. Brion and L. A. R. Olsen, *J. Phys. B* **3**, 1020 (1970).
- [161] J. A. Simpson, G. E. Chamberlain and S. R. Mielczarek, *Phys. Rev. A* **139**, 1039 (1965).
- [162] K. Siegbahn, C. Nordling, G. Johansson, J. Hedman, P. F. Heden, K. Hamrin, U. Gelius, T. Bergmark, L. O. Werme, R. Manne and Y. Baer, 'ESCA: Applied to Free Molecules', (North-Holland, Amsterdam), p.152 (1969).
- [163] A. Zangwill and P. Soven, *Phys. Rev. A* **20**, 978 (1979).
- [164] A. F. Starace, *Phys. Rev. A* **2**, 118 (1970).
- [165] S. T. Manson and J. W. Cooper, *Phys. Rev.* **165**, 126 (1968).
- [166] B. F. Rozsnyai, *Phys. Rev. A* **42**, 286 (1990).
- [167] P. Lee and G. L. Weissler, *Phys. Rev.* **99**, 540 (1955).
- [168] R. E. Huffman, Y. Tanaka and J. C. Larrabee, *J. Chem. Phys.* **39**, 902 (1963).
- [169] A. P. Lukirskii and T. M. Zimkina, *Bull. Acad. Sci. USSR, Phys. Ser.* **27**, 808 (1963).
- [170] A. P. Lukirskii, I. A. Brytov and T. M. Zimkina, *Opt. Spectrosc.* **17**, 234 (1964).
- [171] O. P. Rustgi, *J. Opt. Soc. Am.* **54**, 464 (1964).
- [172] D. L. Ederer, *Phys. Rev. Lett.* **13**, 760 (1964).
- [173] P. H. Metzger and G. R. Cook, *J. Opt. Soc. Am.* **55**, 516 (1965).

- [174] R. Haensel, G. Keitel and P. Schreider, *Phys. Rev.* **188**, 1375 (1969).
- [175] D. R. Denne, *J. Phys. D* **3**, 1392 (1970).
- [176] R. W. Carlson, D. L. Judge, M. Ogawa and L. C. Lee, *Appl. Opt.* **12**, 409 (1973).
- [177] J. Lang and W. S. Watson, *J. Phys. B* **8**, L339 (1975).
- [178] J. A. R. Samson and L. Yin, *J. Opt. Soc. Am. B* **6**, 2326 (1989).
- [179] J. A. R. Samson, L. Yin, G. N. Haddad and G. C. Angel, *J. Phys. (Paris) IV, Coll. C1, Supp. II* **1**, 99 (1991).
- [180] Th. M. El-Sherbini and M. J. Van der Wiel, *Physica* **62**, 119 (1972).
- [181] R. S. Knox, *Phys. Rev.* **110**, 375 (1958).
- [182] J. D. Dow. and R. S. Knox, *Phys. Rev.* **152**, 50 (1966).
- [183] Y. K. Kim, M. Inokuti, G. E. Chamberlain and S. R. Mielczarek, *Phys. Rev. Lett.* **21**, 1146 (1968).
- [184] C. M. Lee and K. T. Lu, *Phys. Rev. A* **8**, 1241 (1973).
- [185] C. M. Lee, *Phys. Rev. A* **10**, 584 (1974).
- [186] P. F. Gruzdev and A. V. Loginov, *Opt. Spectrosc.* **38**, 234 (1975).
- [187] P. F. Gruzdev and A. V. Loginov, *Opt. Spectrosc.* **38**, 611 (1975).
- [188] R. Albat, N. Gruen and B. Wirsam, *J. Phys. B* **8**, L82 (1975).
- [189] M. Aymar and M. Coulombe, *At. Data Nucl. Data Tables*, **21**, 537 (1978).
- [190] P. G. Wilkinson, *J. Quant. Spectrosc. Radiat. Transfer* **5**, 503 (1965).
- [191] P. G. Wilkinson, *J. Quant. Spectrosc. Radiat. Transfer* **6**, 823 (1966).
- [192] P. M. Griffin and J. W. Hutchson, *J. Opt. Soc. Am.* **59**, 1607 (1969).
- [193] G. I. Chashchina and E. Ya. Shreider, *Opt. Spectrosc.* **22**, 284 (1967).
- [194] G. I. Chashchina and E. Ya. Shreider, *Opt. Spectrosc.* **27**, 79 (1969).

- [195] D. K. Anderson, Phys. Rev. **137**, A21 (1965).
- [196] R. Turner, Phys. Rev. A **140**, 426 (1965).
- [197] J. L. Morack and C. E. Fairchild, Phys. Rev. **163**, 125 (1967).
- [198] G. M. Lawrence, Phys. Rev. **175**, 40 (1968).
- [199] D. Irwin, A. E. Livingston and J. A. Kernahan, Nucl. Instrum. Methods **110**, 111 (1973).
- [200] W. Wieme and P. Mortier, Physica **65**, 198 (1973).
- [201] E. Matthias, R. A. Rosenberg, E. D. Poliakoff, M. G. White, S. T. Lee and D. A. Shirley, Chem. Phys. Lett. **52**, 239 (1977).
- [202] D. J. Chornay, G. C. King and S. J. Buckman, J. Phys. B **17**, 3173 (1984).
- [203] D. N. Stacey and J. M. Vaughan, Phys. Lett. **11**, 105 (1964).
- [204] J. M. Vaughan, Phys. Rev. **166**, 13 (1968).
- [205] G. H. Copley and D. M. Camm, J. Quant. Spectrosc. Radiat. Transfer **14**, 899 (1974).
- [206] O. Vallee, P. Ranson and J. Chapelle, J. Quant. Spectrosc. Radiat. Transfer **18**, 327 (1977).
- [207] S. D. Kramer, C. H. Chen. and M. G. Payne, Opt. Lett. **9**, 347 (1984).
- [208] J. W. McConkey and F. G. Donaldson, Can. J. Phys. **51**, 914 (1973).
- [209] G. E. Chamberlain, J. G. M. Heideman, J. A. Simpson and C. E. Kuyatt, "Abstracts in Proceedings of the Fourth International Conference on the Physics of Electronic and Atomic Collisions", Quebec, 1965", edited by L. Kerwin and W. Fite, (Science Bookcrafters, Hastings-on-Hudson, 1968).
- [210] J. Geiger, "Proceedings of the Fourth International Conference on Vacuum Ultraviolet Radiation Physics", (Pergamon, New York), p.28 (1974).
- [211] A. Delage and J. D. Carette, Phys. Rev. A **14**, 1345 (1976).
- [212] J. Geiger, Z. Phys. A **282**, 129 (1977).
- [213] J. Geiger, unpublished observations (1978) as quoted in references [139, 143].

- [214] G. P. Li, T. Takayanagi, K. Wakiya, H. Suzuki, T. Ajiro, S. Yagi, S. S. Kano and H. Takuma, *Phys. Rev. A* **38**, 1240 (1988).
- [215] T. Takayanagi, G. P. Li, K. Wakiya, H. Suzuki, T. Ajiro, T. Inaba, S. S. Kano and H. Takuma, *Phys. Rev. A* **41**, 5948 (1990).
- [216] T. Y. Suzuki, Y. Sakai, B. S. Min, T. Takayanagi, K. Wakiya, H. Suzuki, T. Inaba and H. Takuma, *Phys. Rev. A* **43**, 5867 (1991).
- [217] E. Eggarter, *J. Chem. Phys.* **62**, 833 (1975).
- [218] R. P. Madden, D. L. Ederer and K. Codling, *Phys. Rev.* **177**, 136 (1969).
- [219] C. E. Kuyatt, quoted in reference [217] as private communication.
- [220] J. A. R. Samson, *Phys. Rev.* **132**, 2122 (1963).
- [221] K. Codling and R. P. Madden, *Phys. Rev. A* **4**, 2261 (1971).
- [222] D. L. Ederer, *Phys. Rev. A* **4**, 2263 (1971).
- [223] K. Codling and R. P. Madden, *J. Res. Nat. Bur. Stand.* **76A**, 1 (1972).
- [224] A. A. Wills, A. A. Cafolla, F. J. Currell, J. Comer, A. Svensson and M. A. MacDonald, *J. Phys. B* **22**, 3217 (1989).
- [225] A. A. Wills, A. A. Cafolla and J. Comer, *J. Phys. B* **23**, 2029 (1990).
- [226] M. G. Flemming, J. Z. Wu, C. D. Caldwell and M. O. Krause, *Phys. Rev. A* **44**, 1733 (1991).
- [227] C. E. Brion, *Int. J. Quant. Chem.* **19**, 1397 (1986).
- [228] A. O. Bawagan, C. E. Brion, E. R. Davidson and D. Feller, *Chem. Phys.* **113**, 19 (1987).
- [229] A. O. Bawagan and C. E. Brion, *Chem. Phys.* **144**, 167 (1990).
- [230] P. Duffy, M. E. Casida, C. E. Brion and D. P. Chong, *Chem. Phys.* **159**, 347 (1992).
- [231] D. Feller, C. Boyle and E. R. Davidson, *J. Chem. Phys.* **86**, 3424 (1987).
- [232] K. P. Kirby, "Molecular photoabsorption processes" in *Molecular Astrophysics*, edited by T. W. Hartquist, Cambridge University Press, p.159 (1990).

- [233] H. Tawara, "Atomic and molecular data needed in space, fusion and related researches" in *Molecular Processes in space*, edited by T. Watanabe, I. Shimamura, M. Shimizu and Y. Itikawa, Plenum Press, New York and London, p.233 (1990).
- [234] A. C. Allison and A. Dalgarno, *At. Data* **1**, 289 (1970).
- [235] F. J. De Heer and J. D. Carriere, *J. Chem. Phys.* **8**, 3829 (1971).
- [236] D. E. Shemansky, J. M. Ajello and D. T. Hall, *Astrophys. J.* **296**, 765 (1985).
- [237] H. Schmoranzer, J. Imschweiler and T. Noll, "Proceedings on the 9th International Conference on Atomic Physics, Satellite Workshop and Conference Abstracts", Paper A26 (1984).
- [238] G. Herzberg, "Molecular Spectra and Molecular Structure I, Spectra of Diatomic Molecules", (VanNostrand, Princeton, N. J., 1950).
- [239] R. S. Mulliken and C. A. Rieke, *Rept. Prog. Phys.* **8**, 231 (1941).
- [240] H. Shull, *J. Chem Phys.* **20**, 18 (1952).
- [241] S. Ehrenson and P. E. Phillipson, *J. Chem. Phys.* **34**, 1224 (1961).
- [242] J. M. Peek and E. N. Lassettre, *J. Chem. Phys.* **38**, 2392 (1963).
- [243] K. J. Miller and M. Krauss, *J. Chem. Phys.* **47**, 3754 (1967).
- [244] J. Geiger and M. Topschowsky, *Z. Naturforsch.* **21A**, 626 (1966).
- [245] R. W. Nicholls, *Astrophys. J.* **141**, 819 (1965).
- [246] M. Halmann and I. Laulicht, *J. Chem. Phys.* **46**, 2684 (1967).
- [247] R. J. Spindler, *J. Quant. Spectrosc. Radiat. Transfer* **9**, 597 (1969).
- [248] R. J. Spindler, *J. Quant. Spectrosc. Radiat. Transfer* **9**, 627 (1969).
- [249] J. Geiger, *Z. Phys.* **181**, 413 (1964).
- [250] J. Geiger and H. Schmoranzer, *J. Mol. Spectrosc.* **32**, 39 (1969).
- [251] J. E. Hesser, *J. Chem. Phys.* **48**, 2518 (1968).
- [252] J. C. Browne, *Astrophys. J.* **156**, 397 (1969).
- [253] F. A. Matsen and J. C. Browne, *J. Chem. Phys.* **66**, 2332 (1962).
- [254] J. C. Browne and F. A. Matsen, *Phys. Rev. A* **135**, 1227 (1964).

- [255] S. Rothenberg and E. R. Davidson, *J. Mol. Spectrosc.* **22**, 1 (1967).
- [256] W. Kolos and L. Wolniewicz, *J. Chem Phys.* **43**, 2429 (1965).
- [257] A. Dalgarno and A. C. Allison, *Astrophys. J.* **154**, L95 (1968).
- [258] W. Kolos and L. Wolniewicz, *J. Chem. Phys.* **45**, 509 (1966).
- [259] W. Kolos, *Internat. J. Quant. Chem.* **1**, 169 (1967).
- [260] Y. M. Chan and A. Dalgarno, *Mol. Phys.* **14**, 101 (1968).
- [261] L. Wolniewicz, *J. Chem. Phys.* **51**, 5002 (1969).
- [262] A. C. Allison and A. Dalgarno, *Mol. Phys.* **19**, 567 (1970).
- [263] H. Schmoranzer, *J. Phys. B* **8**, 1139 (1975).
- [264] H. Schmoranzer and J. Geiger, *J. Chem. Phys.* **59**, 6153 (1973).
- [265] K. Dressler and L. Wolniewicz, *J. Chem. Phys.* **82**, 4720 (1985).
- [266] G. P. Arrighini, F. Biondi, C. Guidotti, A. Biagi and F. Marinelli, *Chem. Phys.* **52**, 133 (1980).
- [267] M. Glass-Maujean, *At. Data. Nucl. Data Tables* **30**, 301 (1984).
- [268] D. E. Gerhart, *J. Chem. Phys.* **62**, 821 (1975).
- [269] C. R. Jeppesen, *Phys. Rev.* **44**, 165 (1933).
- [270] G. H. Dieke, *J. Mol. Spectrosc.* **2**, 494 (1958).
- [271] G. Herzberg and L. L. Howe, *Can. J. Phys.* **37**, 636 (1959).
- [272] T. Namioka, *J. Chem. Phys.* **40**, 3154 (1964).
- [273] T. Namioka, *J. Chem. Phys.* **41**, 2141 (1964).
- [274] W. A. Chupka and J. Berkowitz, *J. Chem. Phys.* **51**, 4244 (1969).
- [275] S. Takazawa, *J. Chem. Phys.* **52**, 2575 (1970).
- [276] G. Herzberg and Ch. Jungen, *J. Mol. Spectrosc.* **41**, 425 (1972).
- [277] P. M. Dehmer and W. A. Chupka, *J. Chem. Phys.* **65**, 2243 (1976).
- [278] M. A. Baig and J. P. Connerade, *J. Phys B* **18**, L809 (1985).

- [279] G. N. Haddad, K. H. Lokan, A. J. D. Farmer and J. H. Carver, *J. Quant. Spectrosc. Radiat. Transfer* **8**, 1193 (1968).
- [280] J. E. Hesser, N. H. Brooks and G. M. Lawrence, *Astrophys. J.* **153**, L65 (1968).
- [281] J. E. Hesser, N. H. Brooks and G. M. Lawrence, *J. Chem. Phys.* **49**, 5388 (1968).
- [282] W. Fabian and B. R. Lewis, *J. Quant. Spectrosc. Radiat. Transfer* **14**, 523 (1974).
- [283] B. R. Lewis, *J. Quant. Spectrosc. Radiat. Transfer* **14**, 537 (1974).
- [284] M. Glass-Maujean, J. Breton and P. M. Guyon, *Chem. Phys. Lett.* **112**, 25 (1984).
- [285] M. Glass-Maujean, J. Breton and P. M. Guyon, *J. Chem. Phys.* **83**, 1468 (1985).
- [286] M. Glass-Maujean, J. Breton and P. M. Guyon, *Z. Phys. D* **5**, 189 (1987).
- [287] A. P. Hitchcock, C. E. Brion and M. J. Van der Wiel, *Chem. Phys.* **45**, 461 (1980).
- [288] E. N. Lassetre and E. A. Jones, *J. Chem. Phys.* **40**, 1222 (1964).
- [289] C. E. Kuyatt, S. R. Mielczarek and J. A. Simpson, *Phys. Rev. Lett.* **12**, 293 (1964).
- [290] H. G. M. Heideman, C. E. Kuyatt and G. E. Chamberlian, *J. Chem. Phys.* **44**, 440 (1966).
- [291] H. Boersch, J. Geiger and M. Topschowsky, *Phys. Lett.* **17**, 266 (1965).
- [292] J. A. R. Samson and G. Haddad, private communication (1984), as quoted in ref. [30].
- [293] A. C. Allison, quoted as a private communication in ref. [282].
- [294] E. C. Zipf and R. W. McLaughlin, *Planet. Space Sci.* **26**, 449 (1978).
- [295] E. C. Zipf and M. R. Gorman, *J. Chem. Phys.* **73**, 813 (1980).
- [296] J. M. Ajello, G. K. James, B. O. Franklin and D. E. Shemansky, *Phys. Rev. A* **40**, 3524 (1989).

- [297] G. K. James, J. M. Ajello, B. O. Franklin and D. E. Shemansky, *J. Phys. B* **23**, 2055 (1990).
- [298] C. Duzy and R. S. Berry, *J. Chem. Phys.* **64**, 2421 (1976).
- [299] T. N. Rescigno, C. F. Bender, B. V. McKoy and P. W. Langhoff, *J. Chem. Phys.* **68**, 970 (1978).
- [300] W. M. Kosman and S. Wallace, *J. Chem. Phys.* **82**, 1385 (1985).
- [301] J. Rose, T. Shibuya and V. McKoy, *J. Chem. Phys.* **58**, 74 (1973).
- [302] A. U. Hazi, *Phys. Rev. A* **23**, 2232 (1981).
- [303] C. E. Bielschowsky, M. A. C. Nascimento and E. Hollauer, *J. Phys. B* **23**, L787 (1990).
- [304] J. Geiger and B. Schroder, *J. Chem. Phys.* **50**, 7 (1969).
- [305] P. K. Carroll and C. P. Collins, *Can. J. Phys.* **47**, 563 (1969).
- [306] D. Stahel, M. Leoni and K. Dressler, *J. Chem. Phys.* **79**, 2541 (1983).
- [307] P. K. Carroll and Kh. I. Hagim, *Phys. Scr.* **37**, 682 (1988).
- [308] H. Lefebvre-Brion and R. W. Field, "Perturbations in the Spectra of Diatomic Molecules", (Academic Press, Orlando), p.265 (1986).
- [309] J. J. Hopfield, *Phys. Rev.* **29**, 356 (1927).
- [310] R. E. Worley and F. A. Jenkins, *Phys. Rev.* **54**, 305 (1938).
- [311] R. E. Worley, *Phys. Rev.* **64**, 207 (1943).
- [312] G. L. Weissler, P. Lee and E. I. Mohr, *J. Opt. Soc. Am.* **42**, 84 (1952).
- [313] K. C. Clark, *Phys. Rev.* **87**, 271 (1952).
- [314] R. E. Worley, *Phys. Rev.* **89**, 863 (1953).
- [315] J. P. Curtis, *Phys. Rev.* **94**, 908 (1954).
- [316] K. Watanabe and F. F. Marmo, *J. Chem. Phys.* **25**, 965 (1956).
- [317] M. Ogawa and Y. Tanaka, *Can. J. Phys.* **40**, 1593 (1962).
- [318] P. K. Carroll and K. Yoshino, *J. Phys. B* **5**, 1614 (1972).

- [319] J. W. Ledbetter, Jr., *J. Mol. Spectrosc.* **42**, 100 (1972).
- [320] K. Yoshino and D. E. Freeman, *Can. J. Phys.* **62**, 1478 (1984).
- [321] K. Shobatake, A. Hiraya, K. Tabayashi and T. Ibuki, "Vacuum Ultraviolet Photoionization and Photodissociation of Molecules and Clusters: Absorption and Fluorescence Studies of Molecules and Clusters", edited by C. Y. Ng (World Scientific), p.503 (1992).
- [322] A. J. Williams III and J. P. Doering, *Planet. Space Sci.* **17**, 1527 (1969).
- [323] A. J. Williams III and J. P. Doering, *J. Chem. Phys.* **51**, 2859 (1969).
- [324] A. Chutjian, D. C. Cartwright and S. Trajmar, *Phys. Rev. A* **16**, 1052 (1977).
- [325] J. A. R. Samson and R. B. Cairns, *J. Opt. Soc. Am.* **55**, 1035 (1965).
- [326] L. C. Lee, R. W. Carlson, D. L. Judge and M. Ogawa, *J. Quant. Spectrosc. Radiat. Transfer* **13**, 1023 (1973).
- [327] W. S. Watson, J. Lang and D. T. Stewart, *J. Phys. B* **6**, L148 (1973).
- [328] L. De Reilhac and N. Damany, *J. Quant. Spectrosc. Radiat. Transfer* **18**, 121 (1977).
- [329] B. E. Cole and R. N. Dexter, *J. Phys. B* **11**, 1011 (1978).
- [330] K. Watanabe, *Advan. Geophys.* **2**, 153 (1958).
- [331] P. H. Krupenie, *J. Phys. Chem. Ref. Data* **1**, 423 (1972).
- [332] B. R. Lewis, L. Berzins and J. H. Carver, *J. Quant. Spectrosc. Radiat. Transfer* **36**, 209 (1986).
- [333] R. Ladenburg and C. C. Van Voorhis, *Phys. Rev.* **43**, 315 (1933).
- [334] K. Watanabe, E. C. Y. Inn and M. Zelikoff, *J. Chem. Phys.* **21**, 1026 (1953).
- [335] R. W. Ditchburn and P. W. O. Heddle, *Proc. Roy. Soc. (London) A* **220**, 61 (1953).
- [336] P. H. Metzger and G. R. Cook, *J. Quant. Spectrosc. Radiat. Transfer* **4**, 107 (1964).
- [337] R. D. Hudson, V. L. Carter and J. A. Stein, *J. Geophys. Res.* **71**, 2295 (1966).

- [338] A. J. Blake, J. H. Carver and G. N. Haddad, *J. Quant. Spectrosc. Radiat. Transfer* **6**, 451 (1966).
- [339] R. Goldstein and F. N. Mastrup, *J. Opt. Soc. Am.* **56**, 765 (1966).
- [340] S. Ogawa and M. Ogawa, *Can. J. Phys.* **53**, 1854 (1975).
- [341] S. T. Gibson, H. P. F. Gies, A. J. Blake, D. G. McCoy and P. J. Rogers, *J. Quant. Spectrosc. Radiat. Transfer* **30**, 385 (1983).
- [342] J. Wang, D. G. McCoy, A. J. Blake and L. Torop, *J. Quant. Spectrosc. Radiat. Transfer* **38**, 19 (1987).
- [343] R. J. Buenker and S. D. Peyerimhoff, *Chem. Phys. Lett.* **34**, 225 (1975).
- [344] A. C. Allison, S. L. Guberman and A. Dalgarno, *J. Geophys. Res.* **91**, 10193 (1986).
- [345] M. Yoshimine, K. Tanaka, H. Tatewaki, S. Obara, F. Sadaki and K. Ohno, *J. Chem. Phys.* **64**, 2254 (1976).
- [346] R. J. Buenker, S. D. Peyerimhoff and M. Peric, *Chem. Phys. Lett.* **42**, 383 (1976).
- [347] Y. Li, M. Honigmann, K. Bhanuprakash, G. Hirsch, R. J. Buenker, M. A. Dillon and M. Kimura, *J. Chem. Phys.* **96**, 8314 (1992).
- [348] B. R. Lewis, S. T. Gibson, M. Emami and J. H. Carver, *J. Quant. Spectrosc. Radiat. Transfer* **40**, 1 (1988).
- [349] B. R. Lewis, S. T. Gibson, M. Emami and J. H. Carver, *J. Quant. Spectrosc. Radiat. Transfer* **40**, 469 (1988).
- [350] J. Geiger and B. Schroder, *J. Chem Phys.* **49**, 740 (1968).
- [351] R. H. Huebner, R. J. Celotta, S. R. Mielczarek and C. E. Kuyatt, *J. Chem. Phys.* **63**, 241 (1975).
- [352] W. S. Watson, J. Lang and D. T. Stewart, *Phys. Lett. A* **44**, 293 (1973).
- [353] O. Edqvist, E. Lindholm, L. E. Selin and L. Åsbrink, *Phy. Scr.* **1**, 25 (1970).
- [354] R. E. Huffman, J. C. Larrabee and Y. Tanaka, *J. Chem. Phys.* **40**, 356 (1964).
- [355] J. A. R. Samson and R. B. Cairns, *J. Geophys. Res.* **69**, 4583 (1964).

- [356] F. M. Matsunaga and K. Watanabe, *Sci. Light (Tokyo)* **16**, 31 (1967).
- [357] Y. P. Viala, C. Letzelter, M. Eidelsberg and F. Rostas, *Astron. Astrophys.* **193**, 265 (1988).
- [358] M. Eidelsberg and F. Rostas, *Astron. Astrophys.* **235**, 472 (1990).
- [359] J. F. M. Aarts and F. J. De Heer, *J. Chem. Phys.* **52**, 5354 (1970).
- [360] G. K. James, J. M. Ajello, I. Kanik, B. Franklin and D. E. Shemansky, *J. Phys. B* **25**, 1481 (1992).
- [361] W. Coughran, J. Rose, T. Shibuya and V. McKoy, *J. Chem. Phys.* **58**, 2699 (1973).
- [362] M. H. Wood, *Chem. Phys. Lett.* **28**, 477 (1974).
- [363] E. S. Nielsen, P. Jorgensen and J. Oddershede, *J. Chem. Phys.* **73**, 6238 (1980).
- [364] D. Lynch, M. F. Herman and D. L. Yeager, *Chem. Phys.* **64**, 69 (1982).
- [365] N. Padial, G. Csanak, B. V. McKoy and P. W. Langhoff, *J. Chem. Phys.* **69**, 2992 (1978).
- [366] D. M. Cooper and S. R. Langhoff, *J. Chem. Phys.* **74**, 1200 (1981).
- [367] K. Kirby and D. L. Cooper, *J. Chem. Phys.* **90**, 4895 (1989).
- [368] L. Chantranupong, K. Bhanuprakash, M. Honigmann, G. Hirsch and R. J. Buenker, *Chem. Phys.* **161**, 351 (1992).
- [369] P. H. Krupenie, "The Band Spectrum of Carbon Monoxide", vol. 5, NSRDS-NBS 5, Natl. Bur. Stand. (1966).
- [370] S. G. Tilford and J. D. Simmons, *J. Chem. Phys. Ref. Data* **1**, 147 (1972).
- [371] K. P. Huber and G. Herzberg, "Molecular Spectra and Molecular Structure, IV: Constants of Diatomic Molecules", Van Nostrand-Reinhold, New York (1979).
- [372] J. J. Hopfield and R. T. Birge, *Phys. Rev.* **29**, 922 (1927).
- [373] H. J. Henning, *Ann. Phys.* **13**, 599 (1932).
- [374] T. Takamine, Y. Tanaka and M. Iwata, *Sci. Papers Inst. Phys. Chem. Research (Tokyo)* **40**, 371 (1943).

- [375] K. Watanabe, M. Zelikoff and E. C. Y. Inn, Geophys. Res. Paper (U.S.) No. 21, (June 1953).
- [376] H. Sun and G. L. Weissler, J. Chem. Phys. **23**, 1625 (1955).
- [377] G. Herzberg and T. J. Hugo, Can. J. Phys. **33**, 757 (1955).
- [378] Y. Tanaka, A. S. Jursa and F. LeBlanc, J. Chem. Phys. **26**, 862 (1957).
- [379] B. A. Thompson, P. Harteck and R. R. Reeves, Jr., J. Geophys. Res. **68**, 6431 (1963).
- [380] R. E. Huffman, J. C. Larrabee and Y. Tanaka, J. Chem. Phys. **40**, 2261 (1964).
- [381] S. G. Tilford, J. T. Vanderslice and P. G. Wilkinson, Can. J. Phys. **43**, 450 (1965).
- [382] G. P. Cook, P. H. Metzger and M. Ogawa, Can. J. Phys. **43**, 1706 (1965).
- [383] J. D. Simmons and S. G. Tilford, J. Chem. Phys. **45**, 2965 (1966).
- [384] J. D. Simmons and A. M. Bass, Astrophys. J. **155**, 345 (1969).
- [385] J. A. Myer and J. A. R. Samson, J. Chem. Phys. **52**, 266 (1970).
- [386] J. H. Fock, P. Gurtler and E. E. Koch, Chem. Phys. **47**, 87 (1980).
- [387] L. C. Lee and J. A. Guest, J. Phys. B **14**, 3415 (1981).
- [388] C. Letzelter, M. Eidelsberg and F. Rostas, Chem. Phys. **114**, 273 (1987).
- [389] M. Eidelsberg, J. Y. Roncin, A. Le Floch, F. Launay, C. Letzelter and J. Rostas, J. Mol. Spectrosc. **121**, 309 (1987).
- [390] A. C. Le Floch, F. Launay, J. Rostas, R. W. Field, C. M. Brown and K. Yoshino, J. Mol. Spectrosc. **121**, 337 (1987).
- [391] G. Stark, K. Yoshino, P. L. Smith, K. Ito and W. H. Paskinson, Astrophys. J. **369**, 574 (1991).
- [392] M. Eidelsberg, F. Rostas, J. Breton and B. Thieblemont, J. Chem. Phys. **96**, 5585 (1992).
- [393] J. C. Rich, Astrophys. J. **153**, 327 (1968).
- [394] E. H. Fink and K. H. Welge, Zs. Naturforsch. A **23**, 358 (1968).

- [395] J. H. Moore, Jr. and W. Robinson J. Chem. Phys. **48**, 4870 (1968).
- [396] P. J. Le Calve, M. Bourene, M. Schmidt and M. Clerc, J. de Phys. **30**, 807 (1967).
- [397] J. Rogers and R. Anderson, J. Opt. Soc. Am. **60**, 278 (1970).
- [398] J. G. Chervenak and R. A. Anderson, J. Opt. Soc. Am. **61**, 952 (1971).
- [399] R. E. Imhof and F. H. Read, Chem. Phys. Lett. **11**, 326 (1971).
- [400] R. L. Burnham, R. C. Isler and W. C. Wells, Phys. Rev. A **6**, 1327 (1972).
- [401] R. E. Imhof, F. H. Read and S. T. Beckett, J. Phys. B **5**, 896 (1972).
- [402] L. W. Dotchin and E. L. Chupp, J. Chem. Phys. **59**, 3960 (1973).
- [403] A. Pochat, M. Doritch and J. Peresse, J. Chim. Phys. **70**, 936 (1973).
- [404] H. A. Van Sprang, G. R. Mohlmann and F. J. De Heer, Chem. Phys. **24**, 429 (1977).
- [405] W. H. Smith, Phys. Scr. **17**, 513 (1978).
- [406] T. A. Carlson, N. Duric, P. Erman and M. Larsson, Z. Phys. A **287**, 123 (1978).
- [407] R. W. Field, O. Benoist d'Azy, M. Lavollee, R. Lopez-Delgado and A. Tramer, J. Chem. Phys. **78**, 2838 (1983).
- [408] E. Krishnakumar and S. K. Srivastava, Astrophys. J. **307**, 795 (1986).
- [409] V. D. Meyer, A. Skerbele and E. N. Lassetre, J. Chem. Phys. **43**, 805 (1965).
- [410] J. P. Bromberg, J. Chem. Phys. **52**, 1243 (1970).
- [411] G. R. Burton, W. F. Chan, G. Cooper and C. E. Brion, submitted to Chem. Phys..
- [412] W. C. Watson, D. T. Stewart, A. B. Gardner and M. J. Lynch, Planet. Space Sci. **23**, 384 (1975).
- [413] A. W. Potts and T. A. Williams, J. Elect. Spectrosc. Relat. Phenom. **3**, 3 (1974).

- [414] R. W. Field, Ph. D. thesis, Harvard University, 1972.
- [415] A. Le Floch, *Mol. Phys.* **72**, 133 (1991).
- [416] R. L. De Leon, *J. Chem. Phys.* **89**, 20 (1988), and erratum; *J. Chem. Phys.* **91**, 5859 (1989).
- [417] I. S. McDermid and J. B. Laudenslager, *J. Quant. Spectrosc. Radiat. Transfer* **27**, 483 (1982).
- [418] G. Witt, J. Dye and N. Wilhelm, *J. Atm. Terr. Phys.* **38**, 223 (1976).
- [419] M. D. Burrows, S. L. Baughum and R. C. Oldenborg, *Appl. Phys. Lett.* **46**, 22 (1985).
- [420] H. A. Ory, *J. Chem. Phys.* **40**, 562 (1964).
- [421] D. M. Cooper, *J. Quant. Spectrosc. Radiat. Transfer* **27**, 459 (1982).
- [422] R. de Vivie and S. D. Peyerimhoff, *J. Chem. Phys.* **89**, 3028 (1988).
- [423] S. R. Langhoff, C. W. Bauschlicher, Jr. and H. Partridge, *J. Chem. Phys.* **89**, 4909 (1988).
- [424] S. R. Langhoff, H. Partridge, C. W. Bauschlicher, Jr. and A. Komornicki, *J. Chem. Phys.* **94**, 6639 (1991).
- [425] R. Gallusser and K. Dressler, *J. Chem. Phys.* **76**, 4311 (1982).
- [426] G. W. Bethke, *J. Chem. Phys.* **31**, 662 (1959).
- [427] S. W. Leifson, *Astrophys. J.* **63**, 73 (1926).
- [428] Y. Tanaka, *J. Sci. Research Inst. (Tokyo)* **43**, 2328 (1949).
- [429] R. F. Barrow and E. Miescher, *Proc. Phys. Soc. (London)* **70A**, 219 (1957).
- [430] K. P. Huber, *Helv. Phys. Acta* **34**, 929 (1961).
- [431] Ch. Jungen, *Can. J. Phys.* **44**, 3197 (1966).
- [432] B. Narayana and W. C. Price, *J. Phys. B* **5**, 1784 (1972).
- [433] M. Sasanuma, Y. Morioka, E. Ishiguro and M. Nakamura, *J. Chem. Phys.* **60**, 327 (1974).
- [434] E. Miescher, *Can. J. Phys.* **54**, 2074 (1976).

- [435] E. Miescher, Y. T. Lee and P. Gurtler, *J. Chem. Phys.* **68**, 2753 (1978).
- [436] Y. Ono, S. H. Linn, H. F. Prest, C. Y. Ng and E. Miescher, *J. Chem. Phys.* **73**, 4855 (1980).
- [437] E. Miescher and K. Huber, "International Reviews of Science", Physical Chemistry Series 2, Vol. 3, Spectroscopy, ed. by D. A. Ramsay (Butterworths, London) p.37 (1976).
- [438] E. Miescher and F. Alberti, *J. Phys. Chem. Ref. Data* **5**, 309 (1976).
- [439] F. F. Marmo, *J. Opt. Soc. Am.* **43**, 1186 (1953).
- [440] D. Weber and S. S. Penner, *J. Chem. Phys.* **26**, 860 (1957).
- [441] V. Hasson and R. W. Nicholls, *J. Phys. B* **4**, 1769 (1971).
- [442] H. Sun and G. L. Weissler, *J. Chem. Phys.* **23**, 1372 (1955).
- [443] K. Watanabe, F. M. Matsunaga and H. Sakai, *Appl. Opt.* **6**, 391 (1967).
- [444] P. H. Metzger, G. R. Cook and M. Ogawa, *Can. J. Phys.* **45**, 203 (1967).
- [445] A. Gardner, M. Lynch, D. T. Stewart and W. S. Watson, *J. Phys. B* **6**, L262 (1973).
- [446] M. Mandelman and T. Carrington, *J. Quant. Spectrosc. Radiat. Transfer* **14**, 509 (1974).
- [447] A. B. Callear and M. J. Pilling, *Trans. Faraday Soc.* **66**, 1886 (1970).
- [448] A. Pery-Thorne and F. P. Banfield, *J. Phys. B* **3**, 1011 (1970).
- [449] A. J. D. Farmer, V. Hasson and R. W. Nicholls, *J. Quant. Spectrosc. Radiat. Transfer* **12**, 627 (1972).
- [450] A. J. D. Farmer, V. Hasson and R. W. Nicholls, *J. Quant. Spectrosc. Radiat. Transfer* **12**, 635 (1972).
- [451] J. C. Keck, J. C. Camm, B. Kivel and T. Wentink, Jr., *Ann. Phys.* **7**, 1 (1959).
- [452] J. W. Daiber and M. J. Williams, *J. Quant. Spectrosc. Radiat. Transfer* **1**, 135 (1961).
- [453] M. Mandelman, T. Carrington and R. A. Young, *J. Chem. Phys.* **58**, 84 (1973).

- [454] M. Jeunehomme and A. B. F. Duncan, *J. Chem. Phys.* **41**, 1692 (1964).
- [455] M. Jeunehomme, *J. Chem. Phys.* **45**, 4433 (1966).
- [456] J. Brzozowski, N. Elander and P. Erman, *Phys. Scr.* **9**, 99 (1974).
- [457] J. Brzozowski, P. Erman and M. Lyyra, *Phys. Scr.* **14**, 290 (1976).
- [458] H. Zacharias, J. B. Halpern and K. H. Welge, *Chem. Phys. Lett.* **43**, 41 (1976).
- [459] G. R. Mohlmann, H. A. Van Sprang, E. Bloemem and F. J. De Heer, *Chem. Phys.* **32**, 239 (1978).
- [460] T. Hikida, S. Yagi and Y. Mori, *Chem. Phys.* **52**, 399 (1980).
- [461] K. Shibuya and F. Stuhl, *Chem. Phys.* **79**, 367 (1983).
- [462] J. F. Burris, T. J. McGee and J. Barnes, *Chem. Phys. Lett.* **121**, 371 (1985).
- [463] D. J. Hart and J. W. Hepburn, *J. Chem. Phys.* **86**, 1733 (1987).
- [464] K. Tsukiyama, T. Munakata, M. Tsukakoshi and T. Kasuya, *Chem. Phys.* **121**, 55 (1988).
- [465] D. J. Hart and O. L. Bourne, *Chem. Phys.* **133**, 103 (1989).
- [466] G. E. Gadd and T. G. Slanger, *J. Chem. Phys.* **92**, 2194 (1990).
- [467] G. E. Gadd, D. L. Huestis and T. G. Slanger, *J. Chem. Phys.* **95**, 3944 (1991).
- [468] E. T. Antropov, V. N. Kolesnikov, L. Ya. Ostrovskaya and N. N. Sobolev, *Opt. Spectrosc.* **22**, 109 (1966).
- [469] A. B. Callear, M. J. Pilling and I. W. M. Smith, *Trans. Faraday Soc.* **62**, 2997 (1966).
- [470] H. M. Poland and H. P. Broida, *J. Quant. Spectrosc. Radiat. Transfer* **11**, 1863 (1971).
- [471] T. J. McGee, G. E. Miller, J. Burris, Jr. and T. J. McIlrath, *J. Quant. Spectrosc. Radiat. Transfer* **29**, 333 (1983).
- [472] T. J. McGee, J. Burris, Jr. and J. Barnes, *J. Quant. Spectrosc. Radiat. Transfer* **34**, 81 (1985).
- [473] L. G. Piper and L. M. Cowles, *J. Chem. Phys.* **85**, 2419 (1986).

- [474] L. G. Piper, T. R. Tucker and W. P. Cummings, *J. Chem. Phys.* **94**, 7667 (1991).
- [475] E. N. Lassette, A. Skerbele, M. A. Dillon and K. J. Ross, *J. Chem. Phys.* **48**, 5066 (1968).
- [476] O. Edqvist, L. Asbrink and E. Lindholm, *Z. Naturforsch.* **26A**, 1407 (1971).